Bio-inspired self-construction and self-assembly of organic films triggered by electrochemistry

Clément Maerten

UNIVERSITÉ DE STRASBOURG

ÉCOLE DOCTORALE de PHYSIQUE et CHIMIE-PHYSIQUE

Institut Charles Sadron CNRS-UPR22

THÈSE

pour obtenir le grade de : **Docteur de l'université de Strasbourg**

Discipline: Chimie-Physique

présentée et soutenue le **20 septembre 2016** par :

Clément MAERTEN

Bio-inspired self-construction and self-assembly of organic films triggered by electrochemistry

---

THÈSE dirigée par :

BOULMEDAIS Fouzia	Chargée de recherches, HDR, CNRS

RAPPORTEURS :

WOISEL Patrice	Professeur, Université de Lille 1
LAKARD Boris	Professeur, Université de Besançon

AUTRES MEMBRES DU JURY :

ROUCOULES Vincent	Professeur, Université de Mulhouse
SCHAAF Pierre	Professeur, Université de Strasbourg

Summary

List of abreviations

Molecules

AP : alkaline phosphatase

BMP : bone morphogenetic protein

BSA : bovine serum albumin

DNA : Deoxyribonucleic acid

DHPAA : 3,4-dihydroxypehenylacetic acid

Dopa : 3,4-dihydroxyphenyl-L-alanine

DXS : dextran

EDTA : ethylenediaminetetraacetic acid disodium salt dehydrate

EGCG : epigallocatechin-3-gallate

GA : gallic acid

GO : glucose oxidase

HA : hyaluronic acid

Hap : Hydroxyapatite (Hap)

HEPES : 4-(2-Hydroxyethyl) piperazine-1-ethanesulfonic acid

ITO : indium tin oxide

NTA : nitrilotriacetic

PAA : polyacrylic acid

PAH : poly(allylamine hydrochloride)

PDA : polydopamine

PDADMA : poly(diallyldimethylammonium chloride)

PDMS : polydimethylsiloxane

PEG : polyethylene glycol

PEI : polyethylenimine

PLL : poly(-L-lysine)

PLO : poly(L-ornithine)

PNPP : paranitrophenyl phosphate

PSS : poly(styrenesulfonate)

PVP : poly(N-vinlypyrrolidone)

RA : rosmarinic acid

Rh6G-LEDA : N(rhodamine-6G)lactam-ethylenediamine

TA : tannic acid

TUDA : 3,6,9-trioaundecandioic acid

VEGF : vascular endothelial growth factor

Methods

AFM : atomic force microscopy

CE : counter electrode

CV : cyclic voltammetry

EC-QCM-D : quartz crystal microbalance with dissipation coupled to an electrochemical modulus

FTIR : fourier transform infrared spectroscopy

NMR : nuclear magnetic resonance

QCM : quartz crystal microbalance

RE : reference electrode

WE : working electrode

XPS : X-ray photoelectron spectroscopy

Others

ECC-LbL : electrochemical-coupling layer-by-layer

EFDLA *:* electric-field directed layer-by-layer assembly

LbL : layer-by-layer

OCP : open circuit potential

SI-ATRP : surface initiated atom transfer radical polymerization

General introduction

Surface coatings are studied since the first quarter of the XXth century and are largely present in our day life conferring to materials new functionalities such as magnetic, electrical, optical properties, biocompatibility, protection towards corrosion or catalytic properties, etc. Many processes were developed in the last decades to functionalize all types of materials (metals, ceramics, polymers) depending on the desired property.

Electrodeposition of soft matter, a process in which an electrical "signal" is used to direct the assembly of thin films, attracts an increasing attention because it offers broad opportunities for a diverse range of applications. Compared to other polymer coating processes, it presents the advantage of being fast, easily applicable on conductive materials with complex geometries. Moreover, the electrical signal can be applied with a perfect spatiotemporal selectivity, therefore, allowing sequential assembly of different components at separate electrodes.

Five years ago, our team introduced a new concept based on the electrochemical generation of a catalyst gradient triggering the covalent assembly of polymer films: the morphogenic self-construction of films. In biology, morphogenesis, from the Greek *morphê* (shape) and *genesis* (creation), encompasses the rules describing the formation of the shape and the structure of a biological organism. In 1952, the mathematician Alan Turing published a seminal article called "*The Chemical Basis of Morphogenesis" (Philosophical Transactions of the Royal Society, Vol 237, 1953)* where he introduced a model to explain the formation of patterns during the creation of living organisms. According to this model, the conjunction of chemical reactions and molecular diffusion of reactive species, called morphogens, leads spontaneously to spatial variations of the concentrations of these species resulting in the formation of stripe or stain patterns. To illustrate this model, Turing used the examples of cheetah coat spots, hydra's tentacles positioning as well as a phase of embryo development called gastrulation.

In chemistry, a morphogen can be defined as a molecule or ion generated at an interface, that diffuses into the solution leading to a gradient and which locally induces a chemical process. This concept was applied to build polymer films composed of two polymers interacting through covalent bonding. Copper (I), the morphogen here, electrochemically produced at an electrode from copper (II) reduction, catalyzed the click reaction between alkyne and azide bearing polymers leading to their assembly, localized at the electrode. *(Angewandte Chemie International Edition, Vol 123, 2011)*

The purpose of this PhD was to extend this strategy to other systems using a bio-inspired approach. The one-pot morphogen concept was applied to electro-triggered self-construction of polymer and polyphenols films based on mussel-inspired and polyphenols biochemistry. In comparison to the previously described system, the morphogen in this work is not a catalyst that induces a buildup but is an integral part of the final assembly.

The PhD manuscript is divided in five chapters. The first chapter gives a review of the state-of-the-art of the mussel-inspired and polyphenols-based materials and surface coatings as well as the different electrodeposition processes described in the literature. The second chapter presents the material and methods used for this work. The third chapter introduces the self-construction of covalent polymer films triggered by mussel-inspired molecule oxidation. The fourth chapter deals with the electro-induced self-assembly of polyphenols films based on ionic bonds coordination. The application to biosensing of both systems developed is exposed in the last chapter.

The first chapter is subdivided into two parts. A first part aims to present our inspiration which comes from the mussel adhesion phenomenon and the polyphenols role in plants, both based on the phenolic chemistry through catechol or gallol moieties. Materials and coatings that came out from the understanding of these phenomena are also introduced. The second part reviews the different electrodeposition processes, which can be separated on three categories based on the deposition mechanism: electrodeposition through macromolecules precipitation, polyelectrolytes self-assembly and covalent bonds formation between polymers.

The materials and methods used during this PhD are introduced in the second chapter. The commercial and synthesized molecules are described. The characterization and experimental techniques (electrochemical quartz crystal microbalance, cyclic voltammetry, atomic force microscopy and X-ray photoelectrons spectroscopy) are detailed.

The third chapter concentrates on the morphogen electrochemically triggered self-construction of polymer films based on mussel-inspired chemistry. A bis-catechol spacer, acting as the morphogen, was used to electro-crosslink a polyamine. Indeed, catechols can be oxidized into quinone moieties which are reactive towards amine functions. Thus, bis-quinone active molecules diffuse from the electrode reacting on both sides with polyamine leading to the buildup of a film on the surface. The influence of some relevant parameters such as the morphogen concentration or the scan rate was studied. The chemical composition and the morphology of the films are also discussed.

The fourth chapter deals with the electrotriggered self-assembly of metal-polyphenol films. Tannic acid, already widely used to functionalize surfaces, was electro-crosslinked through coordination bonding with Fe(III). Indeed, tannic acid is known to form complexes with metal ions, such as Fe(III) thanks to its gallol moities. Fe(III), the morphogen here, is generated by the oxidation of Fe(II) and induces the assembly of tannic acid from the surface. The influence of some relevant parameters, the chemical composition and the morphology of the films are analyzed. The resulting coatings appear to be stable even at reductive potential. Moreover, the concept is generalized to other phenolic molecules: gallic acid and rosmarinic acid.

Application to biosensing of the systems developed in third and fourth chapter is discussed in the last chapter. Our goal was to immobilize an enzyme on an electrode by a morphogenic process and keep its activity. In a first part, we try to electro-crosslink alkaline phosphatase through quinone/amine covalent bonding. Different phenolic molecules were used: bis-catechol, tannic acid, and a gallol-modified dendrimer. The second part introduces a different strategy: the physical entrapment of alkaline phosphatase in the electrotriggered assembly of metal-polyphenols films.

The manuscript ends with a general conclusion and some outlooks of the PhD work.

CHAPTER 1 : BIBLIOGRAPHIC REVIEW

CHAPTER 1 : BIBLIOGRAPHIC REVIEW

Summary

1.1 Phenolic and Polyphenolic biomimetism

Biomimetism aims at understanding natural phenomena in order to not only broaden our knowledge of Nature but also to find ideas to create new concepts particularly in materials science. Even if tremendous technological advances were made by mankind during the past centuries, nature is still far way beyond us. Therefore, it has been ages since man has been trying to mimic nature for his advantage. Leonardo da Vinci was already trying to design a flying machine mimicking flying birds. Since da Vinci, numerous examples of biomimetic concepts were created. Spiker silk which presents unique mechanical properties has drawn great attention in order to replace Kevlar. Lotus flea's microstructure allowed to create superhydrophobic surfaces. Geckos are able to walk on every surface without falling, leadings to the design of new adhesives. Velcro© was inspired by the tiny hooks on the surface of burs. In this work, our inspiration comes from two observations: the unique capacity of mussels to adhere on all type of surfaces in water in extremely harsh conditions, and the fact that polyphenols are able to coordinate metals contributing to the coloration of plants. Both phenomena are based on the diversified chemistry of catechol and gallol moieties (Figure 1.1). Catechols are benzene derivatives with two *ortho*-hydroxyl groups and are widespread in nature. For example, dopamine is a well-known neurotransmitter, and Dopa is the amino-acid responsible of the strong adhesive properties of the proteins involved in mussel adhesion. Gallols have a chemical structure very similar to catechol, with three neighboring hydroxyl groups instead of two. Along with catechols, they are present in the plant polyphenols.

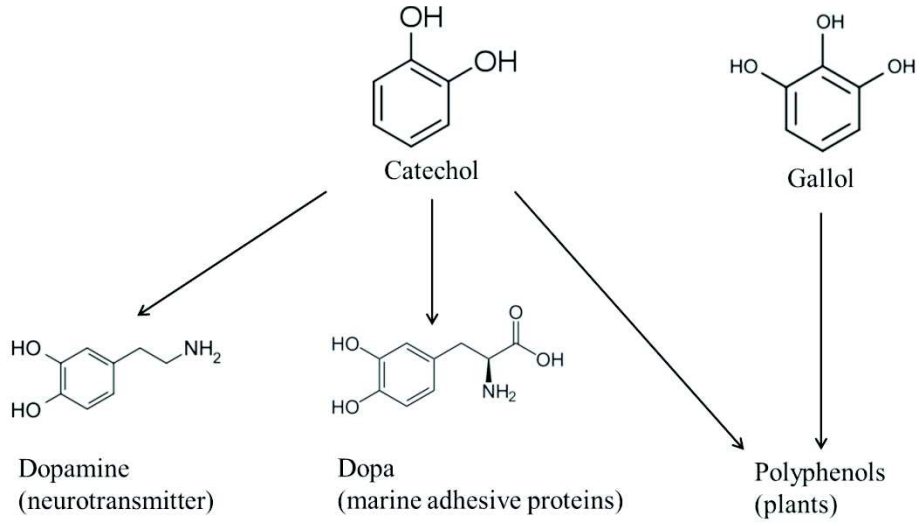

Figure 1.1: *Chemical structure of catechol and gallol moieties with examples of natural phenomena in which they are involved.*

Firstly, we will give a simplified understanding of these two natural phenomena that inspired us and the biomolecules implied. Secondly, we will overview the functional materials inspired by them.

1.1.1 Nature: our source of inspiration

1.1.1.1 Marine adhesive proteins in mussels

Mussels are bivalve molluscs of the marine family *Mytilidae*. These organisms have the property to stick to all kind of materials (glass, wood, organic surface, metal…) under extremely harsh conditions: they endure huge changes of temperature in seawater, fluctuations of salinity, and mechanical solicitation due to waves and currents.

In order to attach to surfaces, mussels secrete a bundle of radially distributed threads called byssus (Figure 1.2). The byssus can be divided into four parts: the attachment plaques in direct contact with the surface, the threads, the stem and the root. The threads are joined to the stem, which inserts into the base of the foot. The byssal tension and movement are controlled by 12 byssal retractor muscles.

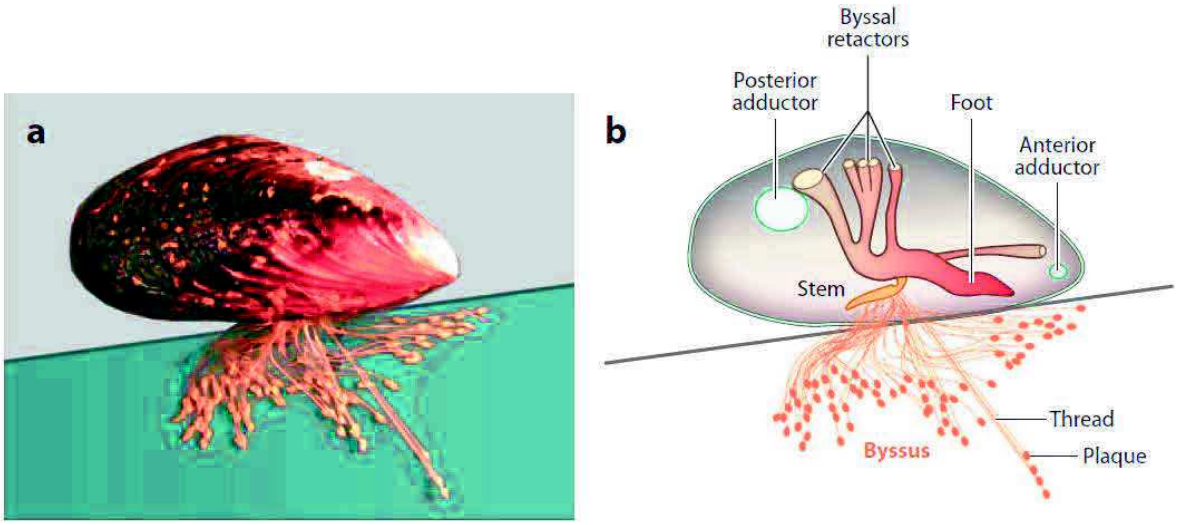

Figure 1.2: *Adhesion in the marine mussel Mytilus californianus. a) Adult mussel (5cm length) displaying an extensive byssus. b) Schematic representation of a mussel on a half-shell. Each byssus is a bundle of threads tipped with adhesive plaques.*[1]

In order to understand how the mussel can adhere to any kind of surfaces, we will focus on the analysis of the chemical composition and the structure of the byssal plaques which are responsible for the strong adhesion of the organism. Around seven different proteins are present in the plaque, five of them are specific: mefp-2, -3, -4, -5, and -6.[1] Having different peptidic sequences, they present a high content in the amino acid 3,4-dihydroxyphenyl-L-alanine (Dopa)

(Figure 1.3b). These proteins are generally called marine adhesive proteins and were observed in other organisms such as tube worms,[2] and barnacles.[3]

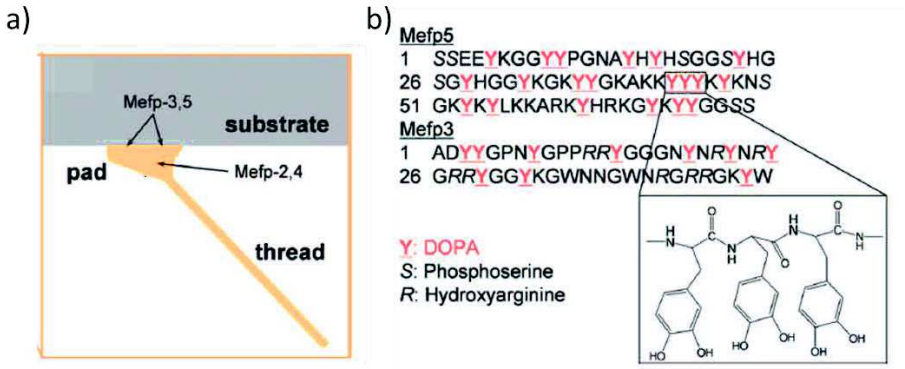

Figure 1.3: *a) Distribution of the mepfs in the attachment plaque or pad. b) The amino acid sequences of mefp-3 and mefp-5, have the highest known Dopa content. The insight shows the chemical structure of Dopa as it appears in the tri-Dopa sequence of mefp-5.*[4]

The mefp-3, -5 proteins, localized in the adhesive part of the plaque in contact with the surface, have the highest Dopa content.[4] Dopa amino acids present catechol moieties (Figure 1.3) which are responsible for the strong adhesion of the plaque. Indeed catechol can interact with atoms or chemical functions in different ways (Figure 1.4): it can form hydrogen bonds, metal-ligand complexes especially with Fe(III) ions,[5] charge-transfer complexes, and covalently react with nucleophiles (amines, thiol) when oxidized.[6]

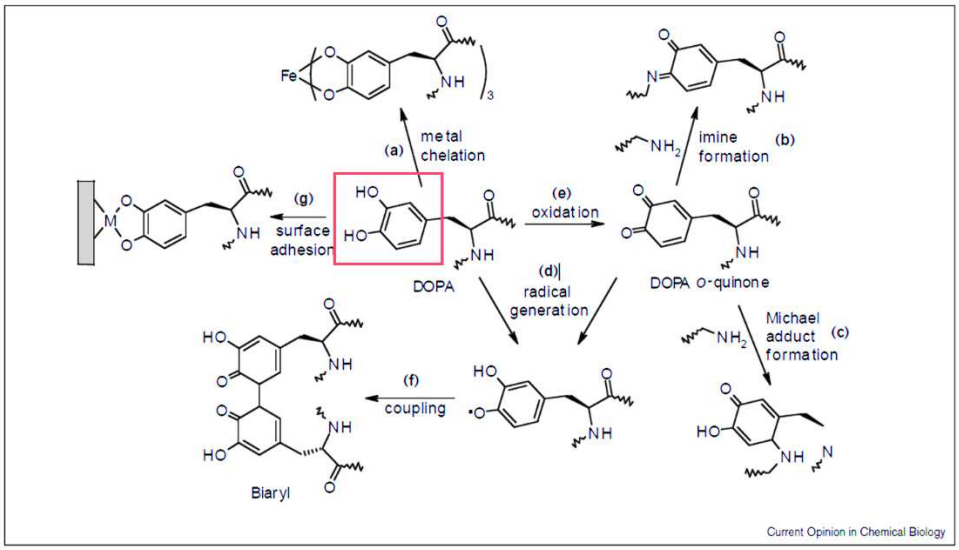

Figure 1.4: *Chemical pathways of different interactions that catechol moieties (red square) are capable of forming.*[6]

Because of the numerous possible interactions of catechols with various atoms and chemical functions, and the diversity of the adhesive proteins contained in the byssus, the mechanism of mussel adhesion has not been fully understood. Yet, important advances were made during the

past decades notably with the pioneering works of Herbert Waite. Different methods such as gel electrophoresis,[7] high-performance liquid chromatography[8-9] and MALDI-TOF,[9-10] were used to determine the chemical structure of the adhesive proteins and the chemical composition of the interface attachment plaque/surface:

It has been highlighted that catechol moieties in marine adhesive proteins can be oxidized whether by auto-oxidation or by a catechol oxidase enzyme which converts catechol into ortho-quinones.[6] Converted quinones contribute to adhesion in two ways. They enhance the insolubility of the plaque mainly by reacting covalently with amine functions from lysine residues or with catechol moieties (through radical reaction) of other marine proteins (Figure 1.5).[2, 10-11] Quinones also enhance adhesion of the plaque on organic surfaces mainly by Michael addition on nucleophilic groups of the surfaces.[4]

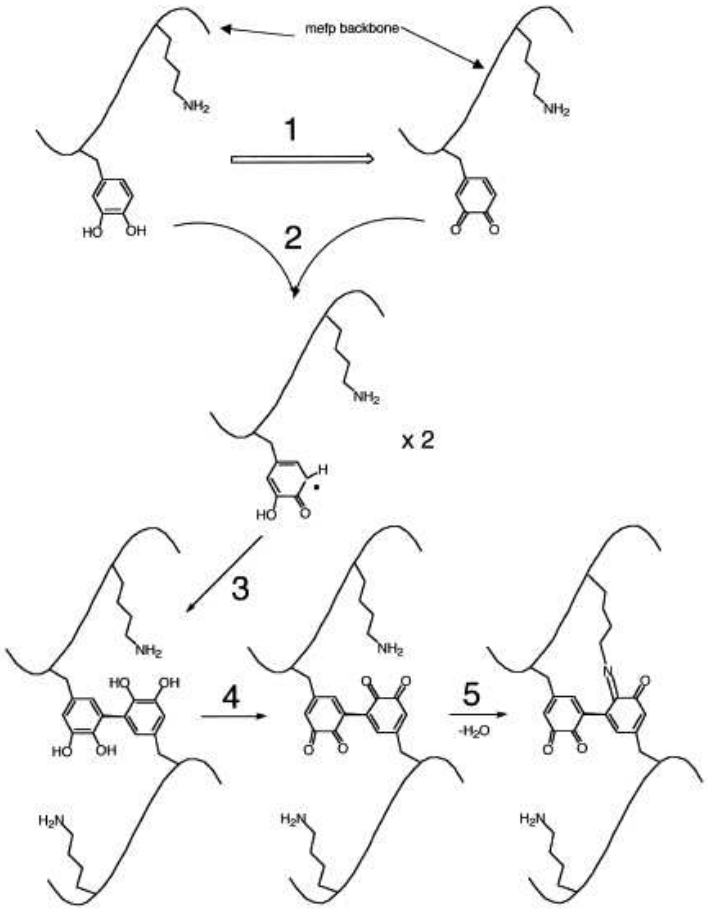

Figure 1.5: *Proposed pathway of Dopa-based cross-linking in plaque proteins. 1) Dopa is converted to Dopa-orthoquinone by catalysis or auto-oxidation. 2) Dopa-quinone reacts with Dopa by a reverse dismutation process to form semiquinone free radicals. 3) Free radicals couple through a ring-ring C-C bond. 4) Di-Dopa is reoxidized once or twice to a diquinone. 5) Schiff-base addition of Dopa-quinone on amine function of lysine.*[10]

The ability of catechols to complex metals also highly contributes to the capacity of catechol bearing molecules to adhere to a surface in a reversible way. Mussel are known to capture high concentrations of metal ions, such as Fe(III) or Ca(II), from seawater[12]. Firstly, ions complexation by Dopa-catechol allows adhesion of the mussel on a surface containing metallic atoms.[4] Secondly, complexation of metallic ions by Dopa or oxidation of Dopa-catechol into Dopa-quinone by the ions induces reinforcement of the matrix byssus whether it is in the plaque,[13] or in the thread.[14]

The interaction Dopa-surface will be different depending on the nature of the surface. For example on TiO_2 surfaces, Dopa interacts with the surface through Ti atom complexation while on mica surfaces the interaction is made through H-bonding.[15] This adhesion can be defined as a "chemical adhesion" because it is due to covalent bonds or coordination bonding. It can be opposed to a "physical adhesion" where adhesion is based on a nanostructuration of the surface which adheres, and weak interactions.

It should be noted that catechols are also involved in other natural phenomena such as neurotransmission with dopamine and others catecholamines.[16]

1.1.1.2 Polyphenols in plants

Polyphenols are a wide class of biomolecules which are present in huge amounts in plants. Nowadays plant polyphenols are known because of their beneficial effect on human health[17-19] and of their presence in fruits, vegetables and in derived beverages or food (wine, chocolate…). It can be explained roughly by their strong antioxidant property and are thus, widely used in the industry. A simple definition would be to include all molecules with several phenolic functions, yet in 1962 E.C Bate Smith, Tony Swain and Edwin Haslam gave a clear definition of the term "polyphenols" as *water-soluble plant phenolic compounds having molecular masses ranging from 500 to 3000-4000 Da and possessing 12 to 16 phenolic hydroxyl groups on five to seven aromatic rings per 1000 Da or relative molecular mass*.[20] More recently, the definition has been enlarged to other plant phenols. According to Haslam, polyphenols can be divided into three classes depending on the reactions from which they derive[21] (Figure 1.6): the proanthocyanidins also called condensed tannins (1), the gallo- and ellagitannins also called hydrolyzable tannins (2), and the phlorotannins (3).

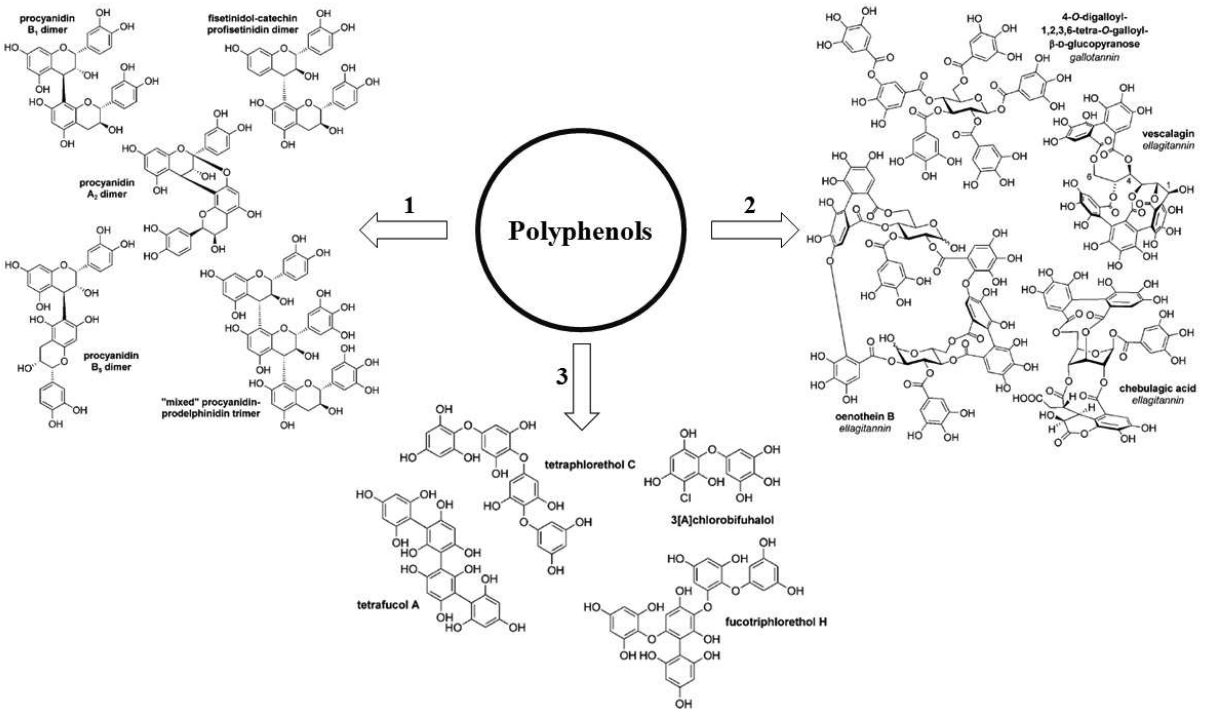

Figure 1.6: *Representative examples of (1) condensed tannins, (2) hydrolyzable tannins and (3) phlorotannins.*[21]

Polyphenols are secondary plant metabolites, which means that they don't contribute directly to the living of the organism's cells but they ensure important ecological functions at different levels. They are involved in the coloration of the leaves and fruits through their phenolic moieties. For example, the color of some blue flowers is attributed to delphinidin.[22] Delphinidin glycosides have a spectral maximum of 535 nm. They thus require a copigment to shift the spectrum to blue (580 nm). The interaction between delphinidin and its copigment is based on hydrogen bonding. More recently, Kondo *et al* highlighted the fact that blue coloration of flowers is mainly attributed to the formation of anthocyanins/metals complexes through phenol/metal complexation.[23] Anthocyanins are a class of polyphenols and more specifically a class of flavonoids. As other polyphenols, they are able to coordinate metals such as magnesium, iron or aluminum. Figure 1.7 represents the anthocyanin called commelinin responsible for the color of a plant called *Commelina communis*.

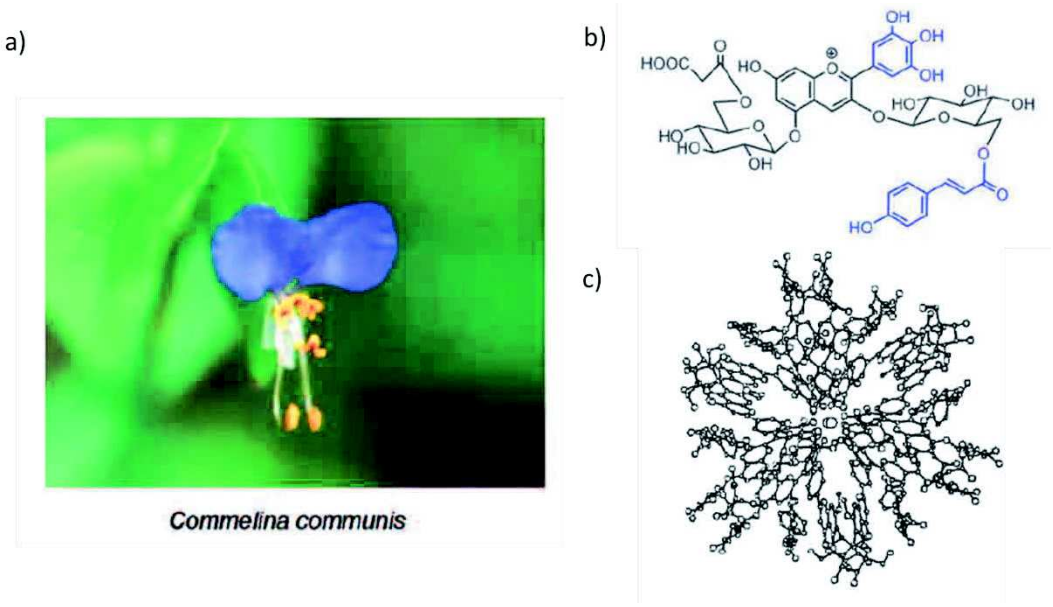

Figure 1.7: a) *Picture of the Commelina communis. b) Chemical structure of the commelinin. c) X-ray crystallographic structure of the commelinin complex with* Mg^{2+}*.*[23]

Polyphenols have also a role of protection against ultraviolet radiation of the sun. UV radiation is divided into three bands, with different energies and different ecological impacts. UV-B (280-315 nm) is the band of highest energy. It can penetrate through the ozone layer and causes damage to plant life. Polyphenols and more specifically flavonoids shield plant from UV-B because, they generally absorb in the 280-315 nm region and are capable of radical scavenging.[22, 24] Polyphenols ensure other functions in the plant metabolism such as enhancing nutrients intake[25-26], ensuring protection against microbial attacks and insects[22, 27], and interaction with other organisms.

1.1.2 Bio-inspired phenolic based materials

Phenomena associated with mussel adhesion and with the presence of polyphenols are based on phenol properties of catechol and gallol moieties leading to an increasing interest of the scientific community on these functions.

1.1.2.1 Mussel-inspired catecholic functional 3D materials

Inspired by the exceptional ability of mussels to adhere on any kind of surface in water and by the catechol based biochemistry behind this adhesion, a huge community of researchers designed different functional materials.

Adhesives are an integral part of our lives but are still limited by one main factor: working in water or in moist air.[28] In order to overcome this limitation, understanding how a simple

mollusk can overpass this drawback is a real challenge. Mussel-inspired gels were mainly developed for adhesive applications. In order to create adhesives with properties similar to the mussel "glue", the first studies were devoted to find synthesis pathways to create polypeptide mimics, pionnered by Hiroyuki Yamamoto.[29-30] In 1998, Deming et al reported the synthesis of water soluble copolymers of Dopa and L-Lysine, amino-acids present in marine adhesive proteins, with a controlled composition and molecular weight.[31] These copolymers were able to form cross-linked gels which displayed moisture-resistant properties upon oxidation with air (oxygen), $NaIO_4$, H_2O_2 and mushroom tyrosinase. Payne and co-workers improved the mechanical properties of chitosan hydrogels by enzymatically oxidizing catechols functionalized chitosan.[32] More precisely, tyrosinase was added to a dopamine-modified chitosan hydrogel to oxidize catechols moieties of dopamine leading to their reaction with amine groups of chitosan (process of tanning) increasing the viscosity and the mechanical properties of the hydrogel.

Messersmith's group greatly contributed to this field during the past twenty years. Many strategies were elaborated to create gels with high Dopa content to enhance their adhesive properties. For example, adhesive copolymers with Dopa amino acids which are able to photopolymerize under UV irradiation in less than one minute were synthesized. Once exposed to UV irradiation, these copolymers form quickly a gel with high Dopa content and thus which exhibits good adhesion properties on titanium.[33] More recently, new mimic hydrogels were designed by photopolymerization of dopamine methacrylamide, 2-methoxyethyl acrylate and ethylene glycol dimethacrylate monomers.[34] Ethylene glycol dimethacrylate was used as a cross-linker to create gels with catechol moieties, presenting good mechanical and adhesion properties.

In order to obtain new materials with magnified adhesion properties, combined mussel and gecko inspired surfaces were developed.[35] These hybrid surfaces were obtained in two steps: electron-beam lithography was used to create gecko-foot-mimetic nanopillar arrays and a marine adhesive protein mimic was deposited on the nanostructured polydimethylsiloxane (PDMS) (Figure 1.8). A hybrid nanoadhesive surface was obtained with combined chemical (mussel) and physical (gecko) adhesion.

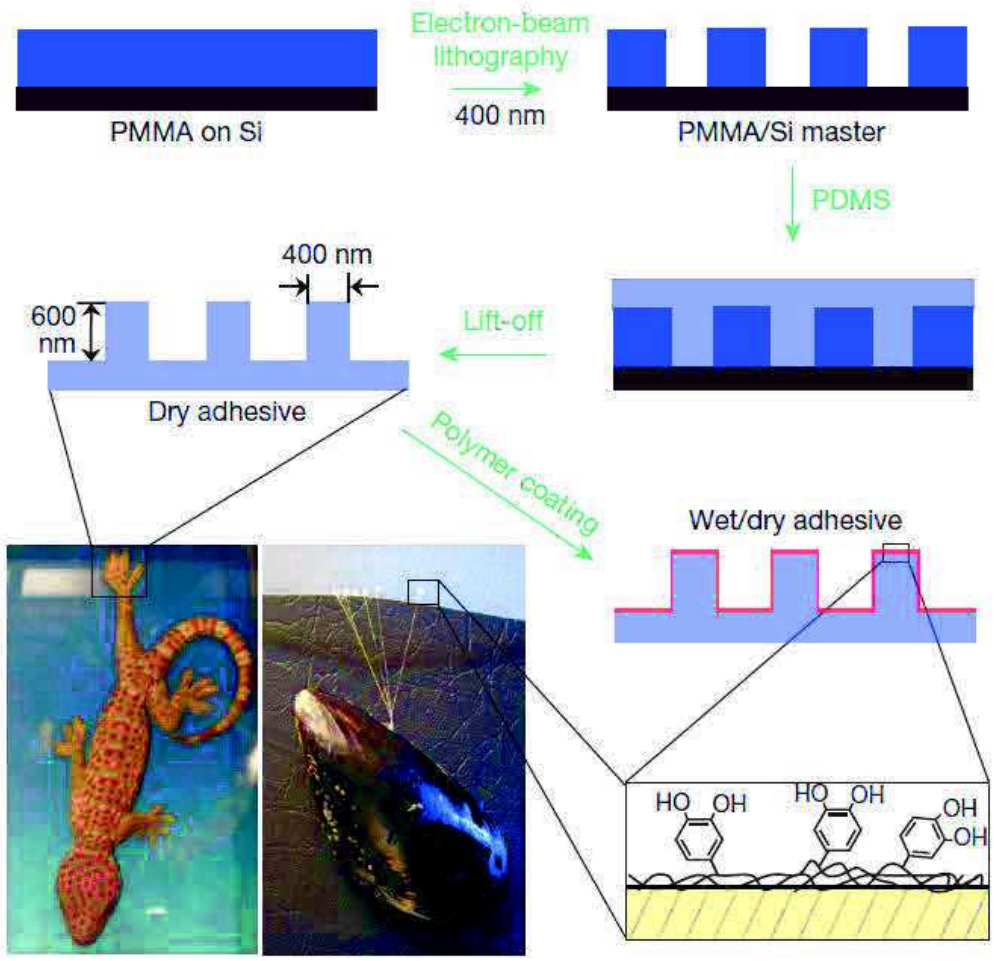

Figure 1.8: *Schematic representation of the fabrication of a hybrid wet/dry nanoadhesive.*[35]

In 2007, on the contrary to the previous examples, Wilker and co-workers designed a new polymer (copolymer from styrene and 3,4-dihydroxystyrene monomers) based on catechol functions.[36] In order to obtain gels with relevant mechanical and adhesion properties, oxidizing agents such as Fe(III), $NaIO_4$ and $Cr_2O_7^{2-}$ have to be used to crosslink those polymers. An extend of this study was to add a third ammonium-containing monomer in order to make the copolymer cationic.[37] Doing so, electrostatic adhesion was added to the catechol adhesion with enhancement of underwater bonding. The same authors have optimized the 3,4-dihydroxystyrene/styrene ratio of the copolymer in order to get the best adhesion properties on various type of surfaces.[38]

Injectable composite hydrogels were designed by mixing catechol-grafted hyaluronic acid (HA-DN on Figure 1.9a) with thiol-modified pluronic (Plu-SH on Figure 1.9a).[39] Indeed as mentioned above, quinones (oxidized catechol moieties) are known to react with various functional groups such as thiol (Figure 1.9b). These gels have the property to be slightly cross-

linked at room temperature keeping an almost liquid state and making them injectable (Figure 1.9a). When brought to the human body temperature (37°C), the cross-linking is enhanced and the mixture goes through a sol-gel transition, leading to gel formation in the organism. In this case, no oxidizing agents are needed to trigger the gelation.

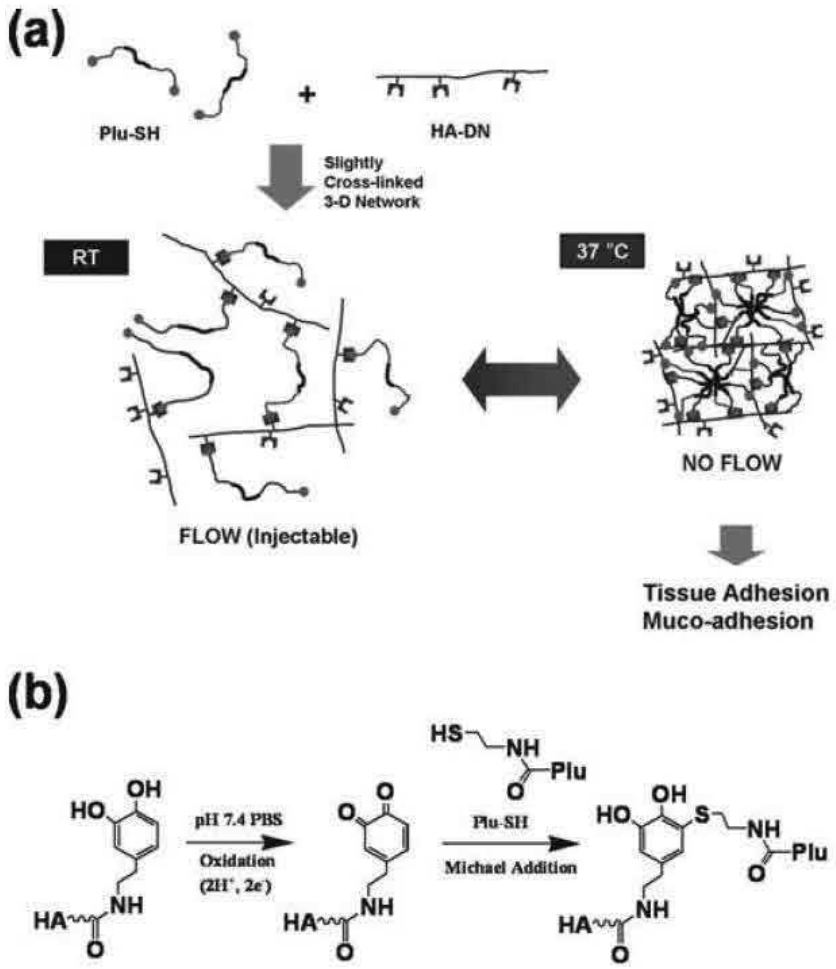

Figure 1.9: *Schematic representation of HA/Pluronic hydrogels. a) Slightly cross-linked 3-D network formation of HA/Pluronic hydrogels and their sol-gel transition behavior. b) The mechanism of Michael-type addition between a quinone on HA and a thiol group on Pluronic.*[39]

A very similar strategy was developed by the same authors with a catechol-grafted chitosan instead of hyaluronic acid for the same application.[40] Mussel mimetic gels based on catechol-modified PEG were also used for biomedical applications such as islet transplantation in the context of diabetes diseases.[41]

A novel approach was designed lately based on the pH-triggered cross-linking of a Dopa-modified PEG by Fe(III) ions (Figure 1.10a).[42] Indeed, Fe(III)/catechol complexes are pH dependent (Figure 1.10b). At low pH values, mono-complexes (catechol/iron ratio 1:1) are formed. Going through more basic pHs, bis-complexes (ratio 2:1) and then tris-complexes (ratio

3:1) are observed. These complexes are notably characterized by green, blue and red colors respectively. In order to avoid the precipitation of iron hydroxide at basic pH, the mixture of the Dopa-modified PEG and Fe(III) was prepared at pH 5. The resulting mixture is a dark green solution (Figure 1.10c). A drop of this solution was deposited on a surface near a drop of alkaline solution. By mixing both droplets, the viscosity of the mixture drastically increased leading to first a dark blue/purple viscous liquid (bis-complexes) and then a dark red gel (tris-complexes). Based on the same principle, gels were assembled with titanium instead of iron ions.

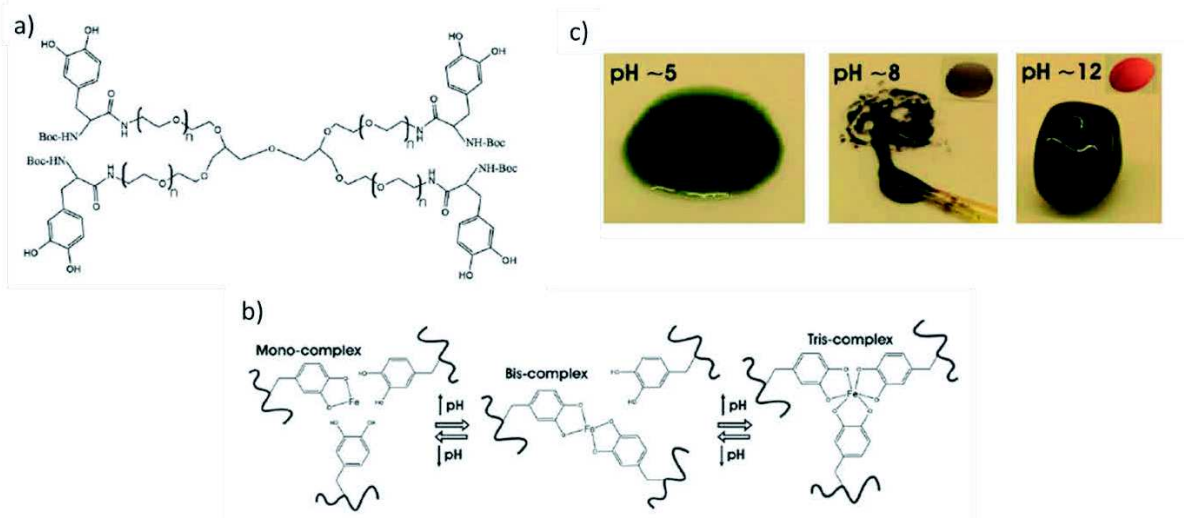

Figure 1.10: *a) Chemical structure of the Dopa-modified polyethylene glycol. b) The pH-dependent stoichiometry of Fe(III)-catechol complexes. c) Physical state and color of Dopa-PEG gels in mono- (green), bis- (purple), and tris-complexes (red).* [42]

pH responsive PEG gels were also formed through boronate-catechol complexation.[43] Catechol can form complexes with boron atoms at basic pH. Thus, by mixing branched catechol-modified PEGs with 1,3-benzenediboronic acid, gels can be obtained at pH =9. If the pH is brought at 3, these gels go back to a liquid state. These gels present self-healing properties. PEGs were also modified with nitrodopamine.[44] The originality of this work is that the o-nitrophenyl ethyl moieties are photocleavable (Figure 1.11a). Thus, these nitrodopamine-modified PEGs can form photo-destructible gels by adding Fe(III) ions or oxidizing agents to the mixture (Figure 1.11b). Patterned gels were formed by using an UV light combined with a template of the desired pattern.

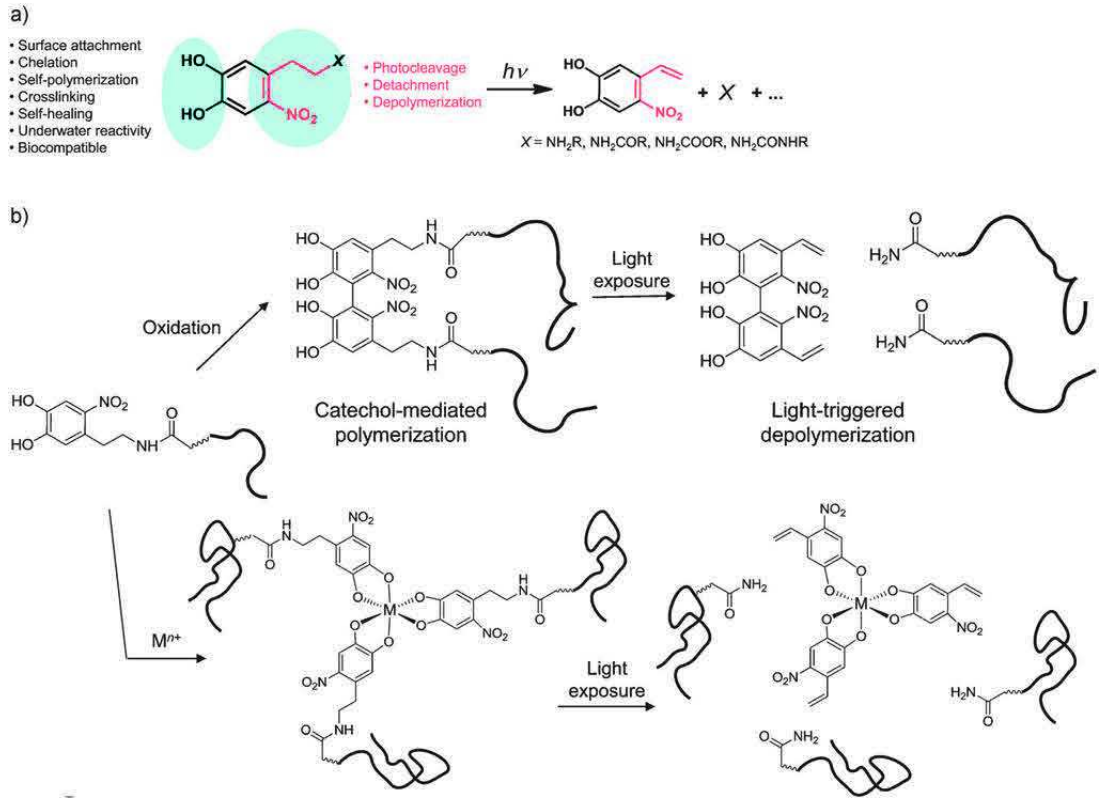

Figure 1.11: *Structure of nitrodopamine derivatives and their photocleavage mechanisms. a) Photolytic reaction of the o-nitrophenyl ethyl moiety. b) Different strategies used to trigger bonding (through oxidation of the catechol unit to quinone and further reaction, or through formation of metal complexes) and debonding upon exposure of nitrodopamine derivatives to light. Catechol reactions may lead to other polymerization products, but the photoreaction cleaves the linked chains in every case.*[44]

1.1.2.2 Mussel-inspired catecholic functional surfaces

Polydopamine and its properties

In 2007, Messersmith and co-workers introduced a mussel-inspired coating based on the polymerization of dopamine.[45-46] Obtained by dip coating of a substrate in an alkaline solution of dopamine, dopamine polymerization into polydopamine occurs at the surface of the object and in solution according to the mechanism described in Figure 1.12a. The coating deposited reached a maximum thickness of 50 nm after 24h (Figure 1.12c). This technique can be applied on any type of surfaces (metal, ceramic, polymers) even with complex geometries. The resulted coatings present free catechol/quinone groups that can be used for electroless metallization through catechol/metal complexes formation and for functionalization with organic species through quinone reaction with thiol or amine functions. Some examples will be given page 22.

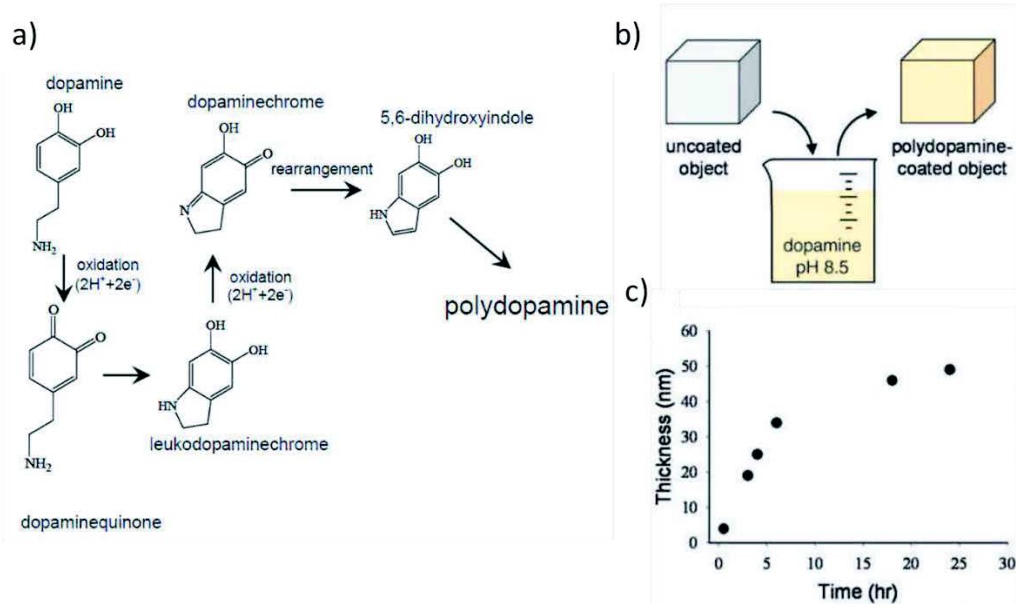

Figure 1.12: *a) Proposed structural evolution and polymerization mechanisms of dopamine. Under an oxidative condition, e.g. alkaline pH, dihydroxyl group protons in dopamine are deprotonated becoming dopamine-quinone, which subsequently rearranges via intramolecular cyclization to leukodopaminechrome. Further oxidation and rearrangement leads to 5,6-dihydroxyindole, whose further oxidation causes inter-molecular cross-linking to yield polydopamine. b) A schematic illustration of thin film deposition of polydopamine by dip-coating an object in an alkaline dopamine solution. c) Thickness evolution of polydopamine coating on Si measured by AFM.*[45]

Recently, polydopamine was used as an ink through microcontact printing to create patterned coatings of polydopamine.[47] A PDMS substrate with the desired pattern was dipped into a solution of dopamine which polymerizes according to the mechanism introduced before (Figure 1.13). Then, the polydopamine-modified PDMS substrate was removed from the solution and printed on a surface. The resulted patterned polydopamine coating can then be used for spatially controlled cell adhesion, protein adsorption and metal deposition.[47]

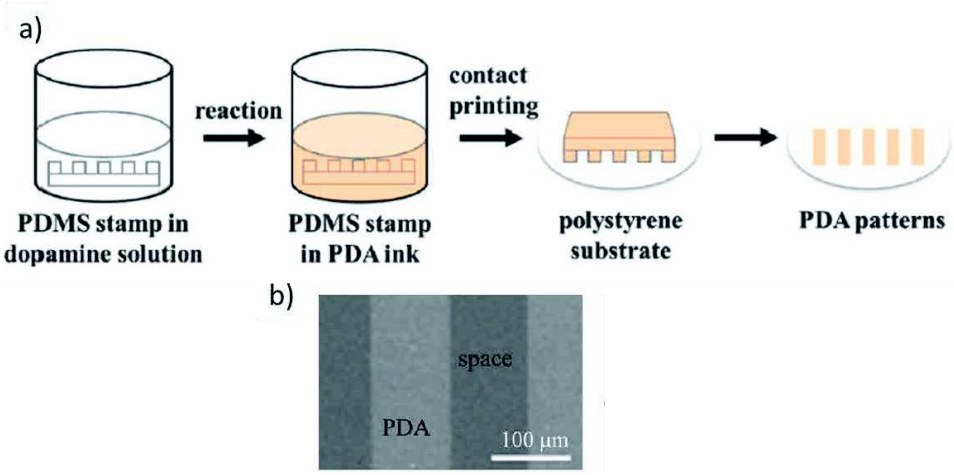

Figure 1.13: *a) Schematic illustration of microcontact printing of polydopamine (PDA) patterns. b) SEM image of imprinted PDA patterns on silicon substrates.*[47]

Polydopamine coatings are hydrophilic and this property was used to deposit by spray silver nanowires on stretchable polydopamine-modified elastomeric substrate.[48] The hydrophilic character of polydopamine allows to transform superhydrophobic surfaces into hydrophilic ones.[49] Moreover by using soft lithography combined with microfluidic apparatus, patterned superhydrophobic surfaces can be designed. To do so a patterned PDMS mold was applied on a superhydrophobic surface (Figure 1.14a). The empty spaces between surface and the PDMS were filled with a dopamine solution which then was polymerized into polydopamine. When the PDMS was removed, only the polydopamine pattern remained on the surface. These coatings allowed to spatially localize droplets onto the surface which kept their position even when the surface was tilted (Figure 1.14c and d).

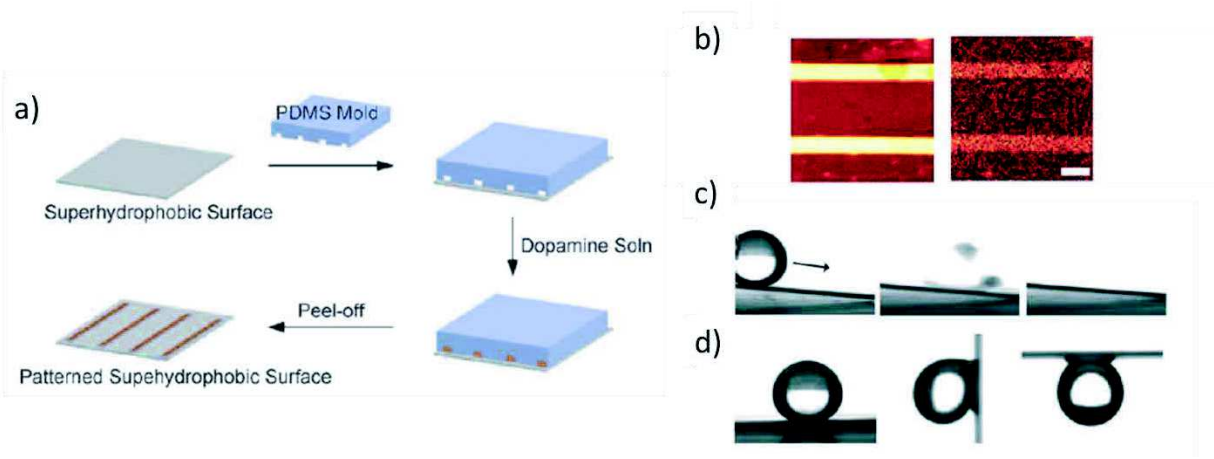

Figure 1.14: *Micropatterning of superhydrophobic surfaces and wetting properties. a) Schematic description for preparing polydopamine-patterned superhydrophobic surfaces. b) ToF-SIMS images of the polydopamine-patterned superhydrophobic surface: CN^- (left) and $C_8H_5N_2O^-$ (right). Scale bar is 100 µm. c,d) Rolling vs. stationary water droplets: c) the water droplet on the unmodified superhydrophobic rapidly rolled down when the surface is tilted (4°). d) The water droplet on the polydopamine-micropatterned superhydrophobic surface remained attached even when the surface is tilted at 90° and 180°.*[49]

Li-ion batteries mainly use polyethylene as separator but polyethylene still lacks compatibility with conventional liquid electrolytes due to its hydrophobic character. Therefore, polyethylene separators were coated with polydopamine making the modified surface hydrophilic.[50] Moreover, polydopamine improved the electrolyte uptake and the ionic conductivity allowing enhanced battery performance compared to batteries with uncoated separators. Furthermore, polydopamine films have an amphiphilic character: it can be negatively charged by deprotonation of catecholic hydroxyl groups or positively charged by protonation of indolic nitrogen atoms. This aspect was used for the creation of electrodes with pH tunable ion permeability.[51] Au-coated Si wafers functionalized with polydopamine occurs to selectively

block cations at pH<3 and anions at pH>11. Recently, Lu and coworkers used polydopamine-modified clay in order to incorporate it in an epoxy resin.[52] The polydopamine coating allows first to promote dispersion of clay into the epoxy matrix through hydrogen bonding between catechol and epoxy, but also to boost its thermomechanical properties (viscosity, storage modulus). Dopamine was also used as reducing agent for graphene oxide reduction.[53] Dopamine not only reduces graphene oxide but also polymerizes on the surface of graphene oxide sheets allowing for further functionalization. This process was also achieved with norepinephrine.[54]

Polydopamine can also be used to promote cell adhesion in surface-mediated drug delivery systems.[55] Surfaces coated by poly(L-lysine) and liposomes were coated with polydopamine (Figure 1.15). Polydopamine promotes cell adhesion and viability and depending on the thickness of the polydopamine layer, allows to control the drug release from lyposome.

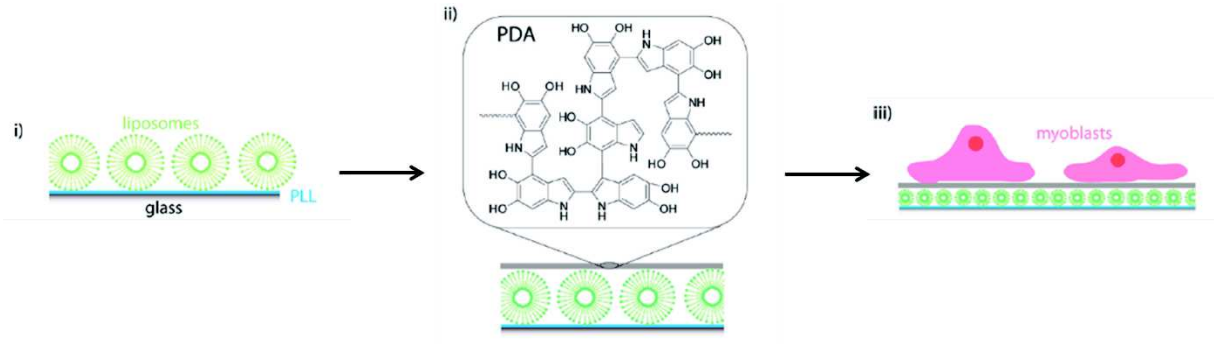

Figure 1.15: *Schematic illustration of adsorption of liposomes, on PLL precoated glass slides (i) followed by the deposition of a polydopamine PDA layer (ii) and the adhesion of myoblast cells on these surfaces (iii).*[55]

As mentioned previously, polydopamine coatings are extremely versatile platforms for secondary functionalization in order to confer diverse functions to a surface. As quinone moieties are reactive towards nucleophiles, biomolecules such as trypsin or growth factors (vascular endothelial growth factor (VEGF) and bone morphogenetic protein (BMP)) can be easily immobilized on polydopamine-coated surfaces.[56-58] This was achieved for trypsin on various types of surfaces.[56] VEGF functionalized surfaces allowed to enhance human dermal microvascular endothelial cells adhesion and viability making them suitable for bone healing and regeneration applications.[57] BMP functionalized TiO_2 nanotubes *via* polydopamine promoted cell growth, differentiation and mineralization with potential application for coated titanium implants with bone regeneration properties.[58] Neural interfaces are devices allowing to monitor a neural signal and transform it into an electric signal that can be read by a computer. Microelectrode arrays of different types (gold, platinum, ITO…) were coated with

polydopamine to functionalize them first with poly-D-lysine and then with neural cells.[59] These neuron-adhesive modified-electrodes, allowed to record neural activity from the neuronal network making them suitable for neural interfaces applications.

In biomedicine, an Au/polypyrrole actuator was covered with polydopamine to enhance bacterial adhesion and accumulation from physiological media.[60] Polydopamine was also used as the basis for triazine-based polymers cross-linked through thioether linkages in order to create a fiber-reinforced adhesive patch for fixation of bones fractures.[61]

As polydopamine appears to be biocompatible, it was used to encapsule yeast cells in order to protect them.[62] In this case, the surface of the cell wall has the role of initiator of polydopamine coating by covalent bonding between polydopamine and amine or thiol functions of proteins present in the cell wall. The entrapped cells maintain their biological activity while being protected. Moreover by using the ability of polydopamine to be functionalized with organic molecules, coated cells were modified with streptavidin for specific immobilization on biotin-modified surfaces. Polydopamine was also used to coat magnetite nanoparticles in the presence of a protein.[63] By removing the protein with an acetic acid rinsing, a coating with the protein print was created making these particles suitable for protein recognition. Recently, Woisel and coworkers used polydopamine as a platform for cyclodextrin-modified polymer immobilization to create drug-release coatings on CoCr vascular stents[64] and TiO_2 implants.[65] Polydopamine occurs also to be a good reducer for silver ions. For example, fibrous structured bacterial cellulose was coated with polydopamine in order to incorporate silver nanoparticles to form an antimicrobial network.[66] Silver nanoparticles were also immobilized on cotton fabrics through polydopamine cotton functionalization to create antibacterial textiles.[67]

The “dopamine concept” can be applied with other derivatives of dopamine as norepinephrine[68] or catechol/amine synthetic polymers such as a copolymer from N-(3,4-dihyroxyphenethyl) methacrylamide and aminoethylmethacrylamide monomers which was used as a DNA immobilization platform for DNA hybridization.[69]

Mussel-inspired layer-by-layer assemblies

Marine adhesive mimic polymers were also used in Layer-by-Layer (LbL) assemblies. Introduced by Decher, the LbL process consists in the exposure of a substrate alternatively to a polycation and polyanion solution with rinsing steps between each deposition step.[70] The buildup process relies on the charge overcompensation observed at each deposition step. A marine adhesive mimic polymer was used in a LbL process in order to create hybrid composite

films with nacre structuration.[71] These films were based on an alternate deposition of inorganic nanometer-sized sheets of Montmorillonite clay and a Dopa-Lys-PEG polymer (Figure 1.16a). Fe(III) post treatment induced a cross-linking, and allowed to obtain a removable film with exceptional mechanical properties compare to the classic nacre inspired assembled coatings (Figure 1.16c). LbL assemblies were also realized with a positively charged copolymer bearing catechol moieties and colloidal synthetic layered silicate.[72] These assemblies were used for anticorrosion applications: catechols are corrosion redox inhibitors and clay gives barrier properties to the films.

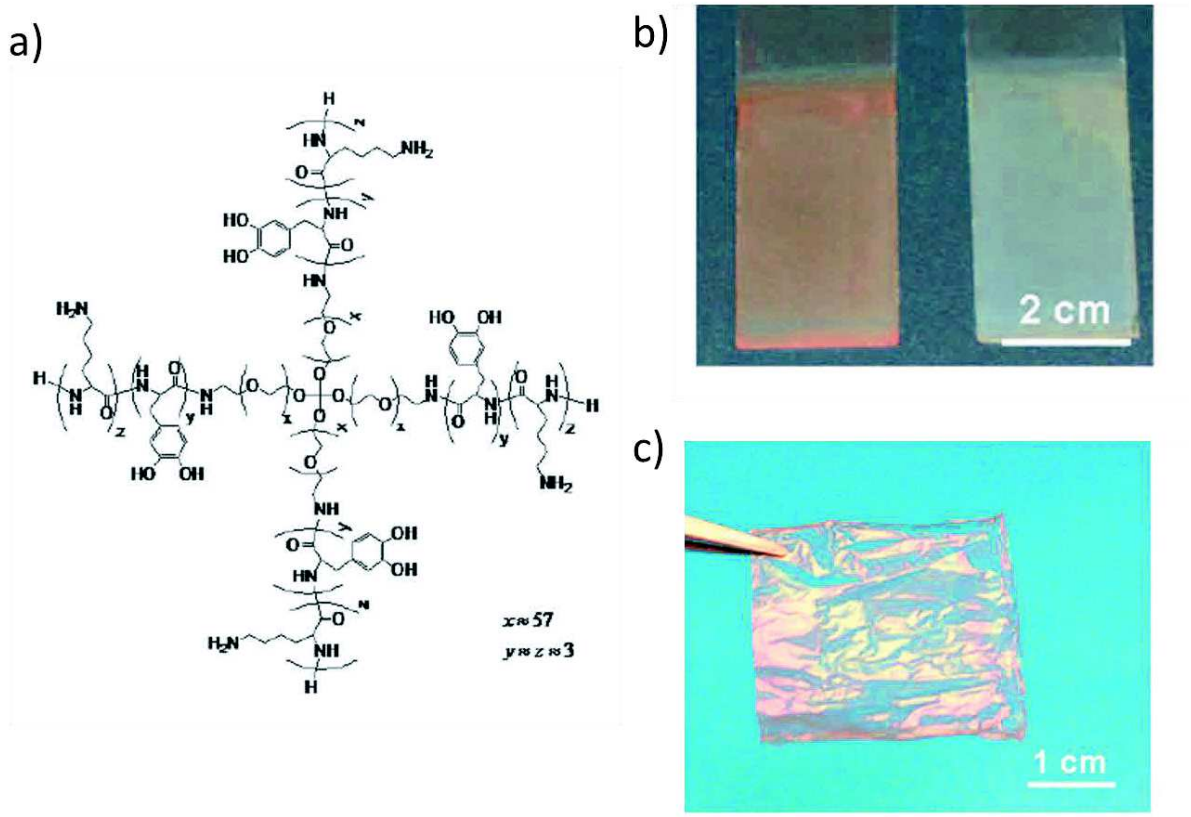

Figure 1.16: *a) Molecular structure of Dopa-PEG-Lys polymer. b) Digital photograph of 300 bilayers Dopa-PEG-Lys/Clay films on microscope glass slide with (left) and without (right) Fe(III) crosslinking. c) Digital photograph of a Fe(III) crosslinked 300 bilayers Dopa-PEG-Lys/Clay free-standing film.*[71]

Mussel-inspired LbL assemblies were also notably used for antibacterial coating design. For example, catechol grafted poly(ethyleneimine) (PEI) and hyaluronic acid (HA) LbL allowed to obtain well controlled assemblies on any kind of substrate, even polymeric ones.[73] Using the redox activity of the catechol moieties, silver nanoparticles were deposited on these coatings conferring them anti-microbial properties. Mussel-inspired LbL films containing silver nanoparticles for antimicrobial applications were also built with polystyrene sulfonate and a copolymer from N-methacrylated Dopa and cationic methacrylate monomers.[74] In 2011,

Detrembleur and coworkers used quinone-grafted poly(methacrylate) with poly(allylamine hydrochloride) (PAH) allowing cross-linking between quinones and amine functions of the PAH ensuring a long time stability to the LbL film.[75] Going further Nisin, an anti-bacterial peptide, was used instead of PAH creating a robust anti-bacterial coating.

Catechol-mediated anchoring for surfaces functionalization

As catechol moieties are known to interact with different type of surfaces, they were widely used as anchors for surface modification both for macroscopic planar surfaces, or for nanoscale surfaces of particles. In 2005, Messesmith and coworkers introduced a surface-initiated atom transfer radical polymerization (SI-ATRP) by using a biomimetic initiator.[76] Starting from dopamine (**1** in Figure 1.17), they designed a bifunctional molecule (**2** in Figure 1.17) with a catechol on one side (mussel mimetism) for anchoring on the surface and an alkyl bromine to initiate ATRP (**3** to 4 on Figure 1.17). The obtained surfaces were anti-fouling towards cell adhesion. By using a Ti substrate coated with pattern photoresist through standard photomask lithography, the biomimetic initiator was selectively anchored on the bare Ti area allowing to spatially control the SI-ATRP. More recently, PEG dendrimers with a catecholic anchor were immobilized on TiO_2 surfaces.[77] The obtained films were less hydrated that the ones build from linear PEGs and showing good non-fouling properties for proteins.

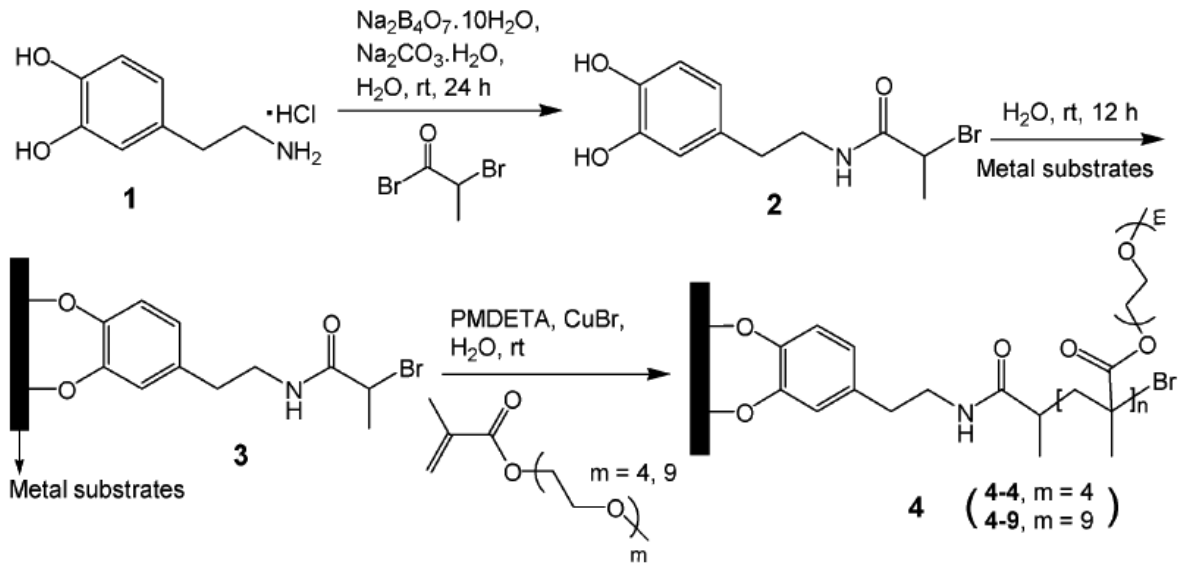

Figure 1.17: *Synthesis and anchoring of the biomimetic initiator and subsequent SI-ATRP.*[76]

Other bio-inspired antifouling surfaces were designed. An antifouling peptidomimetic polymer was synthesized to be immobilized on metallic surfaces.[78] It was composed of two parts: a short functional peptide domain made of alternate Dopa and Lysine residues which allows anchoring of the polymer on a metallic surface and an N-substituted glycine oligomer of different size,

resistant to protein and cell adhesion. Saxer et al. designed a copolymer poly(L-lysine) grafted with 3,4-dihydroxypehenylacetic acid (DHPAA) and PEGs that was assembled in monolayer on TiO_2 surfaces.[79] Immobilization operates *via* the catechol moiety of DHPAA (strong binding) and lysine residues (long range electrostatic interactions) while bacterial and cellular adhesion were prevented by PEG chains. Dopamine modified surfaces *via* catechol anchoring were used to further immobilize the tripeptide Arg-Gly-Asp (RGD) and collagen on a surface.[80] These functional surfaces were used to study the effect of the type of adhesive ligand (RGD or collagen) on the bacterial and fibroblast adhesion in order to create a selective antifouling surface that inhibits bacterial activity while promoting cell adhesion.

Catechol-driven anchoring was used to design antimicrobial coatings. For example, a hybrid molecule was developed by Gademann and coworkers with an anachelin chromophore linked to vancomycin through a PEG linker.[81] The anachelin chromophore presents a catechol moiety to immobilize the molecule on a surface and vancomycin is an antibiotic giving the desired antimicrobial property against *Bacillus subtilis*. Antimicrobial functional surfaces were also created by dip-coating of a surface in a solution of a copolymer synthesized by free-radical polymerization from dodecyl quaternary ammonium, catechol and methoxyethyl containing monomers.[82]

Catechol-driven anchoring allows to functionalize not only macroscopic planar surfaces but also nano-scaled surfaces. Its ability to coordinate metals make it a suitable candidate for metallic nanoparticle functionalization. Magnetite nanoparticles (Fe_3O_4) were functionalized with different catechol-modified PEG to improve their biocompatibility,[83-84] catechol–modified porphyrin for cancer therapy,[85] catechol-conjugated bisphosphonate for uranyl ions removal treatment in blood,[86] catechol-anchoring mediated luminescent terbium complexes for imaging applications,[87] and dopamine-grafted biotin for the formation of heterodimers of magnetite and silver nanoparticles.[88] PEG functionalized magnetite nanoparticles were used as reducers of non-specific uptake by cell macrophages.[89] Catechol-stabilized iron oxide nanoparticles were used as MRI contrast and anticancer agents.[90] HA modified with dopamine was immobilized on magnetite nanoparticles.[91] HA is known to interact with specific receptors giving a targeting functionality to the coated particles. Dopamine-modified magnetite nanoparticles were used to create magnetic and transparent composites by covalently grafting it (through amine functions of dopamine) in a polymethylhydrosiloxane network modified with crystal liquids.[92] Dumbbell nanoparticles are two nanoparticles of different chemical nature that are linked to each other. Magnetite-gold dumbbell nanoparticles were functionalized with an antibody through catechol

anchoring for magnetite and with PEG through thiol anchoring for gold.[93] Through the antibody functionality, these particles acted both as magnetic and optical probes. Recently, Sun and coworkers coupled a rhodamine derivative, N(rhodamine-6G)lactam-ethylenediamine (Rh6G-LEDA, **1a** on Figure 1.18) to PEG-dopamine modified magnetite nanoparticles (**1b** on Figure 1.18).[94] Rh6G-LEDA were bound to metal ions such as Fe(III) (**1c** on Figure 1.18) which enhanced greatly its fluorescence. Thus, these particles were used for Fe(III) sensing applications.

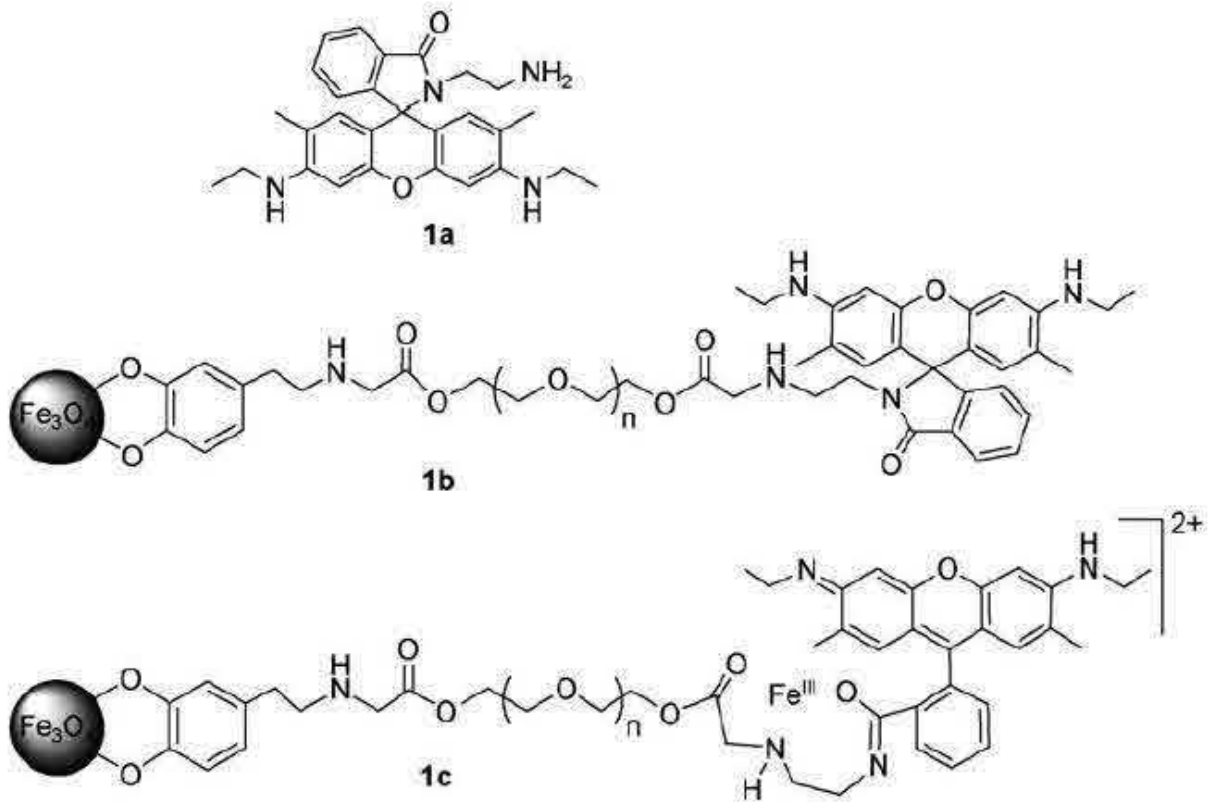

Figure 1.18: *Structural illustration of Rh6G-LEDA (**1a**), its coupling with PEG-Fe_3O_4 NP (**1b**), and its complex with Fe(III) (**1c**) along with the structural change that enhances its fluorescence property.*[94]

TiO_2 nanoparticles were functionalized with dopamine in a first step and then biotin in a second step by covalent reaction of the valeric acid chain of biotin with the amine function of dopamine.[95] These modified TiO_2 nanoparticles were deposited on an ITO electrode to further immobilize avidin on the coated electrode. TiO_2-entrapped *Chlorella* cells were also functionalized through catechol chemistry.[96] TiO_2 nanorods were functionalized with a diblock polymer with a catechol anchor to form hairy rod mesogens (Figure 1.19) which can be aligned under application of an electric field leading to liquid crystals formation.[97]

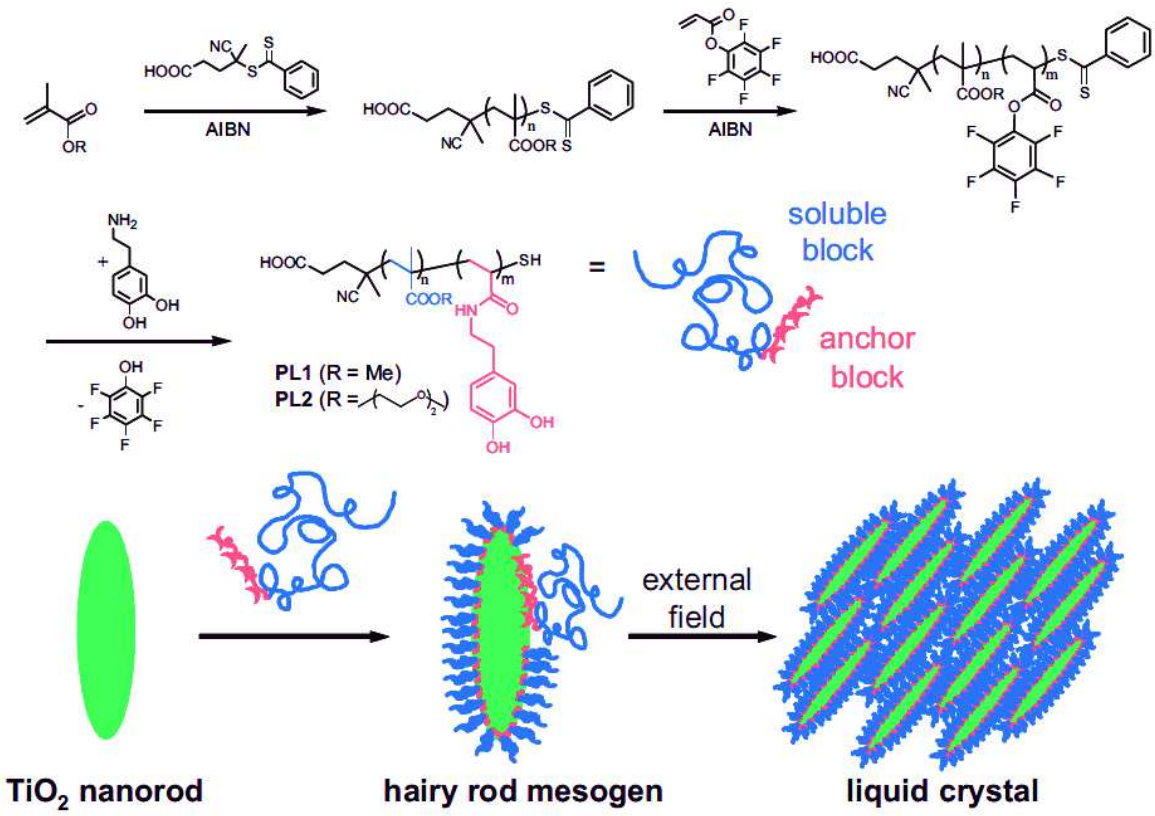

Figure 1.19: *Buildup of defined diblock copolymers with an anchor and a soluble block for the functionalization of TiO2 nanorods to form the hairy rod mesogen.*[97]

Along the same idea, ZnO nanorods were functionalized with dopamine-modified polystyrene.[98] In order to functionalized MoS_2, nanoparticles Tahir et al. synthesized a polymer grafted with nitrilotriacetic (NTA) and dopamine groups acting as two different anchor functions.[99] A Ni atom act as an "anchoring ion", it is partially coordinated by NTA on one side and by the surface S atoms of the external part of the MoS_2 nanoparticles. The modified nanoparticles, soluble in polar solvents, were immobilized through catechol groups of the ligand on surfaces to create hybrid materials with diverse functionalities. Gold nanoparticles were coated with dopamine-modified fluorescein-hyaluronic acid in order to probe reactive oxygen species formation in macrophage cells.[100] Indeed, reactive oxygen species induce cleavage of HA chains and thus a fluorescence recovery signal which can be measured. Alumina nanoparticles were also functionalized with PEGs but through gallol anchoring instead of catechol, allowing to disperse them in a solution at higher concentrations.[101] Recently, Hirsemann et al. modified kaolinite with catechol (covalent grafting) and a Ruthenium complex (ion exchange).[102] This bi-modification allows to enhance the difference in chemical nature of the two opposited basal surfaces of kaolinite expressing the Janus character of the mineral. As it was recalled before, dopamine promotes reduction of graphene oxide into graphene.

Dopamine modified with an alkyne function on the amine side was used to reduce graphene oxide into graphene and further functionalize it through click reaction between alkyne and azide functions (Cu(I) catalyzed)[103] or alkyne and thiol functions.[104] Azide-modified dopamine were used for ZnO nanoparticle functionalization with alkyne-modified poly(3-hexylthiophene),[105] magnetite nanoparticle functionalization,[106] nanodiamond particle modification with poly-N-isopropylacrylamide.[107] Magnetite nanoparticles were also modified with maleimide-grafted dopamine for functionalization through click reaction between maleimide and thiol functions.[108]

Catecholic polymers were also used as adhesive re-inforcers of carbon nanotube fibers.[109] A star-branched catechol-grafted (PEI) was infiltrated in the carbon nanotube fibers during the post spinning treatment. Then by evaporation of the solvent and curing at 120°C a final densification of the carbon nanotubes through the PEI-catechol was obtained. This process allows to produce carbon nanotubes fibers with greatly improved tensile and mechanical strength.

The mussel-inspired chemistry and the new materials described here are far from being exhaustive. Ss some recent reviews give a more complete state of the art on this topic.[110-111]

1.1.2.3 Tannic acid coatings and hydrogels

Tannic acid (TA) is a polyphenol present in abundance in nature and easily accessible. Mankind used the properties of TA and others polyphenols for a very long time. Polyphenols are called “tannins”, a word that comes from the action “to tan”, a process already used by the antique greek civilization. This process consists in the use of natural substances issued from plants in order to turn animal skins into leather (Figure 1.20).

Figure 1.20: *Traditional process of tanning*[112]

During the past decade, TA draw a great attention from the scientific community in the nanoscience field. In 2005, Lvov and coworkers were the first to used TA in LbL assemblies.[113] TA was used as negatively charged molecule in combination with two different polycations: poly(dimethyldiallylamine) and PAH in order to build nanofilms on planar surfaces. The interactions between TA and polycations are based on electrostatic interactions and hydrogen bonding. Two years later, it was shown that tea polyphenols interact with polymers *via* different types of interactions: hydrogen bonding, hydrophobic effect (Van der walls) and π-π stacking depending on the chemical structure of the polymer.[114]

TA was used to create hydrogen-bonded LbL assemblies with neutral polymers. The resulted coatings were stable at high pH in contrary to others H-bond based LbL.[115] Hammond and coworkers exploited this ability to create LbL assemblies through H-bonding to design a drug delivering surface.[116] Block copolymer micelles of poly(ethylene oxide)-*block*-poly(2-hydroxyethylemethacrylate) were conjugated with a chemotherapeutic agent: doxorubicin. These micelles were assembled with TA at pH=7.4 through H-bonding mediated LbL assembly (Figure 1.21). The carbamate linkage between doxorubicin and the polymer backbone is pH sensitive and is cleaved at acidic pHs. Thus when micelles film were brought in contact with an acidic medium, doxorubicin release was triggered. Doxorubicin was also entrapped in TA-poly(N-vinlypyrrolidone) (PVP) H-bonded multilayer capsules.[117]

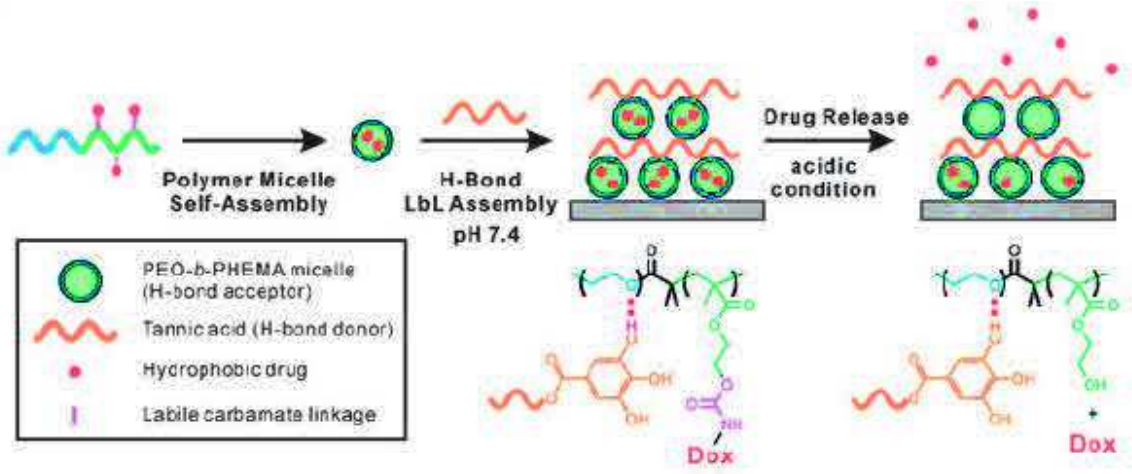

Figure 1.21: *Schematic representation of hydrogen-bonding LbL assembly of doxorubicin-containing micelles with TA.*[116]

Hammond and co-workers showed that as other H-bond based LbL assemblies, TA-containing LbL assemblies can also be dissolved electrochemically when deposited on electrodes by electrochemically producing OH^- ions.[118] Oxygen reduction at the coated-electrode leads to the formation of a hydroxyl gradient from the surface and thus a localized increase of the pH which

triggers the dissolution of the film. H-bonded TA LbL were also realized with poly(N-isopropylacrylamide) and poly(2-isopropyl-2-oxazoline).[119] TA/thrombin LbL were deposited onto porous gelatin sponges which were shown to promote hemostasis making these functional materials potential coatings to prevent hemorrhage.[120] Hydrogen-bonded TA LbL assemblies were built on silica microparticles in order to create microcapsules by removing the silica.[121] The permeability of the resulting capsules was pH responsive and thus could be tuned, making them suitable for the loading or the releasing of functional molecules. The mechanical properties of these capsules were studied in dry and liquid states.[122] They had an elastic modulus of 700 MPa in dry state and around 0.5 MPa when swollen. The value in liquid could be enhanced and tuned by adding a pre-layer of PEI to the construction and by using a PVP of greater molecular weight. PVP/TA LbL films were deposited on cell surfaces.[123] These coatings are biocompatible and the entrapped cells showed good viability. Moreover, gallol groups of tannic acid allowed surface immobilization of the cells.

In 2013, Caruso and coworkers introduced a new concept: the one-pot assembly of tannic acid/Fe(III) films and capsules.[124] As catechol moieties, gallols coordinate metals such as Fe(III) in a pH dependent manner. Thus by mixing Fe(III) and TA in solution, dipping any substrate (planar surface, microparticles) in this solution and then increasing the pH, a film of TA cross-linked by Fe(III) is assembled on the surface (Figure 1.22). As TA has an affinity with various types of materials, this process is versatile and can be applied to any kind of substrate. The concept was extended to others metallic ions such as aluminum, vanadium, chromium, cobalt…[125] and to small phenolic molecules: gallic acid, pyrogallol and pyrocatechol.[126] As mono-complexes are formed at acidic pH, these capsules can be diassembled in acidic medium. TA/Fe(III) capsules are permeable to macromolecules. Thus, it is possible to load them with drugs and then diassemble them at acidic pH for drug release applications.[127] Europium and terbium/TA capsules can be used for imaging applications.

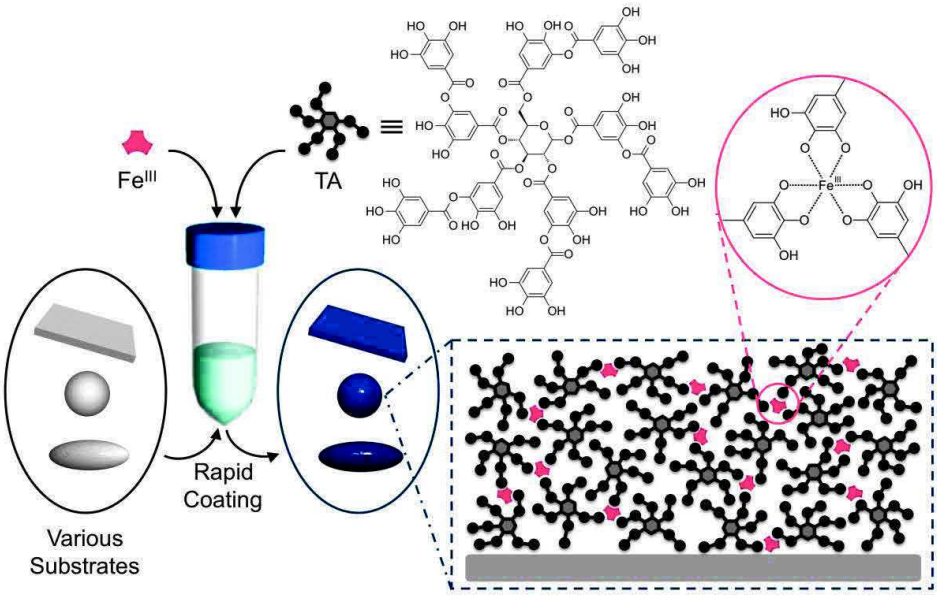

Figure 1.22: *Schematic illustration of the one-step assembly of coordination complexes on various types of substrates.*[128]

LbL were developed based on the same principle.[129] In that case, Fe(III) and TA are not mixed together in solution and the deposition occurs by dipping a substrate alternatively in TA and Fe(III) solutions resulting in a layered organized coating compared to the randomly distributed one-step coating. Recently, Jia and coworkers studied the influence of different parameters on the behavior of TA/Fe LbL films.[130] They showed that the order of addition of TA and Fe(III) greatly changes the film growth. When NaOH is added to the mixture, no significant effect on the thickness of the films was observed. However, the morphology of the films changes going from large aggregates to smaller ones, and the stability of the films was greatly improved. This effect is attributed to the formation of tris-complexes (ratio Fe/gallol: 1/3). Finally, they observed that surfaces with low wettability promote film formation due to hydrophobic effect between the surface and TA. Another study showed that when films are assembled at pH 5, the interaction between Fe(III) layers and TA layers is dominated by electrostatic interactions and not metal-ligand interactions.[131]

TA/Fe(III) were mixed with graphene oxide to improve the late one's mechanical properties.[132] Indeed, this process creates cross-links between the graphene oxide sheets, enhancing their cohesion. TA/Fe(III) films were also deposited on living cells.[133] The films present good cytocompatibility, and cytoprotection towards UV-irradiation, bacterial binding and silver nanoparticles. Moreover, the shell can be easily removed (Figure 1.23) if needed as TA/Fe(III) are easily degradable.

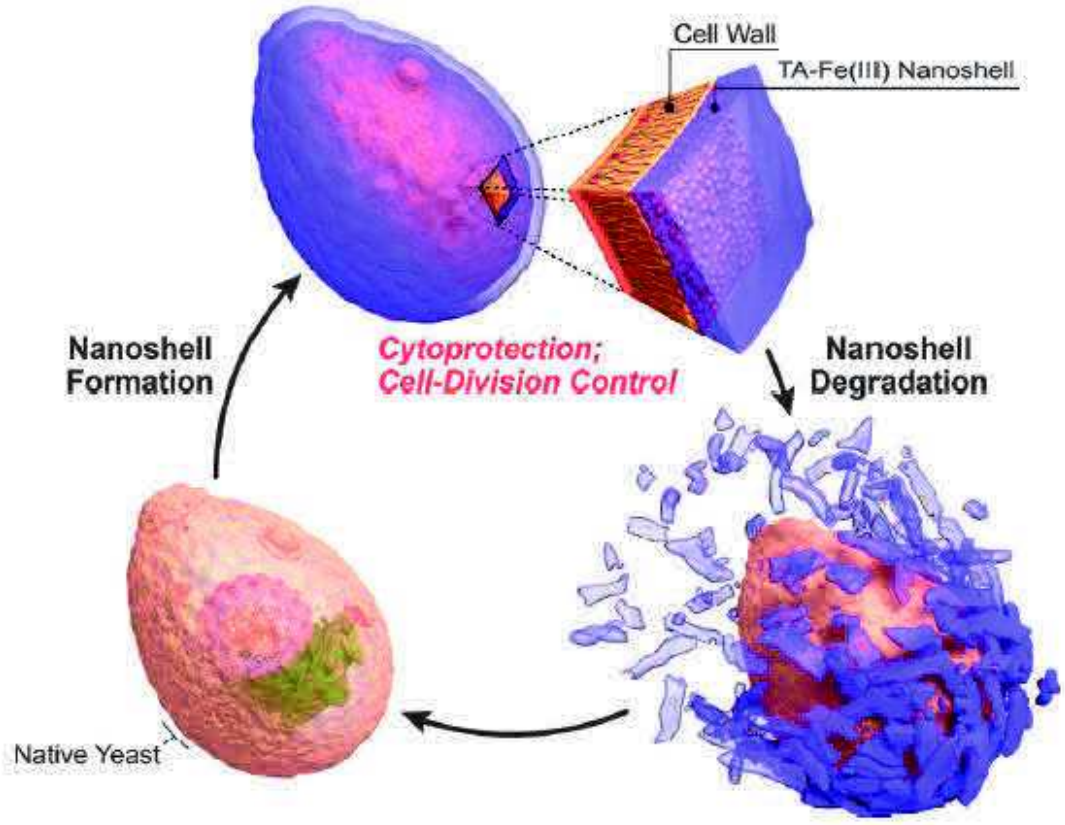

Figure 1.23: *Schematic representation for controlled formation and degradation of the TA–Fe(III) shell on individual S. cerevisiae.*[133]

A melamine sponge was also functionalized with TA/Fe(III) films.[134] Free gallol groups were used for a second step functionalization of the sponge with 1-dodecanethiol through covalent bonding between thiol and oxidized catechol conferring superhydrophobic and fire-resistant properties to the material.

Tannic acid was also used to create 3D gels, by mixing it with Fe(III) and PAH.[135] The process is very similar to the one introduced by Messersmith in 2011 (see above).[42] All three compounds are mixed at acidic pH and the mixture is then brought to more basic pH by adding NaOH. As mentioned before, basification of the solution triggers formation of bis- and tris-gallol/Fe(III) complexes, but also enhances catechols oxidation into quinones which further react on the amine functions of PAH. Thus, the resulting 3D-network is composed of PAH chains covalently cross-linked by TA while TA itself is cross-linked by Fe(III). TA is mixed only with PAH or Fe(III), no gel can be obtained. DNA-TA gels can also be designed.[136] Indeed by simply adding TA to a DNA solution, a hydrogel is spontaneously formed by cross-linking of DNA by TA through hydrogen bonding (Figure 1.24). These gels can be dissolved by TA's ester bond

hydrolysis at basic pH, creating a DNA release. TA was also used as an intermolecular cross-linker through hydrogen bonds in PEG hydrogels.[137]

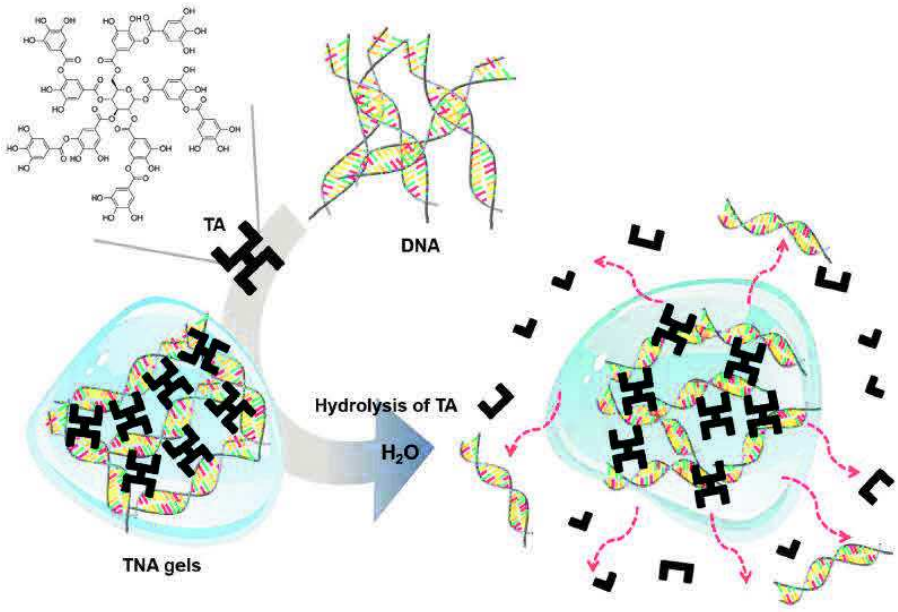

Figure 1.24: *Schematic description of the formation and degradation of DNA-TA hydrogels.*

Polyphenols, in particular TA, can form coatings.[138] The principle is quite simple and consists in the dip coating of a substrate in a solution of polyphenol during several hours without stirring followed by a rinsing step. TA, pyrogallol, epicatechin gallate, epigallocatechin gallate and epigallocatechin, as well as crude extracts of red wine, cacao bean and green tea, were used on various kinds of substrates (metals, polymers etc) and with different shapes (planar surface, particles) (Figure 1.25). Even if the mechanism is not fully understood, it seems to occur through self-polymerization of polyphenols by radical reaction between oxidized phenolic moieties. These coatings allow to immobilize PEG chains for antifouling applications and metals for plasmonic tuning applications. The redox properties of polyphenols can also be used for the design of anti-oxidant coatings.[138] It appears that not all polyphenols can form coatings in these conditions.[139]

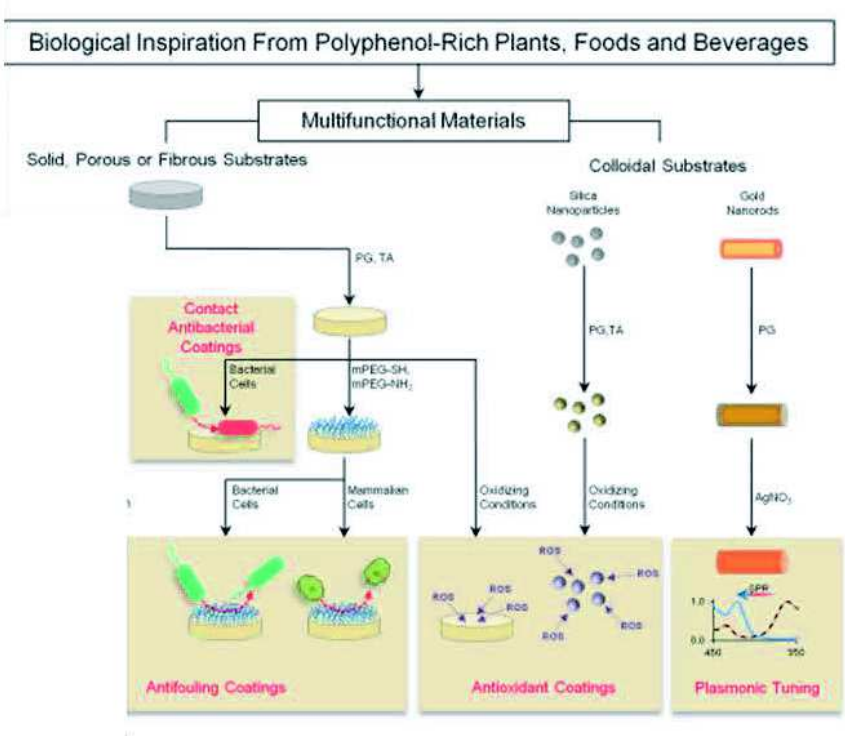

Figure 1.25: *Schematic illustration of compositions, deposition conditions and potential applications of plant polyphenol inspired multifunctional coatings.*[138]

Other polyphenols were used to create functional materials. For example, epigallocatechin-3-gallate (EGCG) was grafted on collagen fibers used as support for palladium nanoparticles through catechol-metal complexation, creating a catalytic network of collagen.[140] More recently, EGCG was used to create assemblies for cancer therapy.[141] More precisely, Herceptin (an anticancer protein) forms nano-micelles through complexation with EGCG. This core was functionalized with EGCG-modified PEG chains to form a protective shell. Herceptin carriers showed greater anticancer impact than the protein alone. Tea polyphenol were also used to create hybrid metal-organic nanostructures.[142] To do so, tea polyphenols were directly extracted from tea leaves, and were mixed with either silver or gold ions. Self-assembly was then triggered by microwave-assisted oxidation leading to covalent cross-linking between tea polyphenols. The resulting nanostructures were made of metallic core and self-polymerized tea polyphenols around the metallic core. Ag/tea polyphenols structures display good antibacterial activity without expressing cell toxicity.

1.2 Electrodeposition of Macromolecules towards the morphogenic approach

Functional materials are predicted to have an enormous impact on many aspects of society, including next generation health care and energy-related technologies. Control of the interactions between material surfaces and their environment can be achieved by tailoring their surface properties, especially through the application of coatings. Bottom-up approaches, using self-assembly principles, are increasingly considered to be one of the most appropriate routes for functional materials design.[143] Different techniques of surface functionalization forming a thin film on a surface, such as Langmuir Blodgett, self-assembled monolayer, adsorption or grafting of polymer and LbL deposition of polymers, have been developed depending on the nature of both the material and the deposited molecules or macromolecules. Since almost 40 years, numerous complex and hierarchical structures have been described.[144] Still, almost all the structures obtained by mixing molecules were realized in solution. Molecular architectures that spontaneously grow exclusively near a surface are rare. This comes from the fact that the molecules composing the architectures generally interact one with the other immediately or rapidly in solution forbidding self-assembly exclusively on a surface. Using a localized stimulus seems to be the best way of inducing a film buildup. Electrodeposition is a process in which imposed electrical "signals" are employed to direct the buildup of thin films. Electrotriggered formation of films can be divided into three categories: precipitation of macromolecules, self-assemblies of polyelectrolytes or physical gel and electrodeposition of polymeric films based on covalent bonds. We will rapidly review them here.

1.2.1 Electrodeposition through macromolecule precipitation

1.2.1.1 Electrodeposition of paints

Electrodeposition of macromolecules through precipitation is a process that has been discovered almost a century ago and is now referenced as electrodeposition of paints. Indeed, some patents from the first half of the XXst century describe examples of electropainting on conductive surfaces.[145-147] All the processes were based on the deposition of natural resinous materials, such as rubber. Finding no application in the industry, research on this topic was somehow forgotten.[148] During the 1950s, coating processes were greatly needed with the explosion of the car industries in order to protect metallic surfaces from rust. Thus, parallel researches were made between Ford Motor & Company and several paints companies in order

to develop water-soluble paints that could be electrodeposited. Figure 1.26 represents the principle of cathodic electrodeposition of paint.

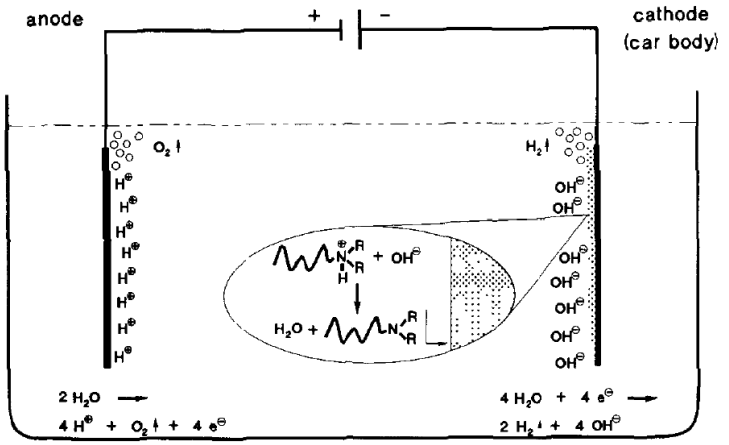

Figure 1.26: *Mechanism of the deposition of a cathodic electrocoating.*[149]

The deposition of a cathodic paint is based on the use of a water-soluble polymer at acidic pH which becomes insoluble at basic pH by deprotonation. A gradient of hydroxyl ions is generated from the electrode by water electrolysis obtained at potential above -2 V, leading to a pH increase and thus to polymer deposition. Anodic paints were also developed corresponding to soluble polymers at basic pH and insoluble at acidic pH. In this case, a gradient of protons is generated by water electrolysis at 50-400 V. Cathodic paints are mostly polycationic and anodic paints are polyanionic. Cathodic paints are mainly used to prevent corrosion in car industry.[149] Numerous papers and reviews, published at the end of the XXst century, describe the fundamental aspect of the electrodeposition process,[150-154] and the chemistry of the paints and the binders.[155-156]

In 2002, Schuhmann and co-workers found new applications of paint electrodeposition in the field of enzymatic biosensors.[157] Indeed, the electrodeposition process allows to co-deposit enzymes by physical entrapment in the coating. It was done for several enzymes or molecules such as glucose oxidase,[157-165] alcohol oxidases,[166-167] alkaline phosphatase[164] and metalloporphyrins.[168] Bi-enzymes sensors were also designed for ATP detection[169] and alcohol sensing.[170-171] In order to improve the electron transfer in the coating, redox polymers were used such as osmium functionalized polymers.[164, 166, 170-177] Different types of electrodes can be functionalized using this process: micro-electrodes,[157] tip-like electrodes[160] or porous electrodes.[163-164] Enzyme loaded electrodeposited films can also be used for biofuel cell applications.[178] It should be noted that electrodeposition of paints were also used to coat Janus

particles by bipolar electrodeposition.[179] Janus anisotropic particles could be used in applications such as e-paper, sensing and photovoltaics.

1.2.1.2 Electrochemical deposition of chitosan hydrogels

1.2.1.2.1 Principle

In 2002, Payne and co-workers opened a new page in the field of electrodeposition of polymers. Instead of using synthetic polymers, they used chitosan, a natural polysaccharide.[180] Chitosan has the same property as a cathodic paint: soluble at pH < pKa (about 6.3)[181-182] due to protonation of the amino groups and insoluble at pH > pKa (Figure 1.27).

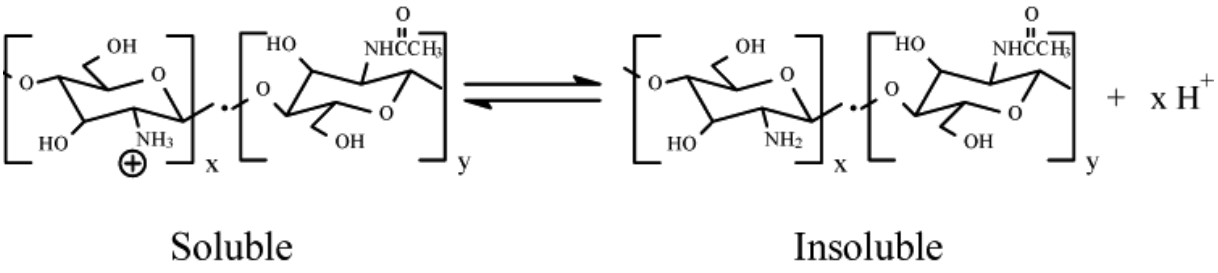

Figure 1.27: *Chemical pathway between soluble and insoluble chitosan.*[180]

Figure 1.28 shows the mechanism of cathodic electrodeposition of chitosan. As for cathodic electrodeposition of paints, a pH gradient is generated from the electrode by water electrolysis (at -2 V) leading to deprotonation of amino groups of chitosan and precipitation in the vicinity of the electrode.

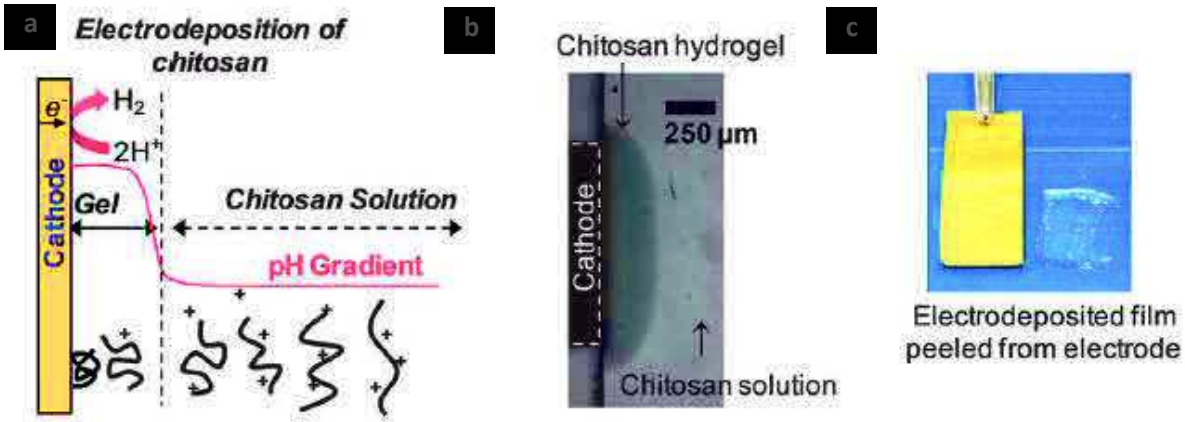

Figure 1.28: *(a) Mechanism of cathodic electrodeposition of chitosan, with pictures of (b) chitosan deposited on a microfluidic device and (c) chitosan hydrogel peeled from an electrode*[183].

The mechanism can be divided into two parts: (i) the electrophoretic motion of charged chitosan chains under the electric field,[184] and (ii) chitosan precipitation due to pH change in the vicinity of the electrode. Using a microfluidic device with sidewall electrodes under an optical microscope, the presence of a pH gradient has been confirmed near the electrode. This gradient triggers the precipitation of chitosan.[185] The electrodeposited chitosan hydrogel has a semi-

crystalline nature.[186] Electrochemically inactive, it is permeable to cationic and anionic probes.[187] Moreover, anionic probes can be confined inside the gel. The deposited thickness is controlled by different parameters such as the time of deposition or the applied current density.[180, 188] The morphology (pores size and connection) of chitosan gels can be tuned by changing the pH, the salt concentration or the nature of the acidic solution used to solubilize chitosan, i.e. acetic solution, malonic acid or citric acid.[189-190] Built at high salt concentration, chitosan gels are less homogeneous. The spatial control of the deposition was shown using a wire electrode,[191] a patterned template with an edge sharpness of 0.5-1.0 µm[192, 188, 193] and confined micropores with a diameter of 3-8 µm (Figure 1.29).[194] Photoconductive cathodes were used to produce hydroxide ions by light illumination and to produce electrochemically patterned chitosan by patterned light.[195]

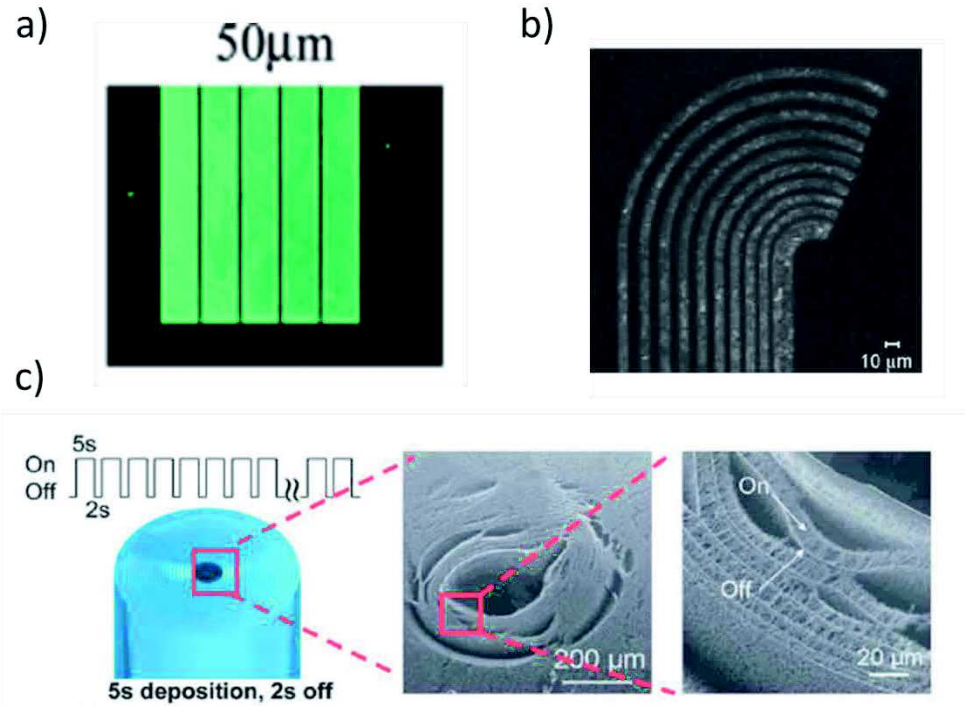

Figure 1.29: *Spatially selective deposition of fluorescently labeled chitosan, in response to an applied voltage, (a) onto a patterned gold surface, the widths between electrodes are 50 µm,[193] (b) and on a curved geometry pattern.[192] (c) Electrodeposition of chitosan on a wire using on/off application of a voltage.[191]*

1.2.1.2.2 Chitosan co-deposition and applications

Since its discovery, electrodeposited chitosan was used for applications in various fields. Co-deposition allows the design of hybrid organic/inorganic coatings for diverse applications. A wide range of enzymes were also entrapped in electrodeposited chitosan for biosensing applications.

Hybrid electrodeposited chitosan

As chitosan can be electrodeposited with various inorganic components, it is an ideal candidate for the microfabrication of nanoparticle platforms. These platforms can be used for electrochemical sensing, *in vivo* imaging, fluorescent labeling and nanocomposite devices. Chitosan was co-deposited with latex nanoparticles,[196] ZnO particles,[197] ZnS quantum dots,[198] carbon dots[199] or magnetic nanoparticles.[200] ZnS quantum dots electrodeposited with chitosan allowed to build fluorescent patterned coatings (Figure 1.30).[198] The fluorescence intensity can be tuned by controlling the deposition parameters such as the deposition time and the concentration in quantum dots.

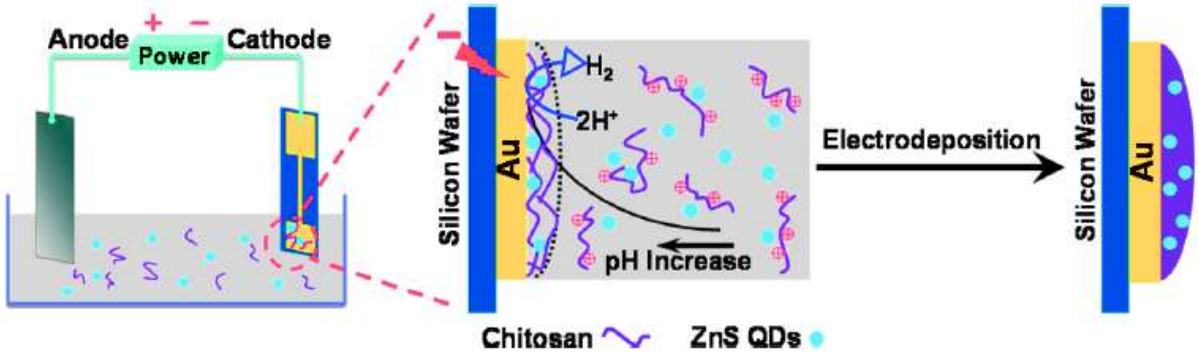

Figure 1.30: *Illustration of electrodeposition of ZnS quantum dots and chitosan on gold electrode.*[198]

Manganese dioxide nanowires were deposited with chitosan for cysteine sensing.[201] Trichloroacetic acid and nitric oxide sensors were designed by depositing chitosan with silver nanoparticles[202] and hemin, and with an iron containing porphyrin, and carbon nanotubes,[203] respectively. Very recently, Payne and co-workers created magnetic soft matter by depositing magnetic nanoparticles with chitosan while applying both electric and magnetic fields leading to the formation of magnetic nanoparticle channels in a chitosan matrix. Moreover, the nanoparticles assembly was reversible and can be removed.[200] These magnetic interfaces could be used for sensing and separation of magnetic beads-modified biological species. Molecularly imprinted hybrid films for p-nitrophenol sensing were developed using phenyltrimethoxysilane, having the ability to self-condensate and to cross-link with chitosan, $HAuCl_4$ salt, as precursor of gold nanoparticles obtained by electrochemical reduction, and p-nitrophenol, as a template, establishing H-bond interactions with chitosan (Figure 1.31).[204]

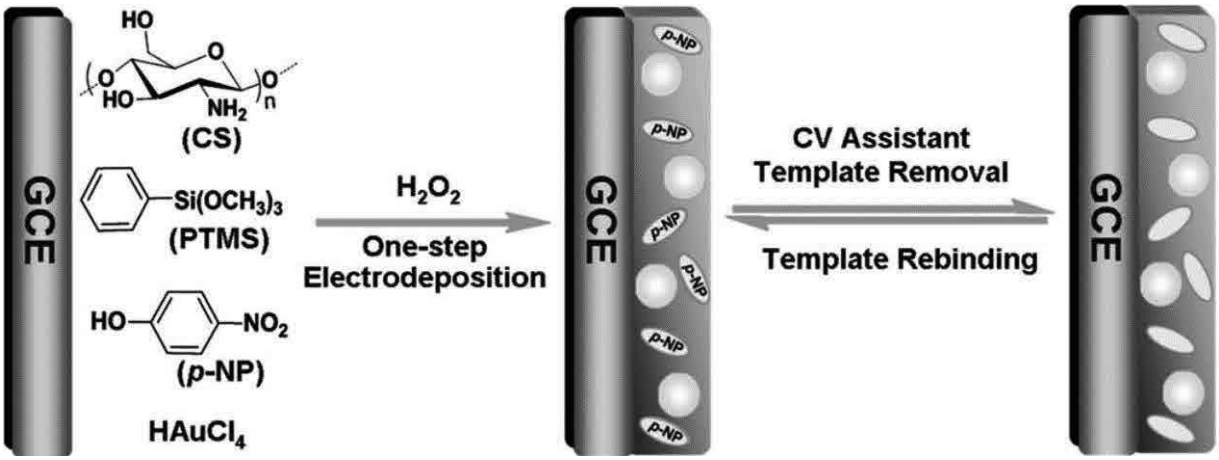

Figure 1.31: *Schematic representation of the fabrication protocol of the p-NP imprinting and imprinted CS/PTMS/AuNPs/GCE for sensing p-NP.*[204]

Chitosan was also co-deposited with alginate and Prussian blue in order to build a microbial fuel cell[205]

Biosensors

Electrodeposited chitosan films were widely used in order to develop biosensors by codeposition with enzymes.[206] The first examples of glucose biosensors were based on chitosan electro-co-deposited with glucose oxidase and inorganic nanomaterials, such as gold nanoparticles,[207-211] carbon nanotubes,[212-214] MnO_2 particles[215-216], nickel nanoparticles[217] and graphene oxide.[218-219] The co-deposition of inorganic nanomaterials improves biosensors properties. Prussian blue modified electrodes[220-221] or ionic liquids[222-224] allow to improve the sensitivity and the stability of the response. Scanning electrochemical microscopy was used to locally immobilize glucose oxidase,[225] horseradish peroxidase[226-227] and carbon nanotubes-chitosan hybrid materials for cytosensing,[228] the impedance of electronic transduction being related to the amount of the adhered cells. Acetylcholine, choline, polyphenol, superoxide anions and adrenaline biosensors were created by co-deposition of chitosan with acetylcholine esterase,[229-234] choline oxidase,[235] laccase,[236] superoxide dismutase,[237] and tyrosinase.[238] More recently, bi-enzyme sensors were created with both glucose oxidase and horseradish peroxidase[239] or β-glucanase.[240] An immunosensor can be designed by cross-linking a specific antibody to chitosan[241] and using chitosan grafted with ferrocene to improve its performance.[242]

Biosensors were also developed by post-functionalization of electrodeposited chitosan with oligonucleotides, virus, phenol or catechol bearing molecules, proteins and enzymes. DNA probes can be cross-linked on the film through glutaraldehyde chemistry.[243-244] A filamentous virus, the tobacco mosaic virus was assembled on patterned chitosan through nucleic acid hybridization.[245] It should be noted that DNA hybridization was also detected by depositing

chitosan and an oligonucleotide-probe on a cantilever.[246] By using a chitosan chemically modified with biotin moieties, streptavidin was adsorbed on microelectrodes allowing spatial selectivity of biotinylated protein assemblies.[247]

Proteins can be grafted on chitosan gels by electrochemistry. Electrogenerated reactive mediators, such as HOCl and OCl^- obtained at 0.9 V (anodic potential) in the presence of NaCl, can oxidize chitosan to generate aldehydes which react with primary amines through Schiff base formation to cross-link proteins,[248] such as glucose oxidase.[249] Azide-tagged proteins were cross-linked on chitosan gels by electro-click chemistry based on Cu(I) catalyzed Huisgen reaction.[250] Cross-linking of phenol or catechol based molecules to chitosan was done by applying an anodic potential[251-254] or by tyrosinase, an enzyme known to oxidize catechol.[255] Oxidized phenol and polyphenol can react with amino groups of chitosan, improving the mechanical[251, 256] and the electrochemical[252] properties of chitosan gels. Catechol modified-chitosan gels present a redox activity and allow to amplify the electrochemical signal of redox probes.[257] Even if the catechol-modified chitosan is not conductive, it improves redox signal detection through exchange of electrons with redox probe and the catechol moieties (Figure 1.32). These gels can be considered for electrons storage applications.

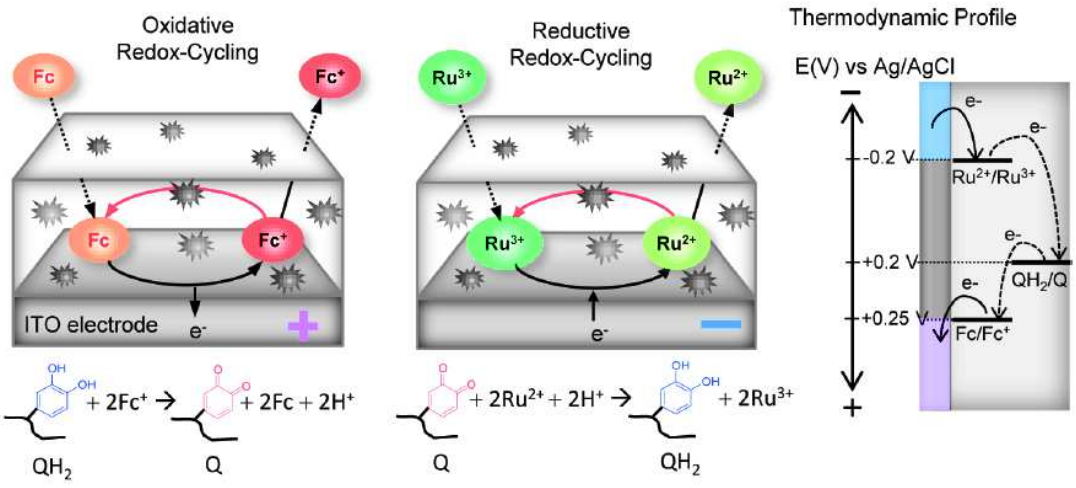

Figure 1.32: *Schematics and thermodynamic profile of the two mediators (Fc and Ru(III)) that can engage oxidative and reductive redox-cycling mechanisms between the phenolic film (QH_2/Q) and ITO electrode.*[258]

The reactivity of phenolic compounds (containing catechol moieties) with chitosan was used to develop an antioxidant phenol film.[259] The phenolic compounds diffuse through the chitosan film to the electrode where they are anodically oxidized and undergo reactions with the chitosan film. This reaction has an effect on the optical properties of the colorless and transparent chitosan gels. The properties of catechol modified chitosan was used to detect a redox bacterial metabolite, the pyocyanin,[260] for clozapine sensors,[261-263] natural phenols (melanin, lignin and

humic acid),[258] to develop insoluble clove[264] and antipsychotics.[265] GFP proteins,[266-267] gelatin,[268-269] tyrosine-peptides[268-269] and chlorogenic acid[270] with catechol moieties were cross-linked to chitosan gels using tyrosinase. Crosslinking of caffeic acid improved the mechanical and redox properties of the electrodeposited chitosan gel.[271] A fusion protein, named HLPT and bearing tyrosine, was covalently cross linked to a chitosan electrodeposited film in order to electronically induced collective bacterial behavior.[272]

Biomedical applications

Hydroxyapatite (Hap) which is a natural mineral, is the major mineral constituent of tooth enamel, dentin and bones and is widely used in biomedical applications. Chitosan is known to be biocompatible. Thus hybrid biocompatible coatings were developed by electro-deposition of chitosan and Hap,[273-275] poly(ethylene oxide),[276] gelatin[277] and bioactive glass.[278-281] Electrochemical studies of chitosan co-deposited with Hap,[273, 282-283] in combination with silica [284], $CaSiO_3$ particles[285], carbon nanotubes[286-287] and halloysite nanotubes,[288] show the prevention of corrosion of the substrate. Different bioactivities were implemented in chitosan gels by incorporation of carbon nanotubes and proteins to enhance cell adhesion,[289] of hexagonal boron nitride,[290] TiO_2,[290] silver nanoparticles[291-292, 293 294] and antibiotic[295] to confer antimicrobial properties and heparin to improve blood compatibility.[296] Electrodeposited chitosan gels were co-deposited to create drug delivering surfaces, with bioglass and an antibiotic,[297 298] gelatin loaded with ampicillin,[299] insuline and layered double hydroxide[300] and ibuprofen.[301-302] The release of ibuprofen is obtained by dissolving the film with the application of an anodic potential. A micro-robotic drug-delivery device was developed by co-depositing a model drug: the Brilliant Green, in intravitreous injections capsules used by a robotic device.[303]

1.2.1.3. Electrochemical deposition of other polymers

Others polysaccharides were electrodeposited. Alginate[304] or hyaluronic acid[305] were also electrodeposited but by applying an anodic potential, leading to a pH decrease in the vicinity of the coated electrode. Indeed, alginate in contrary to chitosan is soluble at basic pH and insoluble at acidic pH. An amperometric biosensor was created by co-deposition of alginate with horseradish peroxidase.[306] As for chitosan, these composite films were prepared by electro co-deposition with other compounds such as carbon nanotubes,[286] cellulose nano-crystals,[307] PHBV microspheres,[308] bioactive glass,[309] nanostructured TiO_2,[310] and hydroxyapatite.[311] A multilayer system can be created by applying alternatively a cathodic potential for chitosan electroprecipitation and an anodic potential for alginate electrodeposition[312]. It should be noted that electrodeposition was also carried out for chiral polymers such as poly(L-lysine) and

poly(L-ornithine)[313]. Other polymers were also electrodeposited, such as poly[-3(3-N,N-diethylaminopropoxy)thiophène] and poly[9,9-bis(diethylaminopropyl)-2,7-fluorene-co-1,4-phenylene],[314-315] poly(acrylic acid).[316-317]

1.2.1.4 Electro-precipitation of enzymes

Electro-precipitation of enzymes is a process based on the application of an electric potential to induce the precipitation of an enzyme on the surface of an electrode. Two different processes are described in the literature: the electrochemical deposition and the electrophoretic deposition of enzymes.[318] Both are based on the electrolysis of water which generates a proton gradient in an enzymatic solution and thus leads to the aggregation and precipitation of enzymes when the local pH reaches the isoelectric point (pI) of the enzyme.

1.2.1.4.1 Electrochemical deposition of enzymes

Electrochemical deposition of enzymes is based on the application of relatively low constant voltages (0-2V) and on the use of highly conductive solution. Buffer with high ionic strength are often used to screen the enzyme surface charge which limits its motion in an electric field. Only enzymes present in the vicinity of the electrode are deposited leading to thin coatings (few hundreds of nm). Electrochemical deposition of enzymes was introduced by Wang *et al*. to create collagen-enzyme biocatalytic membranes.[319] The process was also performed for various enzymes or proteins such as glucose oxidase,[320-323] horseradish peroxidase,[324] laccase,[325] or avidin.[326] Electrochemical deposition of enzymes can be coupled with electropolymerization of conductive polymers to physically entrap enzymes in a conductive matrix.[327] It was done with polyaniline,[328] polypyrolle,[329-331] poly(3,4-ethylenedioxythiophene),[332] poly-o-aminophenol,[325, 333] or poly(o-phenylenediamine).[334] These coatings were mainly used for biosensors and micro-biofuel cell application.[335] To improve the performance of the obtained coatings, enzymes were codeposited with other compounds such as anionic clay,[336] carbon nanotubes,[236, 332] palladium nanoparticles[337] or redox mediators/polymers.[335, 338] Electrochemical deposition was processed on various conductive substrate such as porous copper films,[339] platinum black modified electrode,[340-341] or colloidal gold solutions.[342]

1.2.1.4.2 Electrophoretic deposition of enzymes

Electrophoretic deposition of enzymes is based on the electrophoretic motion of enzymes. In this process, high voltage (few hundreds of volts) are applied using low ionic strength solutions of enzymes.[343] Having a high surface charge due to low charge screening, all the enzymes present in solution contribute to the film buildup. The obtained coatings are much thicker (several μm) than the one deposited by electrochemical deposition. Electrophoretic deposition

of enzymes was introduced in 2009 by Ammam and coworkers using glucose oxidase.[344] Different enzymes, such as β-galactosidase,[345] laccase,[346-347] catalase,[347-348] or glutamate oxidase[349] were immobilized using this process for biosensing and micro-biofuel cell applications. Electropolymerization of polypyrrole was coupled with electrophoretic deposition.[346, 349]

1.2.1.5 Electrogelation of silk

Recently, the electrogelation of silk, obtained from silkworm, has been developed using high potentials (up to 30 V).[350-351] By applying the electrical potential, silk gels were deposited from a silk solution around the positive electrode (Figure 1.33).[350] The gel, stable when the electrical potential is stopped, can be dissolved by reversing the polarity of the electrode while a new gel is created on the other electrode (Figure 1.33*)*.

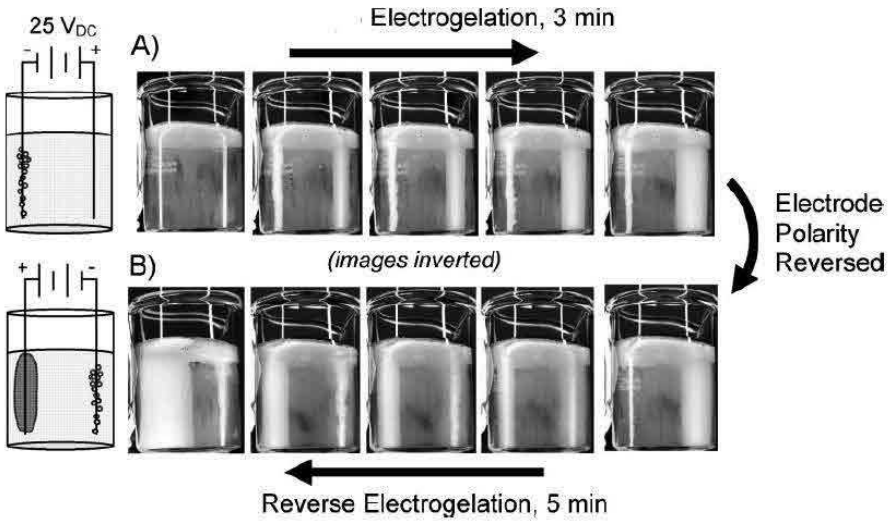

Figure 1.33: *Electrogelation of silk using pencil-lead electrodes: a) the gel forms around the positive electrode for 3 min; b) gelation is reversed with the application of reversed polarity DC voltage.*[350]

In order to understand the gel deposition mechanism, one must have notions on silk fibroin's structure. Silk fibroin is a high molecular weight block copolymer made of heavy and light chains linked by a single disulfide bond.[352] The heavy chain consists of alternating arrays of 12 repetitive hydrophobic peptide domains, rich in alanine and glycine residues, and 11 small hydrophilic charged amorphous domains. The N terminus and the amorphous domains contain acidic groups, whereas only the last amorphous domain and the C terminus contain basic groups.[353] For a pH above its pI (4.2), silk protein is negatively charged, and intermolecular self-assembly is prevented by electrostatic repulsion (Figure 1.31*)*. When the pH value decreased in the vicinity of the positive electrode due to proton generation from water

electrolysis, protonation of acidic groups enables intermolecular self-assembly of silk's macromolecule (Figure 1.34*).*[354]

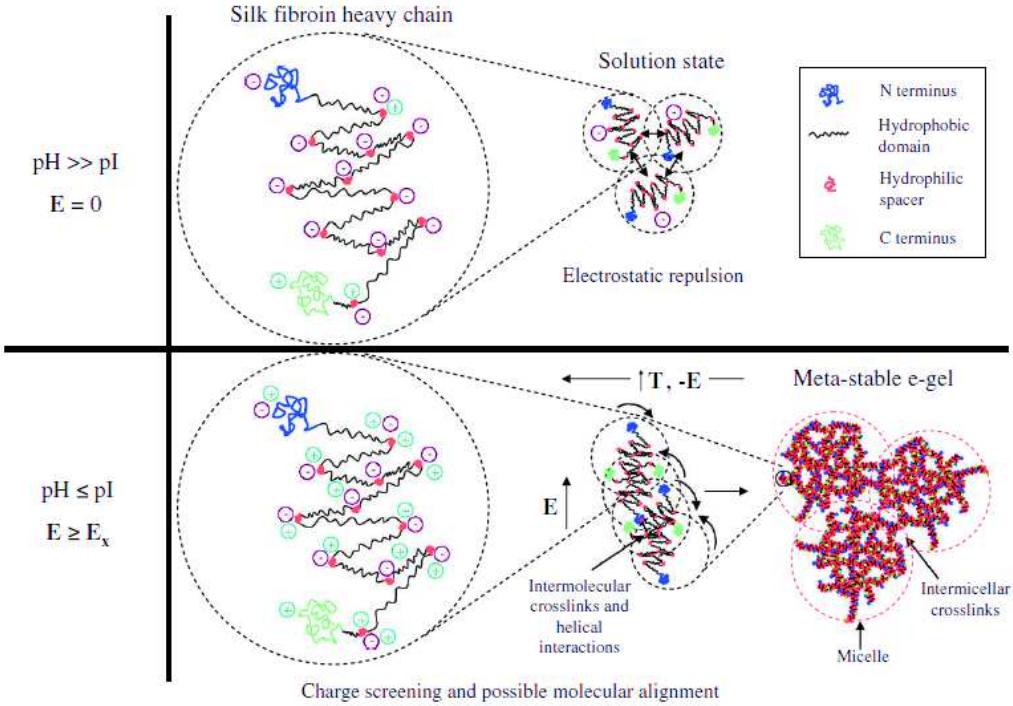

Figure 1.34: *Silk fibroin electrogelation mechanism.*[354]

These gels exhibit spherical micellar structures obtained from the assembly of 10 nm diameter particles into microspheres of larger diameters (from tens to several hundreds of nm) which in turn assemble in large microspheres (Figure 1.35).[355]

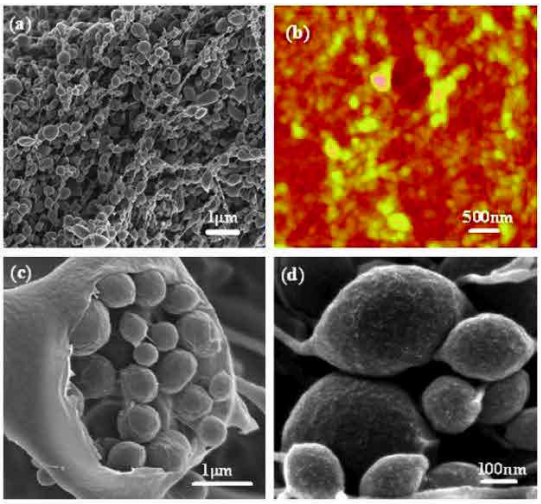

Figure 1.35: *Morphology of electrodeposited gels using pencil lead electrodes: (a) SEM; (b) AFM; (c) inside structure of large microspheres in the gel; (d) magnified images of microspheres in the gel.*[355]

Theoretical finite-element electrodiffusion model using classic diffusion and ion migration equations under an electrical potential supports experimental pH measurement.[356] These models confirm that silk electro-gel construction is governed by the proton gradient generated from the

electrode. Such gels can be deposited on different electrode materials such as copper, aluminum, gold or platinum with various geometries.[350] By using a ring-shaped electrode a thin transparent film with no underlying surface was obtained.[357] This new fabrication process allows to confer three dimensionality and crystallinity to the gels which was not reached with the previously described processes. Their mechanical properties can be tuned with the time of application or the intensity of the electric potential.[358-359] Mainly in random coil state, silk gels are lacking thermal and mechanical stability for biomedical applications. Cross-linking of the gel was obtained chemically by using glutaraldehyde and physically by inducing β-sheet cross-links through ethanol dehydration.[360] Very recently, these gels were studied as potential coatings for bone implants[361]. To add a biological activity to the gel, silk fibroin was chemically modified with tetracycline, an antibiotic. Making the protein positively charged, electrophoretic deposition was proceed on a titanium cathode.[362] These coatings show acceptable cell affinity and good antibacterial activity.

1.2.2 Electrochemical deposition through polyelectrolytes self-assembly

1.2.2.1 Electric-field assisted Layer-by-Layer

A derivate technic of the LbL process, the electric-field directed layer-by-layer assembly (EFDLA), was introduced by Gao and co-workers in 2002.[363] Figure 1.36 shows a schematic illustration of the EFDLA, based on the enhancement of the electrostatic interactions between polyelectrolytes and the substrate by the application of an electric potential.[364] When a polycation (linear poly(ethyleneimine), LPEI) is putted in contact with the electrode, a negative potential is applied to render the surface negatively charged. When the polyanion (poly(acrylic acid), PAA) is adsorbed the applied potential is reverse to a positive value to render the surface positively charged. In comparison with the classic LbL process, patterned multilayers can be easily designed using micro-electrodes.[364-365] A recent study on weak polyelectrolytes/nanoparticles multilayers shows that EFDLA leads to more adsorbed amount of materials on the surface than the classic LbL process.[366]

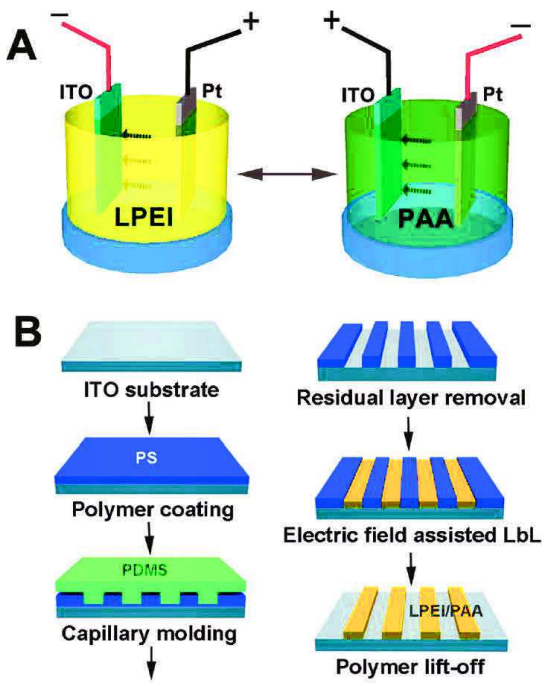

Figure 1.36: *Schematic illustrations of (A) electric-field assisted layer-by-layer assembly and (B) pattern formation*[364].

EFDLA allows to design enzyme/polyelectrolytes multilayers for biosensing applications,[367-368] multilayers functionalized membranes for isopropanol-water separation,[369-370] multilayers sensors for pH measurement,[371] PEI/Graphene Oxide multilayers for ultrahigh hydrogen barriers,[372] conductive multilayer assemblies,[373] hydrophobic films by depositing chitosan/lignosulfonate multilayers[374] or quantum-dots modified electrodes as photo-electrochemical device for reduction of carbon dioxide.[375]

1.2.2.2 Electro-self-assembly of polyelectrolytes

First studies about the adsorption of macromolecules by the application of an electric potential deals mainly with proteins.[376-381] Already in these results, a surprising phenomenon was observed: adsorption of positively charged proteins occurs also when a positive potential is applied on the surface. In 2003, the adsorption of poly(vinyl pyrolidone) on an electrode was studied with the application of different electric potentials.[382-383] These articles underline the fact that the adsorption of polyelectrolytes on a charged electrode (obtained during the potential application) is not only driven by electrostatic interactions. Indeed even when the electrode is positively charged, poly(vinyl pyrolidone) still adsorbs on the surface. This counterintuitive result was also observed for poly(L-lysine)-grafted-poly(ethylene glycol) under a range of anodic potentials going from 0 to 1.5 V (vs Ag/AgCl),[384] during the buildup of poly(L-Lysine)/dextran sulfate (PLL/DSX) and poly(allylamine)/poly(styrene sulfonate) (PAH/PSS)[385] multilayers at potentials ranging from 1.0 to 2.0 V (vs Ag/AgCl), and for

PLL/DNA multilayers at 1.2 V (vs Ag/AgCl).[386] The following argument was raised: when no electric potential is applied, polyelectrolytes adopt a flat conformation on the surface preventing further adsorption of polymers while under an applied potential, they adopt a random coil conformation allowing more material to be immobilized on the surface and thus to thicker layers. Van Tassel and coworkers highlighted a phenomenon of continuous adsorption of a polyelectrolyte during the application of a potential (between 1.2 to 1.5 V (vs Ag/AgCl)).[387] A continuous adsorption applying an anodic potential (positive) was observed for several polycations such as PLL, poly(L-ornithine) and PAH. These results were explained by a polymer-polymer binding due to weak interactions (Van der Walls, close-range) and counterion condensation.[388] In 2012, Van Tassel wrote a review to make a summary of the influence of an electrical potential on assembly and disassembly of polyelectrolytes.[389]

Very recently, our team introduced a new way to electrotrigger the assembly of oppositely charged polyelectrolytes by using a charge shifting polymer.[390] More precisely a polycation, (PAH) was modified with dimethylmaleic functions turning the polycation into a charge shifting polyanion PAHd (Figure 1.37a).

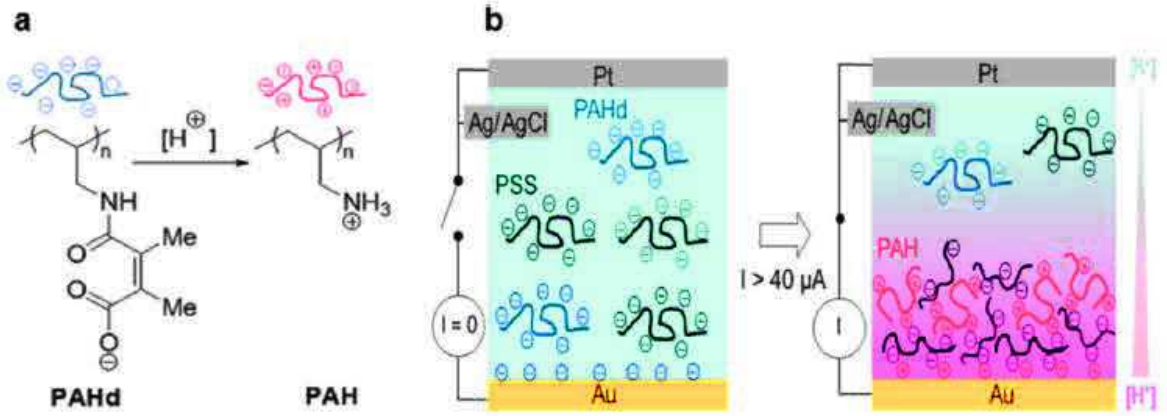

Figure 1.37: *(a) Principle of the charge-shifting polyelectrolytes: PAHd (negatively charged) hydrolyzes under acidic conditions into PAH (positively charged). (b) Schematic representation of the one-pot self-assembly of the PAH/PSS film triggered by the application of a constant current leading to a pH decrease, transforming PAHd into PAH that complexes with PSS present in the solution near the electrode.*[390]

PAHd is negatively charged at basic pH. When the pH is decreased, PAHd is hydrolyzed into positively charged PAH. PAHd was mixed with another polyanion, poly(styrene sulfonate) (PSS). Due to electrostatic repulsion, there is no interactions. In the presence of hydroquinone in the polyanionic mixture, the application of an anodic current allows generating protons by oxidation of hydroquinone leading to an acidic pH gradient in the vicinity of the electrode. The hydrolysis of PAHd into PAH is obtained in a confined area and triggers the localized assembly

of PAH and PSS through electrostatic interactions on the electrode (Figure 1.37b). Another charge shifting polymer was also used for the electrotriggered self-assembly of polyampholytes using the same strategy.[391]

1.2.2.3 Electro-self-assembly through ionic activation

Self-assembly of alginate gel can be obtained by an ionic activation. Alginate is an acidic polysaccharide that forms a biocompatible hydrogel in the presence of divalent cations, such as calcium ions. These cations ionically crosslink carboxylate groups of alginate, leading to a gel formation.[392] In 2009, Payne and co-workers found a way to build a calcium alginate gel from a surface under an electrical potential (Figure 1.38a).[393] An electrode is immersed in a mixed solution of alginate and insoluble calcium carbonate $CaCO_3$. An anodic current is applied to induce by water electrolysis a pH gradient near the anode. The protons reach out $CaCO_3$ particles to dissolve them (partially) releasing free calcium ions. Then, calcium ions interact with alginate to form a gel from the surface.[394]

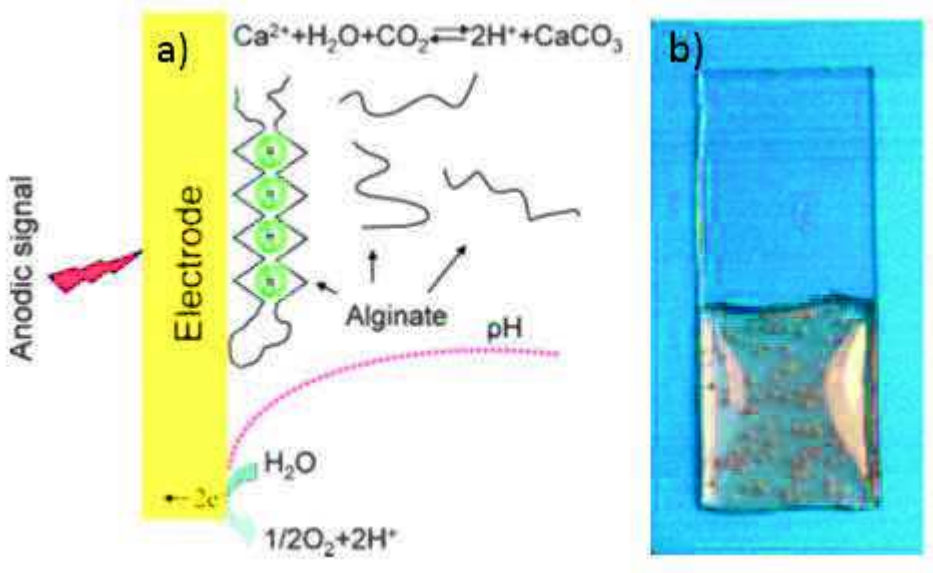

Figure 1.38: *a) Mechanism for calcium alginate electrodeposition. b) Electrodeposition of calcium alginate gel on an ITO-coated glass slide for 5 min at a current density of 3 A/m².*[393]

Figure 1.35b shows an electrodeposited calcium alginate gel with a thickness of 6 µm. The thickness is tunable by changing the deposition time and the current density.[393-394] The opacity of the gel is due to entrapped $CaCO_3$ particles. A major advantage of the electrodeposition is the ability to spatially control the film deposition using patterned electrodes. Thus, calcium alginate was deposited on a patterned chip (Figure 1.39). It is even possible to use an insulating paper to induce the formation of the gel with a define shape depending on the pattern on the paper.[395]

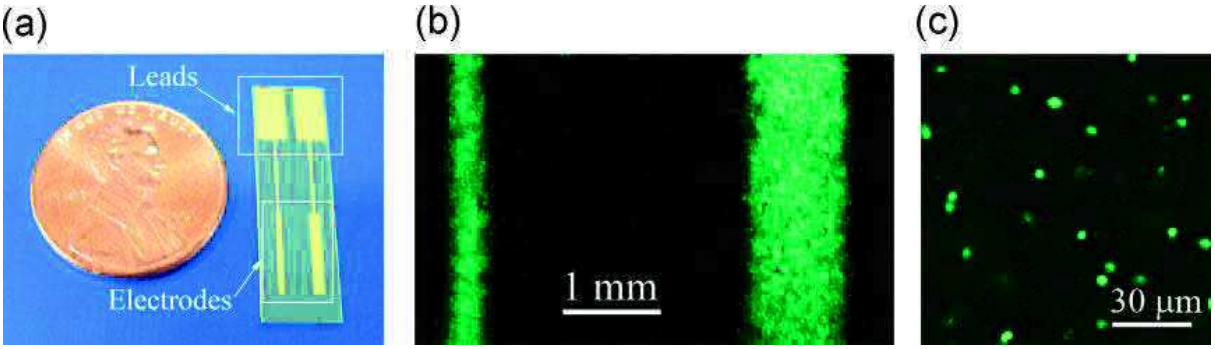

Figure 1.39: *Spatial selectivity of calcium alginate electrodeposition on a patterned chip. a) The chip is a silicon wafer with two patterned gold electrodes. b) Fluorescence photomicrograph of electrodeposited calcium alginate gels with entrapped fluorescent microparticles. c) Confocal fluorescence image from the middle depth of the alginate gel with entrapped fluorescent microparticles.*[393]

Going further, these gels can be co-deposited with cells or bacteria on patterned surfaces in microfluidic devices allowing in-time visualization of the film growth (Figure 1.40a).[396-397] Cells or bacteria entrapped in an electrodeposited calcium alginate gel remain viable.[393, 397] Moreover, different types of bacteria can be deposited simultaneously or separately in multilayers. By using a patterned ITO electrodes, Matsue et al. achieved to obtain cells spheroids culture in alginate gel microwells.[398]

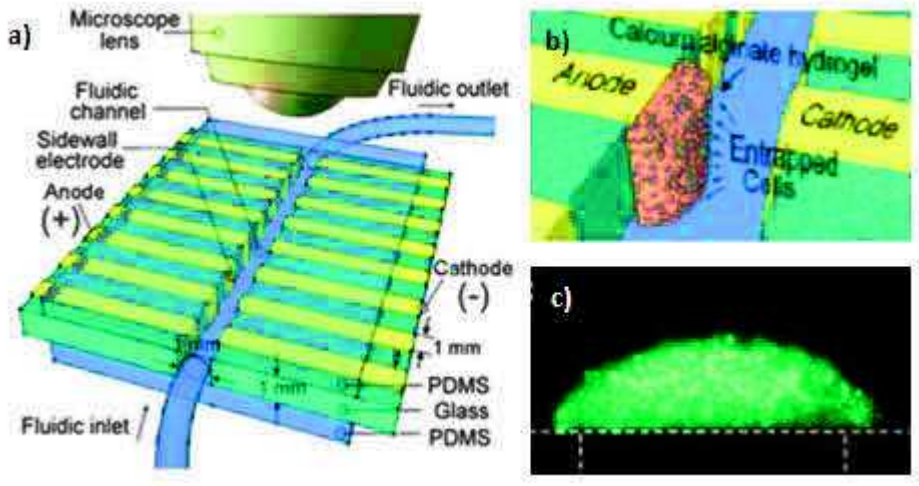

Figure 1.40: *Schematic representation of (a) microfluidic device and (b) cells assembled on one sidewall electrode in a microfluidic device. (c) Fluorescence micrograph of living cells, fluorescently labeled in green, encapsulated in an electrodeposited alginate hydrogel.*[396]

Because these gels are highly hydrated, molecules and macromolecules can diffuse within the gel. Thus, cells and bacteria remains sensitive to chemical stimuli allowing to design model biofilms to study cell signaling[397] or immunoanalysis.[399] Alginate was co-deposited with hemoglobin onto a porous Co-Ni film to obtain drug delivery platforms.[400] It should be noted

that vascular-like structures were developed by co-deposition of alginate calcium with cells on a platinum wire electrode.[401]

In 2013 to obtain $CaCO_3$ particles free alginate gel, Payne and co-workers improved their method.[402] A first layer of electrodeposited alginate/$CaCO_3$ particles gel was used as a reservoir of calcium ions to form a second layer of alginate when put in contact with a calcium free alginate solution (Figure 1.41). Very recently, the electrodeposition of alginate was coupled with a magnetic device in order to create 3D organized assemblies of cells in the alginate-calcium electrodeposited gel.[403]

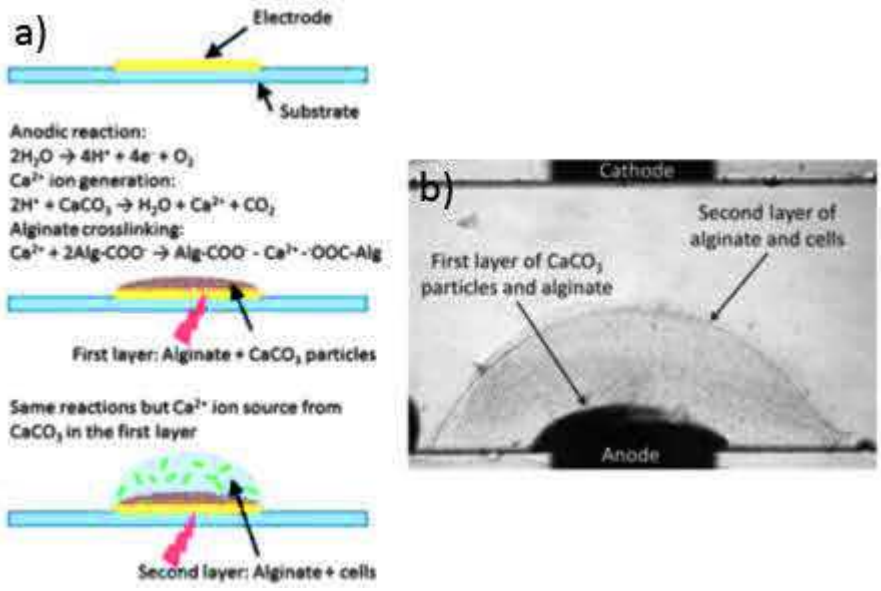

Figure 1.41: *a) Schematic illustration of the method to deposit an optically clear alginate gel at an electrode surface. b) Calcium alginate gel formed by the bilayer method.*[402]

1.2.3 Electrochemical deposition of polymers through covalent bond formation

1.2.3.1 Electropolymerization

Since 1980's, electropolymerization provides a major route for the synthesis of conducting polymers such as polypyrrole or polyaniline. Electropolymerization employs electrochemical oxidation of a monomer, creating a reactive radical, which polymerizes and generates an insoluble polymer film. This kind of reaction is limited to monomers that can undergo an oxidation to form a radical. Electropolymerization has been widely used to design enzymatic biosensor.[404-406] Indeed, enzyme molecules that are present in the immediate vicinity of the electrode surface can be physically incorporated within the growing polymer network. Most of electropolymerized films used for biomolecule immobilization are conducting polymers.

Electropolymerization is a field itself and will not be discussed in detail here as it was already done in several of reviews.[407-409]

1.2.3.2 Electrochemical-Coupling Layer-by-Layer

Electrochemical-coupling Layer-by-Layer (ECC-LbL) consists in an enhanced version of LbL assembly, where an electrotriggered cross-linking of the polymer layers is added between each deposition step. In 2010, the first example described was based on two polyelectrolytes bearing alkyne or azide functions able to cross-link thanks to Cu(I) catalyzed Sharpless-Huisgens click reaction.[410] At each adsorption step of the alkyne-modified polymer and the azide-modified polymer, a reductive potential (-0.35 V vs Ag/AgCl) was applied in the presence of Cu(II) to generate Cu(I). Cu(I) gradient allows triggering the click reaction between alkyne and azide functions leading to covalent cross-link of each layer. Yet, Ariga and coworkers were the first to use the designation "ECC-LbL".[411] They applied the concept to immobilize carbazole functionalized porphyrin, fullerene and fluorine by electrochemically triggered N-alkylcarbazole dimerization (Figure 1.42). As for other electrochemically triggered systems, ECC-LbL can be performed on patterned electrode for spatial control of the assembly[412] and have potential applications in the photovoltaic field.[413-414]

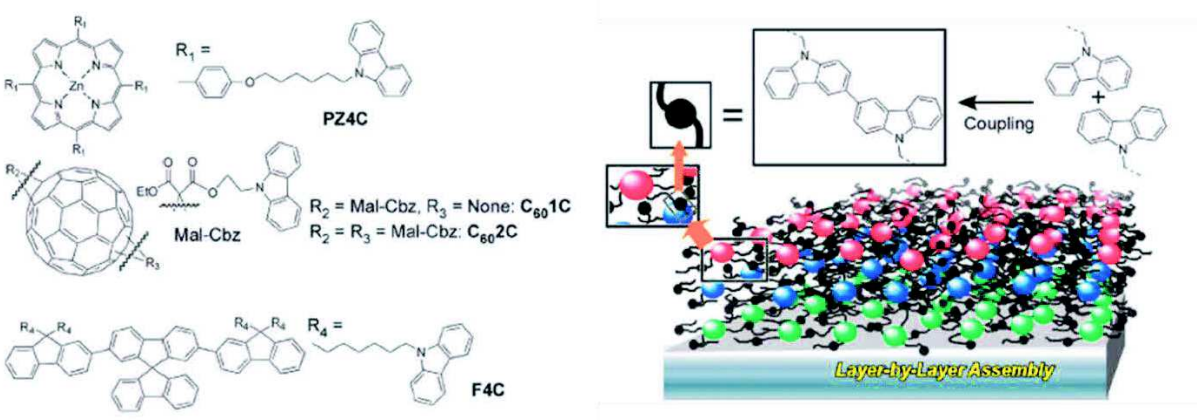

Figure 1.42: *Molecules used for electrochemical-coupling layer-by-layer (ECC_LbL) assembly through cross-linking of peripheral N-alkylcarbazole units.*[411]

1.2.3.3 Electro-crosslinking of polymers

In 2011, our group introduced a new concept in the field of electrodeposition of polymers that can be named electro-crosslinking of polymers.[415] No example of electrodeposition of pre-existing polymers assemblies based on covalent bonds were described previously. Electrotriggered Cu^{I}-catalyzed click reaction between azide and alkyne functionalized polymers solution was used .[416] Figure 1.43 illustrates the concept based on two chemically modified polymers, one bearing azide functions and one bearing alkyne functions. These two polymers are putted together in solution with Cu (II) and are unable to interact with each other.

When an electric potential (cyclic voltammetry from 0.35 V to 0.5 V vs Ag/AgCl) is applied, Cu (II) is reduced to Cu (I) and the reaction between the azide and the alkyne functions is triggered leading to the film assembly from the surface of the electrode. The same principle was also used with an alkyne-grafted polymers and a short azide-modified ethylene glycol spacer.[417] By playing with the size of the ethylene glycol spacer, the thickness and the morphology can be tuned. Different type of polymers can also be used, for example mixture of alkynylated chitosan and azidated chitosan can be electro-crosslinked in presence of Cu (I).[418] Click-based electrocrosslinking of polymers was also used to assemble films based on supramolecular interactions.[419-420]

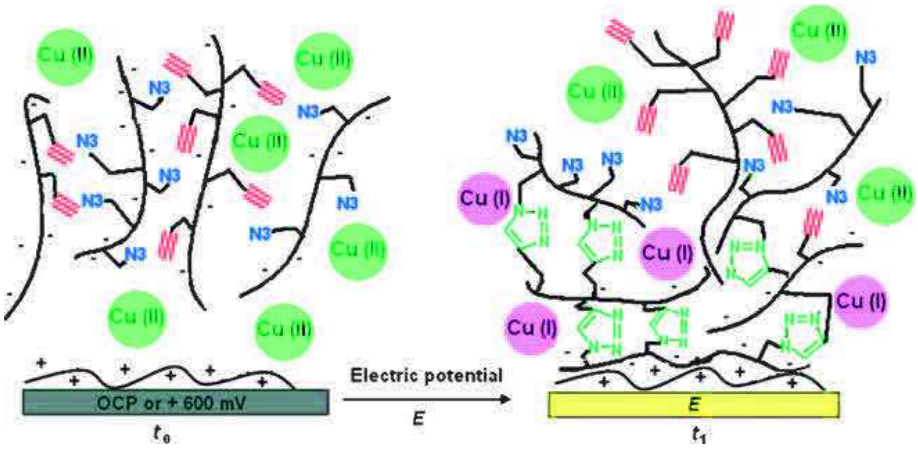

Figure 1.43: *One-pot formation of films using electrochemically controlled click chemistry.*[415]

Another system based on another chemical reaction was described by Payne and co-workers in 2012. Using a solution containing chloride ions, the application a constant current density (4 A/m^2) induces the electrogeneration of chlorine species. In the presence of chitosan, chlorine partially oxidize the polysaccharide forming aldehydes that can further react covalently with amine moities present in chitosan structure (Figure 1.44).[421] Recently, redox polymers were electro-crosslinked by using short protected bis-thiol or bis-amine spacers, which deprotect in acidic or basic conditions.[175] Thus, by generating a proton or hydroxyl gradient by water electrolysis, the spacers were activated in the vicinity of the electrode leading to the cross-linking of the redox polymers on the surface.

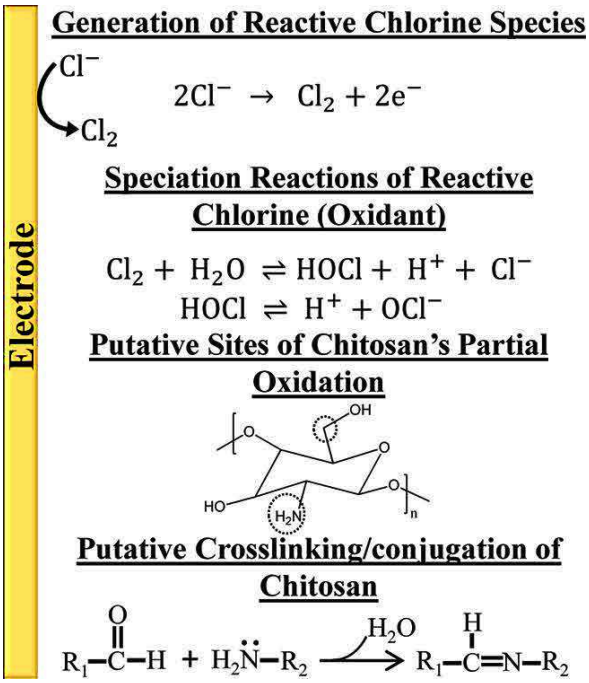

Figure 1.44: *Mechanism for anodic electrodeposition of chitosan.*[421]

References

1. Lee, B. P.; Messersmith, P. B.; Israelachvili, J. N.; Waite, J. H. Mussel-Inspired Adhesives and Coatings. In *Annual Review of Materials Research, Vol 41*, Clarke, D. R.; Fratzl, P., Eds., 2011; Vol. 41, pp 99.

2. Waite, J. H.; Jensen, R. A.; Morse, D. E. Cement Precursor Proteins of the Reef-Building Polychaete Phragmatopoma-Californica (Fewkes). *Biochemistry* **1992,** *31*, 5733.

3. Otness, J. S. M., D.G. Chemical and Physical Characterization of Barnacle Cement. *Comparative Biochemistry and Physiology B: Biochemistry and Molecular Biology* **1972,** *43*, 443.

4. Lee, H.; Scherer, N. F.; Messersmith, P. B. Single-Molecule Mechanics of Mussel Adhesion. *Proceedings of the National Academy of Sciences of the United States of America* **2006,** *103*, 12999.

5. Monahan, J.; Wilker, J. J. Specificity of Metal Ion Cross-Linking in Marine Mussel Adhesives. *Chemical Communications* **2003**, 1672.

6. Deming, T. J. Mussel Byssus and Biomolecular Materials. *Current Opinion in Chemical Biology* **1999,** *3*, 100.

7. Waite, J. H.; Tanzer, M. L. Polyphenolic Substance of Mytilus-Edulis - Novel Adhesive Containing L-Dopa and Hydroxyproline. *Science* **1981,** *212*, 1038.

8. Waite, J. H.; Housley, T. J.; Tanzer, M. L. Peptide Repeats in a Mussel Glue Protein - Theme and Variations. *Biochemistry* **1985,** *24*, 5010.

9. Papov, V. V.; Diamond, T. V.; Biemann, K.; Waite, J. H. Hydroxyarginine-Containing Polyphenolic Proteins in the Adhesive Plaques of the Marine Mussel Mytilus-Edulis. *Journal of Biological Chemistry* **1995,** *270*, 20183.

10. Waite, J. H. Adhesion a La Moule. *Integrative and Comparative Biology* **2002,** *42*, 1172.

11. Burzio, L. A.; Waite, J. H. Cross-Linking in Adhesive Quinoproteins: Studies with Model Decapeptides. *Biochemistry* **2000,** *39*, 11147.

12. Taylor, S. W.; Luther, G. W.; Waite, J. H. Polarographic and Spectrophotometric Investigation of Iron(Iii) Complexation to 3,4-Dihydroxyphenylalanine-Containing Peptides and Proteins from Mytilus-Edulis. *Inorganic Chemistry* **1994,** *33*, 5819.

13. Taylor, S. W.; Chase, D. B.; Emptage, M. H.; Nelson, M. J.; Waite, J. H. Ferric Ion Complexes of a Dopa-Containing Adhesive Protein from Mytilus Edulis. *Inorganic Chemistry* **1996,** *35*, 7572.

14. Zeng, H. B.; Hwang, D. S.; Israelachvili, J. N.; Waite, J. H. Strong Reversible Fe3+-Mediated Bridging between Dopa-Containing Protein Films in Water. *Proceedings of the National Academy of Sciences of the United States of America* **2010,** *107*, 12850.

15. Anderson, T. H.; Yu, J.; Estrada, A.; Hammer, M. U.; Waite, J. H.; Israelachvili, J. N. The Contribution of Dopa to Substrate-Peptide Adhesion and Internal Cohesion of Mussel-Inspired Synthetic Peptide Films. *Advanced Functional Materials* **2010,** *20*, 4196.

16. Bromberg-Martin, E. S.; Matsumoto, M.; Hikosaka, O. Dopamine in Motivational Control: Rewarding, Aversive, and Alerting. *Neuron* **2010,** *68*, 815.

17. Pandey, K. B.; Rizvi, S. I. Plant Polyphenols as Dietary Antioxidants in Human Health and Disease. *Oxidative Medicine and Cellular Longevity* **2009,** *2*, 270.

18. Ross, J. A.; Kasum, C. M. Dietary Flavonoids: Bioavailability, Metabolic Effects, and Safety. *Annual Review of Nutrition* **2002,** *22*, 19.

19. Del Rio, D.; Rodriguez-Mateos, A.; Spencer, J. P. E.; Tognolini, M.; Borges, G.; Crozier, A. Dietary (Poly)Phenolics in Human Health: Structures, Bioavailability, and Evidence of Protective Effects against Chronic Diseases. *Antioxidants & Redox Signaling* **2013,** *18*, 1818.

20. Lattanzio, V.; Kroon, P. A.; Quideau, S.; Treutter, D. *Plant Phenolics - Secondary Metabolites with Diverse Functions* 2008; Vol. 1. p 1.

21. Quideau, S.; Deffieux, D.; Douat-Casassus, C.; Pouysegu, L. Plant Polyphenols: Chemical Properties, Biological Activities, and Synthesis. *Angewandte Chemie-International Edition* **2011,** *50*, 586.

22. Harborne, J. B.; Williams, C. A. Advances in Flavonoid Research since 1992. *Phytochemistry* **2000,** *55*, 481.

23. Yoshida, K.; Mori, M.; Kondo, T. Blue Flower Color Development by Anthocyanins: From Chemical Structure to Cell Physiology. *Natural Product Reports* **2009,** *26*, 884.

24. Cooper-Driver, G. A.; Bhattacharya, M. Role of Phenolics in Plant Evolution. *Phytochemistry* **1998,** *49*, 1165.

25. Hattenschwiler, S.; Vitousek, P. M. The Role of Polyphenols in Terrestrial Ecosystem Nutrient Cycling. *Trends in Ecology & Evolution* **2000,** *15*, 238.

26. Lattanzio, V.; Cardinali, A.; Ruta, C.; Fortunato, I. M.; Lattanzio, V. M. T.; Linsalata, V.; Cicco, N. Relationship of Secondary Metabolism to Growth in Oregano (Origanum Vulgare L.) Shoot Cultures under Nutritional Stress. *Environmental and Experimental Botany* **2009,** *65*, 54.

27. Treutter, D. Significance of Flavonoids in Plant Resistance: A Review. *Environmental Chemistry Letters* **2006,** *4*, 147.

28. Waite, J. H. Nature's Underwater Adhesive Specialist. *Int. J. Adhesion and Adhesives* **1987,** *7*.

29. Yamamoto, H.; Hayakawa, T. Synthesis of Sequential Polypeptides Containing L-Beta-3,4-Dihydroxyphenyl-Alpha-Alanine (Dopa) and L-Lysine. *Biopolymers* **1982,** *21*, 1137.

30. Yamamoto, H. Marine Adhesive Proteins and Some Biotechnological Applications. In *Biotechnology and Genetic Engineering Reviews, Vol 13*, Tombs, M. P., Ed., 1996; Vol. 13, pp 133.

31. Yu, M. E.; Deming, T. J. Synthetic Polypeptide Mimics of Marine Adhesives. *Macromolecules* **1998,** *31*, 4739.

32. Yamada, K.; Chen, T. H.; Kumar, G.; Vesnovsky, O.; Topoleski, L. D. T.; Payne, G. F. Chitosan Based Water-Resistant Adhesive. Analogy to Mussel Glue. *Biomacromolecules* **2000,** *1*, 252.

33. Lee, B. P.; Chao, C. Y.; Nunalee, F. N.; Motan, E.; Shull, K. R.; Messersmith, P. B. Rapid Gel Formation and Adhesion in Photocurable and Biodegradable Block Copolymers with High Dopa Content. *Macromolecules* **2006,** *39*, 1740.

34. Chung, H. Y.; Glass, P.; Pothen, J. M.; Sitti, M.; Washburn, N. R. Enhanced Adhesion of Dopamine Methacrylamide Elastomers Via Viscoelasticity Tuning. *Biomacromolecules* **2011,** *12*, 342.

35. Lee, H.; Lee, B. P.; Messersmith, P. B. A Reversible Wet/Dry Adhesive Inspired by Mussels and Geckos. *Nature* **2007,** *448*, 338.

36. Westwood, G.; Horton, T. N.; Wilker, J. J. Simplified Polymer Mimics of Cross-Linking Adhesive Proteins. *Macromolecules* **2007,** *40*, 3960.

37. White, J. D.; Wilker, J. J. Underwater Bonding with Charged Polymer Mimics of Marine Mussel Adhesive Proteins. *Macromolecules* **2011,** *44*, 5085.

38. Matos-Perez, C. R.; White, J. D.; Wilker, J. J. Polymer Composition and Substrate Influences on the Adhesive Bonding of a Biomimetic, Cross-Linking Polymer. *Journal of the American Chemical Society* **2012,** *134*, 9498.

39. Lee, Y.; Chung, H. J.; Yeo, S.; Ahn, C. H.; Lee, H.; Messersmith, P. B.; Park, T. G. Thermo-Sensitive, Injectable, and Tissue Adhesive Sol-Gel Transition Hyaluronic Acid/Pluronic Composite Hydrogels Prepared from Bio-Inspired Catechol-Thiol Reaction. *Soft Matter* **2010,** *6*, 977.

40. Ryu, J. H.; Lee, Y.; Kong, W. H.; Kim, T. G.; Park, T. G.; Lee, H. Catechol-Functionalized Chitosan/Pluronic Hydrogels for Tissue Adhesives and Hemostatic Materials. *Biomacromolecules* **2011,** *12*, 2653.

41. Brubaker, C. E.; Kissler, H.; Wang, L. J.; Kaufman, D. B.; Messersmith, P. B. Biological Performance of Mussel-Inspired Adhesive in Extrahepatic Islet Transplantation. *Biomaterials* **2010,** *31*, 420.

42. Holten-Andersen, N.; Harrington, M. J.; Birkedal, H.; Lee, B. P.; Messersmith, P. B.; Lee, K. Y. C.; Waite, J. H. Ph-Induced Metal-Ligand Cross-Links Inspired by Mussel Yield Self-Healing Polymer Networks with near-Covalent Elastic Moduli. *Proceedings of the National Academy of Sciences of the United States of America* **2011,** *108*, 2651.

43. He, L. H.; Fullenkamp, D. E.; Rivera, J. G.; Messersmith, P. B. Ph Responsive Self-Healing Hydrogels Formed by Boronate-Catechol Complexation. *Chemical Communications* **2011,** *47*, 7497.

44. Shafiq, Z.; Cui, J. X.; Pastor-Perez, L.; San Miguel, V.; Gropeanu, R. A.; Serrano, C.; del Campo, A. Bioinspired Underwater Bonding and Debonding on Demand. *Angewandte Chemie-International Edition* **2012,** *51*, 4332.

45. Lee, H.; Dellatore, S. M.; Miller, W. M.; Messersmith, P. B. Mussel-Inspired Surface Chemistry for Multifunctional Coatings. *Science* **2007,** *318*, 426.

46. Waite, J. H. Surface Chemistry - Mussel Power. *Nature Materials* **2008,** *7*, 8.

47. Chien, H. W.; Kuo, W. H.; Wang, M. J.; Tsai, S. W.; Tsai, W. B. Tunable Micropatterned Substrates Based on Poly(Dopamine) Deposition Via Microcontact Printing. *Langmuir* **2012,** *28*, 5775.

48. Akter, T.; Kim, W. S. Reversibly Stretchable Transparent Conductive Coatings of Spray-Deposited Silver Nanowires. *Acs Applied Materials & Interfaces* **2012,** *4*, 1855.

49. Kang, S. M.; You, I.; Cho, W. K.; Shon, H. K.; Lee, T. G.; Choi, I. S.; Karp, J. M.; Lee, H. One-Step Modification of Superhydrophobic Surfaces by a Mussel-Inspired Polymer Coating. *Angewandte Chemie-International Edition* **2010,** *49*, 9401.

50. Ryou, M. H.; Lee, Y. M.; Park, J. K.; Choi, J. W. Mussel-Inspired Polydopamine-Treated Polyethylene Separators for High-Power Li-Ion Batteries. *Advanced Materials* **2011,** *23*, 3066.

51. Yu, B.; Liu, J. X.; Liu, S. J.; Zhou, F. Pdop Layer Exhibiting Zwitterionicity: A Simple Electrochemical Interface for Governing Ion Permeability. *Chemical Communications* **2010,** *46*, 5900.

52. Yang, L. P.; Phua, S. L.; Teo, J. K. H.; Toh, C. L.; Lau, S. K.; Ma, J.; Lu, X. H. A Biomimetic Approach to Enhancing Interfacial Interactions: Polydopamine-Coated Clay as Reinforcement for Epoxy Resin. *Acs Applied Materials & Interfaces* **2011,** *3*, 3026.

53. Xu, L. Q.; Yang, W. J.; Neoh, K. G.; Kang, E. T.; Fu, G. D. Dopamine-Induced Reduction and Functionalization of Graphene Oxide Nanosheets. *Macromolecules* **2010,** *43*, 8336.

54. Kang, S. M.; Park, S.; Kim, D.; Park, S. Y.; Ruoff, R. S.; Lee, H. Simultaneous Reduction and Surface Functionalization of Graphene Oxide by Mussel-Inspired Chemistry. *Advanced Functional Materials* **2011,** *21*, 108.

55. Lynge, M. E.; Ogaki, R.; Laursen, A. O.; Lovmand, J.; Sutherland, D. S.; Stadler, B. Polydopamine/Liposome Coatings and Their Interaction with Myoblast Cells. *Acs Applied Materials & Interfaces* **2011,** *3*, 2142.

56. Lee, H.; Rho, J.; Messersmith, P. B. Facile Conjugation of Biomolecules onto Surfaces Via Mussel Adhesive Protein Inspired Coatings. *Advanced Materials* **2009,** *21*, 431.

57. Poh, C. K.; Shi, Z. L.; Lim, T. Y.; Neoh, K. G.; Wang, W. The Effect of Vegf Functionalization of Titanium on Endothelial Cells in Vitro. *Biomaterials* **2010,** *31*, 1578.

58. Lai, M.; Cai, K. Y.; Zhao, L.; Chen, X. Y.; Hou, Y. H.; Yang, Z. X. Surface Functionalization of Tio2 Nanotubes with Bone Morphogenetic Protein 2 and Its Synergistic Effect on the Differentiation of Mesenchymal Stem Cells. *Biomacromolecules* **2011,** *12*, 1097.

59. Kang, K.; Choi, I. S.; Nam, Y. A Biofunctionalization Scheme for Neural Interfaces Using Polydopamine Polymer. *Biomaterials* **2011,** *32*, 6374.

60. Liu, A. R.; Zhao, L.; Bai, H.; Zhao, H. X.; Xing, X. H.; Shi, G. Q. Polypyrrole Actuator with a Bioadhesive Surface for Accumulating Bacteria from Physiological Media. *Acs Applied Materials & Interfaces* **2009,** *1*, 951.

61. Nordberg, A.; Antoni, P.; Montanez, M. I.; Hult, A.; Von Holst, H.; Malkoch, M. Highly Adhesive Phenolic Compounds as Interfacial Primers for Bone Fracture Fixations. *Acs Applied Materials & Interfaces* **2010,** *2*, 654.

62. Yang, S. H.; Kang, S. M.; Lee, K. B.; Chung, T. D.; Lee, H.; Choi, I. S. Mussel-Inspired Encapsulation and Functionalization of Individual Yeast Cells. *Journal of the American Chemical Society* **2011,** *133*, 2795.

63. Zhou, W. H.; Lu, C. H.; Guo, X. C.; Chen, F. R.; Yang, H. H.; Wang, X. R. Mussel-Inspired Molecularly Imprinted Polymer Coating Superparamagnetic Nanoparticles for Protein Recognition. *Journal of Materials Chemistry* **2010,** *20*, 880.

64. Sobocinski, J.; Laure, W.; Taha, M.; Courcot, E.; Chai, F.; Simon, N.; Addad, A.; Martel, B.; Haulon, S.; Woisel, P.; Blanchemain, N.; Lyskawa, J. Mussel Inspired Coating of a Biocompatible Cyclodextrin Based Polymer onto Cocr Vascular Stents. *Acs Applied Materials & Interfaces* **2014,** *6*, 3575.

65. Perez-Anes, A.; Gargouri, M.; Laure, W.; Van Den Berghe, H.; Courcot, E.; Sobocinski, J.; Tabary, N.; Chai, F.; Blach, J. F.; Addad, A.; Woisel, P.; Douroumis, D.; Martel, B.; Blanchemain, N.; Lyskawa, J. Bioinspired Titanium Drug Eluting Platforms Based on a Poly-Beta-Cyclodextrin-Chitosan Layer-by-Layer Self-Assembly Targeting Infections. *Acs Applied Materials & Interfaces* **2015,** *7*, 12882.

66. Sureshkumar, M.; Siswanto, D. Y.; Lee, C. K. Magnetic Antimicrobial Nanocomposite Based on Bacterial Cellulose and Silver Nanoparticles. *Journal of Materials Chemistry* **2010,** *20*, 6948.

67. Xu, H.; Shi, X.; Ma, H.; Lv, Y. H.; Zhang, L. P.; Mao, Z. P. The Preparation and Antibacterial Effects of Dopa-Cotton/Agnps. *Applied Surface Science* **2011,** *257*, 6799.

68. Kang, S. M.; Rho, J.; Choi, I. S.; Messersmith, P. B.; Lee, H. Norepinephrine: Material-Independent, Multifunctional Surface Modification Reagent. *Journal of the American Chemical Society* **2009,** *131*, 13224.

69. Ham, H. O.; Liu, Z. Q.; Lau, K. H. A.; Lee, H.; Messersmith, P. B. Facile DNA Immobilization on Surfaces through a Catecholamine Polymer. *Angewandte Chemie-International Edition* **2011,** *50*, 732.

70. Decher, G. Fuzzy Nanoassemblies: Toward Layered Polymeric Multicomposites. *Science* **1997,** *277*, 1232.

71. Podsiadlo, P.; Liu, Z. Q.; Paterson, D.; Messersmith, P. B.; Kotov, N. A. Fusion of Seashell Nacre and Marine Bioadhesive Analogs: High-Strength Nanocompoisite by Layer-by-Layer

Assembly of Clay and L-3,4-Dihydroxyphenylaianine Polymer. *Advanced Materials* **2007,** *19*, 949.

72. Faure, E.; Halusiak, E.; Farina, F.; Giamblanco, N.; Motte, C.; Poelman, M.; Archambeau, C.; Van De Weerdt, C.; Martial, J.; Jerome, C.; Duwez, A. S.; Detrembleur, C. Clay and Dopa Containing Polyelectrolyte Multilayer Film for Imparting Anticorrosion Properties to Galvanized Steel. *Langmuir* **2012,** *28*, 2971.

73. Lee, H.; Lee, Y.; Statz, A. R.; Rho, J.; Park, T. G.; Messersmith, P. B. Substrate-Independent Layer-by-Layer Assembly by Using Mussel-Adhesive-Inspired Polymers. *Advanced Materials* **2008,** *20*, 1619.

74. Charlot, A.; Sciannamea, V.; Lenoir, S.; Faure, E.; Jerome, R.; Jerome, C.; Van De Weerdt, C.; Martial, J.; Archambeau, C.; Willet, N.; Duwez, A. S.; Fustin, C. A.; Detrembleur, C. All-in-One Strategy for the Fabrication of Antimicrobial Biomimetic Films on Stainless Steel. *Journal of Materials Chemistry* **2009,** *19*, 4117.

75. Faure, E.; Lecomte, P.; Lenoir, S.; Vreuls, C.; Van De Weerdt, C.; Archambeau, C.; Martial, J.; Jerome, C.; Duwez, A. S.; Detrembleur, C. Sustainable and Bio-Inspired Chemistry for Robust Antibacterial Activity of Stainless Steel. *Journal of Materials Chemistry* **2011,** *21*, 7901.

76. Fan, X. W.; Lin, L. J.; Dalsin, J. L.; Messersmith, P. B. Biomimetic Anchor for Surface-Initiated Polymerization from Metal Substrates. *Journal of the American Chemical Society* **2005,** *127*, 15843.

77. Gillich, T.; Benetti, E. M.; Rakhmatullina, E.; Konradi, R.; Li, W.; Zhang, A.; Schluter, A. D.; Textor, M. Self-Assembly of Focal Point Oligo-Catechol Ethylene Glycol Dendrons on Titanium Oxide Surfaces: Adsorption Kinetics, Surface Characterization, and Nonfouling Properties. *Journal of the American Chemical Society* **2011,** *133*, 10940.

78. Statz, A. R.; Meagher, R. J.; Barron, A. E.; Messersmith, P. B. New Peptidomimetic Polymers for Antifouling Surfaces. *Journal of the American Chemical Society* **2005,** *127*, 7972.

79. Saxer, S.; Portmann, C.; Tosatti, S.; Gademann, K.; Zurcher, S.; Textor, M. Surface Assembly of Catechol-Functionalized Poly(L-Lysine)-Graft-Poly(Ethylene Glycol) Copolymer on Titanium Exploiting Combined Electrostatically Driven Self-Organization and Blomimetic Strong Adhesion. *Macromolecules* **2010,** *43*, 1050.

80. He, T.; Shi, Z. L.; Fang, N.; Neoh, K. G.; Kang, E. T.; Chan, V. The Effect of Adhesive Ligands on Bacterial and Fibroblast Adhesions to Surfaces. *Biomaterials* **2009,** *30*, 317.

81. Wach, J. Y.; Bonazzi, S.; Gademann, K. Antimicrobial Surfaces through Natural Product Hybrids. *Angewandte Chemie-International Edition* **2008,** *47*, 7123.

82. Han, H.; Wu, J. F.; Avery, C. W.; Mizutani, M.; Jiang, X. M.; Kamigaito, M.; Chen, Z.; Xi, C. W.; Kuroda, K. Immobilization of Amphiphilic Polycations by Catechol Functionality for Antimicrobial Coatings. *Langmuir* **2011,** *27*, 4010.

83. Amstad, E.; Gillich, T.; Bilecka, I.; Textor, M.; Reimhult, E. Ultrastable Iron Oxide Nanoparticle Colloidal Suspensions Using Dispersants with Catechol-Derived Anchor Groups. *Nano Letters* **2009,** *9*, 4042.

84. Na, H. B.; Palui, G.; Rosenberg, J. T.; Ji, X.; Grant, S. C.; Mattoussi, H. Multidentate Catechol-Based Polyethylene Glycol Oligomers Provide Enhanced Stability and Biocompatibility to Iron Oxide Nanoparticies. *Acs Nano* **2012,** *6*, 389.

85. Gu, H. W.; Xu, K. M.; Yang, Z. M.; Chang, C. K.; Xu, B. Synthesis and Cellular Uptake of Porphyrin Decorated Iron Oxide Nanoparticles - a Potential Candidate for Bimodal Anticancer Therapy. *Chemical Communications* **2005**, 4270.

86. Wang, L.; Yang, Z. M.; Gao, J. H.; Xu, K. M.; Gu, H. W.; Zhang, B.; Zhang, X. X.; Xu, B. A Biocompatible Method of Decorporation: Bisphosphonate-Modified Magnetite Nanoparticles to Remove Uranyl Ions from Blood. *Journal of the American Chemical Society* **2006,** *128*, 13358.

87. Wang, B. D.; Hai, J.; Wang, Q.; Li, T. R.; Yang, Z. Y. Coupling of Luminescent Terbium Complexes to Fe3o4 Nanoparticles for Imaging Applications. *Angewandte Chemie-International Edition* **2011,** *50*, 3063.

88. Gu, H. W.; Yang, Z. M.; Gao, J. H.; Chang, C. K.; Xu, B. Heterodimers of Nanoparticles: Formation at a Liquid-Liquid Interface and Particle-Specific Surface Modification by Functional Molecules. *Journal of the American Chemical Society* **2005,** *127*, 34.

89. Xie, J.; Xu, C.; Kohler, N.; Hou, Y.; Sun, S. Controlled Pegylation of Monodisperse Fe3o4 Nanoparticles for Reduced Non-Specific Uptake by Macrophage Cells. *Advanced Materials* **2007,** *19*, 3163.

90. Gao, J. H.; Liang, G. L.; Cheung, J. S.; Pan, Y.; Kuang, Y.; Zhao, F.; Zhang, B.; Zhang, X. X.; Wu, E. X.; Xu, B. Multifunctional Yolk-Shell Nanoparticles: A Potential Mri Contrast and Anticancer Agent. *Journal of the American Chemical Society* **2008,** *130*, 11828.

91. Lee, Y. H.; Lee, H.; Kim, Y. B.; Kim, J. Y.; Hyeon, T.; Park, H.; Messersmith, P. B.; Park, T. G. Bioinspired Surface Immobilization of Hyaluronic Acid on Monodisperse Magnetite Nanocrystals for Targeted Cancer Imaging. *Advanced Materials* **2008,** *20*, 4154.

92. Song, H. M.; Kim, J. C.; Hong, J. H.; Lee, Y. B.; Choi, J.; Lee, J. I.; Kim, W. S.; Kim, J. H.; Hur, N. H. Magnetic and Transparent Composites by Linking Liquid Crystals to Ferrite Nanoparticles through Covalent Networks. *Advanced Functional Materials* **2007,** *17*, 2070.

93. Xu, C.; Xie, J.; Ho, D.; Wang, C.; Kohler, N.; Walsh, E. G.; Morgan, J. R.; Chin, Y. E.; Sun, S. Au-Fe3o4 Dumbbell Nanoparticles as Dual-Functional Probes. *Angewandte Chemie-International Edition* **2008,** *47*, 173.

94. Wang, B. D.; Hai, J.; Liu, Z. C.; Wang, Q.; Yang, Z. Y.; Sun, S. H. Selective Detection of Iron(Iii) by Rhodamine-Modified Fe3o4 Nanoparticles. *Angewandte Chemie-International Edition* **2010,** *49*, 4576.

95. de la Garza, L.; Saponjic, Z. V.; Rajh, T.; Dimitrijevic, N. M. Photoelectroactivity of a Hybrid System Constructed by Immobilization of Avidin onto Biotinylated Tio2 Electrodes. *Chemistry of Materials* **2006,** *18*, 2682.

96. Yang, S. H.; Ko, E. H.; Choi, I. S. Cytocompatible Encapsulation of Individual Chlorella Cells within Titanium Dioxide Shells by a Designed Catalytic Peptide. *Langmuir* **2012,** *28*, 2151.

97. Meuer, S.; Oberle, P.; Theato, P.; Tremel, W.; Zentel, R. Liquid Crystalline Phases from Polymer-Functionalized Tio2 Nanorods. *Advanced Materials* **2007,** *19*, 2073.

98. Zorn, M.; Tahir, M. N.; Bergmann, B.; Tremel, W.; Grigoriadis, C.; Floudas, G.; Zentel, R. Orientation and Dynamics of Zno Nanorod Liquid Crystals in Electric Fields. *Macromolecular Rapid Communications* **2010,** *31*, 1101.

99. Tahir, M. N.; Zink, N.; Eberhardt, M.; Therese, H. A.; Kolb, U.; Theato, P.; Tremel, W. Overcoming the Insolubility of Molybdenum Disulfide Nanoparticles through a High Degree of Sidewall Functionalization Using Polymeric Chelating Ligands. *Angewandte Chemie-International Edition* **2006,** *45*, 4809.

100. Lee, H.; Lee, K.; Kim, I. K.; Park, T. G. Fluorescent Gold Nanoprobe Sensitive to Intracellular Reactive Oxygen Species. *Advanced Functional Materials* **2009,** *19*, 1884.

101. Studart, A. R.; Amstad, E.; Gauckler, L. J. Colloidal Stabilization of Nanoparticles in Concentrated Suspensions. *Langmuir* **2007,** *23*, 1081.

102. Hirsemann, D.; Shylesh, S.; De Souza, R. A.; Diar-Bakerly, B.; Biersack, B.; Mueller, D. N.; Martin, M.; Schobert, R.; Breu, J. Large-Scale, Low-Cost Fabrication of Janus-Type Emulsifiers by Selective Decoration of Natural Kaolinite Platelets. *Angewandte Chemie-International Edition* **2012,** *51*, 1348.

103. Kaminska, I.; Das, M. R.; Coffinier, Y.; Niedziolka-Jonsson, J.; Sobczak, J.; Woisel, P.; Lyskawa, J.; Opallo, M.; Boukherroub, R.; Szunerits, S. Reduction and Functionalization of Graphene Oxide Sheets Using Biomimetic Dopamine Derivatives in One Step. *Acs Applied Materials & Interfaces* **2012,** *4*, 1016.

104. Kaminska, I.; Qi, W.; Barras, A.; Sobczak, J.; Niedziolka-Jonsson, J.; Woisel, P.; Lyskawa, J.; Laure, W.; Opallo, M.; Li, M. S.; Boukherroub, R.; Szunerits, S. Thiol-Yne Click Reactions on Alkynyl-Dopamine-Modified Reduced Graphene Oxide. *Chemistry-a European Journal* **2013,** *19*, 8673.

105. Awada, H.; Mezzasalma, L.; Blanc, S.; Flahaut, D.; Dagron-Lartigau, C.; Lyskawa, J.; Woisel, P.; Bousquet, A.; Billon, L. Biomimetic Mussel Adhesive Inspired Anchor to Design Zno@Poly(3-Hexylthiophene) Hybrid Core@Corona Nanoparticles. *Macromolecular Rapid Communications* **2015,** *36*, 1486.

106. Mazur, M.; Barras, A.; Kuncser, V.; Galatanu, A.; Zaitzev, V.; Turcheniuk, K. V.; Woisel, P.; Lyskawa, J.; Laure, W.; Siriwardena, A.; Boukherroub, R.; Szunerits, S. Iron Oxide Magnetic Nanoparticles with Versatile Surface Functions Based on Dopamine Anchors. *Nanoscale* **2013,** *5*, 2692.

107. Barras, A.; Lyskawa, J.; Szunerits, S.; Woisel, P.; Boulcherroub, R. Direct Functionalization of Nanodiamond Particles Using Dopamine Derivatives. *Langmuir* **2011,** *27*, 12451.

108. Arslan, M.; Gevrek, T. N.; Lyskawa, J.; Szunerits, S.; Boukherroub, R.; Sanyal, R.; Woisel, P.; Sanyal, A. Bioinspired Anchorable Thiol-Reactive Polymers: Synthesis and Applications toward Surface Functionalization of Magnetic Nanoparticles. *Macromolecules* **2014,** *47*, 5124.

109. Ryu, S.; Lee, Y.; Hwang, J. W.; Hong, S.; Kim, C.; Park, T. G.; Lee, H.; Hong, S. H. High-Strength Carbon Nanotube Fibers Fabricated by Infiltration and Curing of Mussel-Inspired Catecholamine Polymer. *Advanced Materials* **2011,** *23*, 1971.

110. Faure, E.; Falentin-Daudre, C.; Jerome, C.; Lyskawa, J.; Fournier, D.; Woisel, P.; Detrembleur, C. Catechols as Versatile Platforms in Polymer Chemistry. *Progress in Polymer Science* **2013,** *38*, 236.

111. Sedo, J.; Saiz-Poseu, J.; Busque, F.; Ruiz-Molina, D. Catechol-Based Biomimetic Functional Materials. *Advanced Materials* **2013,** *25*, 653.

112. Bentley, W. E.; Payne, G. F. Nature's Other Self-Assemblers. *Science* **2013,** *341*, 136.

113. Shutava, T.; Prouty, M.; Kommireddy, D.; Lvov, Y. Ph Responsive Decomposable Layer-by-Layer Nanofilms and Capsules on the Basis of Tannic Acid. *Macromolecules* **2005,** *38*, 2850.

114. Huang, J. H.; Huang, K. L.; Liu, S. Q.; Luo, Q.; Xu, M. C. Adsorption Properties of Tea Polyphenols onto Three Polymeric Adsorbents with Amide Group. *Journal of Colloid and Interface Science* **2007,** *315*, 407.

115. Erel-Unal, I.; Sukhishvili, S. A. Hydrogen-Bonded Multilayers of a Neutral Polymer and a Polyphenol. *Macromolecules* **2008,** *41*, 3962.

116. Kim, B. S.; Lee, H.; Min, Y. H.; Poon, Z.; Hammond, P. T. Hydrogen-Bonded Multilayer of Ph-Responsive Polymeric Micelles with Tannic Acid for Surface Drug Delivery. *Chemical Communications* **2009**, 4194.

117. Liu, F.; Kozlovskaya, V.; Zavgorodnya, O.; Martinez-Lopez, C.; Catledge, S.; Kharlampieva, E. Encapsulation of Anticancer Drug by Hydrogen-Bonded Multilayers of Tannic Acid. *Soft Matter* **2014,** *10*, 9237.

118. Schmidt, D. J.; Hammond, P. T. Electrochemically Erasable Hydrogen-Bonded Thin Films. *Chemical Communications* **2010,** *46*, 7358.

119. Erel, I.; Schlaad, H.; Demirel, A. L. Effect of Structural Isomerism and Polymer End Group on the Ph-Stability of Hydrogen-Bonded Multilayers. *Journal of Colloid and Interface Science* **2011,** *361*, 477.

120. Shukla, A.; Fang, J. C.; Puranam, S.; Jensen, F. R.; Hammond, P. T. Hemostatic Multilayer Coatings. *Advanced Materials* **2012,** *24*, 492.

121. Kozlovskaya, V.; Kharlampieva, E.; Drachuk, I.; Cheng, D.; Tsukruk, V. V. Responsive Microcapsule Reactors Based on Hydrogen-Bonded Tannic Acid Layer-by-Layer Assemblies. *Soft Matter* **2010,** *6*, 3596.

122. Lisunova, M. O.; Drachuk, I.; Shchepelina, O. A.; Anderson, K. D.; Tsukruk, V. V. Direct Probing of Micromechanical Properties of Hydrogen-Bonded Layer-by-Layer Microcapsule Shells with Different Chemical Compositions. *Langmuir* **2011,** *27*, 11157.

123. Kozlovskaya, V.; Harbaugh, S.; Drachuk, I.; Shchepelina, O.; Kelley-Loughnane, N.; Stone, M.; Tsukruk, V. V. Hydrogen-Bonded Lbl Shells for Living Cell Surface Engineering. *Soft Matter* **2011,** *7*, 2364.

124. Ejima, H.; Richardson, J. J.; Liang, K.; Best, J. P.; van Koeverden, M. P.; Such, G. K.; Cui, J.; Caruso, F. One-Step Assembly of Coordination Complexes for Versatile Film and Particle Engineering. *Science* **2013,** *341*, 154.

125. Guo, J. L.; Ping, Y.; Ejima, H.; Alt, K.; Meissner, M.; Richardson, J. J.; Yan, Y.; Peter, K.; von Elverfeldt, D.; Hagemeyer, C. E.; Caruso, F. Engineering Multifunctional Capsules through the Assembly of Metal-Phenolic Networks. *Angewandte Chemie-International Edition* **2014,** *53*, 5546.

126. Rahim, M. A.; Kempe, K.; Mullner, M.; Ejima, H.; Ju, Y.; van Koeverden, M. P.; Suma, T.; Braunger, J. A.; Leeming, M. G.; Abrahams, B. F.; Caruso, F. Surface-Confined Amorphous

Films from Metal-Coordinated Simple Phenolic Ligands. *Chemistry of Materials* **2015,** *27*, 5825.

127. Ping, Y.; Guo, J. L.; Ejima, H.; Chen, X.; Richardson, J. J.; Sun, H. L.; Caruso, F. Ph-Responsive Capsules Engineered from Metal-Phenolic Networks for Anticancer Drug Delivery. *Small* **2015,** *11*, 2032.

128. Ejima, H.; Richardson, J. J.; Caruso, F. Phenolic Film Engineering for Template-Mediated Microcapsule Preparation. *Polymer Journal* **2014,** *46*, 452.

129. Rahim, M. A.; Ejima, H.; Cho, K. L.; Kempe, K.; Mullner, M.; Best, J. P.; Caruso, F. Coordination-Driven Multistep Assembly of Metal-Polyphenol Films and Capsules. *Chemistry of Materials* **2014,** *26*, 1645.

130. Yang, L. W.; Han, L. L.; Ren, J.; Wei, H. L.; Jia, L. Y. Coating Process and Stability of Metal-Polyphenol Film. *Colloids and Surfaces a-Physicochemical and Engineering Aspects* **2015,** *484*, 197.

131. Ringwald, C.; Ball, V. Layer-by-Layer Deposition of Tannic Acid and Fe3+ Cations Is of Electrostatic Nature but Almost Ionic Strength Independent at Ph 5. *Journal of Colloid and Interface Science* **2015,** *450*, 119.

132. Liu, R. Y.; Xu, A. W. Byssal Threads Inspired Ionic Cross-Linked Narce-Like Graphene Oxide Paper with Superior Mechanical Strength. *Rsc Advances* **2014,** *4*, 40390.

133. Park, J. H.; Kim, K.; Lee, J.; Choi, J. Y.; Hong, D.; Yang, S. H.; Caruso, F.; Lee, Y.; Choi, I. S. A Cytoprotective and Degradable Metal-Polyphenol Nanoshell for Single-Cell Encapsulation. *Angewandte Chemie-International Edition* **2014,** *53*, 12420.

134. Huang, S. Y.; Li, X.; Jiao, Y. Q.; Shi, J. F. Fabrication of a Superhydrophobic, Fire-Resistant, and Mechanical Robust Sponge Upon Polyphenol Chemistry for Efficiently Absorbing Oils/Organic Solvents. *Industrial & Engineering Chemistry Research* **2015,** *54*, 1842.

135. Krogsgaard, M.; Andersen, A.; Birkedal, H. Gels and Threads: Mussel-Inspired One-Pot Route to Advanced Responsive Materials. *Chemical Communications* **2014,** *50*, 13278.

136. Shin, M.; Ryu, J. H.; Park, J. P.; Kim, K.; Yang, J. W.; Lee, H. DNA/Tannic Acid Hybrid Gel Exhibiting Biodegradability, Extensibility, Tissue Adhesiveness, and Hemostatic Ability. *Advanced Functional Materials* **2015,** *25*, 1270.

137. Kim, K.; Shin, M.; Koh, M. Y.; Ryu, J. H.; Lee, M. S.; Hong, S.; Lee, H. Tape: A Medical Adhesive Inspired by a Ubiquitous Compound in Plants. *Advanced Functional Materials* **2015,** *25*, 2402.

138. Sileika, T. S.; Barrett, D. G.; Zhang, R.; Lau, K. H. A.; Messersmith, P. B. Colorless Multifunctional Coatings Inspired by Polyphenols Found in Tea, Chocolate, and Wine. *Angewandte Chemie-International Edition* **2013,** *52*, 10766.

139. Barrett, D. G.; Sileika, T. S.; Messersmith, P. B. Molecular Diversity in Phenolic and Polyphenolic Precursors of Tannin-Inspired Nanocoatings. *Chemical Communications* **2014,** *50*, 7265.

140. Wu, H.; Wu, C.; He, Q.; Liao, X. P.; Shi, B. Collagen Fiber with Surface-Grafted Polyphenol as a Novel Support for Pd(0) Nanoparticles: Synthesis, Characterization and Catalytic Application. *Materials Science & Engineering C-Materials for Biological Applications* **2010,** *30*, 770.

141. Chung, J. E.; Tan, S.; Gao, S. J.; Yongvongsoontorn, N.; Kim, S. H.; Lee, J. H.; Choi, H. S.; Yano, H.; Zhuo, L.; Kurisawa, M.; Ying, J. Y. Self-Assembled Micellar Nanocomplexes Comprising Green Tea Catechin Derivatives and Protein Drugs for Cancer Therapy. *Nature Nanotechnology* **2014,** *9*, 907.

142. Fei, J. B.; Zhao, J.; Du, C. L.; Wang, A. H.; Zhang, H.; Dai, L. R.; Li, J. B. One-Pot Ultrafast Self-Assembly of Autofluorescent Polyphenol-Based Core@Shell Nanostructures and Their Selective Antibacterial Applications. *Acs Nano* **2014,** *8*, 8529.

143. Whitesides, G. M.; Grzybowski, B. Self-Assembly at All Scales. *Science* **2002,** *295*, 2418.

144. Whitesides, G. M.; Boncheva, M. Beyond Molecules: Self-Assembly of Mesoscopic and Macroscopic Components. *Proceedings of the National Academy of Sciences of the United States of America* **2002,** *99*, 4769.

145. Samuel E. Sheppard, L. W. E. Process of Electrodepositing Rubber Upon a Metal Wire1926.

146. Samuel E. Sheppard, C. L. B. Electrodeposition of Organic Material 1932.

147. Clayton, C. G. S. R. I. J. W. Process of Protecing Metal Surfaces by Electrodeposition1940.

148. Brewer, G. E. F. Electrophoretic Painting. *Journal of Applied Electrochemistry* **1983,** *13*, 269.

149. Niemann, J. Waterborne Coatings for the Automotive Industry. *Progress in Organic Coatings* **1992,** *21*, 189.

150. Beck, F. Fundamental Aspects of Electrodeposition of Paint. *Progress in Organic Coatings* **1976**.

151. Krylova, I. A.; Zubov, P. I. Formation and Properties of Coatings Produced by Electrodeposition of Paints. *Progress in Organic Coatings* **1984,** *12*, 129.

152. Beck, F. Electrodeposition of Polymer-Coatings. *Electrochimica Acta* **1988,** *33*, 839.

153. Krylova, I. Painting by Electrodeposition on the Eve of the 21st Century. *Progress in Organic Coatings* **2001,** *42*, 119.

154. Nobuo Furuno, H. K., Yoshiaki Oyabu. Mechanism of Film Formation by the Electrodeposition Coating. *Journal of Colloid and Interface Science* **1975,** *55*.

155. Bieganska, B.; Zubielewicz, M.; Smieszek, E. Anticorrosive Water-Borne Paints. *Progress in Organic Coatings* **1987,** *15*, 33.

156. Schenck, H. U.; Spoor, H.; Marx, M. Chemistry of Binders for Electrodeposition. *Progress in Organic Coatings* **1979,** *7*, 1.

157. Kurzawa, C.; Hengstenberg, A.; Schuhmann, W. Immobilization Method for the Preparation of Biosensors Based on Ph Shift-Induced Deposition of Biomolecule-Containing Polymer Films. *Analytical Chemistry* **2002,** *74*, 355.

158. Reiter, S.; Ruhlig, D.; Ngounou, B.; Neugebauer, S.; Janiak, S.; Vilkanauskyte, A.; Erichsen, T.; Schuhmann, W. An Electrochemical Robotic System for the Optimization of Amperometric Glucose Biosensors Based on a Library of Cathodic Electrodeposition Paints. *Macromolecular Rapid Communications* **2004,** *25*, 348.

159. Ngounou, B.; Neugebauer, S.; Frodl, A.; Reiter, S.; Schuhmann, W. Combinatorial Synthesis of a Library of Acrylic Acid-Based Polymers and Their Evaluation as Immobilisation Matrix for Amperometric Biosensors. *Electrochimica Acta* **2004,** *49*, 3855.

160. Reddy, K. R. C.; Turcu, F.; Schulte, A.; Kayastha, A. M.; Schuhmann, W. Fabrication of a Potentiometric/Amperometric Bifunctional Enzyme Microbiosensor. *Analytical Chemistry* **2005,** *77*, 5063.

161. Neugebauer, S.; Isik, S.; Schulte, A.; Schuhmann, W. Acrylic Acid-Based Copolymers as Immobilization Matrix for Amperometric Biosensors. *Analytical Letters* **2003,** *36*, 2005.

162. Ngounou, B.; Aliyev, E. H.; Guschin, D. A.; Sultanov, Y. M.; Efendiev, A. A.; Schuhmann, W. Parallel Synthesis of Libraries of Anodic and Cathodic Functionalized Electrodeposition Paints as Immobilization Matrix for Amperometric Biosensors. *Bioelectrochemistry* **2007,** *71*, 81.

163. Szamocki, R.; Velichko, A.; Muecklich, F.; Reculusa, S.; Ravaine, S.; Neugebauer, S.; Schuhmann, W.; Hempelmann, R.; Kuhn, A. Improved Enzyme Immobilization for Enhanced Bioelectrocatalytic Activity of Porous Electrodes. *Electrochemistry Communications* **2007,** *9*, 2121.

164. Neugebauer, S.; Stoica, L.; Guschin, D.; Schuhmann, W. Redox-Amplified Biosensors Based on Selective Modification of Nanopore Electrode Structures with Enzymes Entrapped within Electrodeposition Paints. *Microchimica Acta* **2008,** *163*, 33.

165. Guschin, D. A.; Shkil, H.; Schuhmann, W. Electrodeposition Polymers as Immobilization Matrices in Amperometric Biosensors: Improved Polymer Synthesis and Biosensor Fabrication. *Analytical and Bioanalytical Chemistry* **2009,** *395*, 1693.

166. Vilkanauskyte, A.; Erichsen, T.; Marcinkeviciene, L.; Laurinavicius, V.; Schuhmann, W. Reagentless Biosensors Based on Co-Entrapment of a Soluble Redox Polymer and an Enzyme within an Electrochemically Deposited Polymer Film. *Biosensors and Bioelectronics* **2002,** *17*, 1025.

167. Shkotova, L. V.; Soldatkin, A. P.; Gonchar, M. V.; Schuhmann, W.; Dzyadevych, S. V. Amperometric Biosensor for Ethanol Detection Based on Alcohol Oxidase Immobilised within Electrochemically Deposited Resydrol Film. *Materials Science & Engineering C-Biomimetic and Supramolecular Systems* **2006,** *26*, 411.

168. Isik, S.; Oni, J.; Rjabova, V.; Neugebauer, S.; Schuhmann, W. Entrapment of Metalloporphyrins within an Electrodeposition Paint Layer as a Basis for Developing a Nitric Oxide Sensor. *Microchimica Acta* **2004,** *148*, 59.

169. Kueng, A.; Kranz, C.; Mizaikoff, B. Amperometric Atp Biosensor Based on Polymer Entrapped Enzymes. *Biosensors and Bioelectronics* **2004,** *19*, 1301.

170. Alpeeva, I. S.; Vilkanauskyte, A.; Ngounou, B.; Csoregi, E.; Sakharov, I. Y.; Gonchar, M.; Schuhmann, W. Bi-Enzyme Alcohol Biosensors Based on Genetically Engineered Alcohol Oxidase and Different Peroxidases. *Microchimica Acta* **2005,** *152*, 21.

171. Smutok, O.; Ngounou, B.; Pavlishko, H.; Gayda, G.; Gonchar, M.; Schuhmann, W. A Reagentless Bienzyme Amperometric Biosensor Based on Alcohol Oxidase/Peroxidase and an Os-Complex Modified Electrodeposition Paint. *Sensors and Actuators B-Chemical* **2006,** *113*, 590.

172. Hudak, N. S.; Gallaway, J. W.; Barton, S. C. Formation of Mediated Biocatalytic Cathodes by Electrodeposition of a Redox Polymer and Laccase. *Journal of Electroanalytical Chemistry* **2009,** *629*, 57.

173. Guschin, D. A.; Castillo, J.; Dimcheva, N.; Schuhmann, W. Redox Electrodeposition Polymers: Adaptation of the Redox Potential of Polymer-Bound Os Complexes for Bioanalytical Applications. *Analytical and Bioanalytical Chemistry* **2010,** *398*, 1661.

174. Poller, S.; Schuhmann, W. A Miniaturized Voltammetric Ph Sensor Based on Optimized Redox Polymers. *Electrochimica Acta* **2014,** *140*, 101.

175. Poller, S.; Koster, D.; Schuhmann, W. Stabilizing Redox Polymer Films by Electrochemically Induced Crosslinking. *Electrochemistry Communications* **2013,** *34*, 327.

176. Chen, X. X.; Shao, M. L.; Poller, S.; Guschin, D.; Pinyou, P.; Schuhmann, W. Pqq-Sgdh Bioelectrodes Based on Os-Complex Modified Electrodeposition Polymers and Carbon Nanotubes. *Journal of the Electrochemical Society* **2014,** *161*, H3058.

177. Pinyou, P.; Poller, S.; Chen, X. X.; Schuhmann, W. Optimization of Os-Complex Modified Redox Polymers for Improving Biocatalysis of Pqq-Sgdh Based Electrodes. *Electroanalysis* **2015,** *27*, 200.

178. Ackermann, Y.; Guschin, D. A.; Eckhard, K.; Shleev, S.; Schuhmann, W. Design of a Bioelectrocatalytic Electrode Interface for Oxygen Reduction in Biofuel Cells Based on a Specifically Adapted Os-Complex Containing Redox Polymer with Entrapped Trametes Hirsuta Laccase. *Electrochemistry Communications* **2010,** *12*, 640.

179. Loget, G.; Roche, J.; Gianessi, E.; Bouffier, L.; Kuhn, A. Indirect Bipolar Electrodeposition. *Journal of the American Chemical Society* **2012,** *134*, 20033.

180. Wu, L. Q.; Gadre, A. P.; Yi, H. M.; Kastantin, M. J.; Rubloff, G. W.; Bentley, W. E.; Payne, G. F.; Ghodssi, R. Voltage-Dependent Assembly of the Polysaccharide Chitosan onto an Electrode Surface. *Langmuir* **2002,** *18*, 8620.

181. Rinaudo, M.; Pavlov, G.; Desbrieres, J. Influence of Acetic Acid Concentration on the Solubilization of Chitosan. *Polymer* **1999,** *40*, 7029.

182. Sorlier, P.; Denuziere, A.; Viton, C.; Domard, A. Relation between the Degree of Acetylation and the Electrostatic Properties of Chitin and Chitosan. *Biomacromolecules* **2001,** *2*, 765.

183. Payne, G. F.; Kim, E.; Cheng, Y.; Wu, H. C.; Ghodssi, R.; Rubloff, G. W.; Raghavan, S. R.; Culver, J. N.; Bentley, W. E. Accessing Biology's Toolbox for the Mesoscale Biofabrication of Soft Matter. *Soft Matter* **2013,** *9*, 6019.

184. Simchi, A.; Pishbin, F.; Boccaccini, A. R. Electrophoretic Deposition of Chitosan. *Materials Letters* **2009,** *63*, 2253.

185. Cheng, Y.; Luo, X. L.; Betz, J.; Buckhout-White, S.; Bekdash, O.; Payne, G. F.; Bentley, W. E.; Rubloff, G. W. In Situ Quantitative Visualization and Characterization of Chitosan Electrodeposition with Paired Sidewall Electrodes. *Soft Matter* **2010,** *6*, 3177.

186. Cheng, Y.; Gray, K. M.; David, L.; Royaud, I.; Payne, G. F.; Rubloff, G. W. Characterization of the Cathodic Electrodeposition of Semicrystalline Chitosan Hydrogel. *Materials Letters* **2012,** *87*, 97.

187. Zangmeister, R. A.; Park, J. J.; Rubloff, G. W.; Tarlov, M. J. Electrochemical Study of Chitosan Films Deposited from Solution at Reducing Potentials. *Electrochimica Acta* **2006,** *51*, 5324.

188. Fernandes, R.; Wu, L. Q.; Chen, T. H.; Yi, H. M.; Rubloff, G. W.; Ghodssi, R.; Bentley, W. E.; Payne, G. F. Electrochemically Induced Deposition of a Polysaccharide Hydrogel onto a Patterned Surface. *Langmuir* **2003,** *19*, 4058.

189. Altomare, L.; Draghi, L.; Chiesa, R.; De Nardo, L. Morphology Tuning of Chitosan Films Via Electrochemical Deposition. *Materials Letters* **2012,** *78*, 18.

190. Liu, Y.; Zhang, B.; Gray, K. M.; Cheng, Y.; Kim, E.; Rubloff, G. W.; Bentley, W. E.; Wang, Q.; Payne, G. F. Electrodeposition of a Weak Polyelectrolyte Hydrogel: Remarkable Effects of Salt on Kinetics, Structure and Properties. *Soft Matter* **2013,** *9*, 2703.

191. Yan, K.; Ding, F. Y.; Bentley, W. E.; Deng, H. B.; Du, Y. M.; Payne, G. F.; Shi, X. W. Coding for Hydrogel Organization through Signal Guided Self-Assembly. *Soft Matter* **2014,** *10*, 465.

192. Buckhout-White, S. L.; Rubloff, G. W. Spatial Resolution in Chitosan-Based Programmable Biomolecular Scaffolds. *Soft Matter* **2009,** *5*, 3677.

193. Wu, L. Q.; Yi, H. M.; Li, S.; Rubloff, G. W.; Bentley, W. E.; Ghodssi, R.; Payne, G. F. Spatially Selective Deposition of a Reactive Polysaccharide Layer onto a Patterned Template. *Langmuir* **2003,** *19*, 519.

194. Wei, X. Q.; Payne, G. F.; Shi, X. W.; Du, Y. M. Electrodeposition of a Biopolymeric Hydrogel in Track-Etched Micropores. *Soft Matter* **2013,** *9*, 2131.

195. Huang, S. H.; Wei, L. S.; Chu, H. T.; Jiang, Y. L. Light-Addressed Electrodeposition of Enzyme-Entrapped Chitosan Membranes for Multiplexed Enzyme-Based Bioassays Using a Digital Micromirror Device. *Sensors* **2013,** *13*, 10711.

196. Wu, L. Q.; Lee, K.; Wang, X.; English, D. S.; Losert, W.; Payne, G. F. Chitosan-Mediated and Spatially Selective Electrodeposition of Nanoscale Particles. *Langmuir* **2005,** *21*, 3641.

197. Li, Y.; Wu, K.; Zhitomirsky, I. Electrodeposition of Composite Zinc Oxide-Chitosan Films. *Colloids and Surfaces a-Physicochemical and Engineering Aspects* **2010,** *356*, 63.

198. Wang, Y. F.; Geng, Z. H.; Guo, M. M.; Chen, Y. J.; Guo, X. C.; Wang, X. Electroaddressing of Zns Quantum Dots by Codeposition with Chitosan to Construct Fluorescent and Patterned Device Surface. *Acs Applied Materials & Interfaces* **2014,** *6*, 15510.

199. Wang, Y. F.; Wang, X.; Geng, Z. H.; Xiong, Y. F.; Wu, W. C.; Chen, Y. J. Electrodeposition of a Carbon Dots/Chitosan Composite Produced by a Simple in Situ Method

and Electrically Controlled Release of Carbon Dots. *Journal of Materials Chemistry B* **2015,** *3*, 7511.

200. Li, Y.; Liu, Y.; Gao, T. R.; Zhang, B.; Song, Y. Y.; Terrell, J. L.; Barber, N.; Bentley, W. E.; Takeuchi, I.; Payne, G. F.; Wang, Q. Self-Assembly with Orthogonal-Imposed Stimuli to Impart Structure and Confer Magnetic Function to Electrodeposited Hydrogels. *Acs Applied Materials & Interfaces* **2015,** *7*, 10587.

201. Bai, Y. H.; Xu, J. J.; Chen, H. Y. Selective Sensing of Cysteine on Manganese Dioxide Nanowires and Chitosan Modified Glassy Carbon Electrodes. *Biosensors and Bioelectronics* **2009,** *24*, 2985.

202. Liu, B. Z.; Deng, Y. H.; Hu, X. B.; Gao, Z. Q.; Sun, C. Electrochemical Sensing of Trichloroacetic Acid Based on Silver Nanoparticles Doped Chitosan Hydrogel Film Prepared with Controllable Electrodeposition. *Electrochimica Acta* **2012,** *76*, 410.

203. Santos, R. M.; Rodrigues, M. S.; Laranjinha, J.; Barbosa, R. M. Biomimetic Sensor Based on Hemin/Carbon Nanotubes/Chitosan Modified Microelectrode for Nitric Oxide Measurement in the Brain. *Biosensors and Bioelectronics* **2013,** *44*, 152.

204. Li, S. S.; Du, D.; Huang, J.; Tu, H. Y.; Yang, Y. Q.; Zhang, A. D. One-Step Electrodeposition of a Molecularly Imprinting Chitosan/Phenyltrimethoxysilane/Aunps Hybrid Film and Its Application in the Selective Determination of P-Nitrophenol. *Analyst* **2013,** *138*, 2761.

205. Krishnaraj, R. N.; Karthikeyan, R.; Berchmans, S.; Chandran, S.; Pal, P. Functionalization of Electrochemically Deposited Chitosan Films with Alginate and Prussian Blue for Enhanced Performance of Microbial Fuel Cells. *Electrochimica Acta* **2013,** *112*, 465.

206. Suginta, W.; Khunkaewla, P.; Schulte, A. Electrochemical Biosensor Applications of Polysaccharides Chitin and Chitosan. *Chemical Reviews* **2013,** *113*, 5458.

207. Luo, X. L.; Xu, J. J.; Du, Y.; Chen, H. Y. A Glucose Biosensor Based on Chitosan-Glucose Oxidase-Gold Nanoparticles Biocomposite Formed by One-Step Electrodeposition. *Analytical Biochemistry* **2004,** *334*, 284.

208. Du, Y.; Luo, X. L.; Xu, J. J.; Chen, H. Y. A Simple Method to Fabricate a Chitosan-Gold Nanoparticles Film and Its Application in Glucose Biosensor. *Bioelectrochemistry* **2007,** *70*, 342.

209. Zhou, Q. M.; Xie, Q. J.; Fu, Y. C.; Su, Z. H.; Jia, X.; Yao, S. Z. Electrodeposition of Carbon Nanotubes-Chitosan-Glucose Oxidase Biosensing Composite Films Triggered by Reduction of P-Benzoquinone or H2o2. *Journal of Physical Chemistry B* **2007,** *111*, 11276.

210. Li, J. J.; Yuan, R.; Chai, Y. Q. Simple Construction of an Enzymatic Glucose Biosensor Based on a Nanocomposite Film Prepared in One Step from Iron Oxide, Gold Nanoparticles, and Chitosan. *Microchimica Acta* **2011,** *173*, 369.

211. Song, Y. H.; Liu, H. Y.; Wang, Y.; Wang, L. A Glucose Biosensor Based on Cytochrome C and Glucose Oxidase Co-Entrapped in Chitosan- Gold Nanoparticles Modified Electrode. *Analytical Methods* **2013,** *5*, 4165.

212. Luo, X. L.; Xu, J. J.; Wang, J. L.; Chen, H. Y. Electrochemically Deposited Nanocomposite of Chitosan and Carbon Nanotubes for Biosensor Application. *Chemical Communications* **2005**, 2169.

213. Liang, R. P.; Fan, L. X.; Wang, R.; Qiu, J. D. One-Step Electrochemically Deposited Nanocomposite Film of Cs-Fc/Mwnts/God for Glucose Biosensor Application. *Electroanalysis* **2009,** *21*, 1685.

214. Che, X.; Yuan, R.; Chai, Y. Q.; Li, J. J.; Song, Z. J.; Li, W. J.; Zhong, X. A Glucose Biosensor Based on Chitosan-Prussian Blue-Multiwall Carbon Nanotubes-Hollow Ptco Nanochains Formed by One-Step Electrodeposition. *Colloids and Surfaces B-Biointerfaces* **2011,** *84*, 454.

215. Xu, J. J.; Luo, X. L.; Du, Y.; Chen, H. Y. Application of Mno2 Nanoparticles as an Eliminator of Ascorbate Interference to Amperometric Glucose Biosensors. *Electrochemistry Communications* **2004,** *6*, 1169.

216. Bai, Y. H.; Zhang, H.; Xu, J. J.; Chen, H. Y. Relationship between Nanostructure and Electrochemical/Biosensing Properties of Mno(2) Nanomaterials for H(2)O(2)/Choline. *Journal of Physical Chemistry C* **2008,** *112*, 18984.

217. Yang, J.; Yu, J. H.; Strickler, J. R.; Chang, W. J.; Gunasekaran, S. Nickel Nanoparticle-Chitosan-Reduced Graphene Oxide-Modified Screen-Printed Electrodes for Enzyme-Free Glucose Sensing in Portable Microfluidic Devices. *Biosensors and Bioelectronics* **2013,** *47*, 530.

218. Yang, S. L.; Lu, Z. Z.; Luo, S. L.; Liu, C. B.; Tang, Y. H. Direct Electrodeposition of a Biocomposite Consisting of Reduced Graphene Oxide, Chitosan and Glucose Oxidase on a Glassy Carbon Electrode for Direct Sensing of Glucose. *Microchimica Acta* **2013,** *180*, 127.

219. Lu, Z. Z.; Yang, S. L.; Yang, Q.; Luo, S. L.; Liu, C. B.; Tang, Y. H. A Glassy Carbon Electrode Modified with Graphene, Gold Nanoparticles and Chitosan for Ultrasensitive Determination of Lead(Ii). *Microchimica Acta* **2013,** *180*, 555.

220. Xue, M. H.; Xu, Q.; Zhou, M.; Zhu, J. J. In Situ Immobilization of Glucose Oxidase in Chitosan-Gold Nanoparticle Hybrid Film on Prussian Blue Modified Electrode for High-Sensitivity Glucose Detection. *Electrochemistry Communications* **2006,** *8*, 1468.

221. Wang, X. Y.; Gu, H. F.; Yin, F.; Tu, Y. F. A Glucose Biosensor Based on Prussian Blue/Chitosan Hybrid Film. *Biosensors and Bioelectronics* **2009,** *24*, 1527.

222. Xi, F. N.; Liu, L. J.; Wu, Q.; Lin, X. F. One-Step Construction of Biosensor Based on Chitosan-Ionic Liquid-Horseradish Peroxidase Biocomposite Formed by Electrodeposition. *Biosensors and Bioelectronics* **2008,** *24*, 29.

223. Zeng, X. D.; Li, X. F.; Xing, L.; Liu, X. Y.; Luo, S. L.; Wei, W. Z.; Kong, B.; Li, Y. H. Electrodeposition of Chitosan-Ionic Liquid-Glucose Oxidase Biocomposite onto Nano-Gold Electrode for Amperometric Glucose Sensing. *Biosensors and Bioelectronics* **2009,** *24*, 2898.

224. MansouriMajd, S.; Teymourian, H.; Salimi, A.; Hallaj, R. Fabrication of Electrochemical Theophylline Sensor Based on Manganese Oxide Nanoparticles/Ionic Liquid/Chitosan Nanocomposite Modified Glassy Carbon Electrode. *Electrochimica Acta* **2013,** *108*, 707.

225. Chen, P. C.; Chen, R. L. C.; Cheng, T. J.; Wittstock, G. Localized Deposition of Chitosan as Matrix for Enzyme Immobilization. *Electroanalysis* **2009,** *21*, 804.

226. Luo, X. L.; Xu, J. J.; Zhang, Q.; Yang, G. J.; Chen, H. Y. Electrochemically Deposited Chitosan Hydrogel for Horseradish Peroxidase Immobilization through Gold Nanoparticles Self-Assembly. *Biosensors and Bioelectronics* **2005,** *21*, 190.

227. Tangkuaram, T.; Ponchio, C.; Kangkasomboon, T.; Katikawong, P.; Veerasai, W. Design and Development of a Highly Stable Hydrogen Peroxide Biosensor on Screen Printed Carbon Electrode Based on Horseradish Peroxidase Bound with Gold Nanoparticles in the Matrix of Chitosan. *Biosensors and Bioelectronics* **2007,** *22*, 2071.

228. Hao, C.; Ding, L.; Zhang, X. J.; Ju, H. X. Biocompatible Conductive Architecture of Carbon Nanofiber-Doped Chitosan Prepared with Controllable Electrodeposition for Cytosensing. *Analytical Chemistry* **2007,** *79*, 4442.

229. Du, D.; Ding, J. W.; Cai, J.; Zhang, A. D. One-Step Electrochemically Deposited Interface of Chitosan-Gold Nanoparticles for Acetylcholinesterase Biosensor Design. *Journal of Electroanalytical Chemistry* **2007,** *605*, 53.

230. Song, Y. H.; Zhang, M.; Wang, L.; Wan, L. L.; Xiao, X. P.; Ye, S. H.; Wang, J. R. A Novel Biosensor Based on Acetylecholinesterase/Prussian Blue-Chitosan Modified Electrode for Detection of Carbaryl Pesticides. *Electrochimica Acta* **2011,** *56*, 7267.

231. Zhai, C.; Sun, X.; Zhao, W. P.; Gong, Z. L.; Wang, X. Y. Acetylcholinesterase Biosensor Based on Chitosan/Prussian Blue/Multiwall Carbon Nanotubes/Hollow Gold Nanospheres

Nanocomposite Film by One-Step Electrodeposition. *Biosensors and Bioelectronics* **2013,** *42*, 124.

232. Du, D.; Ding, J. W.; Cai, J.; Zhang, A. D. Electrochemical Thiocholine Inhibition Sensor Based on Biocatalytic Growth of Au Nanoparticles Using Chitosan as Template. *Sensors and Actuators B-Chemical* **2007,** *127*, 317.

233. Du, D.; Ding, J. W.; Cai, J.; Zhang, A. D. Determination of Carbaryl Pesticide Using Amperometric Acetylcholinesterase Sensor Formed by Electrochemically Deposited Chitosan. *Colloids and Surfaces B-Biointerfaces* **2007,** *58*, 145.

234. Gong, J. M.; Liu, T.; Song, D. D.; Zhang, X. B.; Zhang, L. Z. One-Step Fabrication of Three-Dimensional Porous Calcium Carbonate-Chitosan Composite Film as the Immobilization Matrix of Acetylcholinesterase and Its Biosensing on Pesticide. *Electrochemistry Communications* **2009,** *11*, 1873.

235. Bai, Y. H.; Du, Y.; Xu, J. J.; Chen, H. Y. Choline Biosensors Based on a Bi-Electrocatalytic Property of Mno2 Nanoparticles Modified Electrodes to H2o2. *Electrochemistry Communications* **2007,** *9*, 2611.

236. Diaconu, M.; Litescu, S. C.; Radu, G. L. Laccase-Mwcnt-Chitosan Biosensor-a New Tool for Total Polyphenolic Content Evaluation from in Vitro Cultivated Plants. *Sensors and Actuators B-Chemical* **2010,** *145*, 800.

237. Wang, L.; Wen, W.; Xiong, H. Y.; Zhang, X. H.; Gu, H. S.; Wang, S. F. A Novel Amperometric Biosensor for Superoxide Anion Based on Superoxide Dismutase Immobilized on Gold Nanoparticle-Chitosan-Ionic Liquid Biocomposite Film. *Analytica Chimica Acta* **2013,** *758*, 66.

238. Ye, H. Z.; Xu, H. F.; Xu, X. Q.; Zheng, C. S.; Li, X. H.; Wang, L. L.; Liu, X. X.; Chen, G. N. An Electrochemiluminescence Sensor for Adrenaline Assay Based on the Tyrosinase/Sic/Chitosan Modified Electrode. *Chemical Communications* **2013,** *49*, 7070.

239. Li, F.; Wang, Z.; Chen, W.; Zhang, S. S. A Simple Strategy for One-Step Construction of Bienzyme Biosensor by in-Situ Formation of Biocomposite Film through Electrodeposition. *Biosensors and Bioelectronics* **2009,** *24*, 3030.

240. Wang, B. B.; Ji, X. P.; Zhao, H. Y.; Wang, N.; Li, X. R.; Ni, R. X.; Liu, Y. H. An Amperometric Beta-Glucan Biosensor Based on the Immobilization of Bi-Enzyme on Prussian Blue-Chitosan and Gold Nanoparticles-Chitosan Nanocomposite Films. *Biosensors and Bioelectronics* **2014,** *55*, 113.

241. Liang, R. P.; Peng, H. Z.; Qiu, J. D. Fabrication, Characterization, and Application of Potentiometric Immunosensor Based on Biocompatible and Controllable Three-Dimensional Porous Chitosan Membranes. *Journal of Colloid and Interface Science* **2008,** *320*, 125.

242. Qiu, J. D.; Liang, R. P.; Wang, R.; Fan, L. X.; Chen, Y. W.; Xia, X. H. A Label-Free Amperometric Immunosensor Based on Biocompatible Conductive Redox Chitosan-Ferrocene/Gold Nanoparticles Matrix. *Biosensors and Bioelectronics* **2009,** *25*, 852.

243. Yi, H. M.; Wu, L. Q.; Sumner, J. J.; Gillespie, J. B.; Payne, G. F.; Bentley, W. E. Chitosan Scaffolds for Biomolecular Assembly: Coupling Nucleic Acid Probes for Detecting Hybridization. *Biotechnology and Bioengineering* **2003,** *83*, 646.

244. Yi, H. M.; Wu, L. Q.; Ghodssi, R.; Rubloff, G. W.; Payne, G. F.; Bentley, W. E. A Robust Technique for Assembly of Nucleic Acid Hybridization Chips Based on Electrochemically Templated Chitosan. *Analytical Chemistry* **2004,** *76*, 365.

245. Yi, H. M.; Nisar, S.; Lee, S. Y.; Powers, M. A.; Bentley, W. E.; Payne, G. F.; Ghodssi, R.; Rubloff, G. W.; Harris, M. T.; Culver, J. N. Patterned Assembly of Genetically Modified Viral Nanotemplates Via Nucleic Acid Hybridization. *Nano Letters* **2005,** *5*, 1931.

246. Koev, S. T.; Powers, M. A.; Yi, H.; Wu, L. Q.; Bentley, W. E.; Rubloff, G. W.; Payne, G. F.; Ghodssi, R. Mechano-Transduction of DNA Hybridization and Dopamine Oxidation through Electrodeposited Chitosan Network. *Lab on a Chip* **2007,** *7*, 103.

247. Shi, X. W.; Liu, Y.; Lewandowski, A. T.; Wu, L. Q.; Wu, H. C.; Ghodssi, R.; Rubloff, G. W.; Bentley, W. E.; Payne, G. F. Chitosan Biotinylation and Electrodeposition for Selective Protein Assembly. *Macromolecular Bioscience* **2008,** *8*, 451.

248. Shi, X. W.; Yang, X. H.; Gaskell, K. J.; Liu, Y.; Kobatake, E.; Bentley, W. E.; Payne, G. F. Reagentless Protein Assembly Triggered by Localized Electrical Signals. *Advanced Materials* **2009,** *21*, 984.

249. Meyer, W. L.; Liu, Y.; Shi, X. W.; Yang, X. H.; Bentley, W. E.; Payne, G. F. Chitosan-Coated Wires: Conferring Electrical Properties to Chitosan Fibers. *Biomacromolecules* **2009,** *10*, 858.

250. Shi, X. W.; Qiu, L.; Nie, Z.; Xiao, L.; Payne, G. F.; Du, Y. M. Protein Addressing on Patterned Microchip by Coupling Chitosan Electrodeposition and 'Electro-Click' Chemistry. *Biofabrication* **2013,** *5*.

251. Wu, L. Q.; Ghodssi, R.; Elabd, Y. A.; Payne, G. F. Biomimetic Pattern Transfer. *Advanced Functional Materials* **2005,** *15*, 189.

252. Kim, E.; Liu, Y.; Shi, X. W.; Yang, X. H.; Bentley, W. E.; Payne, G. F. Biomimetic Approach to Confer Redox Activity to Thin Chitosan Films. *Advanced Functional Materials* **2010,** *20*, 2683.

253. Kim, E.; Gordonov, T.; Liu, Y.; Bentley, W. E.; Payne, G. F. Reverse Engineering to Suggest Biologically Relevant Redox Activities of Phenolic Materials. *ACS Chemical Biology* **2013,** *8*, 716.

254. Kim, E.; Liu, Y.; Bentley, W. E.; Payne, G. F. Redox Capacitor to Establish Bio-Device Redox-Connectivity. *Advanced Functional Materials* **2012,** *22*, 1409.

255. Payne, G. F.; Bentley, W. E. Enzymatic Writing to Soft Films: Potential to Filter, Store, and Analyse Biologically Relevant Chemical Information. *Advanced Functional Materials* **2013**.

256. Wu, L. Q.; McDermott, M. K.; Zhu, C.; Ghodssi, R.; Payne, G. E. Mimicking Biological Phenol Reaction Cascades to Confer Mechanical Function. *Advanced Functional Materials* **2006,** *16*, 1967.

257. Liu, Y.; Kim, E.; White, I. M.; Bentley, W. E.; Payne, G. F. Information Processing through a Bio-Based Redox Capacitor: Signatures for Redox-Cycling. *Bioelectrochemistry* **2014,** *98*, 94.

258. Kim, E.; Liu, Y.; Leverage, W. T.; Yin, J. J.; White, I. M.; Bentley, W. E.; Payne, G. F. Context-Dependent Redox Properties of Natural Phenolic Materials. *Biomacromolecules* **2014,** *15*, 1653.

259. Liu, Y.; Gaskell, K. J.; Cheng, Z. H.; Yu, L. L.; Payne, G. F. Chitosan-Coated Electrodes for Bimodal Sensing: Selective Post-Electrode Film Reaction for Spectroelectrochemical Analysis. *Langmuir* **2008,** *24*, 7223.

260. Kim, E.; Gordonov, T.; Bentley, W. E.; Payne, G. F. Amplified and in Situ Detection of Redox-Active Metabolite Using a Biobased Redox Capacitor. *Analytical Chemistry* **2013,** *85*, 2102.

261. Ben-Yoav, H.; Winkler, T. E.; Kim, E.; Chocron, S. E.; Kelly, D. L.; Payne, G. F.; Ghodssi, R. Redox Cycling-Based Amplifying Electrochemical Sensor for in Situ Clozapine Antipsychotic Treatment Monitoring. *Electrochimica Acta* **2014,** *130*, 497.

262. Ben-Yoav, H.; Chocron, S. E.; Winkler, T. E.; Kim, E.; Kelly, D. L.; Payne, G. F.; Ghodssi, R. An Electrochemical Micro-System for Clozapine Antipsychotic Treatment Monitoring. *Electrochimica Acta* **2015,** *163*, 260.

263. Winkler, T. E.; Ben-Yoav, H.; Chocron, S. E.; Kim, E.; Kelly, D. L.; Payne, G. F.; Ghodssi, R. Electrochemical Study of the Catechol-Modified Chitosan System for Clozapine Treatment Monitoring. *Langmuir* **2014,** *30*, 14686.

264. Lee, M. E.; Kim, E.; Liu, Y.; March, J. C.; Bentley, W. E.; Payne, G. F. Rapid and Repeatable Redox Cycling of an Insoluble Dietary Antioxidant: Electrochemical Analysis. *Journal of Agricultural and Food Chemistry* **2014,** *62*, 9760.

265. Kim, E.; Chocron, S. E.; Ben-Yoav, H.; Winkler, T. E.; Liu, Y.; Glassman, M.; Wolfram, C.; Kelly, D. L.; Ghodssi, R.; Payne, G. F. Programmable "Semismart" Sensor: Relevance to Monitoring Antipsychotics. *Advanced Functional Materials* **2015,** *25*, 2156.

266. Chen, T. H.; Small, D. A.; Wu, L. Q.; Rubloff, G. W.; Ghodssi, R.; Vazquez-Duhalt, R.; Bentley, W. E.; Payne, G. F. Nature-Inspired Creation of Protein-Polysaccharide Conjugate and Its Subsequent Assembly onto a Patterned Surface. *Langmuir* **2003,** *19*, 9382.

267. Lewandowski, A. T.; Yi, H. M.; Luo, X. L.; Payne, G. F.; Ghodssi, R.; Rubloff, G. W.; Bentley, W. E. Protein Assembly onto Patterned Microfabricated Devices through Enzymatic Activation of Fusion Pro-Tag. *Biotechnology and Bioengineering* **2008,** *99*, 499.

268. Yi, H. M.; Wu, L. Q.; Ghodssi, R.; Rubloff, G. W.; Payne, G. F.; Bentley, W. E. Signal-Directed Sequential Assembly of Biomolecules on Patterned Surfaces. *Langmuir* **2005,** *21*, 2104.

269. Yang, X. H.; Shi, X. W.; Liu, Y.; Bentley, W. E.; Payne, G. F. Orthogonal Enzymatic Reactions for the Assembly of Proteins at Electrode Addresses. *Langmuir* **2009,** *25*, 338.

270. Liba, B. D.; Kim, E.; Martin, A. N.; Liu, Y.; Bentley, W. E.; Payne, G. F. Biofabricated Film with Enzymatic and Redox-Capacitor Functionalities to Harvest and Store Electrons. *Biofabrication* **2013,** *5*.

271. Liu, Y.; Zhang, B. C.; Javvaji, V.; Kim, E.; Lee, M. E.; Raghavan, S. R.; Wang, Q.; Payne, G. F. Tyrosinase-Mediated Grafting and Crosslinking of Natural Phenols Confers Functional Properties to Chitosan. *Biochemical Engineering Journal* **2014,** *89*, 21.

272. Gordonov, T.; Kim, E.; Cheng, Y.; Ben-Yoav, H.; Ghodssi, R.; Rubloff, G.; Yin, J. J.; Payne, G. F.; Bentley, W. E. Electronic Modulation of Biochemical Signal Generation. *Nature Nanotechnology* **2014,** *9*, 605.

273. Redepenning, J.; Venkataraman, G.; Chen, J.; Stafford, N. Electrochemical Preparation of Chitosan/Hydroxyapatite Composite Coatings on Titanium Substrates. *Journal of Biomedical Materials Research Part A* **2003,** *66A*, 411.

274. Zhitomirsky, I. Electrophoretic Deposition of Organic-Inorganic Nanocomposites. *Journal of Materials Science* **2006,** *41*, 8186.

275. Boccaccini, A. R.; Keim, S.; Ma, R.; Li, Y.; Zhitomirsky, I. Electrophoretic Deposition of Biomaterials. *Journal of the Royal Society Interface* **2010,** *7*, S581.

276. Cassani, D. A. D.; Altomare, L.; De Nardo, L.; Variola, F. Physicochemical and Nanomechanical Investigation of Electrodeposited Chitosan:Peo Blends. *Journal of Materials Chemistry B* **2015,** *3*, 2641.

277. Jiang, T.; Zhang, Z.; Zhou, Y.; Liu, Y.; Wang, Z. W.; Tong, H.; Shen, X. Y.; Wang, Y. N. Surface Functionalization of Titanium with Chitosan/Gelatin Via Electrophoretic Deposition: Characterization and Cell Behavior. *Biomacromolecules* **2010,** *11*, 1254.

278. Zhitomirsky, D.; Roether, J. A.; Boccaccini, A. R.; Zhitomirsky, I. Electrophoretic Deposition of Bioactive Glass/Polymer Composite Coatings with and without Ha Nanoparticle Inclusions for Biomedical Applications. *Journal of Materials Processing Technology* **2009,** *209*, 1853.

279. Pishbin, F.; Simchi, A.; Ryan, M. P.; Boccaccini, A. R. Electrophoretic Deposition of Chitosan/45s5 Bioglass (R) Composite Coatings for Orthopaedic Applications. *Surface & Coatings Technology* **2011,** *205*, 5260.

280. Seuss, S.; Lehmann, M.; Boccaccini, A. R. Alternating Current Electrophoretic Deposition of Antibacterial Bioactive Glass-Chitosan Composite Coatings. *International Journal of Molecular Sciences* **2014,** *15*, 12231.

281. Patel, K. D.; El-Fiqi, A.; Lee, H. Y.; Singh, R. K.; Kim, D. A.; Lee, H. H.; Kim, H. W. Chitosan-Nanobioactive Glass Electrophoretic Coatings with Bone Regenerative and Drug Delivering Potential. *Journal of Materials Chemistry* **2012,** *22*, 24945.

282. Pang, X.; Zhitomirsky, I. Electrodeposition of Composite Hydroxyapatite-Chitosan Films. *Materials Chemistry and Physics* **2005,** *94*, 245.

283. Pang, X.; Zhitomirsky, I. Electrophoretic Deposition of Composite Hydroxyapatite-Chitosan Coatings. *Materials Characterization* **2007,** *58*, 339.

284. Grandfield, K.; Zhitomirsky, I. Electrophoretic Deposition of Composite Hydroxyapatite-Silica-Chitosan Coatings. *Materials Characterization* **2008,** *59*, 61.

285. Pang, X.; Casagrande, T.; Zhitomirsky, I. Electrophoretic Deposition of Hydroxyapatite-Casio3-Chitosan Composite Coatings. *Journal of Colloid and Interface Science* **2009,** *330*, 323.

286. Grandfield, K.; Sun, F.; FitzPatrick, M.; Cheong, M.; Zhitomirsky, I. Electrophoretic Deposition of Polymer-Carbon Nanotube-Hydroxyapatite Composites. *Surface & Coatings Technology* **2009,** *203*, 1481.

287. Batmanghelich, F.; Ghorbani, M. Effect of Ph and Carbon Nanotube Content on the Corrosion Behavior of Electrophoretically Deposited Chitosan-Hydroxyapatite-Carbon Nanotube Composite Coatings. *Ceramics International* **2013,** *39*, 5393.

288. Deen, I.; Pang, X.; Zhitomirsky, I. Electrophoretic Deposition of Composite Chitosan-Halloysite Nanotube-Hydroxyapatite Films. *Colloids and Surfaces a-Physicochemical and Engineering Aspects* **2012,** *410*, 38.

289. Patel, K. D.; Kim, T. H.; Lee, E. J.; Han, C. M.; Lee, J. Y.; Singh, R. K.; Kim, H. W. Nanostructured Biointerfacing of Metals with Carbon Nanotube/Chitosan Hybrids by Electrodeposition for Cell Stimulation and Therapeutics Delivery. *Acs Applied Materials & Interfaces* **2014,** *6*, 20214.

290. Raddaha, N. S.; Cordero-Arias, L.; Cabanas-Polo, S.; Virtanen, S.; Roether, J. A.; Boccaccini, A. R. Electrophoretic Deposition of Chitosan/H-Bn and Chitosan/H-Bn/Tio2 Composite Coatings on Stainless Steel (316l) Substrates. *Materials* **2014,** *7*, 1814.

291. Pang, X.; Zhitomirsky, I. Electrodeposition of Hydroxyapatite-Silver-Chitosan Nanocomposite Coatings. *Surface & Coatings Technology* **2008,** *202*, 3815.

292. Pishbin, F.; Mourino, V.; Gilchrist, J. B.; McComb, D. W.; Kreppel, S.; Salih, V.; Ryan, M. P.; Boccaccini, A. R. Single-Step Electrochemical Deposition of Antimicrobial Orthopaedic Coatings Based on a Bioactive Glass/Chitosan/Nano-Silver Composite System. *Acta Biomaterialia* **2013,** *9*, 7469.

293. Li, P. H.; Zhang, X. M.; Xu, R. Z.; Wang, W. H.; Liu, X. M.; Yeung, K. W. K.; Chu, P. K. Electrochemically Deposited Chitosan/Ag Complex Coatings on Biomedical Niti Alloy for Antibacterial Application. *Surface & Coatings Technology* **2013,** *232*, 370.

294. Wang, Y. F.; Guo, X. C.; Pan, R. H.; Han, D.; Chen, T.; Geng, Z. H.; Xiong, Y. F.; Chen, Y. J. Electrodeposition of Chitosan/Gelatin/Nanosilver: A New Method for Constructing Biopolymer/Nanoparticle Composite Films with Conductivity and Antibacterial Activity. *Materials Science & Engineering C-Materials for Biological Applications* **2015,** *53*, 222.

295. Ordikhani, F.; Tamjid, E.; Simchi, A. Characterization and Antibacterial Performance of Electrodeposited Chitosan-Vancomycin Composite Coatings for Prevention of Implant-Associated Infections. *Materials Science & Engineering C-Materials for Biological Applications* **2014,** *41*, 240.

296. Sun, F.; Pang, X.; Zhitomirsky, I. Electrophoretic Deposition of Composite Hydroxyapatite-Chitosan-Heparin Coatings. *Journal of Materials Processing Technology* **2009,** *209*, 1597.

297. Ordikhani, F.; Simchi, A. Long-Term Antibiotic Delivery by Chitosan-Based Composite Coatings with Bone Regenerative Potential. *Applied Surface Science* **2014,** *317*, 56.

298. Pishbin, F.; Mourino, V.; Flor, S.; Kreppel, S.; Salih, V.; Ryan, M. P.; Boccaccini, A. R. Electrophoretic Deposition of Gentamicin-Loaded Bioactive Glass/Chitosan Composite Coatings for Orthopaedic Implants. *Acs Applied Materials & Interfaces* **2014,** *6*, 8796.

299. Patel, K. D.; Singh, R. K.; Lee, E. J.; Han, C. M.; Won, J. E.; Knowles, J. C.; Kim, H. W. Tailoring Solubility and Drug Release from Electrophoretic Deposited Chitosan-Gelatin Films on Titanium. *Surface & Coatings Technology* **2014,** *242*, 232.

300. Zhao, P. K.; Liu, Y. Y.; Xiao, L.; Deng, H. B.; Du, Y. M.; Shi, X. W. Electrochemical Deposition to Construct a Nature Inspired Multilayer Chitosan/Layered Double Hydroxides Hybrid Gel for Stimuli Responsive Release of Protein. *Journal of Materials Chemistry B* **2015,** *3*, 7577.

301. Liu, Y. Y.; Yan, K.; Jiang, G. X.; Xiong, Y.; Du, Y. M.; Shi, X. W. Electrical Signal Guided Ibuprofen Release from Electrodeposited Chitosan Hydrogel. *International Journal of Polymer Science* **2014**.

302. Zhao, P. K.; Liu, H. Y.; Deng, H. B.; Xiao, L.; Qin, C. Q.; Du, Y. M.; Shi, X. W. A Study of Chitosan Hydrogel with Embedded Mesoporous Silica Nanoparticles Loaded by Ibuprofen as a Dual Stimuli-Responsive Drug Release System for Surface Coating of Titanium Implants. *Colloids and Surfaces B-Biointerfaces* **2014,** *123*, 657.

303. Fusco, S.; Chatzipirpiridis, G.; Sivaraman, K. M.; Ergeneman, O.; Nelson, B. J.; Pane, S. Chitosan Electrodeposition for Microrobotic Drug Delivery. *Advanced Healthcare Materials* **2013,** *2*, 1037.

304. Cheong, M.; Zhitomirsky, I. Electrodeposition of Alginic Acid and Composite Films. *Colloids and Surfaces a-Physicochemical and Engineering Aspects* **2008,** *328*, 73.

305. Ma, R.; Epand, R. F.; Zhitomirsky, I. Electrodeposition of Hyaluronic Acid and Hyaluronic Acid-Bovine Serum Albumin Films from Aqueous Solutions. *Colloids and Surfaces B-Biointerfaces* **2010,** *77*, 279.

306. Liu, C. H.; Guo, X. L.; Cui, H. T.; Yuan, R. An Amperometric Biosensor Fabricated from Electro-Co-Deposition of Sodium Alginate and Horseradish Peroxidase. *Journal of Molecular Catalysis B-Enzymatic* **2009,** *60*, 151.

307. Chen, Q.; de Larraya, U. P.; Garmendia, N.; Lasheras-Zubiate, M.; Cordero-Arias, L.; Virtanen, S.; Soccaccini, A. R. Electrophoretic Deposition of Cellulose Nanocrystals (Cns) and Cns/Alginate Nanocomposite Coatings and Free Standing Membranes. *Colloids and Surfaces B-Biointerfaces* **2014,** *118*, 41.

308. Chen, Q.; Li, W.; Goudouria, O. M.; Ding, Y. P.; Cabanas-Polo, S.; Boccaccini, A. R. Electrophoretic Deposition of Antibiotic Loaded Phbv Microsphere-Alginate Composite Coating with Controlled Delivery Potential. *Colloids and Surfaces B-Biointerfaces* **2015,** *130*, 199.

309. Cordero-Arias, L.; Cabanas-Polo, S.; Goudouri, O. M.; Misra, S. K.; Gilabert, J.; Valsami-Jones, E.; Sanchez, E.; Virtanen, S.; Boccaccini, A. R. Electrophoretic Deposition of Zno/Alginate and Zno-Bioactive Glass/Alginate Composite Coatings for Antimicrobial Applications. *Materials Science & Engineering C-Materials for Biological Applications* **2015,** *55*, 137.

310. Cordero-Arias, L.; Cabanas-Polo, S.; Gilabert, J.; Goudouri, O. M.; Sanchez, E.; Virtanen, S.; Boccaccini, A. R. Electrophoretic Deposition of Nanostructured Tio2/Alginate and Tio2-Bioactive Glass/Alginate Composite Coatings on Stainless Steel. *Advances in Applied Ceramics* **2014,** *113*, 42.

311. Deen, I.; Zhitomirsky, I. Electrophoretic Deposition of Composite Halloysite Nanotube-Hydroxyapatite-Hyaluronic Acid Films. *Journal of Alloys and Compounds* **2014,** *586*, S531.

312. Wang, Z. L.; Zhang, X. Q.; Gu, J. M.; Yang, H. T.; Nie, J.; Ma, G. P. Electrodeposition of Alginate/Chitosan Layer-by-Layer Composite Coatings on Titanium Substrates. *Carbohydrate Polymers* **2014,** *103*, 38.

313. Wang, Y.; Pang, X.; Zhitomirsky, I. Electrophoretic Deposition of Chiral Polymers and Composites. *Colloids and Surfaces B-Biointerfaces* **2011,** *87*, 505.

314. Wu, K. M.; Imin, P.; Sun, Y. C.; Pang, X.; Adronov, A.; Zhitomirsky, I. Electrophoretic Deposition of Composite Films from Solutions of Conjugated Polymers and Their Supramolecular Complexes with Carbon Nanotubes. *Materials Letters* **2012,** *67*, 248.

315. Casagrande, T.; Imin, P.; Cheng, F. Y.; Botton, G. A.; Zhitomirsky, I.; Adronov, A. Synthesis and Electrophoretic Deposition of Single-Walled Carbon Nanotube Complexes with a Conjugated Polyelectrolyte. *Chemistry of Materials* **2010,** *22*, 2741.

316. Wang, Y.; Deen, I.; Zhitomirsky, I. Electrophoretic Deposition of Polyacrylic Acid and Composite Films Containing Nanotubes and Oxide Particles. *Journal of Colloid and Interface Science* **2011,** *362*, 367.

317. Yoshioka, T.; Chavez-Valdez, A.; Roether, J. A.; Schubert, D. W.; Boccaccini, A. R. Ac Electrophoretic Deposition of Organic-Inorganic Composite Coatings. *Journal of Colloid and Interface Science* **2013,** *392*, 167.

318. Ammam, M. Electrochemical and Electrophoretic Deposition of Enzymes: Principles, Differences and Application in Miniaturized Biosensor and Biofuel Cell Electrodes. *Biosensors and Bioelectronics* **2014,** *58*, 121.

319. Wang, S. S. V., W.R. Collagen-Enzyme Complex Membranes and Their Performance in Biocatalytic Modules. *Biotechnology and Bioengineering* **1973,** *15*, 93.

320. Im, D. M.; Jang, D. H.; Oh, S. M.; Striebel, C.; Wiemhofer, H. D.; Gauglitz, G.; Gopel, W. Electrodeposited God/Bsa Electrodes - Ellipsometric Study and Glucose-Sensing Behavior. *Sensors and Actuators B-Chemical* **1995,** *24*, 149.

321. Strike, D. J.; Derooij, N. F.; Koudelkahep, M. Electrodeposition of Glucose-Oxidase for the Fabrication of Miniature Sensors. *Sensors and Actuators B-Chemical* **1993,** *13*, 61.

322. Matsumoto, N.; Chen, X. H.; Wilson, G. S. Fundamental Studies of Glucose Oxidase Deposition on a Pt Electrode. *Analytical Chemistry* **2002,** *74*, 362.

323. Chen, X. H.; Matsumoto, N.; Hu, Y. B.; Wilson, G. S. Electrochemically Mediated Electrodeposition/Electropolymerization to Yield a Glucose Microbiosensor with Improved Characteristics. *Analytical Chemistry* **2002,** *74*, 368.

324. Stonehuerner, J. G.; Zhao, J.; Odaly, J. P.; Crumbliss, A. L.; Henkens, R. W. Comparison of Colloidal Gold Electrode Fabrication Methods - the Preparation of a Horseradish-Peroxidase Enzyme Electrode. *Biosensors and Bioelectronics* **1992,** *7*, 421.

325. Palys, B.; Marzec, M.; Rogalski, J. Poly-O-Aminophenol as a Laccase Mediator and Influence of the Enzyme on the Polymer Electrodeposition. *Bioelectrochemistry* **2010,** *80*, 43.

326. Hoshi, T.; Anzai, J.; Osa, T. Electrochemical Deposition of Avidin on the Surface of a Platinum-Electrode for Enzyme Sensor Applications. *Analytica Chimica Acta* **1994,** *289*, 321.

327. Bartlett, P. N.; Cooper, J. M. A Review of the Immobilization of Enzymes in Electropolymerized Films. *Journal of Electroanalytical Chemistry* **1993,** *362*, 1.

328. Iwuoha, E. I.; de Villaverde, D. S.; Garcia, N. P.; Smyth, M. R.; Pingarron, J. M. Reactivities of Organic Phase Biosensors. 2. The Amperometric Behaviour of Horseradish Peroxidase Immobilised on a Platinum Electrode Modified with an Electrosynthetic Polyaniline Film. *Biosensors and Bioelectronics* **1997,** *12*, 749.

329. Rishpon, J.; Gottesfeld, S. Investigation of Polypyrrole Glucose-Oxidase Electrodes by Ellipsometric, Microgravimetric and Electrochemical Measurements. *Biosensors and Bioelectronics* **1991,** *6*, 143.

330. Fortier, G.; Brassard, E.; Belanger, D. Optimization of a Polypyrrole Glucose-Oxidase Biosensor. *Biosensors and Bioelectronics* **1990,** *5*, 473.

331. Wang, J. J.; Myung, N. V.; Yun, M. H.; Monbouquette, H. G. Glucose Oxidase Entrapped in Polypyrrole on High-Surface-Area Pt Electrodes: A Model Platform for Sensitive Electroenzymatic Biosensors. *Journal of Electroanalytical Chemistry* **2005,** *575*, 139.

332. Chiu, J. Y.; Yu, C. M.; Yen, M. J.; Chen, L. C. Glucose Sensing Electrodes Based on a Poly(3,4-Ethylenedioxythiophene)/Prussian Blue Bilayer and Multi-Walled Carbon Nanotubes. *Biosensors and Bioelectronics* **2009,** *24*, 2015.

333. Zhang, Z. E.; Liu, H. Y.; Deng, J. Q. A Glucose Biosensor Based on Immobilization of Glucose Oxidase in Electropolymerized O-Aminophenol Film on Platinized Glassy Carbon Electrode. *Analytical Chemistry* **1996,** *68*, 1632.

334. Malitesta, C.; Palmisano, F.; Torsi, L.; Zambonin, P. G. Glucose Fast-Response Amperometric Sensor Based on Glucose-Oxidase Immobilized in an Electropolymerized Poly(Ortho-Phenylenediamine) Film. *Analytical Chemistry* **1990,** *62*, 2735.

335. Ammam, M.; Fransaer, J. Micro-Biofuel Cell Powered by Glucose/O-2 Based on Electro-Deposition of Enzyme, Conducting Polymer and Redox Mediators: Preparation, Characterization and Performance in Human Serum. *Biosensors and Bioelectronics* **2010,** *25*, 1474.

336. Mignani, A.; Scavetta, E.; Tonelli, D. Electrodeposited Glucose Oxidase/Anionic Clay for Glucose Biosensors Design. *Analytica Chimica Acta* **2006,** *577*, 98.

337. Lim, S. H.; Wei, J.; Lin, J. Y.; Li, Q. T.; KuaYou, J. A Glucose Biosensor Based on Electrodeposition of Palladium Nanoparticles and Glucose Oxidase onto Nafion-Solubilized Carbon Nanotube Electrode. *Biosensors and Bioelectronics* **2005,** *20*, 2341.

338. Gao, Z. Q.; Binyamin, G.; Kim, H. H.; Barton, S. C.; Zhang, Y. C.; Heller, A. Electrodeposition of Redox Polymers and Co-Electrodeposition of Enzymes by Coordinative Crosslinking. *Angewandte Chemie-International Edition* **2002,** *41*, 810.

339. Remirez, C. P.; Caruana, D. J. Immobilisation of Glucose Oxidase in Electrodeposited Copper. *Electrochemistry Communications* **2006,** *8*, 450.

340. Johnson, K. W. Reproducible Electrodeposition of Biomolecules for the Fabrication of Miniature Electroenzymatic Biosensors. *Sensors and Actuators B-Chemical* **1991,** *5*, 85.

341. Kim, C. S.; Oh, S. M. Enzyme Sensors Prepared by Electrodeposition on Platinized Platinum Electrodes. *Electrochimica Acta* **1996,** *41*, 2433.

342. Crumbliss, A. L.; Perine, S. C.; Stonehuerner, J.; Tubergen, K. R.; Zhao, J. G.; Henkens, R. W. Colloidal Gold as a Biocompatible Immobilization Matrix Suitable for the Fabrication of Enzyme Electrodes by Electrodeposition. *Biotechnology and Bioengineering* **1992,** *40*, 483.

343. Ammam, M. Electrophoretic Deposition under Modulated Electric Fields: A Review. *Rsc Advances* **2012,** *2*, 7633.

344. Ammam, M.; Fransaer, J. Ac-Electrophoretic Deposition of Glucose Oxidase. *Biosensors and Bioelectronics* **2009,** *25*, 191.

345. Ammam, M.; Fransaer, J. Two-Enzyme Lactose Biosensor Based on Beta-Galactosidase and Glucose Oxidase Deposited by Ac-Electrophoresis: Characteristics and Performance for Lactose Determination in Milk. *Sensors and Actuators B-Chemical* **2010,** *148*, 583.

346. Ammam, M.; Fransaer, J. Glucose/O2 Biofuel Cell Based on Enzymes, Redox Mediators, and Multiple-Walled Carbon Nanotubes Deposited by Ac-Electrophoresis Then Stabilized by Electropolymerized Polypyrrole. *Biotechnology and Bioengineering* **2012,** *109*, 1601.

347. Ammam, M.; Fransaer, J. Combination of Laccase and Catalase in Construction of H2o2-O-2 Based Biocathode for Applications in Glucose Biofuel Cells. *Biosensors and Bioelectronics* **2013,** *39*, 274.

348. Ammam, M.; Fransaer, J. Ac-Electrophoretic Deposition of Metalloenzymes: Catalase as a Case Study for the Sensitive and Selective Detection of H2o2. *Sensors and Actuators B-Chemical* **2011,** *160*, 1063.

349. Ammam, M.; Fransaer, J. Highly Sensitive and Selective Glutamate Microbiosensor Based on Cast Polyurethane/Ac-Electrophoresis Deposited Multiwalled Carbon Nanotubes and Then Glutamate Oxidase/Electrosynthesized Polypyrrole/Pt Electrode. *Biosensors and Bioelectronics* **2010,** *25*, 1597.

350. Leisk, G. G.; Lo, T. J.; Yucel, T.; Lu, Q.; Kaplan, D. L. Electrogelation for Protein Adhesives. *Advanced Materials* **2010,** *22*, 711.

351. Maniglio, D.; Bonani, W.; Bortoluzzi, G.; Servoli, E.; Motta, A.; Migliaresi, C. Electrodeposition of Silk Fibroin on Metal Substrates. *Journal of Bioactive and Compatible Polymers* **2010,** *25*, 441.

352. Inoue, S.; Tanaka, K.; Arisaka, F.; Kimura, S.; Ohtomo, K.; Mizuno, S. Silk Fibroin of Bombyx Mori Is Secreted, Assembling a High Molecular Mass Elementary Unit Consisting of H-Chain, L-Chain, and P25, with a 6 : 6 : 1 Molar Ratio. *Journal of Biological Chemistry* **2000,** *275*, 40517.

353. Zhou, C. Z.; Confalonieri, F.; Medina, N.; Zivanovic, Y.; Esnault, C.; Yang, T.; Jacquet, M.; Janin, J.; Duguet, M.; Perasso, R.; Li, Z. G. Fine Organization of Bombyx Mori Fibroin Heavy Chain Gene. *Nucleic Acids Research* **2000,** *28*, 2413.

354. Yucel, T.; Kojic, N.; Leisk, G. G.; Lo, T. J.; Kaplan, D. L. Non-Equilibrium Silk Fibroin Adhesives. *Journal of Structural Biology* **2010,** *170*, 406.

355. Lu, Q.; Huang, Y. L.; Li, M. Z.; Zuo, B. Q.; Lu, S. Z.; Wang, J. N.; Zhu, H. S.; Kaplan, D. L. Silk Fibroin Electrogelation Mechanisms. *Acta Biomaterialia* **2011,** *7*, 2394.

356. Kojic, N.; Panzer, M. J.; Leisk, G. G.; Raja, W. K.; Kojic, M.; Kaplan, D. L. Ion Electrodiffusion Governs Silk Electrogelation. *Soft Matter* **2012,** *8*, 6897.

357. Bressner, J. E.; Marelli, B.; Qin, G. K.; Klinker, L. E.; Zhang, Y. J.; Kaplan, D. L.; Omenetto, F. G. Rapid Fabrication of Silk Films with Controlled Architectures Via Electrogelation. *Journal of Materials Chemistry B* **2014,** *2*, 4983.

358. Tabatabai, A. P.; Kaplan, D. L.; Blair, D. L. Rheology of Reconstituted Silk Fibroin Protein Gels: The Epitome of Extreme Mechanics. *Soft Matter* **2015,** *11*, 756.

359. Jose, R. R.; Elia, R.; Tien, L. W.; Kaplan, D. L. Electroresponsive Aqueous Silk Protein as "Smart" Mechanical Damping Fluid. *Acs Applied Materials & Interfaces* **2014,** *6*, 6212.

360. Lin, Y. N.; Xia, X. X.; Shang, K.; Elia, R.; Huang, W. E.; Cebe, P.; Leisk, G.; Omenetto, F.; Kaplan, D. L. Tuning Chemical and Physical Cross-Links in Silk Electrogels for Morphological Analysis and Mechanical Reinforcement. *Biomacromolecules* **2013,** *14*, 2629.

361. Elia, R.; Michelson, C. D.; Perera, A. L.; Brunner, T. F.; Harsono, M.; Leisk, G. G.; Kugel, G.; Kaplan, D. L. Electrodeposited Silk Coatings for Bone Implants. *Journal of Biomedical Materials Research Part B-Applied Biomaterials* **2015,** *103*, 1602.

362. Zhang, Z.; Qu, Y. Y.; Li, X. S.; Zhang, S.; Wei, Q. S.; Shi, Y. S.; Chen, L. L. Electrophoretic Deposition of Tetracycline Modified Silk Fibroin Coatings for Functionlization of Titanium Surfaces. *Applied Surface Science* **2014,** *303*, 255.

363. Sun, J. Q.; Gao, M. Y.; Zhu, M.; Feldmann, J.; Mohwald, H. Layer-by-Layer Depositions of Polyelectrolyte/Cdte Nanocrystal Films Controlled by Electric Fields. *Journal of Materials Chemistry* **2002,** *12*, 1775.

364. Ko, Y. H.; Kim, Y. H.; Park, J.; Nam, K. T.; Park, J. H.; Yoo, P. J. Electric-Field-Assisted Layer-by-Layer Assembly of Weakly Charged Polyelectrolyte Multilayers. *Macromolecules* **2011,** *44*, 2866.

365. Gao, M. Y.; Sun, J. Q.; Dulkeith, E.; Gaponik, N.; Lemmer, U.; Feldmann, J. Lateral Patterning of Cdte Nanocrystal Films by the Electric Field Directed Layer-by-Layer Assembly Method. *Langmuir* **2002,** *18*, 4098.

366. Omura, Y.; Kyung, K. H.; Shiratori, S.; Kim, S. H. Effects of Applied Voltage and Solution Ph in Fabricating Multilayers of Weakly Charged Polyelectrolytes and Nanoparticles. *Industrial & Engineering Chemistry Research* **2014,** *53*, 11727.

367. Shi, L. X.; Lu, Y. X.; Sun, J.; Zhang, J.; Sun, C. Q.; Liu, J. Q.; Shen, J. C. Site-Selective Lateral Multilayer Assembly of Bienzyme with Polyelectrolyte on Ito Electrode Based on Electric Field-Induced Directly Layer-by-Layer Deposition. *Biomacromolecules* **2003,** *4*, 1161.
368. Wu, F. H.; Hu, Z. C.; Wang, L. W.; Xu, J. J.; Xian, Y. Z.; Tian, Y.; Jin, L. T. Electric Field Directed Layer-by-Layer Assembly of Horseradish Peroxidase Nanotubes Via Anodic Aluminum Oxide Template. *Electrochemistry Communications* **2008,** *10*, 630.
369. Zhang, P.; Qian, J. W.; Yang, Y.; An, Q. F.; Liu, X. Q.; Gui, Z. L. Polyelectrolyte Layer-by-Layer Self-Assembly Enhanced by Electric Field and Their Multilayer Membranes for Separating Isopropanol-Water Mixtures. *Journal of Membrane Science* **2008,** *320*, 73.
370. Zhang, P.; Qian, J. W.; An, Q. F.; Liu, X. Q.; Zhao, Q.; Jin, H. T. Surface Morphology and Pervaporation Performance of Electric Field Enhanced Multilayer Membranes. *Journal of Membrane Science* **2009,** *328*, 141.
371. Zamarreno, C. R.; Goicolechea, J.; Matias, I. R.; Arregui, F. J. Laterally Selective Adsorption of Ph Sensing Coatings Based on Neutral Red by Means of the Electric Field Directed Layer-by-Layer Self Assembly Method. *Thin Solid Films* **2009,** *517*, 3776.
372. Zhao, L. L.; Yuan, B. B.; Geng, Y. R.; Yu, C. N.; Kim, N. H.; Lee, J. H.; Li, P. Fabrication of Ultrahigh Hydrogen Barrier Polyethyleneimine/Graphene Oxide Films by Lbl Assembly Fine-Tuned with Electric Field Application. *Composites Part a-Applied Science and Manufacturing* **2015,** *78*, 60.
373. Wang, S. W.; Chen, Z.; Umar, A.; Wang, Y.; Yin, P. G. Electric-Field Induced Layer-by-Layer Assembly Technique with Single Component for Construction of Conjugated Polymer Films. *Rsc Advances* **2015,** *5*, 58499.
374. Ye, J. R.; Chen, L.; Zhang, Y.; Zhang, Q. C.; Shen, Q. Turning the Chitosan Surface from Hydrophilic to Hydrophobic by Layer-by-Layer Electro-Assembly. *Rsc Advances* **2014,** *4*, 58200.
375. Guzman, D.; Isaacs, M.; Osorio-Roman, I.; Garcia, M.; Astudino, J.; Ohlbaum, M. Photoelectrochemical Reduction of Carbon Dioxide on Quantum-Dot-Modified Electrodes by Electric Field Directed Layer-by-Layer Assembly Methodology. *Acs Applied Materials & Interfaces* **2015,** *7*, 19865.
376. Fraaije, J.; Kleijn, J. M.; Vandergraaf, M.; Dijt, J. C. Orientation of Adsorbed Cytochrome-C as a Function of the Electrical Potential of the Interface Studied by Total Internal-Reflection Fluorescence. *Biophysical Journal* **1990,** *57*, 965.
377. Brusatori, M. A.; Van Tassel, P. R. Biosensing under an Applied Voltage Using Optical Waveguide Lightmode Spectroscopy. *Biosensors and Bioelectronics* **2003,** *18*, 1269.

378. Khan, G. F.; Shinohara, H.; Ikariyama, Y.; Aizawa, M. Electrochemical-Behavior of Monolayer Quinoprotein Adsorbed on the Electrode Surface. *Journal of Electroanalytical Chemistry* **1991,** *315*, 263.

379. Morrissey, B. W.; Smith, L. E.; Stromberg, R. R.; Fenstermaker, C. A. Ellipsometric Investigation of Effect of Potential on Blood Protein Conformation and Adsorbance. *Journal of Colloid and Interface Science* **1976,** *56*, 557.

380. Mattson, J. S.; Smith, C. A. Enhanced Protein Adsorption at the Solid-Solution Interface: Dependence on Surface Charge. *Science (New York, N.Y.)* **1973,** *181*, 1055.

381. Kleijn, J. M. Influence of the Electric Potential of the Interface on the Adsorption of Proteins. *Colloids and Surfaces B-Biointerfaces* **1994,** *3*, 91.

382. Barten, D.; Kleijn, J. M.; Stuart, M. A. C. Adsorption of a Linear Polyelectrolyte on a Gold Electrode. *Physical Chemistry Chemical Physics* **2003,** *5*, 4258.

383. Kleijn, J. M.; Barten, D.; Stuart, M. A. C. Adsorption of Charged Macromolecules at a Gold Electrode. *Langmuir* **2004,** *20*, 9703.

384. Bearinger, J. P.; Voros, J.; Hubbell, J. A.; Textor, M. Electrochemical Optical Waveguide Lightmode Spectroscopy (Ec-Owls): A Pilot Study Using Evanescent-Field Optical Sensing under Voltage Control to Monitor Polycationic Polymer Adsorption onto Indium Tin Oxide (Ito)-Coated Waveguide Chips. *Biotechnology and Bioengineering* **2003,** *82*, 465.

385. Ngankam, A. P.; Van Tassel, P. R. In Situ Layer-by-Layer Film Formation Kinetics under an Applied Voltage Measured by Optical Waveguide Lightmode Spectroscopy. *Langmuir* **2005,** *21*, 5865.

386. Dieguez, L.; Darwish, N.; Graf, N.; Voros, J.; Zambelli, T. Electrochemical Tuning of the Stability of Pll/DNA Multilayers. *Soft Matter* **2009,** *5*, 2415.

387. Ngankam, A. P.; Van Tassel, P. R. Continuous Polyelectrolyte Adsorption under an Applied Electric Potential. *Proceedings of the National Academy of Sciences of the United States of America* **2007,** *104*, 1140.

388. Olsen, C.; Van Tassel, P. R. Polyelectrolyte Adsorption Kinetics under an Applied Electric Potential: Strongly Versus Weakly Charged Polymers. *Journal of Colloid and Interface Science* **2009,** *329*, 222.

389. Van Tassel, P. R. Polyelectrolyte Adsorption and Layer-by-Layer Assembly: Electrochemical Control. *Current Opinion in Colloid & Interface Science* **2012,** *17*, 106.

390. Dochter, A.; Garnier, T.; Pardieu, E.; Chau, N. T. T.; Maerten, C.; Senger, B.; Schaaf, P.; Jierry, L.; Boulmedais, F. Film Self-Assembly of Oppositely Charged Macromolecules Triggered by Electrochemistry through a Morphogenic Approach. *Langmuir* **2015,** *31*, 10208.

391. Garnier, T.; Dochter, A.; Chau, N. T. T.; Schaaf, P.; Jierry, L.; Boulmedais, F. Surface Confined Self-Assembly of Polyampholytes Generated from Charge-Shifting Polymers. *Chemical Communications* **2015,** *51*, 14092.

392. Kuo, C. K.; Ma, P. X. Ionically Crosslinked Alginate Hydrogels as Scaffolds for Tissue Engineering: Part 1. Structure, Gelation Rate and Mechanical Properties. *Biomaterials* **2001,** *22*, 511.

393. Shi, X. W.; Tsao, C. Y.; Yang, X. H.; Liu, Y.; Dykstra, P.; Rubloff, G. W.; Ghodssi, R.; Bentley, W. E.; Payne, G. F. Electroaddressing of Cell Populations by Co-Deposition with Calcium Alginate Hydrogels. *Advanced Functional Materials* **2009,** *19*, 2074.

394. Cheng, Y.; Luo, X. L.; Betz, J.; Payne, G. F.; Bentley, W. E.; Rubloff, G. W. Mechanism of Anodic Electrodeposition of Calcium Alginate. *Soft Matter* **2011,** *7*, 5677.

395. Wan, W. F.; Dai, G. L.; Zhang, L. J.; Shen, Y. J. Paper-Based Electrodeposition Chip for 3d Alginate Hydrogel Formation. *Micromachines* **2015,** *6*, 1546.

396. Cheng, Y.; Luo, X. L.; Tsao, C. Y.; Wu, H. C.; Betz, J.; Payne, G. F.; Bentley, W. E.; Rubloff, G. W. Biocompatible Multi-Address 3d Cell Assembly in Microfluidic Devices Using Spatially Programmable Gel Formation. *Lab on a Chip* **2011,** *11*, 2316.

397. Cheng, Y.; Tsao, C. Y.; Wu, H. C.; Luo, X. L.; Terrell, J. L.; Betz, J.; Payne, G. F.; Bentley, W. E.; Rubloff, G. W. Electroaddressing Functionalized Polysaccharides as Model Biofilms for Interrogating Cell Signaling. *Advanced Functional Materials* **2012,** *22*, 519.

398. Ozawa, F.; Ino, K.; Arai, T.; Ramon-Azcon, J.; Takahashi, Y.; Shiku, H.; Matsue, T. Alginate Gel Microwell Arrays Using Electrodeposition for Three-Dimensional Cell Culture. *Lab on a Chip* **2013,** *13*, 3128.

399. Yang, X. H.; Kim, E.; Liu, Y.; Shi, X. W.; Rubloff, G. W.; Ghodssi, R.; Bentley, W. E.; Pancer, Z.; Payne, G. F. In-Film Bioprocessing and Immunoanalysis with Electroaddressable Stimuli-Responsive Polysaccharides. *Advanced Functional Materials* **2010,** *20*, 1645.

400. Garcia-Torres, J.; Gispert, C.; Gomez, E.; Valles, E. Alginate Electrodeposition onto Three-Dimensional Porous Co-Ni Films as Drug Delivery Platforms. *Physical Chemistry Chemical Physics* **2015,** *17*, 1630.

401. Ozawa, F.; Ino, K.; Takahashi, Y.; Shiku, H.; Matsue, T. Electrodeposition of Alginate Gels for Construction of Vascular-Like Structures. *Journal of Bioscience and Bioengineering* **2013,** *115*, 459.

402. Betz, J. F.; Cheng, Y.; Tsao, C. Y.; Zargar, A.; Wu, H. C.; Luo, X. L.; Payne, G. F.; Bentleyad, W. E.; Rubloff, G. W. Optically Clear Alginate Hydrogels for Spatially Controlled Cell Entrapment and Culture at Microfluidic Electrode Surfaces. *Lab on a Chip* **2013,** *13*, 1854.

403. Huang, S. H.; Chu, H. T.; Liou, Y. M.; Huang, K. S. Light-Addressable Electrodeposition of Magnetically-Guided Cells Encapsulated in Alginate Hydrogels for Three-Dimensional Cell Patterning. *Micromachines* **2014,** *5*, 1173.

404. Cosnier, S. Biomolecule Immobilization on Electrode Surfaces by Entrapment or Attachment to Electrochemically Polymerized Films. A Review. *Biosensors and Bioelectronics* **1999,** *14*, 443.

405. Ahuja, T.; Mir, I. A.; Kumar, D.; Rajesh. Biomolecular Immobilization on Conducting Polymers for Biosensing Applications. *Biomaterials* **2007,** *28*, 791.

406. Schuhmann, W. Conducting Polymer Based Amperometric Enzyme Electrodes. *Mikrochimica Acta* **1995,** *121*, 1.

407. Waltman, R. J.; Bargon, J. Electrically Conducting Polymers - a Review of the Electropolymerization Reaction, of the Effects of Chemical-Structure on Polymer Film Properties, and of Applications Towards Technology. *Canadian Journal of Chemistry-Revue Canadienne De Chimie* **1986,** *64*, 76.

408. Wojcik, K.; Iwan, A. Electrochemical Polymerization of Polymers for Photovoltaic Cell Applications. *Polimery* **2016,** *61*, 239.

409. Plamper, F. A. Polymerizations under Electrochemical Control. *Colloid and Polymer Science* **2014,** *292*, 777.

410. Rydzek, G.; Thomann, J. S.; Ben Ameur, N.; Jierry, L.; Mesini, P.; Ponche, A.; Contal, C.; El Haitami, A. E.; Voegel, J. C.; Senger, B.; Schaaf, P.; Frisch, B.; Boulmedais, F. Polymer Multilayer Films Obtained by Electrochemically Catalyzed Click Chemistry. *Langmuir* **2010,** *26*, 2816.

411. Li, M.; Ishihara, S.; Akada, M.; Liao, M. Y.; Sang, L. W.; Hill, J. P.; Krishnan, V.; Ma, Y. G.; Ariga, K. Electrochemical-Coupling Layer-by-Layer (Ecc-Lbl) Assembly. *Journal of the American Chemical Society* **2011,** *133*, 7348.

412. Li, M.; Ishihara, S.; Ji, Q. M.; Ma, Y. G.; Hill, J. P.; Ariga, K. Electrochemical Coupling Layer-by-Layer (Ecc-Lbl) Assembly in Patterning Mode. *Chemistry Letters* **2012,** *41*, 383.

413. Gu, C.; Zhang, Z. B.; Sun, S. H.; Pan, Y. Y.; Zhong, C. M.; Lv, Y.; Li, M.; Ariga, K.; Huang, F.; Ma, Y. G. In Situ Electrochemical Deposition and Doping of C-60 Films Applied to High-Performance Inverted Organic Photovoltaics. *Advanced Materials* **2012,** *24*, 5727.

414. Rydzek, G.; Ji, Q. M.; Li, M.; Schaaf, P.; Hill, J. P.; Boulmedais, F.; Ariga, K. Electrochemical Nanoarchitectonics and Layer-by-Layer Assembly: From Basics to Future. *Nano Today* **2015,** *10*, 138.

415. Rydzek, G.; Jierry, L.; Parat, A.; Thomann, J. S.; Voegel, J. C.; Senger, B.; Hemmerle, J.; Ponche, A.; Frisch, B.; Schaaf, P.; Boulmedais, F. Electrochemically Triggered Assembly of Films: A One-Pot Morphogen-Driven Buildup. *Angewandte Chemie-International Edition* **2011,** *50*, 4374.

416. Kolb, H. C.; Finn, M. G.; Sharpless, K. B. Click Chemistry: Diverse Chemical Function from a Few Good Reactions. *Angewandte Chemie-International Edition* **2001,** *40*, 2004.

417. Rydzek, G.; Polavarapu, P.; Rios, C.; Tisserant, J. N.; Voegel, J. C.; Senger, B.; Lavalle, P.; Frisch, B.; Schaaf, P.; Boulmedais, F.; Jierry, L. Morphogen-Driven Self-Construction of Covalent Films Built from Polyelectrolytes and Homobifunctional Spacers: Buildup and Ph Response. *Soft Matter* **2012,** *8*, 10336.

418. Hu, L. J.; Zhao, P. K.; Deng, H. B.; Xiao, L.; Qin, C. Q.; Du, Y. M.; Shi, X. W. Electrical Signal Guided Click Coating of Chitosan Hydrogel on Conductive Surface. *Rsc Advances* **2014,** *4*, 13477.

419. Rydzek, G.; Parat, A.; Polavarapu, P.; Baehr, C.; Voegel, J. C.; Hemmerle, J.; Senger, B.; Frisch, B.; Schaaf, P.; Jierry, L.; Boulmedais, F. One-Pot Morphogen Driven Self-Constructing Films Based on Non-Covalent Host-Guest Interactions. *Soft Matter* **2012,** *8*, 446.

420. Rydzek, G.; Garnier, T.; Schaaf, P.; Voegel, J. C.; Senger, B.; Frisch, B.; Haikel, Y.; Petit, C.; Schlatter, G.; Jierry, L.; Boulmedais, F. Self-Construction of Supramolecular Polyrotaxane Films by an Electrotriggered Morphogen-Driven Process. *Langmuir* **2013,** *29*, 10776.

421. Gray, K. M.; Liba, B. D.; Wang, Y. F.; Cheng, Y.; Rubloff, G. W.; Bentley, W. E.; Montembault, A.; Royaud, I.; David, L.; Payne, G. F. Electrodeposition of a Biopolymeric Hydrogel: Potential for One-Step Protein Electroaddressing. *Biomacromolecules* **2012,** *13*, 1181.

CHAPTER 2: MATERIAL AND METHODS

CHAPTER 2: MATERIAL AND METHODS

Summary

2.1 Material and sample preparation

All the solutions were prepared using ultra-pure water with a resistivity of 18.2 MΩ.cm (Milli-Q-plus system, Millipore).

2.1.1 Low molecular weight molecules

2.1.1.1 Commercial molecules

Sodium nitrate, potassium hexafluorophosphate (KPF6), potassium hexacyanoferrate (II), iron (II) sulfate heptahydrate, 4-(2-Hydroxyethyl) piperazine-1-ethanesulfonic acid (HEPES), ethylenediaminetetraacetic acid disodium salt dehydrate (EDTA) and rosmarinic acid (RA) were purchased from Sigma-Aldrich. Tannic acid (TA) and gallic acid (GA) were purchased from Alfa-Aesar. Table 2.1 gives a view of the structures of all the molecules used.

Tannic acid and iron (II) sulfate heptahydrate were prepared at 1 mg/mL in 150 mM KPF6 solution at pH = 3, unless otherwise stated. Rosmarinic acid, gallic acid were prepared at 1.3 mg/mL and 5.3 mg/mL in 150 mM KPF6 solution at pH = 3 respectively. 100 mM EDTA solutions were prepared in 150 mM KPF6 solution at pH = 3 or pH = 7.4.

Name	Formula	Molecular weight
Sodium nitrate	$NaNO_3$	Mw = 84.99 g/mol
Potassium hexafluorophosphate	KPF_6	Mw = 184.06 g/mol
Potassium hexacyanoferrate (II)	$K_4Fe(CN)_6 \cdot 3H_2O$	Mw = 422.41 g/mol
Iron(II) sulfate heptahydrate	$FeSO_4 \cdot 7H_2O$	Mw = 278.01 g/mol
4-(2-Hydroxyethyl) piperazine-1-ethanesulfonic acid (HEPES)	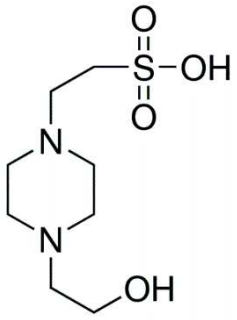	Mw = 238.30 g/mol
Ethylenediaminetetraacetic acid disodium salt dehydrate (EDTA)	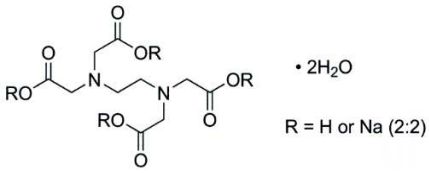	Mw = 372.24 g/mol
Tannic acid (TA)	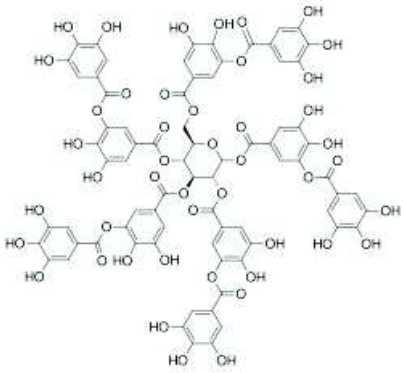	Mw = 1701.23 g/mol
Rosmarinic acid (RA)	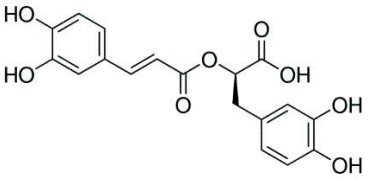	Mw = 360.31 g/mol
Gallic acid (GA)	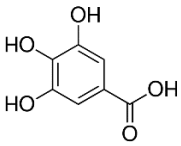	Mw = 170.12 g/mol

Table 2.1: *Molecular representation of the low molecular weight commercial molecules used during the PhD.*

2.1.1.2 Synthesized molecules

Bis-catechol

Bis-catechol is an original molecule displaying a catechol group at each end of a linear oligoethylene oxide chain, prepared in five steps from dopamine and 3,6,9-trioaundecandioic acid (TUDA) by Dr. Tony Garnier (post doctorant). The general synthetic pathway to get bis-catechol is shown in Figure 2.1.

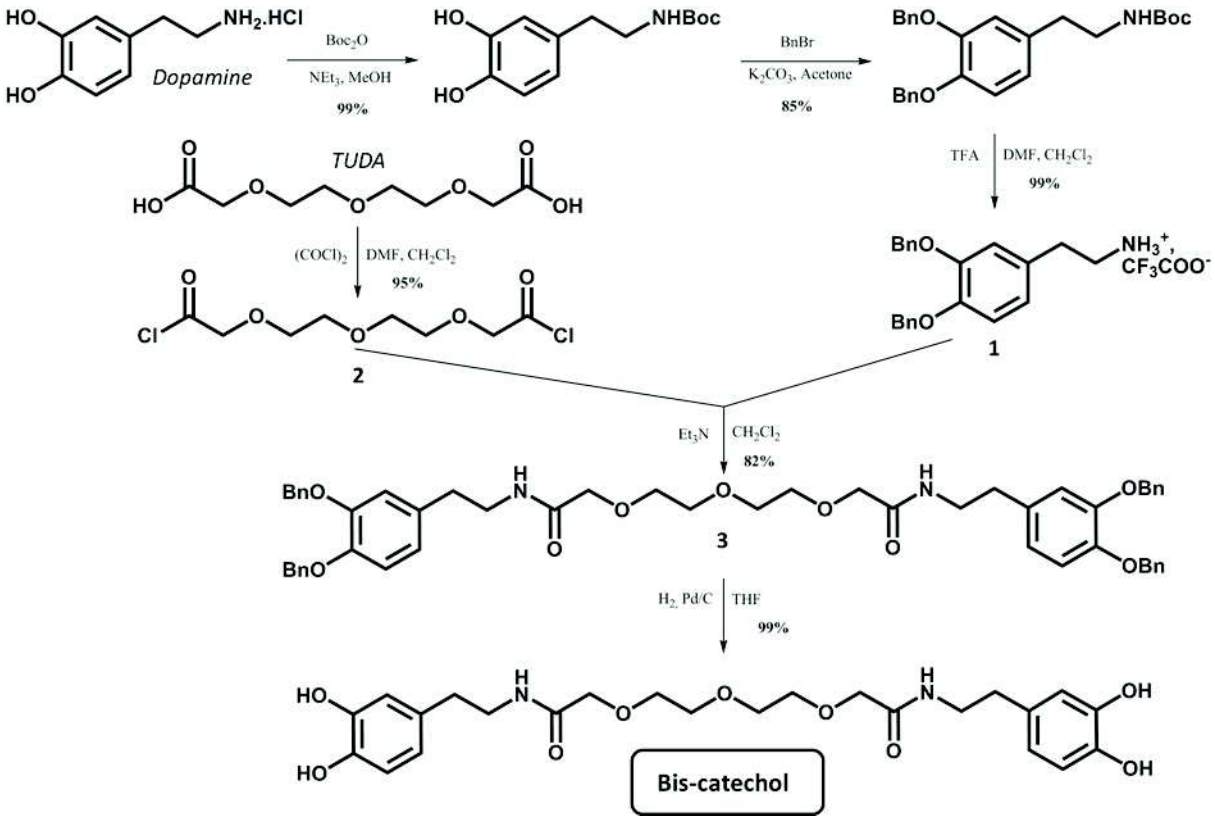

Figure 2.1: *Synthetic pathway to prepare bis-catechol in five steps from commercially available dopamine and TUDA.*

General information: All starting materials were obtained from commercial suppliers and were used without further purification. Dopamine hydrochloride was purchased from Aldrich. TUDA was purchased from Iris Biotech. All dried solvents were purchased from Acros Organics. ^{1}H NMR and ^{13}C NMR spectra were recorded on Bruker Advance DPX400 (400 MHz) spectrometers. The NMR chemical shifts are reported in ppm relative to tetramethylsilane (DMSO-*d*6, CDCl3 or MeO-d_4) or *tert*-butanol (1.24 ppm) in D_2O (s: singlet, t: triplet, q: quadruplet, dd: doublet of doublet, m: multiplet, br: broad). The ^{1}H NMR chemical shifts in deuterated water are reported in ppm relative to tert-butanol (1.24 ppm). Infrared spectra were obtained on a Vertex 70 spectrometer (Bruker, Germany). The spectra were recorded in the Attenuated Total Reflection (ATR) mode. Merck RP-18 F254S plates were used

for analytical thin layer chromatography. Silica gel 60 (particle: 40 – 60 μm) was used for flash chromatography. High-resolution mass spectra (HRMS) were recorded with an MicroTOF-Q (BRÜKER) mass spectrometer at the *Service de Spectrométrie de Masse de la Faculté de Chimie (University of Strasbourg)* and are given in m/z.

***N-tert*-Butoxycarbonyl-3,4-dihydroxiphenylethylamine**

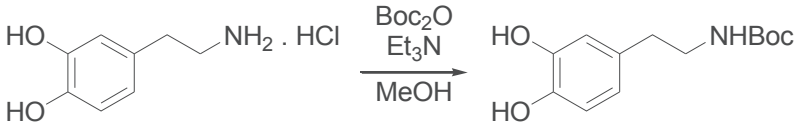

Dopamine hydrochloride (4.00 g, 21.1 mmol, 1.0 eq.) was dissolved in MeOH (100 mL). Ar gas was bubbled through the solution during dissolution to remove oxygen gas (few minutes). Then, Et_3N (3.24 mL, 23.2 mmol, 1.1 eq.) was added followed by Boc_2O (5.06 g, 23.2 mmol, 1.1 eq.). The reaction mixture was stirred under Ar for 1h and the solvent was removed under reduce pressure. The remaning residue was dissolved in $CHCl_3$ (200 mL) and quickly washed with a 1M aqueous HCl (2 × 50 mL) and brine (100 mL). The organic layer was then dried over $MgSO_4$, filtered and evaporated to give the desired product (5.35 g, quantitative yield) as a white solid which was used in the next step without further purification; FTIR (neat, cm^{-1}) 3486, 3375, 3061, 1675; ^{1}H NMR ($CDCl_3$, 400 MHz) δ 1.44 (s, 9H), 2.66 (t, J = 6.9 Hz, 2H), 3.32 (bs, 2H), 6.60 (dd, J = 1.8, 8.0 Hz, 1H), 6.71 (d, J = 1.8 Hz, 1H), 6.79 (d, J = 8.0 Hz, 1H); ^{13}C NMR (CD_3OD, 100 MHz) δ 158.4, 146.2, 144.6, 132.2, 121.1, 116.9, 116.3, 79.9, 43.3, 36.6, 28.8.

***N-tert*-Butoxycarbonyl-3,4-dibenzyloxyphenylethylamine**

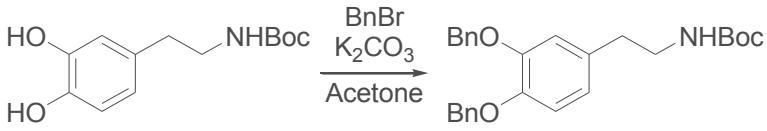

Boc-dopamine (5.35 g, 21.1 mmol, 1.0 eq.) was dissolved in acetone (150 mL) under Ar. Then K_2CO_3 (20.4 g, 147.7 mmol, 7.0 eq.) was added in one portion followed by BnBr (12.6 mL, 105.5 mmol, 5.0 eq.). The flask was wrapped with Al foil and the resulting mixture was stirred under Ar for 15 h. The crude was filtered to remove K_2CO_3 and rinse with additional acetone. The filtrate was evaporated and the residue was purified by recrystallization (AcOEt / *n*-Hex) to give the desired product as a white solid (7.84 g, 85%); FTIR (neat, cm^{-1}) 3378, 3069, 1679; ^{1}H NMR ($CDCl_3$, 400 MHz) δ 1.45 (s, 9H), 2.70 (t, J = 7.0 Hz, 2H), 3.25-3.35 (m, 2H), 4.49 (bs, 1H), 5.13 (s, 2H), 5.14 (s, 2H), 6.70 (dd, J = 1.9, 8.1 Hz, 1H), 6.80 (bs, 1H), 6.88 (d, J = 8.2 Hz, 1H), 7.27-7.47 (m, 10H); ^{13}C NMR ($CDCl_3$, 100 MHz) δ 155.8, 149.1, 147.7, 137.4,

137.3, 132.4, 128.4 (two carbons overlapped), 127.8, 127.7, 127.4, 127.3, 121.7, 116.0, 115.5, 79.2, 71.5, 71.4, 41.8, 35.7, 28.4.

Trifluoroacetate salt of 2-(3,4-bis-benzyloxyphenyl)-ethylamine

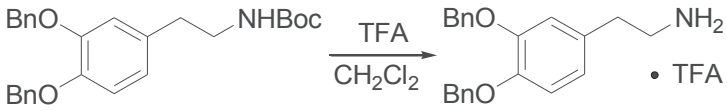

N-tert-Butoxycarbonyl-3,4-dibenzyloxyphenylethylamine (6.74 g, 15.5 mmol, 1.0 eq.) was dissolved in CH_2Cl_2 (40 mL) and treated with TFA (5 mL) for 4h. The resulting reaction mixture was then concentrated under reduce pressure to give the desired product as a colorless oil (7 g, quantitative yield) which was used in the next step without further purification. ^{1}H NMR ($CDCl_3$, 400 MHz) δ 2.79 (t, J = 6.7 Hz, 2H), 3.04-3.15 (m, 2H), 5.10 (s, 4H), 6.68 (dd, J = 2.0, 8.2 Hz, 1H), 6.74 (d, J = 2.0 Hz, 1H), 6.90 (d, J = 8.2 Hz, 1H), 7.27-7.44 (m, 10H).

Trioxaundecanedioyl chloride

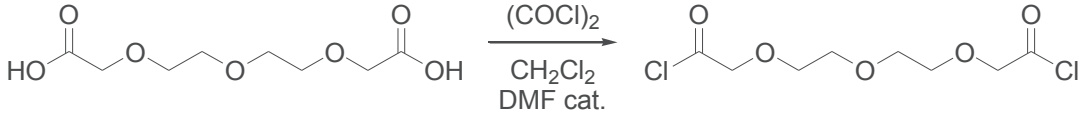

3,6,9-trioxaundecandioic acid (TUDA, 1.57 g, 7.07 mmol, 1.0 eq.) was dissolved in CH_2Cl_2 (20 mL) at room temperature and oxalyl chloride (4.8 mL, 56.54 mmol, 8.0 eq.) was added in one portion. One drop of DMF was added, resulting to the formation of bubbles. The reaction mixture was stirred until no more bubbling (30 min) and evaporated to give the desired product as a pale yellow oil (1.74 g, 95%) which was used in the next step without further purification. ^{1}H NMR ($CDCl_3$, 400 MHz) δ 3.65-3.69 (m, 4H), 3.77-3.80 (m, 4H), 4.50 (s, 4H).

Benzyl protected bis-catechol

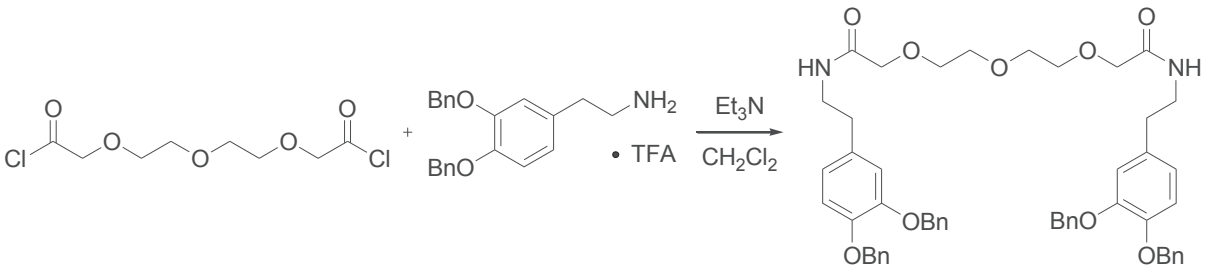

To a stirred cold solution (0 °C) of Trioxaundecanedioyl chloride (1.74 g, 6.72 mmol, 1.0 eq.) in CH_2Cl_2 (15 mL) was added dropwise Et_3N (9.4 mL, 67.2 mmol, 10.0 eq.) and a solution of Trifluoroacetate salt of 2-(3,4-bis-benzyloxyphenyl)-ethylamine (6.61 g, 14.8 mmol, 2.2 eq.) in CH_2Cl_2 (20 mL). The reaction mixture was allowed to warm to room temperature and stirred under Ar overnight. The mixture was quenched with saturated aqueous $NaHCO_3$ (50 mL) and

extracted with CH_2Cl_2 (3 × 40 mL). The combined organic layers were washed with water (50 mL), dried over $MgSO_4$, filtered and evaporated. The resulting oily residue was purified by column chromatography, eluting with CH_2Cl_2 / MeOH (1:0 to 97:3) to give the desired product as a pale orange oil (4.68 g, 82%). FTIR (neat, cm^{-1}); 3346, 3069, 2920, 2866, 1665, 1510, 1453, 1133; ^1H NMR ($CDCl_3$, 400 MHz) δ 2.71 (t, J = 7.3 Hz, 4H), 3.41-3.55 (m, 12H), 3.93 (s, 4H), 5.11 (s, 4H), 5.12 (s, 4H), 6.70 (dd, J = 2.1, 8.1 Hz, 2H), 6.76-6.91 (m, 6H), 7.27-7.49 (m, 20H); ^{13}C NMR ($CDCl_3$, 100 MHz) δ 169.5, 149.1, 147.7, 137.3, 137.2, 132.2, 128.4, 128.4, 127.8, 127.7, 127.32, 127.26, 121.6, 115.8, 115.4, 71.44, 71.37, 70.7, 70.5, 70.1, 40.0, 35.1.

Bis-catechol

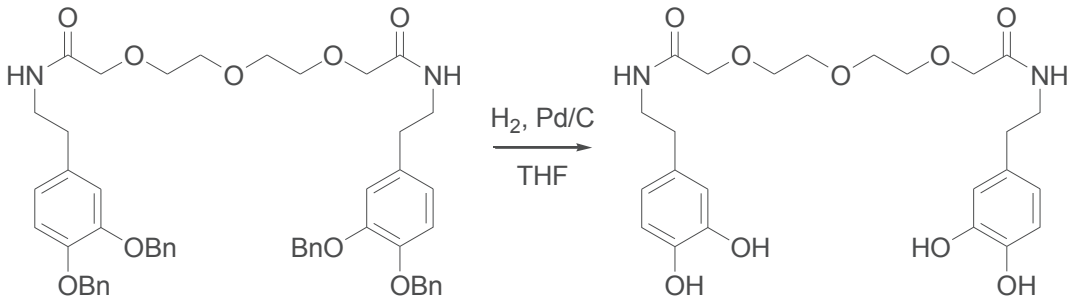

Debenzylation of benzyl protected bis-catechol (4.63 g, 5.43 mmol, 1.0 eq.) in THF (60 mL) was carried out under H_2 atmosphere 24 h at room temperature in the presence of 10 % palladium on carbon (130 mg). The reaction mixture was filtered through Celite and the solid was washed with THF. Evaporation of the filtrate afford the desired product as a white highly hygroscopic solid (2.7 g, quantitative yield). FTIR (neat, cm^{-1}); 3465, 3315, 2926, 1643, 1519, 1441, 1108; ^1H NMR (CD_3OD, 400 MHz) δ 2.65 (t, J = 7.2 Hz, 4H), 3.40 (t, J = 7.1 Hz, 4H), 3.58 (s, 8H), 3.94 (s, 4H), 6.52 (dd, J = 2.1, 8.0 Hz, 2H), 6.64 (d, J = 1.9 Hz, 2H), 6.68 (d, J = 8.0 Hz, 2H); ^{13}C NMR (CD_3OD, 100 MHz) δ 172.5, 146.3, 144.8, 131.8, 121.1, 116.9, 116.4, 71,8, 71.2, 71.1, 41.6, 35.7.

Gallol-dendrimer

1,3,5-tris(prop-2-ynyloxy)benzene

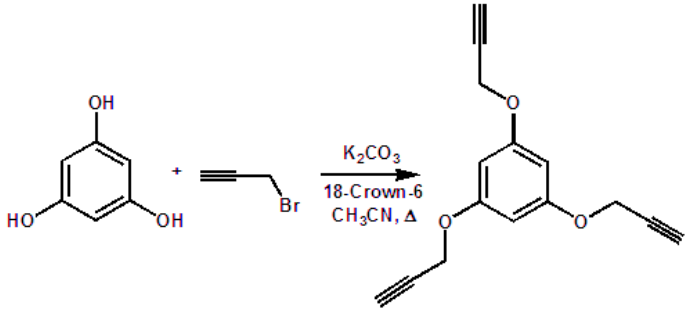

1,3,5-tris(benzyloxy)benzoic acid

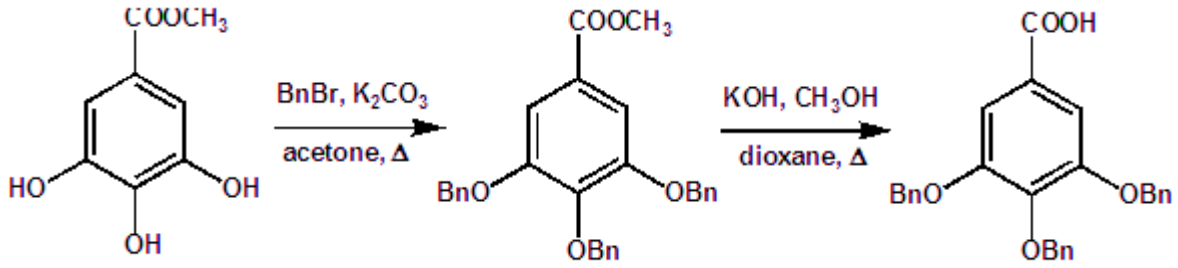

Methyl 1,3,5-tris(benzyloxy)benzoate (1.500 g, 3.30 mmol, 1 eq.) was dissolved in CH_3OH/dioxane 1:1 (80 mL) and KOH (1.85 g, 33.00 mmol, 10 eq.) was added in small portions. The reaction mixture was stirred at reflux for 1 hour. The solvents were removed, the residue dissolved in water (60 mL), the organic layer was extracted with ethyl acetate (3 x 50 mL), washed with aqueous 1M HCl (30 mL), brine (3 x 50 mL), dried with $MgSO_4$, filtered and evaporated. The desired product was obtained as white solid (1.400 g, 97% yield) and used without further purification. ^{1}H NMR ($CDCl_3$, 400 MHz) δ 5.14 (brs, 6H), 7.26 (brs, 2H), 7.32-7.43 (m, 15H). ^{13}C NMR ($CDCl_3$, 100 MHz) δ 71.50, 75.39, 109.94, 124.34, 127.70, 128.20, 128.29, 128.43, 128.73, 128.79, 136.79, 137.62, 143.48, 152.83, 171.20.

N-(2-{2-[2-(2-{2-[2-(2-Azido-ethoxy)-ethoxy]-ethoxy}-ethoxy)-ethoxy]-ethoxy}-ethyl)-3,4,5-tris-benzyloxy-benzamide

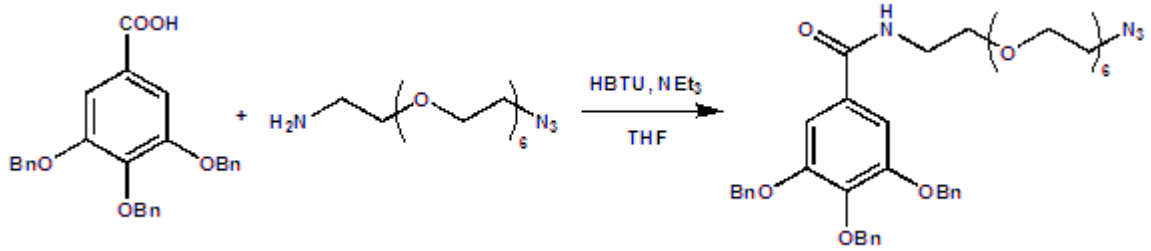

1,3,5-tris(benzyloxy)benzoic acid (0.400 g, 0.90 mmol, 1.1 eq.), and H_2N-PEG_{11}-N_3 (0.290 g, 0.82 mmol, 1.0 eq.) were dissolved in anhydrous THF (20 mL). The solution was kept at T = 0°C and Et_3N (0.164 g, 228 µL, 1.64 mmol, 2.0 eq.) was slowly added. Then 2-(1H-Benzotriazol-1-yl)-1,1,3,3-tetramethyluronoium hexafluorphosphate (HBTU, 0.466 g, 1.23 mmol, 1.5 eq.) was added in small portions. The reaction mixture was stirred at r.t. for 24 hrs. Then the solvent was removed by evaporation and the resulting oil was purified by SiO_2 column chromatography, eluting with CH_2Cl_2 / CH_3OH 90:10 to give the desired product as a colorless oil (0.475 g, 75%). ^{1}H NMR ($CDCl_3$, 400 MHz) δ 3.33 (dd, $J_1 = J_2 = 5.0$ Hz, 2H), 3.55-3.65 (m, 26H), 3.55 (brs, 4H), 3.58 (m, 10H), 3.61 (m, 6H), 3.63 (m, 6H), 5.07 (s, 2H), 5.13 (s, 4H),

7.17 (s, 2H), 7.24 (m, 3H), 7.35 (m, 8H), 7.42 (m, 4H). ^{13}C NMR ($CDCl_3$, 100 MHz) □□ 50.89, 70.18, 70.33, 70.48, 70.71, 70.76, 71.64, 75.39, 107.38, 127.80, 128.14, 128.20, 128.75, 130.27, 137.07, 137.78, 141.41, 152.96, 167.34.

1,3,5-Tris-{1-[2-(2-{2-[2-(2-{2-[2-(3,4,5-Tris-benzyloxy-benzoylamino)-ethoxy]-ethoxy}-ethoxy)-ethoxy]-ethoxy}-ethoxy)-ethyl]-1H-[1,2,3]triazol-4-ylmethoxy}-benzene

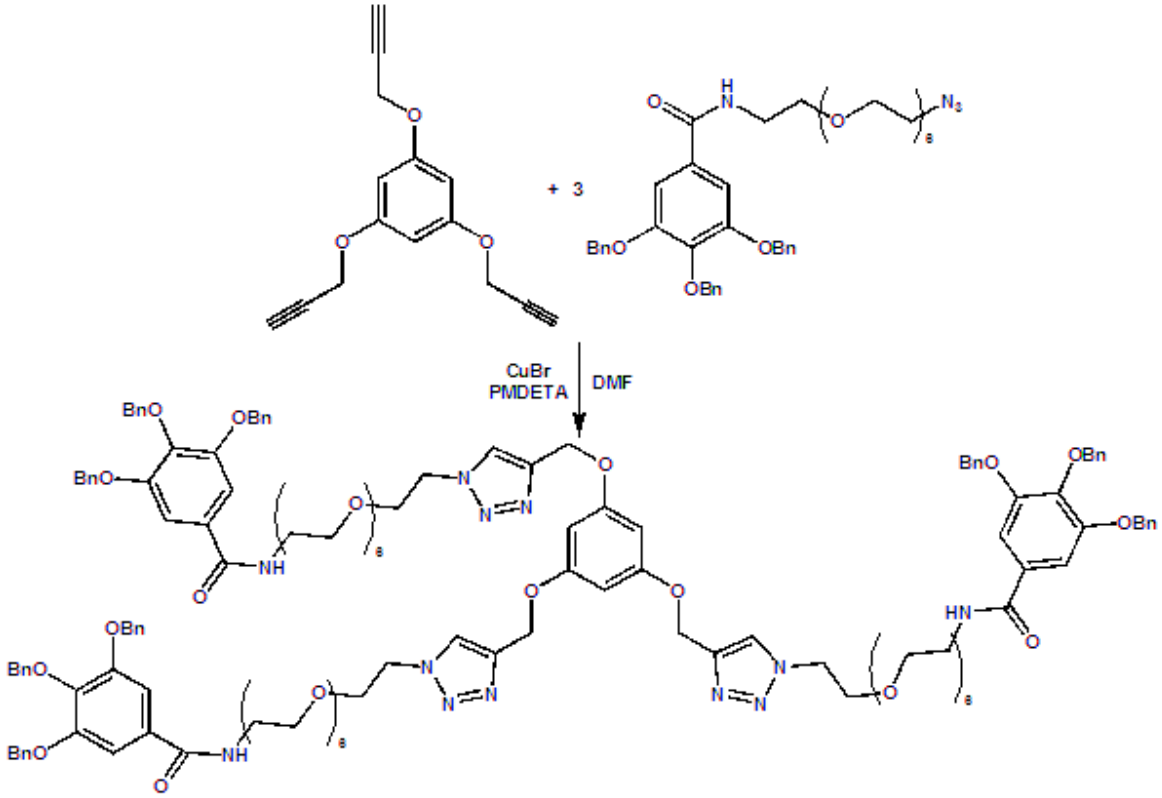

1,3,5-tris-(prop-2-ynyloxy)benzene (0.048 g, 0.20 mmol, 1 eq.) and N-(2-{2-[2-(2-{2-[2-(2-Azido-ethoxy)-ethoxy]-ethoxy}-ethoxy)-ethoxy]-ethoxy}-ethyl)-3,4,5-tris-benzyloxy-benzamide (0.470 mg, 0.60 mmol, 3 eq.) were dissolved in DMF (15 mL). Pentamethyldiethylendiamine (PMDETA, 0.098 g, 0.60 mmol, 3 eq.) and CuBr (0.086 mg, 0.60 mmol, 3 eq.) were added at room temperature and the reaction mixture was stirred at room temperature for 20 hrs. The solvent was then evaporated and THF (20 mL) was added. The mixture was stirred with Dowex, (2.00 g) filtered through a celite path and evaporated. The resulting oil was purified by SiO_2 column chromatography, eluting with CH_2Cl_2 / CH_3OH 95:5 to give the desired product as a colorless oil (0.337 g, 65%). ^{1}H NMR ($CDCl_3$, 400 MHz) δ 3.51-3.64 (m, 72H), 3.79 (dd, $J_1 = J_2 = 5.0$ Hz, 6H), 4.47 (dd, $J_1 = J_2 = 5.0$ Hz, 6H), 5.06 (s, 6H), 5.09 (s, 6H), 5.12 (s, 6H), 6.27, (s, 3H), 7.20 (brs, 6H), 7.24 (brs, 3H), 7.31-7.42 (m, 45H), 7.79 (s, 3H).

Gallol-dendrimer: 1,3,5-Tris-{1-[2-(2-{2-[2-(2-{2-[2-(3,4,5-Trihydroxy-benzoylamino)-ethoxy]-ethoxy}-ethoxy)-ethoxy]-ethoxy}-ethoxy)-ethyl]-1H-[1,2,3]triazol-4-ylmethoxy}-benzene

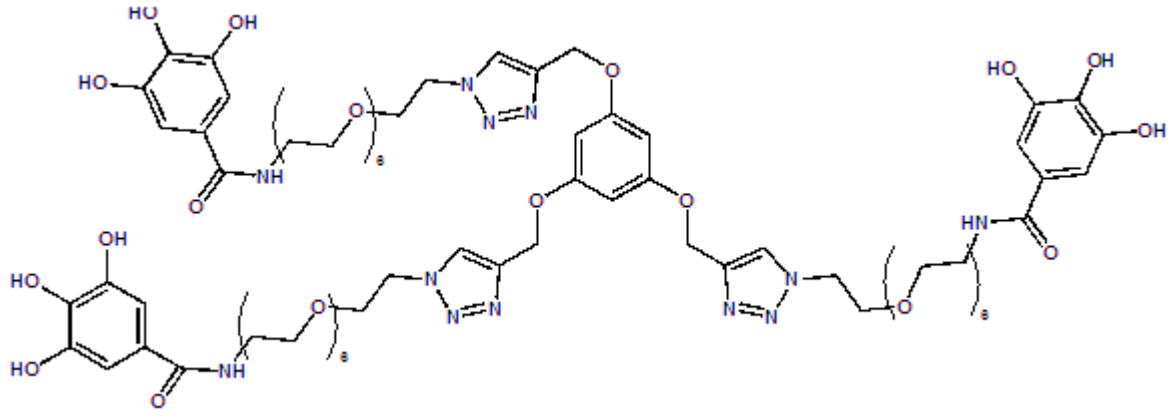

1,3,5-Tris-{1-[2-(2-{2-[2-(2-{2-[2-(3,4,5-Tris-benzyloxy-benzoylamino)-ethoxy]-ethoxy}-ethoxy)-ethoxy]-ethoxy}-ethoxy)-ethyl]-1H-[1,2,3]triazol-4-ylmethoxy}-benzene (0.320 g, 0.12 mmol) was dissolved in CH_3OH/THF 9/1 mixture (25 mL). Pd,C 10% (0.030 g) was added and the reaction mixture was purged with H_2. The mixture was kept stirring under H_2 (ca. 1 atm.) for 18 hrs. The mixture was then filtered on a celite path and the solvents were evaporated. The resulting oil was purified by SiO_2 column chromatography, eluting with CH_2Cl_2 / CH_3OH / AcOH 4:1:0.5 to give the desired product as an oil (0.147 g, 70%). ^1H NMR (CD_3OD, 400 MHz) δ 3.57 (m, 72H), 3.88 (dd, $J_1 = J_2 = 5.0$ Hz, 6H), 4.59 (dd, $J_1 = J_2 = 5.0$ Hz, 6H), 5.13 (s, 6H), 6.34 (s, 3H), 6.89 (s, 6H), 8.11 (s, 3H).

HRMS (ESI) *m/z* calculated for $C_{78}H_{115}N_{12}O_{33}$ $(M+H)^+$ 1747.768, found: 1747.770

2.1.2 Polymers

Poly(allylamine hydrochloride) (PAH) and poly(diallyldimethylammonium chloride) (PDADMA) were purchased from Sigma-Aldrich. Table 2.2 represents the structures and gives the molecular weight of each polymer used. For all polymers, the molecular weights Mw were supplied by the provider. PAH has a pKa of 8.5 and PDADMA is a strong polycation. Polymers were solubilized in aqueous solution of 10 mM HEPES – 150 mM $NaNO_3$ pH=7.4 buffer at a concentration 1 mg/mL, unless otherwise stated.

Name	Formula	Molecular weight
Poly(allylamine hydrochloride) (PAH)	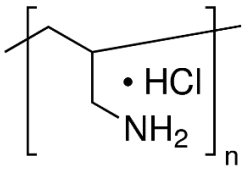	Mw : 15000 g/mol 58000 g/mol
Poly(diallyldimethylammonium chloride) (PDADMA)	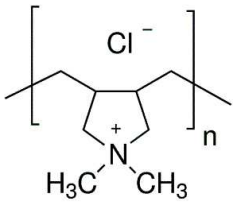	Mw : 90000 g/mol

Table 2.2: *Molecular representation of poly(allylamine hydrochloride) and poly(diallyldimethylammonium chloride).*

2.1.3 Enzyme

Alkaline phosphatase (AP) with an isoelectric point between 4.4 and 5.8 was purchased from Tokyo Chemical Industry.

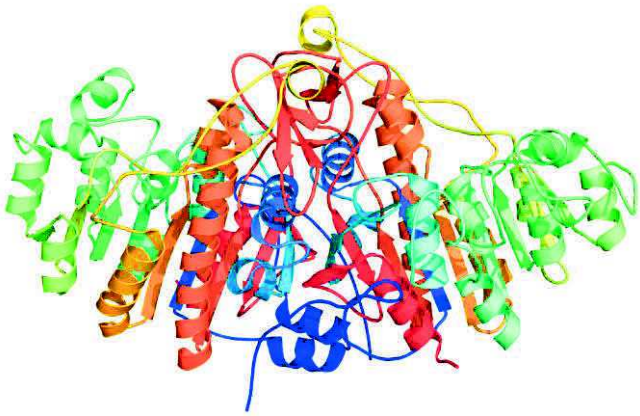

Figure 2.2: *Model representation of alkaline phosphatase*

2.2 Methods

2.2.1 Electrochemical Methods

Different electrochemical methods have been used in order to trigger the self-construction of films from an electrode: cyclic voltammetry (CV), chronopotentiometry and chronoamperometry. All these methods are described in the following paragraph.

2.2.1.1 Three-electrode electrochemical set up

In order to perform electrochemical measurements in our system, the quartz crystal microbalance has been coupled with an electrochemical workstation (CHI660E) and a three-electrode set up. We first describe a classic set up in electrochemistry which consists of a working electrode, a reference electrode and an auxiliary electrode (Figure 2.3).

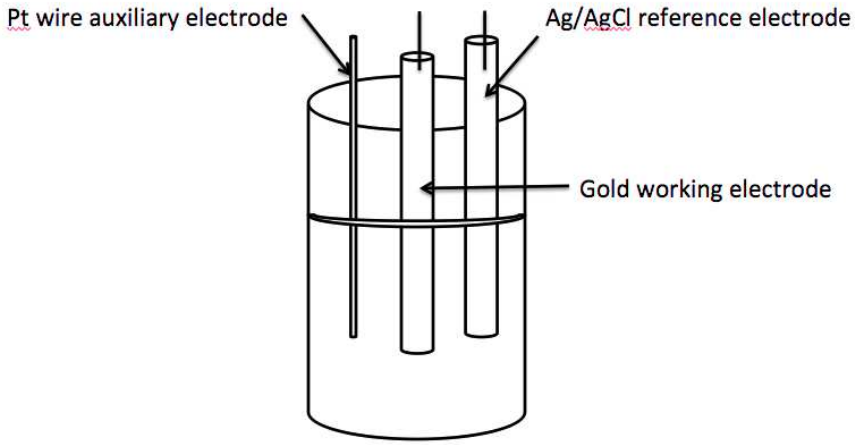

Figure 2.3: *A typical 3-cell electrode used in cyclic voltammetry*

Working electrode: the WE is made of a quartz crystal coated on both side with a conductive layer, gold or indium tin oxide (ITO) in our case. More precisely the working electrode is the top layer of the crystal which is in contact with the solution containing the electro-active species.

Reference electrode: the RE usually contains a redox couple which has a stable and well-known potential. Thus, when a potential difference is measured, knowing the reference electrode potential, one obtains the potential of the working electrode. It is conventionally accepted that redox couple $2H^+/H_2$ has 0V standard potential (at pH=0 and $p(H_2)$=1 atm) and the potential of other redox reactions are referred to it. This redox couple is defined as *standard hydrogen electrode (SHE)*. However, it is rarely used as RE due to its complicated set up. For this work, we used a silver chloride electrode based on the *Ag/AgCl* redox couple as reference electrode. Its standard potential is 0.208 V SHE at 25°C (vs hydrogen electrode). Hence, all the potential in the manuscript are referred to Ag/AgCl electrode.

Counter electrode: the CE is made of platinum in our case and its role is to provide the second electrode to pass the current in WE-CE circuit, i.e. to polarize WE (note that no current can be passed in WE-RE circuit in order to keep the potential of RE constant). In galvanostatic/galvanodynamic methods, the current passes through WE-CE circuit and the

potential of WE is measured from WE-RE voltage. In potentiostatic/potentiodynamic methods, the potential of WE (controlled via WE-RE voltage) is adjusted to a certain value by passing a current in WE-CE circuit.

2.2.1.2 Cyclic voltammetry

Cyclic voltammetry is a method that uses the three electrode set-up in order to characterize oxydo-reduction reactions at electrode/electrolyte interface. A potential of WE is changed linearly in time and the current flowing through WE is measured as a function of the applied potential. The measured current contains the contribution from the charging of interfacial layer by adsorbing/desorbing electrolyte ions (forming so-called interfacial double layer, see also chapter 2.2.1.3). When an electrochemical reaction (oxidation or reduction) occurs at the WE, an additional current is recorded.

The range of potentials (E_i and E_f) and the scan rate of the potential $v = \frac{|dE|}{dt}$ are chosen by the operator. The cycle of potential applied is a triangular signal represented on Figure 2.4. One cycle can be divided into two steps: a first step where the potential increases linearly from an initial potential E_i to a final potential E_f and a second step where it decreases linearly from E_f to E_i. The number of cycles is also chosen by the operator.

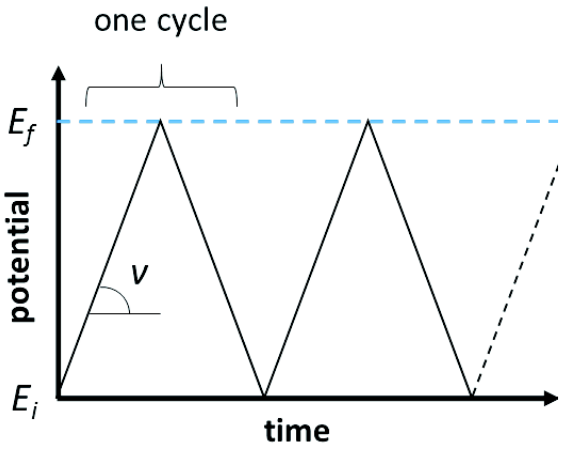

Figure 2.4: *Potential cycles applied at the working electrode as a function of time.*

A simple redox system can be described by the following chemical equation:

$$x \times Ox + n \times e^{-} = y \times Red$$

Ox and *Red* are respectively the oxidizing and the reductive species, *x* and *y* are the stoichiometric numbers and *n* represents the number of electron involved in the reaction.

Oxidation and reduction reactions on the WE induce a current, and the intensity of this current depends on the surface area of the WE and on the rate of this electrochemical reaction. Usually, the current density $J = \frac{i}{S}$ is used in order to become independent of the area of the surface (S).

A typical *i(E)* curve called "voltammogram" monitored during a cyclic voltammetry experiment for a reversible redox couple is represented in Figure 2.5. Several conventions exist for the presentation of a voltammogram: in this work, in accordance with the IUPAC convention the electric potential varies from negative (left) to positive (right) and the current is taken negative for a reduction reaction and positive for an oxidation.

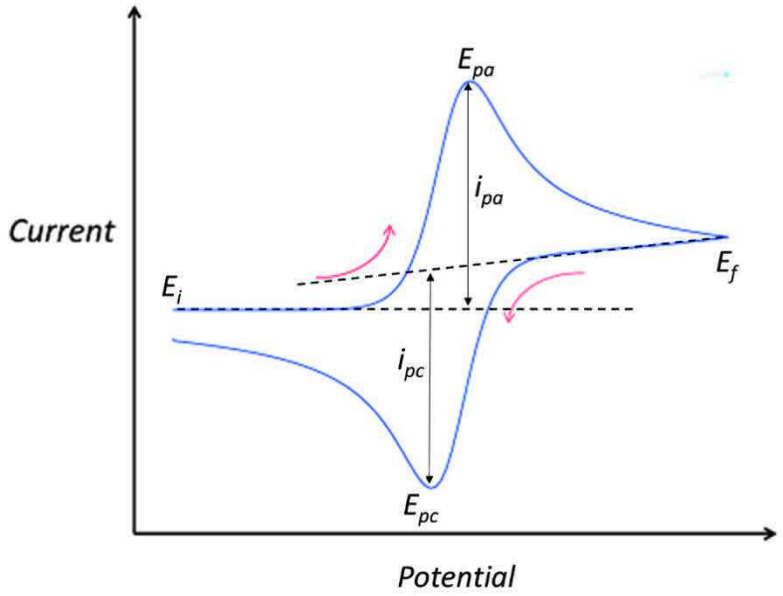

Figure 2.5: *Typical voltammogram of a reversible system displaying one oxidation peak E_{pa} of intensity i_{pa} and one reduction peak E_{pc} of intensity i_{pc}.*

The potential ranges from a minimum value E_i to a maximum value E_f. For the reversible redox reaction introduced above, two current peaks are observed: a first one at a potential E_{pa} with an intensity i_{pa} corresponding to an oxidation and a second one at a potential E_{pc} with an intensity i_{pc} corresponding to a reduction. The redox potential characteristic of the redox couple is determined with the following equation:

$$E_{1/2} = \frac{E_{pa} + E_{pc}}{2}$$

The equilibrium potential for a redox couple is given by the Nernst equation:

$$E = E_0 + \frac{RT}{nF} \ln\left(\frac{[Ox]^x}{[Red]^y}\right)$$

Where E, the equilibrium potential is in V, E_0 is the standard potential characteristic of the redox couple (i.e. potential of redox couple with standard concentrations of Ox and Red) in V, R the perfect gas constant, T the temperature in K, n the number of the electrons involved in the electrochemical reaction, F the Faraday constant in C/mol and *[Ox]* and *[Red]* are respectively the concentrations of the oxidizing and the reducing species.

The oxidation reaction corresponds to an electronic transfer of an electroactive molecule in the vicinity of the electrode surface. The current intensity observed in Figure 2.5 decreases beyond the E_{pa} potential. This is due to a diffusion limitation of the *Red*: it is consumed much faster than it diffuses toward the electrode. Thus, when the potential exceeds E_{pa}, its concentration at the interface decreases and the current decreases too even if the reaction is more favored. The same mechanism happens in the second half cycle with the oxidized molecule.

The voltammogram allows the qualitative evaluation of the electron transfer reversibility: it can be irreversible, quasi-reversible or reversible. Reversible electron transfer reaction is the case of fast electrochemical reaction; the shape of voltammogram is determined in this case by the conditions of mass transport of Red and Ox species. This results in a symmetrical voltammogram (for the same concentrations of Red and Ox) with peaks potential separation exactly close to $\frac{RT}{nF}$. In contrast to this case, if the electron transfer rate is slow, the peaks separation is larger than 0.2 V and the system is called irreversible. Also, if one of the electrochemical processes (reduction or oxidation) is much slower, oxidation and reduction peaks of very different intensities are observed: the system is also called irreversible. Voltammetry showing peaks with a potential difference between them larger than $\frac{RT}{nF}$ is characteristic of a quasi-reversible system.

2.2.1.3 Capacitive and faradic currents

The intensity of the current measured during a cyclic voltammetry experiment is attributed to two phenomena at the electrode|solution interface: the capacitive current and the faradic current. Thus, the current can be written with the following equation:

$$i = i_f + i_c$$

Where i is the measured current and i_f and i_c are the faradic and capacitive current intensities, respectively.

The capacitive current is due to a molecular organization of the solvent and the ions at the electrode|solution interface. Because they are charged species, ions in the vicinity of the electrode surface order themselves under the application of an electric potential and compensate the electrode surface charge. This is described by the "electrochemical double-layer" model also called Stern model[1] which is represented in Figure 2.6.

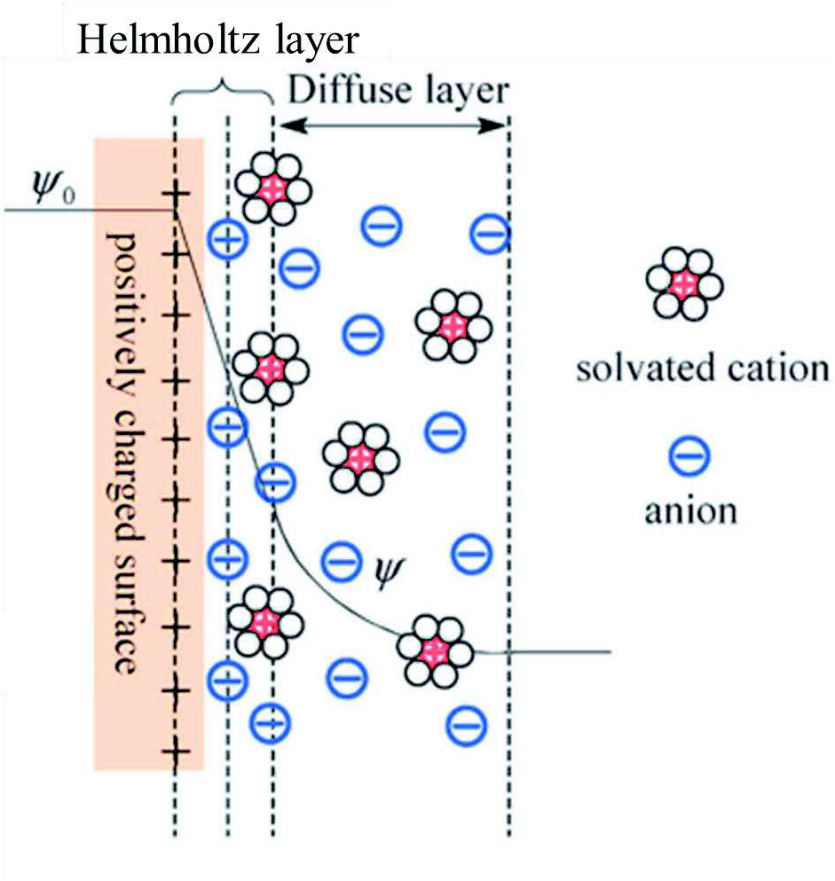

Figure 2.6: *Schematic representation of the Stern model.*

As it is mentioned in its name, this model separates the electrode|solution into two layers. A first dense layer, called Helmholtz layer, which is composed of desolvated ions of opposite charges with respect to the electrode surface. These ions, which have a low ionic mobility, screen the electrode surface charge and so decrease the electrode surface charge. Thus, this layer behaves as a resistance but as it is very thin it is negligible. The second layer is a diffuse layer of a few (or up to tens of) nanometers composed of ions. In this layer, the concentration of ions of opposite charges with respect to the electrode surface charge is higher than in the rest of the solution. These ions feel less the surface potential than the ones in the Helmholtz layer. As the distance from the surface increases, the heterogeneous ion composition decreases to reach a homogeneous ion composition (solution). At low ionic strength, the ion distribution is

predicted by Boltzmann-Hückel theory. The diffuse layer has an electric charge capacity and thus electrode/electrolyte interface behaves as a capacitor.

An analogy can be made between the charging of electrode|solution interface and a classic Resistance-Capacitor (RC) circuit: the current of charging i_c passing after application of potential step ΔE can be calculated with the following same equation for both systems:

$$i(t)_c = \frac{\Delta E}{R} \times e^{\frac{-t}{RC}}$$

Here R is the total resistance of the electrode/electrolyte interface (mainly due to the diffuse layer and bulk electrolyte) and C is its capacitance.

A faradic current is observed when an electroactive molecule is present in solution, and that an effective electronic transfer occurs between the electrode and the electroactive molecule. Thus, an electrochemical reaction must take place at the electrode to measure a faradic contribution. Electroactive species have to diffuse from the solution to the WE and adsorb onto it. Hence, diffusion of the electroactive species is of primary importance because the faradic current measured results from an interplay between the speed of consumption of the species at the electrode/solution interface and the diffusion of these species to the electrode. Once the electronic transfer has occurred, the oxidized or reduced species desorb from the electrode and diffuse into the solution.

When the concentration of the electro-active compound is very low, the capacitive current cannot be neglected but in our case the capacitive current is of the order of several microAmperes while the faradic current is of the order of hundreds of microAmperes. Thus, only the faradic part of the current resulting from electrochemical reactions at the WE will be considered.

2.2.2 Quartz Crystal Microbalance with Dissipation coupled to an electrochemical modulus (EC-QCM-D)

Quartz Crystal Microbalance is a device which allows following mass deposition on a surface with a detection limit of the order of 1 ng/cm^2. Depending on the nature of the material deposited on the surface (metal, polymer…) and on the environment (air, water), different mathematical models allow to calculate the mass and the thickness of the deposit. It should be noted that the thickness calculated is valid for homogenous deposits and one must be cautious for inhomogeneous deposits.

2.2.2.1 Quartz Crystal Microbalance basics

The Quartz Crystal Microbalance (QCM) was developed by Sauerbrey in the early 60th. It is based on the piezoelectric properties of a quartz crystal. Indeed, as other piezoelectric materials, when quartz is submitted to an electrical field, it is mechanically deformed (Figure 2.7) and vice versa. A quartz crystal sandwiched by two conducting layers of gold is used in our device.

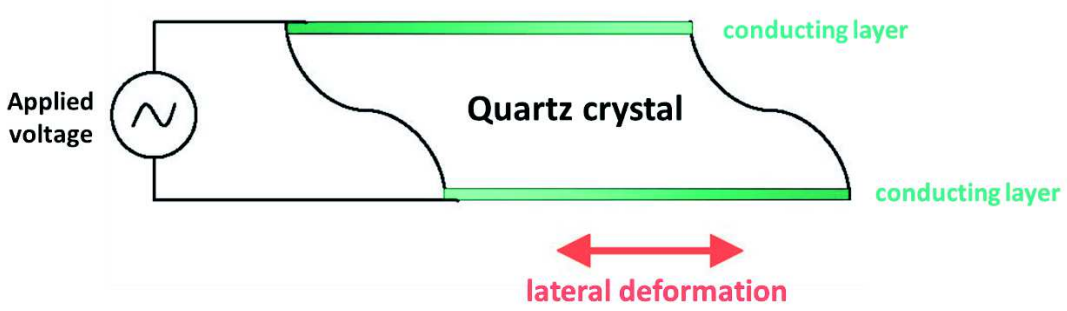

Figure 2.7: *Schematic representation of a sandwiched quartz crystal submitted to an electric field and vibrating in the lateral direction.*

This system behaves as a harmonic oscillator with an associated resonance frequency f_r which can be written:

$$f_r = \frac{1}{2\pi}\sqrt{\frac{k}{M}}$$

where k is the stiffness constant of the quartz crystal in N/m and M is its mass in kg. Hence, one can see that if the mass of the crystal is changed by depositing material on it, unavoidably its resonance frequency will decrease (Figure 2.8). By following the evolution of the resonance frequency of the crystal, it is therefore possible to follow the mass deposited on the crystal.

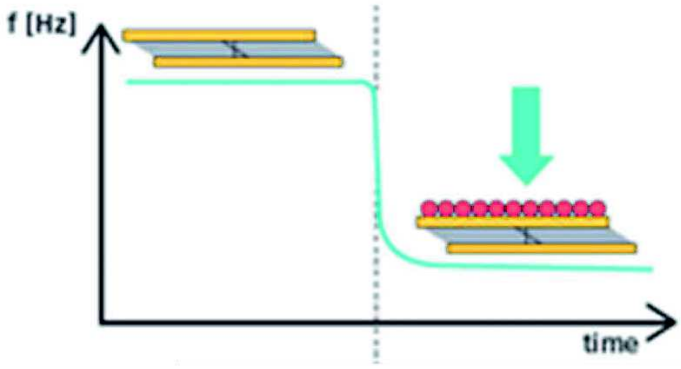

Figure 2.8: *Schematic representation of the frequency shift measured by QCM during the adsorption of material on the crystal.*

In the case of a small amount of material deposited, on top of the crystal, of a mass m with $m<<M$, the resonance frequency can be written:

$$f = \frac{1}{2\pi}\sqrt{\frac{k}{m+M}} \approx f_r\left(1 - \frac{m}{2M}\right)$$

Therefore, the difference of frequency *Δf* can be written as:

$$\Delta f = f - f_r = -\frac{f_r m}{2M} = -\frac{m}{C}$$

with *C* a characteristic constant of the crystal also called "Sauerbrey's constant" defined as:

$$C = \frac{2M}{f_r}$$

By measuring the resonance frequency shift of the system during an experiment, QCM allows to determine the mass deposited on the crystal with a precision of ng/cm^2. It is also possible to measure the frequency shifts of the odd harmonics during an experiment. The Sauerbrey equation can thus be written:

$$m = -C\frac{\Delta f_v}{v}$$

with *v* the number of the considered harmonic. This equation is valid in the case where uniform and rigid layers are deposited in air or in aqueous solutions.[2] The validity of Sauerbrey's relation can be estimated from the fact that the normalized frequency shift $\frac{\Delta f_v}{v}$ measured is independent of the harmonics. However, it cannot be applied for viscous layers which is the case in this work.

The QCM-D also allows the determination of a viscous dissipation factor *D* which corresponds to the sum of all the losses in the system. This parameter is defined by the proportion of dissipated energy at each oscillation with respect to the total stored energy:[3]

$$D = \frac{E_{dissipated\ at\ each\ oscillation}}{2\pi E_{stored}}$$

This dissipation factor is measured by exciting the quartz crystal at its fundamental frequency and the odd harmonics and then by measuring the time needed to relax while its energy is dissipated in the crystal, in the deposit and in the medium in contact (see figure 2.9).

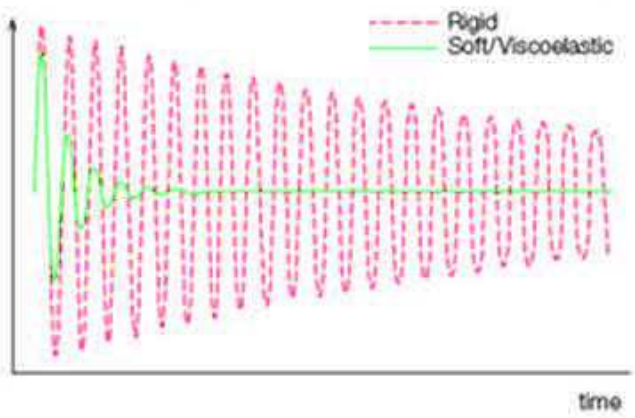

Figure 2.9: *Schematic representation of the time evolution of the potential difference at a quartz crystal in the case of a rigid and visco-elastic coating. The damping observed for a rigid film is low while the damping corresponding to the adsorption of a visco-elastic layer is high due to the dissipative nature of the visco-elastic film towards the acoustic wave generated by the resonator. The dissipation factor D higher for a viscoelastic substrate deposited on the quartz crystal than for a rigid one.*

The *D* factor gives an indication about the viscoelastic character of a coating. If it is superior to a few tens units, the viscous modulus of the deposit cannot be neglected and the Sauerbrey relation is not valid anymore.

2.2.2.2 Coupling of the QCM-D with an electrochemical modulus: EC-QCM-D

The coatings on top of the QCM-D crystals which are in contact with the solution can be either conducting or insulating. When this coating is conducting, the crystals can be used as a WE for electrochemistry experiments. Thus, the crystal surface is both used as the substrate for deposition and as a WE. The two main conducting coatings available are gold and indium tin oxide (ITO). These two coatings have both benefits and drawbacks: the ITO coated crystals are transparent and support a *pdiff* going from -0.5 to several V whereas the gold ones are opaque and support a *pdiff* ranging from -2 V to 0.8 V. Furthermore, the ITO coated crystal surfaces exhibit an AFM topography with large grain size (Figure 2.10, Rms = 2.7 nm) whereas the gold ones haves a topography with small grain size (Figure 2.10, Rms = 0.9 nm).

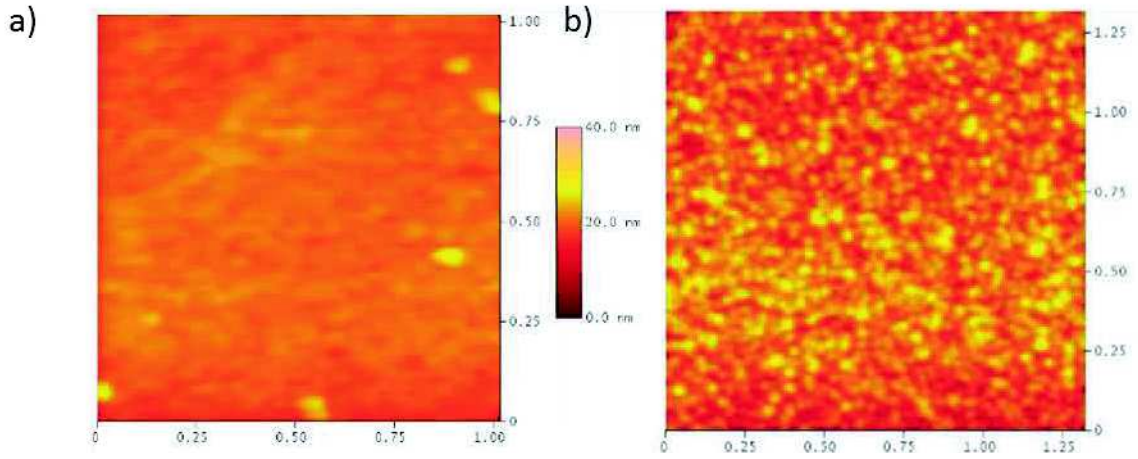

Figure 2.10: *AFM surface topographies obtained in contact mode of (a) a gold coated quartz crystal with thin grain size and (b) of an indium tin oxide coated quartz crystal with large grain size.*

Depending on the range of the *pdiff* used, both types of crystals were used for this work. In the electrochemical three-electrode setup, an *Ag/AgCl* electrode was used as the RE and a platinum electrode was used as the CE. Figure 2.11 schematically represents the EC-QCM-D electrochemical cell.

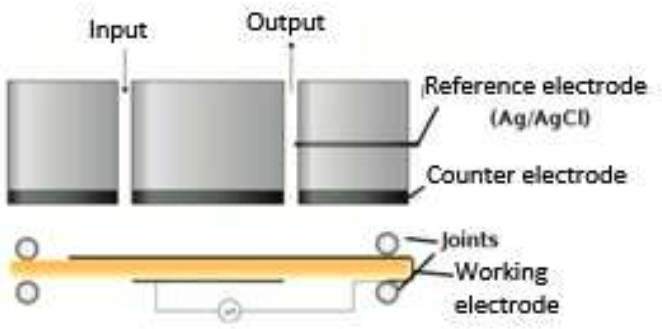

Figure 2.11*: Schematic representation of the three electrode EC-QCM-D electrochemical cell.*

The interest of coupling the QCM-D to an electrochemical modulus lies in the fact that we can both measure the frequency shift of the quartz crystal and its dissipation factor while measuring or applying a *pdiff* or a current.

The frequency shift quantitatively indicates if a mass is depositing on the surface of the crystal and the dissipation factor *D* relates it to its visco-elastic character.

2.2.2.3 EC-QCM-D working principle

The instrument used is the Q-Sense E1 model (Q-Sense AB, Göteborg, Sweden). It is equipped with a QEM 401 electrochemical modulus and with a CHI 660E (CH Instrument, Austin, Texas) potentiostat/galvanostat. The apparatus is composed of a Peltier thermostated cell and includes

a three-electrode electrochemical setup. The electrochemical cell is connected on one hand to a control electronic interface controlled by a software (QSoft) which measures the frequencies shift and the dissipation factors and on the other hand to a potentiostat/galvanostat monitored by the CHI software.

The quartz crystal, used as a sensor, is excited by a sinusoidal tension generator. The excitation frequency corresponds to the fundamental and odd harmonic resonance frequencies and is applied for a few microseconds. At each excitation stop, the crystal oscillates freely at the fundamental and harmonic frequencies thus inducing the apparition of electric oscillations. These are then collected and treated by the QSoft software in order to obtain the frequency shifts and the dissipation factors of the quartz crystal.

2.2.2.4 Experimental protocol

The quartz crystals used in this work are QSX 301 (Q-Sense) crystals coated with a gold layer of 100 nm and QCM-ITO (Microvacuum, Budapest Hungary) coated with an ITO layer. They possess a fundamental resonance frequency f_1 at 5 MHz as well as odd harmonics at 15, 25 and 35 MHz respectively noted as f_3, f_5, and f_7 in the rest of this manuscript. The crystals are treated by UV ozone during 15 minutes to make them hydrophilic before each experiment.

Cyclic voltammetry cycles are then applied between 0 mV and 600 mV with a scan rate of 50 mV/s during 4 cycles in an aqueous buffer solution. The capacitive current is measured in a first place. Figure 2.12 shows an example of the capacitive current on a bare gold crystal.

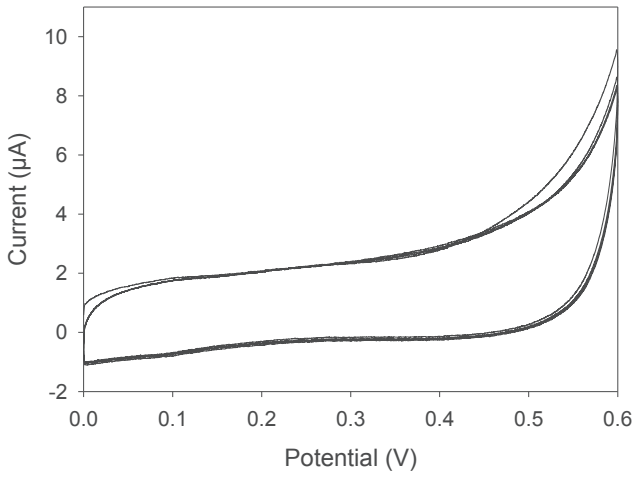

Figure 2.12: *Example of a bare Au quartz crystal voltammogram which does not display any oxidation or reduction peak.*

This voltammogram should not display any peaks because this would mean that an electrochemical reaction is taking place in the vicinity of the WE and thus that the electrode is

polluted. If this is the case, it is possible to decontaminate the crystal by applying a voltammetry cycles between -0.5 and 0.7 V in the presence of 0.6M sulfuric acid H_2SO_4 with a flow rate of 1 ml/min. If the capacitive current is smaller than 10 µA, the WE is not polluted and can be used for an experiment.

In order to ensure that the potentials measured during the experiments are correct, the RE is tested. An aqueous solution of 0.5 mg/ml of tetrapotassium (II) hexacyanoferrate (K_4FeCN_6) is injected in the electrochemical cell. A cyclic voltammetry procedure between 0 mV and 600 mV at 50 mV/s is applied for 4 cycles. Figure 2.13 shows the obtained voltammogram which should display two peaks corresponding to the oxidation and reduction of the electrochemical probe (K_4FeCN_6).

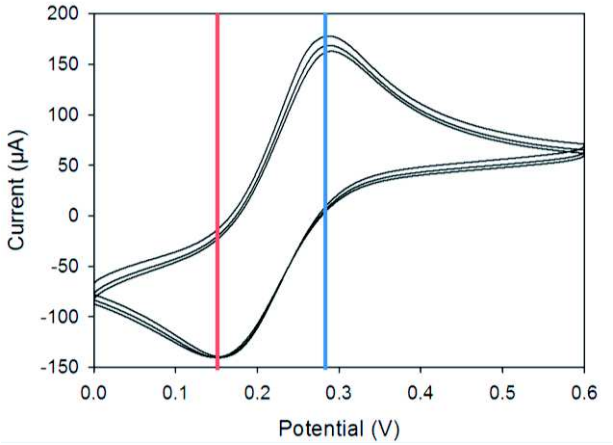

Figure 2.13: *Voltammogram of K_4FeCN_6 at 0.5 mg/ml on QCM Au coated crystals. One oxidation and reduction peak are respectively observed at 250 and 160 mV.*

These characteristic peaks should be obtained at 160 and 250 mV to ensure that the RE is well calibrated. If these two peaks are shifted, i.e. separated by more than 100 mV or located in a lower or higher potential range, the RE is shifted due to an imbalance between silver (Ag^+) and silver salt (AgCl) species. In this case, it is necessary to clean it and to establish the equilibrium between both species. The RE electrode is then first immersed in a sulfuric acid solution at 0.6 M during 20 min and then rinsed to dissolve the possible organic polluting species. After that, it is necessary to re-establish the equilibrium between Ag^+ silver ions in excess and the metallic silver by proceeding to an electrochemical setup. The goal of this step is to form again metallic silver and the silver chloride on the electrode. It is done in a beaker by applying a *pdiff* of -2 V between the *Ag/AgCl* reference electrode and the platinum during few cycles of 15 s in the presence of an aqueous solution of potassium chloride (KCl) at 3M until the stabilization of the measured current. The setup is the following: the *Ag/AgCl* electrode is connected to the

"working electrode" output of the potentiostat while the platinum electrode is connected to the "reference electrode" and "counter electrode" output of the potentiostat.

Once it is confirmed that the two electrodes are not contaminated, the electrochemical setup can be used for the experiment.

The internal temperature is then thermostated at 22°C by means of the QCM-D software. Prior to the injection of the polymer solutions, a measurement of the frequency shifts is taken during at least 15 min until stabilization of the signal in contact with the buffer solution. This serves as a baseline before any material deposition. Once the baseline is done, the solution containing the functional molecules is then injected in the cell. Once the signal stabilizes, the electrochemical stimulus is applied. The mass and the viscoelastic properties of the molecular assembly is characterized in real time by the QCM-D.

2.2.3 Atomic Force Microscopy

Developed in the early 80's by Binnig, Quate and Guerber[4] to overcome the limitation of the scanning tunneling microscope to conducting samples, the atomic force microscope (AFM) is a close field microscopy technique. This technique is based on the interactions between a thin tip in silicon nitride (Si_3N_4) and the surface of the sample to analyze.

The apparatus is constituted of a piezoelectric sample holder and of a thin tip fixed at the extremity of a lever of known stiffness constant k_c (cantilever). The top of the tip reflects a laser beam detected by a four quadrant photodiode. The sample is placed on a magnetized piezoelectric crystal, called piezo tube, which is able to displace itself in three dimensions *(x,y,z).* When the tip is close enough of the surface, it interacts with it leading to a deflection of the cantilever. This deflection of the laser changes the position of the laser spot on the four quadrant photodiode. The spot displacement is transduced by a change in the electrical tension proportional to the tip height variation. Figure 2.14 schematically shows the working principle of an AFM.

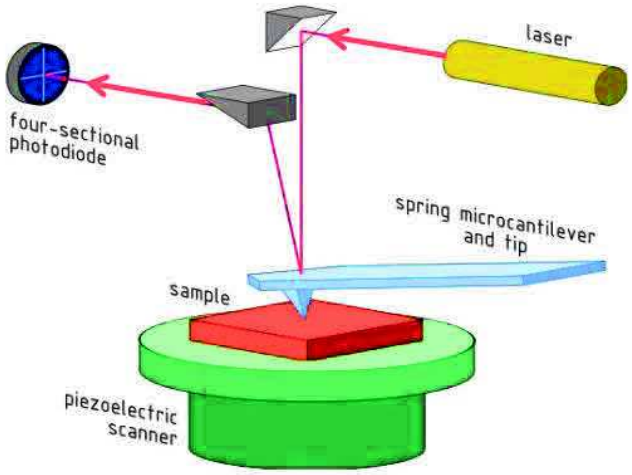

Figure 2.14: *Schematic representation of an atomic force microscope.*[5]

The force *F* exerted between the tip and the sample can be related to the vertical deflection *d* following the Hooke law:

$$F = k_c \times d$$

The apparatus resolution is of the order of a tens of nanometer in the sample displacement plane *(x,y)* and of the order of the nanometer range on the *z* axis. When the tip approaches the surface, different interactions take place between the tip and the sample (e.g: Van der Waals, capillarity, electrostatic, solvation forces, etc). These interactions are attractive at first and when the tip gets closer to the surface, they become repulsive.

The AFM allows to study samples in dry or liquid medium and can be used in several modes (non-contact, intermittent contact, contact), depending on the interaction –and hence the distance- between the tip and the sample. The choice of the mode is made depending on the sample studied and the interaction force tip-sample wanted. Figure 2.15 represents the different modes of the AFM with respect to the distance *d* between the tip and the sample.

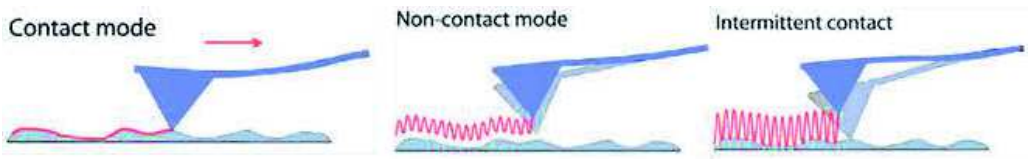

Figure 2.15: *Schematic representation of the contact, non-contact and intermittent contact modes of the AFM.*

Contact mode: the cantilever is in physical contact (repulsive interactions) with the surface of the sample to analyze. In this mode, two possibilities exist: the first one is called at "constant height", in this case the surface is scanned in the plane without changing the height of the

cantilever (*d* varies) and the image is taken by measuring the variations of the deflection of the tip. In the case of the second one called "constant force", the force –and so the deflection- between the sample and the tip is maintained constant (*d* constant) and the image is taken by measuring the displacement of the piezo-tube holding the sample. The second case is the most common used because imaging at constant height implies that the vertical deflection of the cantilever varies while scanning. This can result in damaging the sample and/or the tip when the sample surface is rough. In constant force imaging, the tip-sample distance is maintained constant which allows the tip to follow the surface topography while avoiding a partial destruction of the sample. This mode is particularly adapted to analyze rigid and robust samples.

Non-contact mode: this mode is based on the attractive interactions between the tip and the surface. In this case, the tip is oscillating near the surface without having any physical contact with it. The interaction between the tip/surface can be attractive or repulsive depending on the distance tip/surface and affect the measured oscillation frequency. This mode has the advantage not to destroy the sample by applying a stronger force than necessary. It is however the less convenient mode to use because the interaction tip-sample is weak and can be easily lost while imaging.

Intermittent contact mode or tapping mode: this mode, similar to the non-contact mode, consists in measuring oscillations of the tip closer to the surface and is the most widely used. The lower point of this oscillation makes contact with the sample surface through a repulsive interaction. The lateral forces exerted on the cantilever are much lower than in contact mode considering the small amount of tip-sample contact time. This mode is essentially used to obtain high resolution on fragile sample.

During this work, a Veeco Multimode Nanoscope IIIA microscope from Digital Instrument (Santa Barbara, USA) was used. All the images were taken in contact mode with silicon nitride Si_3N_4 cantilevers possessing a curvature radius of 20 to 40 nm and a stiffness constant of $k_c = 0.6\ N/m$. The AFM images intend to show the surface state (homogeneity, roughness) of the coatings and their thickness by imaging a scratched area of the sample.

2.2.4 X-Ray Photoelectron Spectroscopy (XPS)

X-ray photoelectron spectroscopy (XPS) is an analytical technique which was developed in the 60's by Turner, Price and Siegbahn.[6] Theoretical basis of XPS relies on the photoelectric effect discovered in 1906 by Einstein. A monochromatic source of X-rays with an energy *hv* is used

to excite the atom's core electrons of the sample. The ejected electrons have a kinetic energy T given by:

$$T = h\nu - E_L - W$$

with T the kinetic energy of the emitted electron, E_L the corresponding binding energy and W the electron extraction work in the vacuum (tabulated value).

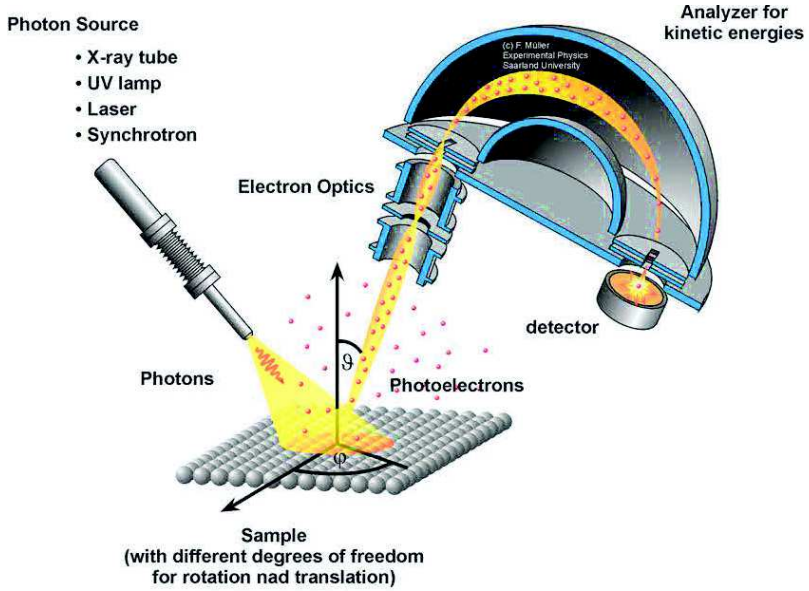

Figure 2.16: Schematic representation of the X-ray photoelectron spectroscopy.[7]

The emitted electrons can be classified depending on their kinetic energy T with respect to the incoming energy *hν* (Figure 2.16). This gives access to the corresponding binding energy E_L for each electron. Since all the atomic orbital energies are classified and specific for each element (ex: N1s: 400 eV, C1s: 285 eV, O1s: 540 eV), it is possible to obtain an elementary analysis of the sample and to know the oxidation state of the atom.

Given the weak free mean path of the incident and emitted rays, the whole measure must be done in a high vacuum of 10^{-2} torr for the irradiating chamber where the sample is exposed and 10^{-5} torr for the kinetic energy analyzer. The penetration depth for organic samples is estimated to be of the order of 9 nm. Thus, XPS gives an insight of the chemical composition of the sample surface.

For this work, two apparatus were used. For the results presented in chapter 3, a Thermo VG Scientific spectrometer equipped with an Al K_α (hν= 1486.6 eV) x-ray source at 225 W was used with a source/analyzer angle of 90°. The analysis was done in two times. A first low resolution spectrum was done with an energy of 50 eV in order to give a general atomic

composition of the sample. Then, to distinguish the different component, high resolution spectra based on atomic transition were performed with an energy of 20 eV. Spectra are represented as a function of the number of photoelectrons detected for a given binding energy. The signal depends on the number of analyzed atoms. Data are treated with the Avantage V.2.26 and CasaXPS software. For the results presented in chapter 4, the analyses were performed with a PHI Quantera SXM (ULVAC-PHI) spectrometer, equipped with an Al Kα X-ray source (1486.6 eV). It operated at 100 W under ultrahigh vacuum (pressure lower than 5.0×10^{-8} mbar). The incidence angle and the source-to-analyzer angle were set to 45° . The probing depth of the technique was estimated to range from 5 to 8 nm. The survey scans were collected from 0 to 1100 eV with pass energy of 280 eV and the high resolution scans were performed with the pass energy adjusted to 55 eV. Raw areas determined after background subtraction were corrected according to Scofield sensitivity factors (C 1s: 1.00, N 1s: 1.80 and O 1s: 2.93). The curve fitting was performed with CasaXPS software, by using a convolution of Gaussian and Lorentzian line shapes with a typical ratio of 60:40. This peak-fitting procedure was repeated until an acceptable fit was obtained with consideration of peak position and full width at half-maximum.

References

[1] A. Bard and L. Faulkner. Electrochemical methods: Fundamentals and applications. *John Wiley & Sons*, 2001.

[2] Rodahl, M.; Kasemo, B. On the measurement of thin liquid overlayers with quartz-crystal microbalance, *Sensors and Actuators A-Physical* **1996,** *54*,448.

[3] Hook, F.; Rodahl, M.; Brzezinski, P.; Kasemo, B. Measurements using the quartz crystal microbalance technique of ferritin monolayers on methylthiolated gold : Dependence of energy dissipation and saturation coverage on salt concentrations. *Journal of Colloid and Interface Science* **1998,** *208*, 63

[4] J.C. Rivoal and C. Frétigny. Microscopie à force atomique (afm). *Techniques de l'ingénieur* R 1 394, 2005

[5] http://fr.slideshare.net/joybiitk/atomic-force-microscope-fundamental-principles

[6] J. M. Hollas. Modern spectroscopy (fourth edition). *Wiley*, 2004.

[7] http://www.rowbo.info/XPS.html

CHAPTER 3: MORPHOGEN ELECTROCHEMICALLY TRIGGERED SELF-CONSTRUCTION OF POLYMERIC FILMS BASED ON MUSSEL-INSPIRED CHEMISTRY

CHAPTER 3: MORPHOGEN ELECTROCHEMICALLY TRIGGERED SELF-CONSTRUCTION OF POLYMERIC FILMS BASED ON MUSSEL-INSPIRED CHEMISTRY

Summary

3.1 Abstract

Inspired by the strong chemical adhesion mechanism of mussels, a catechol based electrochemically triggered self-assembly of films based on short ethylene glycol chains bearing catechol groups on both sides and denoted as bis-catechol molecules was designed. Unable to interact together, commercially available poly(allylamine hydrochloride) (PAH) chains and bis-catechol molecules are mixed in an aqueous solution and brought in contact with an electrode. By application of defined potential cycles, bis-catechol molecules undergo oxidation leading to molecules bearing "reactive" quinone groups which diffuse towards the solution. In this active state, the quinones react with amino groups of PAH through Michael addition and Schiff's base condensation reaction. The application of cyclic voltammetry (CV) between 0 and 500 mV (*vs* Ag/AgCl) of a PAH/bis-catechol solution results in a fast self-construction of a film that reaches a thickness of 40 nm after 60 min. The oxidized bis-catechol molecules thus play the role of a morphogen and, in contrast to previously investigated systems, they are also one of the constituents, after reaction, of the film. The films present a spiky structure which is attributed to the use of bis-functionalized molecules as one component of the films. XPS measurements show the presence of both PAH and bis-catechol cross-linked together in a covalent way. We show that the amine/catechol ratio is an important parameter which governs the film buildup. For a given amine/catechol ratio, it does exist an optimum CV scan rate leading to a maximum of the film thickness as a function of the scan rate.

3.2 Introduction

During the last decades, nature has gradually become an important source of inspiration in science. The study of natural phenomena not only allows understanding the world around us but also permits designing new materials with specific properties. Mussels are common molluscs that can stick to all kinds of materials such as rocks, wood, metals and glass even under extreme conditions (low temperature, salted water). Catechol bearing proteins appear to be directly involved in the adhesion mechanism.[1, 2] Inspired by this extremely strong natural adhesive, researchers attempt to mimic this bio-glue.[3, 4] Catechols present a broad panel of possibilities for chemistry.[5] In particular, they can be oxidized into quinones which undergo Michael addition and Schiff's base formation with nucleophilic groups such as amines or thiols. Several synthetic approaches were developed for the design of novel catechol-based polymer materials and for functionalization of surfaces.[6]

Surface functionalization allows controlling the interaction of materials with their surrounding environment. Catalysis, molecular recognition or cell adhesion are typical examples of such interactions. During the last decades, progress in surface science allowed modifying and tuning material's surface properties in a highly controlled way by the development of new coating methods. Among them, the use of an external stimulus, such as an electric signal or light, appears as a convenient way of inducing a film buildup in a one pot manner. Electrochemically-triggered formation of polymeric films can be divided into three categories: (i) precipitation of polyelectrolytes,[7, 8, 9] (ii) self-assemblies of polyelectrolytes,[10, 11] polysaccharides[12, 13] or proteins[14, 15, 16, 17] and (iii) electropolymerization.[18] Recently, we introduced a forth category of polymeric-film electro-constructions based on the formation of covalent bonds between polymers[19, 20, 21, 22, 23] induced by an electro-generated gradient of "active" molecules called "morphogens". First introduced by Turing,[24] morphogens are specific molecules to which cells respond in a concentration-dependent manner.[25] This definition has been extended to film-buildups on a surface where morphogens are molecules or ions that induce a chemical reaction or interaction in a confined space near a surface. In a first study, we used the Huisgens – Sharpless click reaction to induce the reticulation between two polymers by electro-reduction of Cu^{2+} into Cu^{+}.[19] Generated at the surface of the electrode, Cu^{+} ions (the morphogens) diffuse from the surface to the solution and catalyze the click reaction between azide and alkyne functionalized polymers. As this reaction takes place only in the presence of Cu(I), all the constituents can be mixed in a single solution and the film formation takes place by the simple application of an electrical stimulus. In 2012, Payne and co-workers electro-generated chlorine species (HOCl) to partially oxidize chitosan forming aldehydes that can react covalently with amines (from chitosan itself or proteins) present simultaneously in solution.[26]

Inspired by the chemical versatility of the catechol group to crosslink suitable polymers, we report here a new example of morphogen driven film construction based on short ethylene glycol chains bearing catechol groups on both sides. These molecules will be denoted as bis-catechols (Figure 3.1a). Unable to crosslink together, a commercially available poly(allylamine hydrochloride) (PAH) and these bis-catechol molecules will be mixed in an aqueous solution and put into contact with an electrode. By application of a defined electrochemical potential, the bis-catechol molecules will undergo an oxidation at the electrode, transforming into an “active” state (bis-quinone) (Figure 3.1b). In this active state, the bis-quinone molecules can react with the amino groups of PAH through Michael addition and Schiff’s base condensation (Figure 3.3). The film buildup, occurring exclusively near the electrode, is by far not obvious

because (i) the diffusion of bis-catechol molecules towards the electrode has to be ensured all along the buildup process, even after the beginning of the film formation, and (ii) the two ends of the bifunctionalized molecules could react with the same polymer chain and thereby become unavailable to continue the self-construction process. In contrast to previously reported morphogen driven film constructions, this constitutes the first example of such a film buildup where the morphogen is also an essential component of the film. This represents an extension of the morphogen definition introduced in 2011.[19]

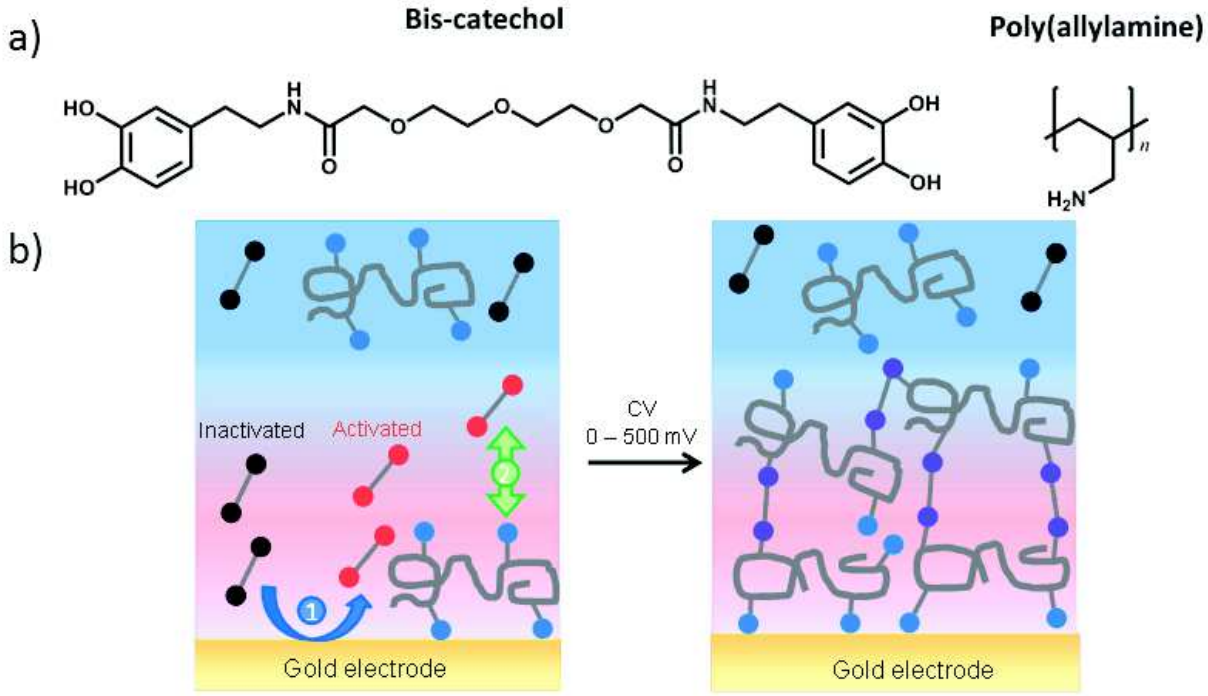

Figure 3.1: *(a) Chemical structures of bis-catechol and poly(allylamine hydrochloride) (PAH). (b) Principle of the one pot self-construction of polymeric film based on oxidation of an organic morphogen (bis-catechol).*

3.3 Synthesis of bis-catechol

Bis-catechol is an original molecule displaying a catechol group at each end of a linear oligoethylene oxide chain. This hydrophilic molecule is stable and water soluble. Bis-catechol was prepared in five steps from dopamine and 3,6,9-trioaundecandioic acid (TUDA), both commercially available starting materials (Figure 3.2). Briefly, first dopamine is modified in three steps according to the literature[27] to get the trifluoroacetate salt of 2-(3,4-bis-benzylyoxyphenyl)-ethylamine **1** in 84% overall yield. Then, in the presence of a half equivalent of trioxaundecanedioyl chloride **2** (prepared in one step from TUDA) in basic conditions, the benzyl-protected bis-catechol **3** is obtained in 82%. Finally, a last hydrogenolysis step provides bis-catechol in a quantitative way. The overall yield of this

synthesis is 68% and it has been realized on a multigram scale. The synthesis of the molecule was done by Dr Tony Garnier (post-doctorant) and the description of the total synthesis is given in the Material and Methods chapter.

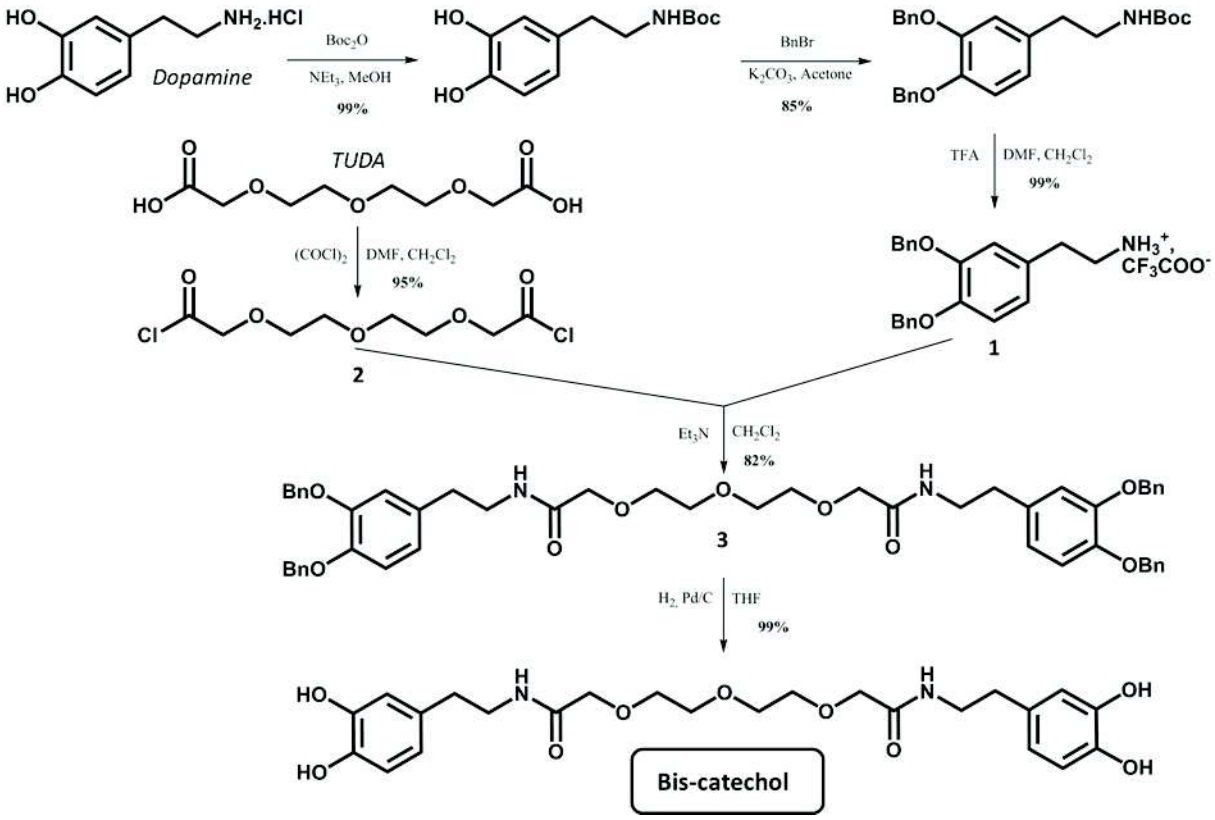

Figure 3.2: *Synthetic pathway to prepare bis-catechol in five steps from commercially available dopamine and TUDA.*

3.4 Electro-triggered self-construction of PAH/bis-catechol films

We first investigated the electrochemical response of bis-catechol molecules (Figure 3.4a) by cyclic voltammetry. A couple of redox peaks can be observed which corresponds to the transformation of catechols to quinones and *vice versa* (see Figure 3.3 step 1).

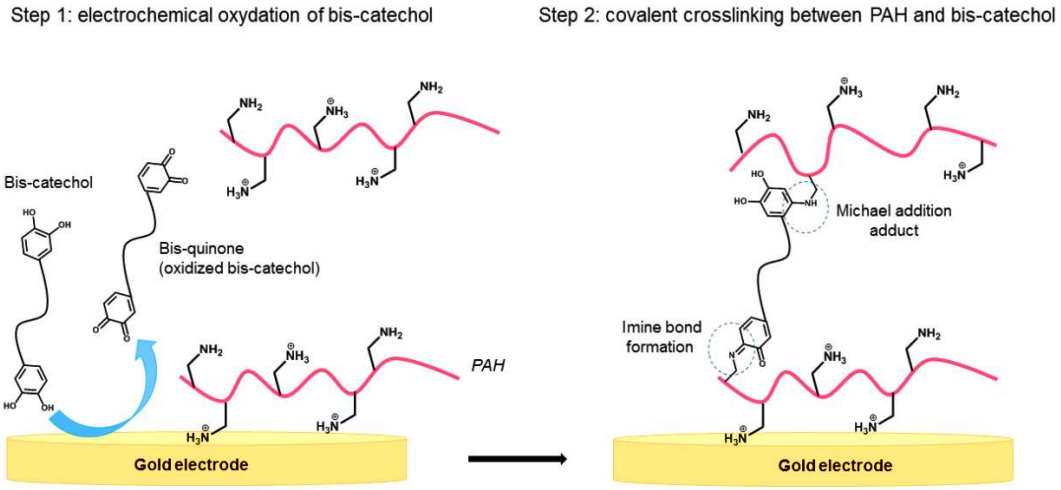

Figure 3.3: *Schematic representation of the two chemical steps of the self-construction buildup leading to covalent crosslinking between PAH and bis-catechol.*

The oxidation and reduction peaks are respectively at 0.4 V and -0.03 V (*vs* Ag/AgCl). This is in good accordance with the literature.[28, 29, 30]

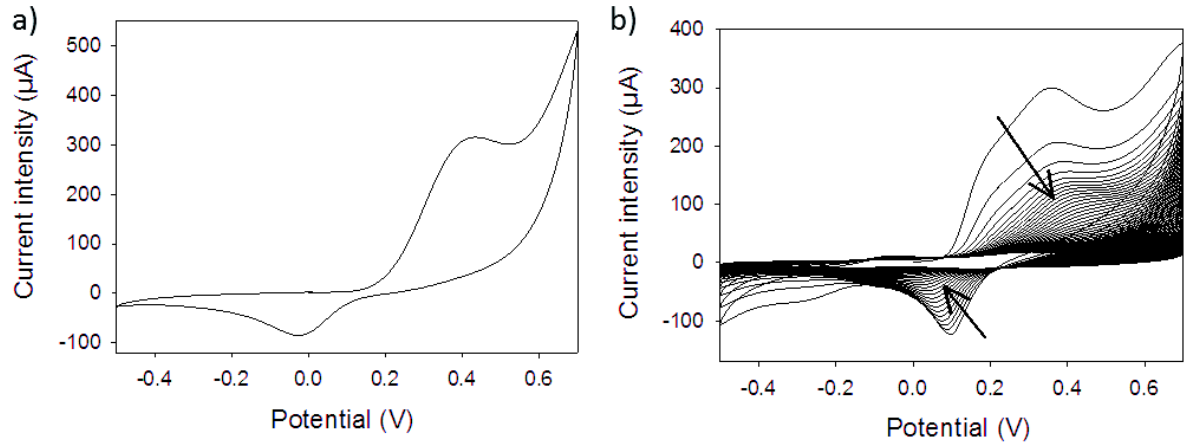

Figure 3.4: *Cyclic voltammograms with (a) 1 cycle of bis-catechol (1 mg/mL) solution and (b) 180 cycles (1h, 20s between each cycle) of bis-catechol (1 mg/mL) and PAH (1 mg/mL) mixture solution (catechol/amine ratio of 0.38) over the potential range of -0.5 to 0.7 V (vs Ag/AgCl, scan rate 50 mV/s). The supporting electrolyte was 10 mM Hepes-150 mM $NaNO_3$ buffer solution at pH 7.4.*

The self-construction of PAH (Mw = 58 000 g/mol) and bis-catechol films was studied by EC-QCM allowing to follow *in-situ* the buildup of the film during the application of the electrical stimulus. PAH and bis-catechol mixtures were prepared in 10 mM HEPES - 150 mM $NaNO_3$ aqueous buffer at pH 7.4. The HEPES buffer compensates the production of H^+ from oxidation of catechol into quinone. Indeed, quinone moieties cannot react with amine functions in acidic conditions. Argon was flushed through all the PAH/bis-catechol solutions to prevent oxidation in solution due to dissolved oxygen. Figure 3.5 shows a typical QCM signal relative to the buildup obtained with a catechol/amine ratio of 0.38 (molar ratio of each chemical group). After

injection of the PAH/bis-catechol mixture, a small increase of the normalized frequency is observed due to PAH electrostatic adsorption (polycation) and coordination bonding between catechol and gold. The application of cyclic voltammetry (CV) between 0 and 500 mV (*vs* Ag/AgCl, scan rate of 50 mV/s) results in a fast increase of the normalized frequency shift reaching a plateau at 1100 Hz after 80 min.

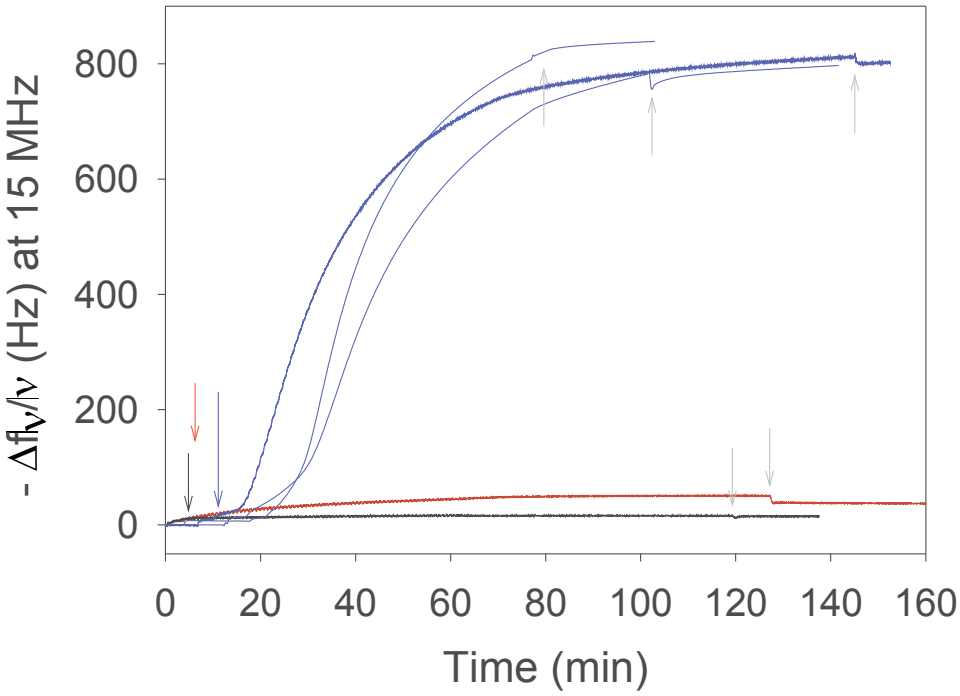

Figure 3.5: *Evolution of the normalized frequency shift, measured by EC-QCM, as a function of time of (blue lines) PAH/bis-catechol mixture (0.38 in catechol/amine molar ratio), (red line) bis-catechol and (black line) PAH solutions during the application of CV between 0 and +500 mV (vs Ag/AgCl, scan rate 50 mV/s). After injection of the solutions, CV was applied as indicated by the respective colored arrows. The grey arrows correspond to the end of CV application.*

Figure 3.4b represents the evolution of the electrochemical signal during the self-construction of a PAH/bis-catechol film. The oxidation currents decrease with the number of cycles to reach the capacitive current after 30 cycles. At the first cycle, the oxidation and reduction peaks of bis-catechol are at 0.37 and 0.10 V, respectively. The oxidation peak shift during the self-construction towards positive values while the reduction peak shift towards the negative value (Figure 3.6a). The overall apparent redox potential, $E_{1/2}=\frac{1}{2}\left(E_{ox}^{p}+E_{red}^{p}\right)$, shifts towards more positive values (Figure 3.6b).

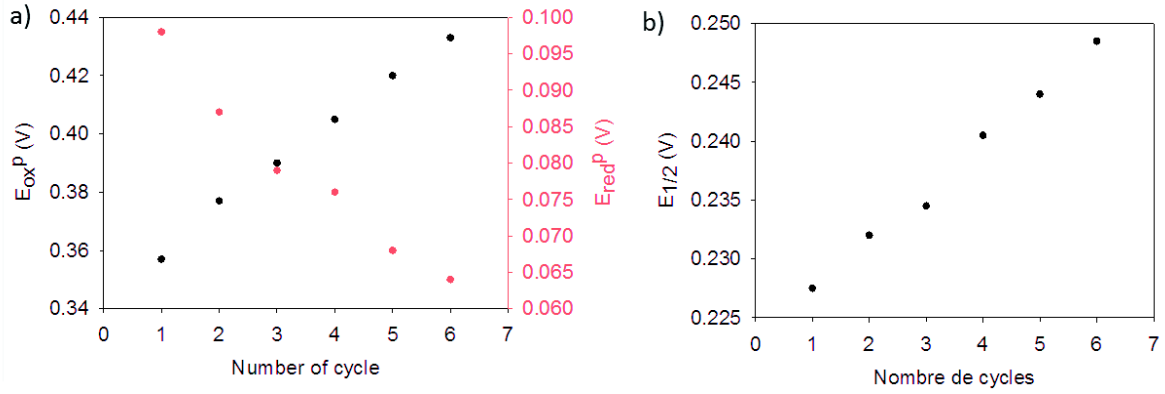

Figure 3.6: *a) Evolution of the oxidation (E_{ox}^{p}) and reduction (E_{red}^{p}) potentials of the bis-catechol for the first six cycles during the application of a CV from -0.5 to 0.7 V (vs Ag/AgCl, scan rate 50 mV/s) for 1h. b) Evolution of the apparent redox potential $E_{1/2}$ of the bis-catechol for the first six cycles during the application of a CV from -0.5 to 0.7 V (vs Ag/AgCl, scan rate 50mV/s) for 1h.*

This may be due to the Donnan potential in the film generated by the positive charges from PAH.[31] The decrease of the current intensity during film construction must originate from the increased limitation of the bis-catechol to diffuse towards the electrode as build up proceeds. This then prevents further oxidation of catechols into quinones, hindering further film buildup.

Indeed when a solution of potassium ferrocyanide is putted in contact with the film and a cyclic voltammetry is performed, no peaks of oxidation or reduction are observed. Tough, even a small molecule can't diffuse through the film to be oxidized or reduced at the electrode (Figure 3.7)

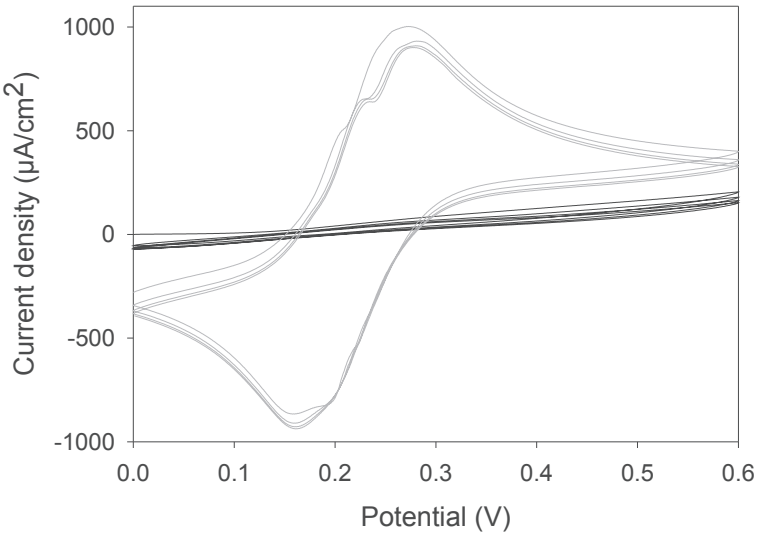

Figure 3.7**:** *Cyclic voltammograms of a solution of potassium ferrocyanide (2 mg/mL) on a bare gold electrode (grey line) and on an electrode coated with a PAH/bis-catechol film (black line) built from a PAH/bis-catechol mixture (0.38 in catechol/amine molar ratio) during the application of CV between 0 and +500 mV (vs Ag/AgCl, scan rate 50 mV/s) for 1h.*

When a PAH solution is used with the same self-construction set up, the QCM signal remains stable (Figure 3.5). In the case of a bis-catechol solution, a small increase of the frequency shift

is observed until 130 Hz after 2 h of CV application. This could be due to a polymerization reaction of bis-catechol as already observed in the literature for catechol-derived compounds.[32, 33] Poly(diallyldimethylammonium chloride) (PDADMA) is a polycation bearing only quarternary amines which cannot react with quinones. When PAH is replaced by PDADMA in the mixture solution keeping the same catechol/amine ratio, no buildup occurs (Figure 3.8).

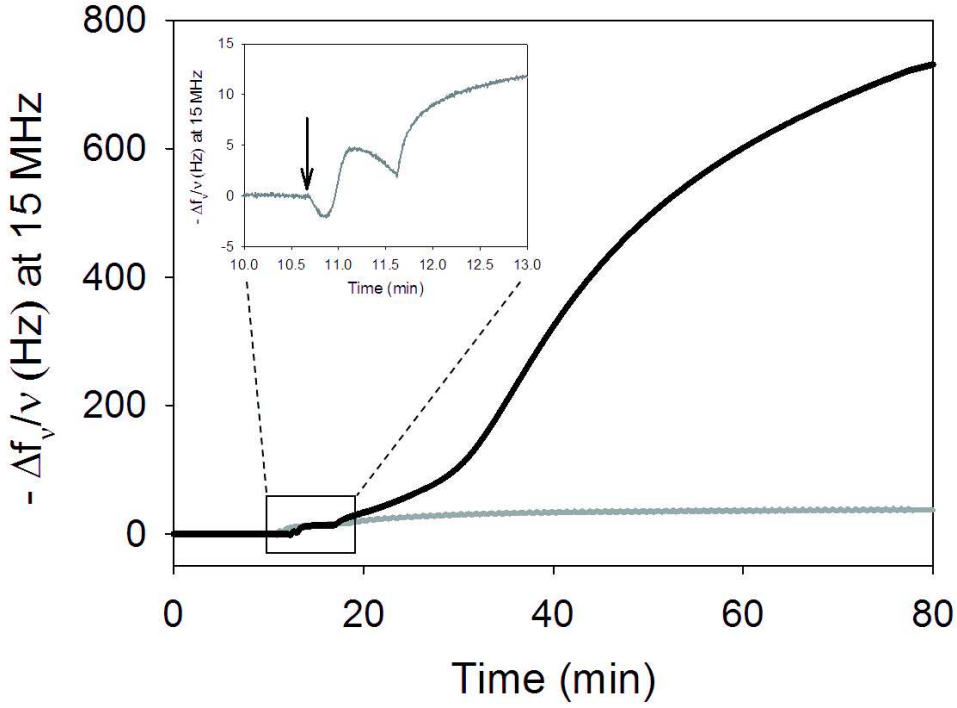

Figure 3.8: *Evolution of the normalized frequency shift of (black line) PAH/bis-catechol mixture and (grey line) PDADMA/bis-catechol mixture during CV application between 0 and +500 mV (vs Ag/AgCl, scan rate 50 mV/s). The inset is a zoom-in of the evolution of the normalized frequency shift overtime of the system of PDADMA/bis-catechol; the black arrow indicates the injection of PDADMA/bis-catechol mixture into the QCM Cell.*

These different control experiments prove that the increase of the QCM signal in the simultaneous presence of PAH and bis-catechol molecules is due to a chemical reaction between both components. Moreover, the self-construction can be stopped and triggered again at any time before the maximum thickness is reached. Figure 3.9 shows the buildup of a bis-catechol/PAH followed by QCM-D where two successive CV of 5 min are applied. When the CV is stopped, the increase of the normalized frequency shift drastically decreases but does not reach zero. After stopping the CV, freshly oxidized molecules still diffuse from the surface of the electrode to the surface of the film and thus continue to contribute to a "slow" self-construction. When a new cyclic voltammetry is applied the buildup starts again with the same speed as previously.

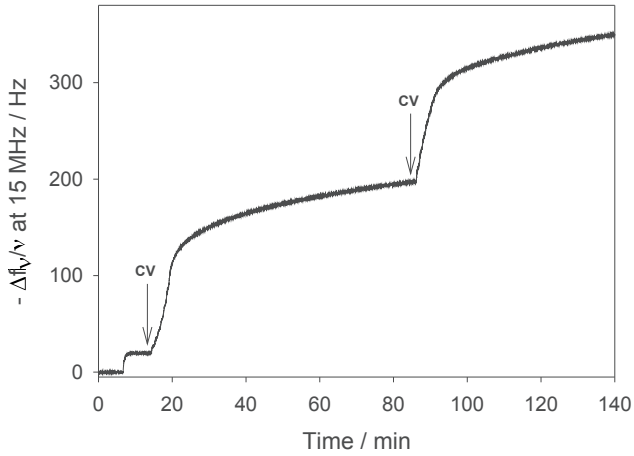

Figure 3.9: *Evolution of the normalized frequency shift, measured by EC-QCM, as a function of time for a PAH/bis-catechol mixture (0.38 in catechol/amine molar ratio) during the application of two successive CV (black arrows)between 0 and +500 mV (vs Ag/AgCl, scan rate 50 mV/s, 5 min).*

3.5 AFM characterization of self-constructed PAH/bis-catechol films

AFM measurements were performed in contact mode and liquid state to characterize the topography of the self-constructed films and also their thicknesses after scratching (Figure 3.10).

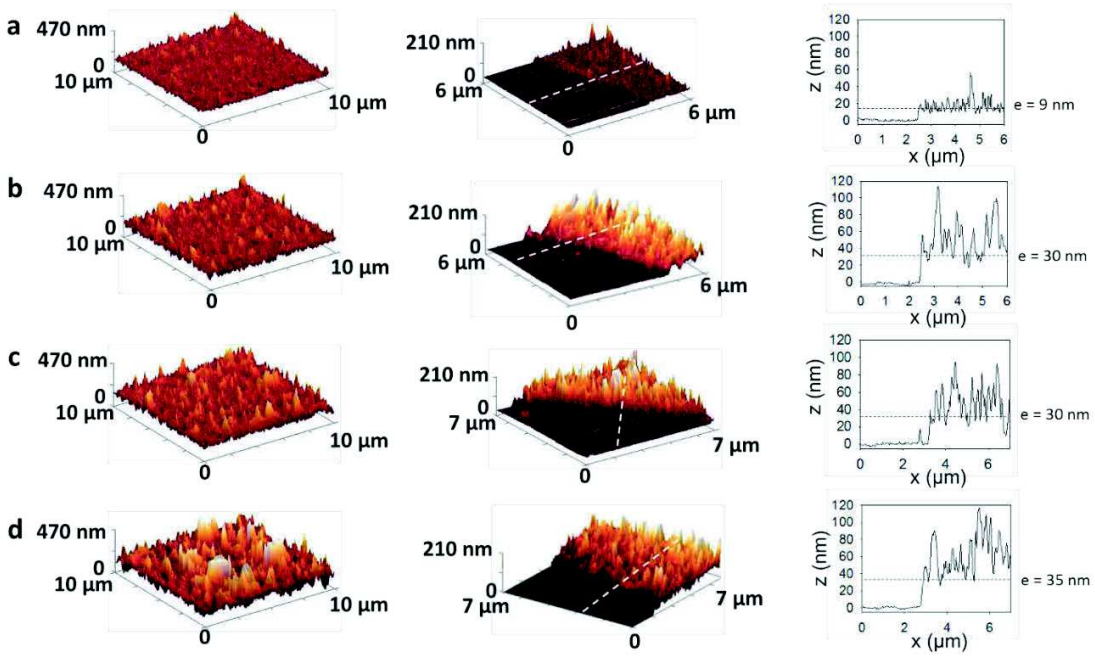

Figure 3.10: *Typical AFM 3D images, obtained in contact mode (liquid state), and their respective cross-section profiles of a scratched PAH/bis-catechol film, obtained after (a) 5 min, (b) 10 min, (c) 20 min and (d) 60 min of self-construction. The film buildup was performed with PAH/bis-catechol solution at 0.38 in catechol/amine molar ratio by applying a CV between 0 and +500 mV (vs Ag/AgCl, scan rate 50 mV/s). The white dashed-lines show the line corresponding to the profiles presented on the right.*

Figure 3.11 shows the evolution of the film thickness (minimal *z* distance between the bare substrate and the surface of the film for which the whole substrate is covered) measured by AFM at different times during the buildup.

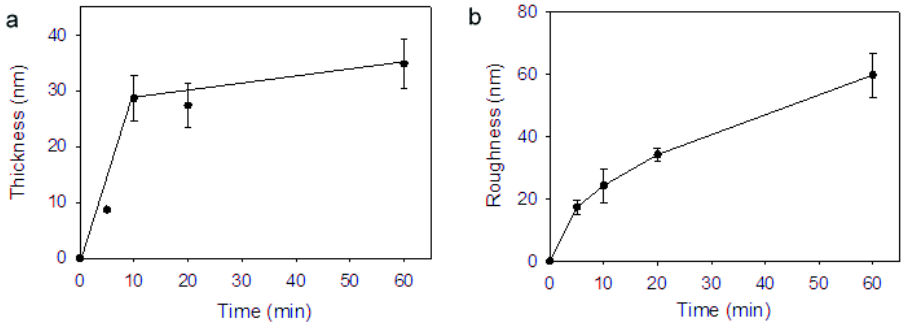

Figure 3.11: *Evolution of the thickness and the roughness, measured by AFM in contact mode and liquid state, as a function of time of the self-constructed film obtained from a PAH/bis-catechol mixture solution at 0.38 in catechol/amine ratio by applying a CV between 0 and +500 mV (vs Ag/AgCl, scan rate 50 mV/s). The roughness was calculated on a 10 µm × 10 µm AFM images.*

After 5 min of CV application, the PAH/bis-catechol film covers uniformly the whole substrate with a thickness of 9 nm. The film thickness increases as a function of the application time of the CV, reaching 35 nm after 60 min of self-construction. One can notice that the thickness of the film increases in the same manner as the normalized frequency shift, *i.e* a high increase during the first 15 min of self-construction followed by a much slower increase. One can also remark that the films are quite rough and that the roughness increases during the film buildup process (Figure 3.11b). Interestingly similarly rough films, corresponding to the presence of a large number of spikes, were obtained for other electrochemically triggered morphogen film buildup examples which involve one component which is a small bis-functionalized molecules.[22, 34] It is thus tempting to correlate this spiky structure with the use of bis-functional ethylene glycol spacers.

3.6 Chemical analysis of the self-constructed PAH/bis-catechol films

XPS analysis provides chemical information about the atomic and the chemical group composition of surface coating. Such analysis has been recently reported for bio-inspired coatings based on catecholamine derivatives.[35, 36] A film self-constructed for 60 min from PAH and bis-catechol according to parameters described in chapter 2 section (described under) has been analyzed by XPS. Representative high-resolution spectra of N 1s, C 1s and O 1s regions of this film are shown in Figure 3.12. The energies and chemical group assignment for each

measured peak are listed in Table 3.1 and are similar to the values reported in the literature. In some cases, there is an overlap of peaks corresponding to atoms involved in several chemical groups. To avoid wrong conclusions we did not calculate any percent contribution coming from the decomposition of the experimental peaks.

Atom (Chemical group)	Binding energy (eV)	Binding energy in litt. (eV)	References
O=C (quinone)	531.0	531.0 ± 0.2	35, 37
O=C (amide)	531.4	531.6	38
O-C	532.5	532.6	39
O of chemisorbed water	535.4	535.9	40
N=C (imine)	397.8	397.8-399.0	35, 37, 41
NH-C	398.8	398.8	37
NH_2-C	399.6	399.1-399.6	42
NHCO (amide)	400.6	400.5-400.7	43
NH_3^+ (ammonium)	402.0	401.8	43
C=**C** (aromatic)	284.4	284.0-284.3	44
C-**C** (aliphatic)	284.9	284.5-285.1	44
C-N (amine) and **C**$_{aromatic}$-OH (phenol)	285.5	285.4-286 (C-N) 285.8 ± 0.1 (C$_{aromatic}$-OH)	35, 45 37
C=N (imine) and **C**-O-C (ether)	286.5	286.5-286.7 (C=N, imine) 286.2-286.7 (C-O-C, ether)	42, 45 46
C=O (quinone)	287.4	287.7 ± 0.4	35, 37, 42
NH**C**O (amide)	288.0	287.9-288.3	45, 46, 47

Table 3.1: *XPS peak binding energy assignments and corresponding references.*

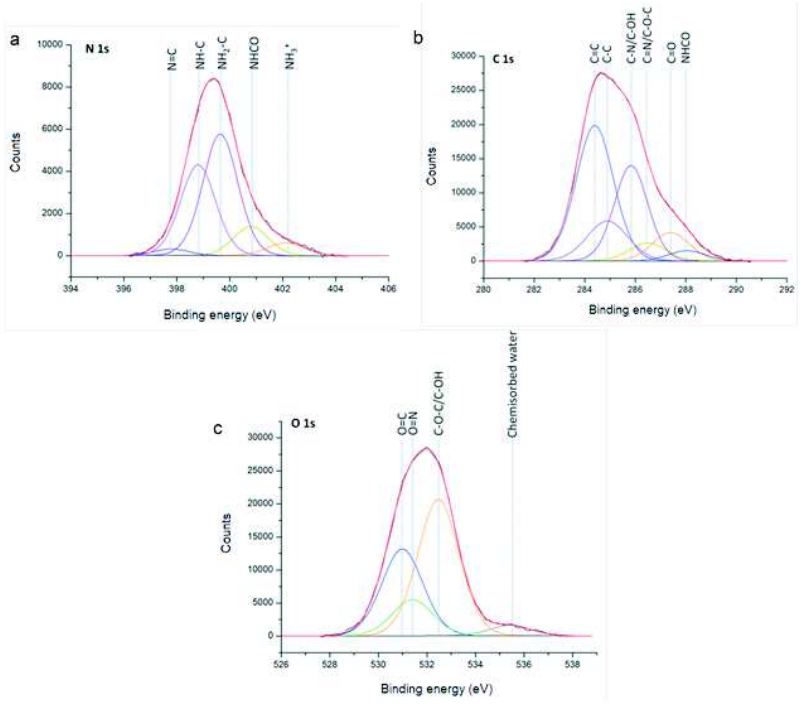

Figure 3.12: *High-resolution XPS spectra of (a) N 1s, (b) C 1s and (c) O 1s regions of a self-constructed film obtained from a PAH/bis-catechol solution at 0.19 in catechol/amine molar ratio by applying a CV between 0 and +500 mV (vs Ag/AgCl, scan rate 50 mV/s) for 60 min.*

As depicted in figure 3.1 and 3.3, nitrogen atoms can come from uncharged primary amine NH_2, from ammonium NH_3^+groups both related to PAH, from secondary amines resulting from the Michael addition from the imines originating from the Schiff's base condensation reaction and from the amide bonds (NHC=O) of the bis-catechol molecules. The N 1s region was thus fitted with five peaks assigned to nitrogen involved in imine (**N**=C), secondary and primary amines (**N**H-C/**N**H_2-C), amide (**N**HC=O) and ammonium (**N**H_3^+) groups. All these peaks seem to be present in the N(1s) band even if the contribution of the peak relative to the imines appears rather small. On the other hand the strong contribution of the secondary amine peak indicates that the catechols have reacted with the amines of PAH through Michael addition (Figure 3.3). Moreover the presence of the primary amine and of the amide peaks confirms the presence of both PAH and of the bis-catechol molecules in the film. In addition, five others peak energies observed in the C 1s region are assigned to **C**-C aromatic, **C**-C aliphatic, **C**-N/**C**-OH aromatic (overlapped), **C**=O (quinone) and NH**C**O, confirming again the presence of both PAH and bis-catechol in the self-constructed film. Oxygen atoms come exclusively from catechol or oxidized catechol (quinone) molecules present in the film. Catechols are composed of two types of oxygen atoms: one coming from the catechol phenolic hydroxyls and ether groups (C-**O** simple bond) and the other one involved in the amide bonds (NHC=**O**). The O 1s peak was thus fitted by using four peaks assigned to **O**-C, **O**=C (quinone, *i.e.* oxidized catechol), **O**=CNH and the oxygen coming from chemisorbed water. The presence of quinone (**O**=C) comes from the oxidation of catechols into quinone occurring during the electrochemical film buildup. They remain present in the self-constructed film as in the case of catecholamine derivatives polymerization leading to a high proportion of stable quinone groups.[35, 36] This presence of quinones is in agreement with our proposed model of a self-constructed film based on catechol oxidation. In summary, the XPS analysis of the self-constructed film reveals the presence of both PAH and bis-catechol covalently linked through secondary amines formation. The presence of quinone groups, resulting from the electro-oxidation of bis-catechol molecules in the close vicinity of the electrode and highlights the concept of morphogens (*i.e.* oxidized bis-catechol) allowing the self-construction of the film.

3.7 Influence of the physico-chemical conditions on the self-construction

The influence of catechol/amine ratio of the PAH/bis-catechol mixture was first studied. According to the conditions previously described, the mixtures were prepared at 1 mg/mL in

PAH and bis-catechol corresponding to a catechol/amine molar ratio of 0.38. Keeping the PAH concentration constant, the bis-catechol concentration was tuned from 0.06 to 2.5 mg/mL, corresponding to catechol/amine molar ratios ranging from 0.02 to 0.95. Figure 3.13a represents the normalized frequency shift obtained after 60 min of self-construction at each studied ratio. The mass deposited increases linearly with the catechol/amine ratio until it reaches a plateau at a ratio of 0.3. This corresponds approximatively to 7 amine functions from PAH for one bis-catechol molecule i.e. 7 amine functions for 2 catechol groups. Above a ratio of 0.3, no change of the buildup kinetic is observed. The limited buildup is thus probably due to the fact that the film becomes dense and that the bis-catechol molecules can no longer diffuse through. This is also suggested by the evolution of the current intensity during the film buildup (figure 3.4b).

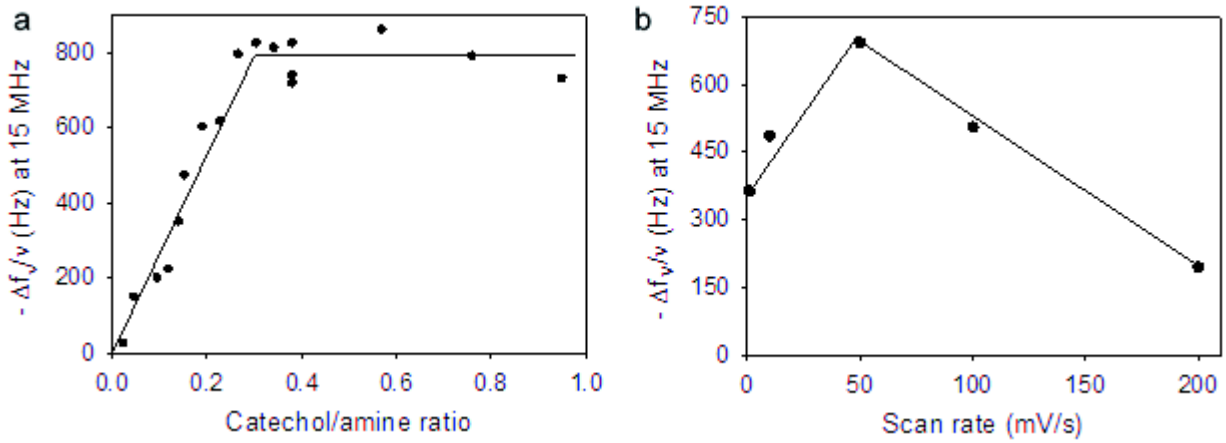

Figure 3.13: *(a) Evolution of the normalized frequency shift of a PAH/bis-catechol mixture, obtained after 60 min of CV application between 0 and +500 mV (vs Ag/AgCl, scan rate 50 mV/s), as a function of catechol/amine ratio. (b) Evolution of the normalized frequency shift of a PAH/bis-catechol mixture (at 0.23 in catechol/amine ratio), obtained after 60 min of CV application between 0 and +500 mV (vs Ag/AgCl) as a function of the scan rate. The lowest scan rate corresponds to 1 mV/s.*

The influence of the scan rate of the CV was also investigated. 50 mV/s in scan rate was applied in all the results reported so far. Figure 12b shows the normalized frequency shift obtained after 60 min of self-construction for the different scan rates at a fixed catechol/amine ratio of 0.23. Figure 3.14a, b and c shows the evolution of the normalized frequency shifts and of the potential during the application of the first four potential-cycles at 1, 50 and 100 mV/s in scan rate, respectively.

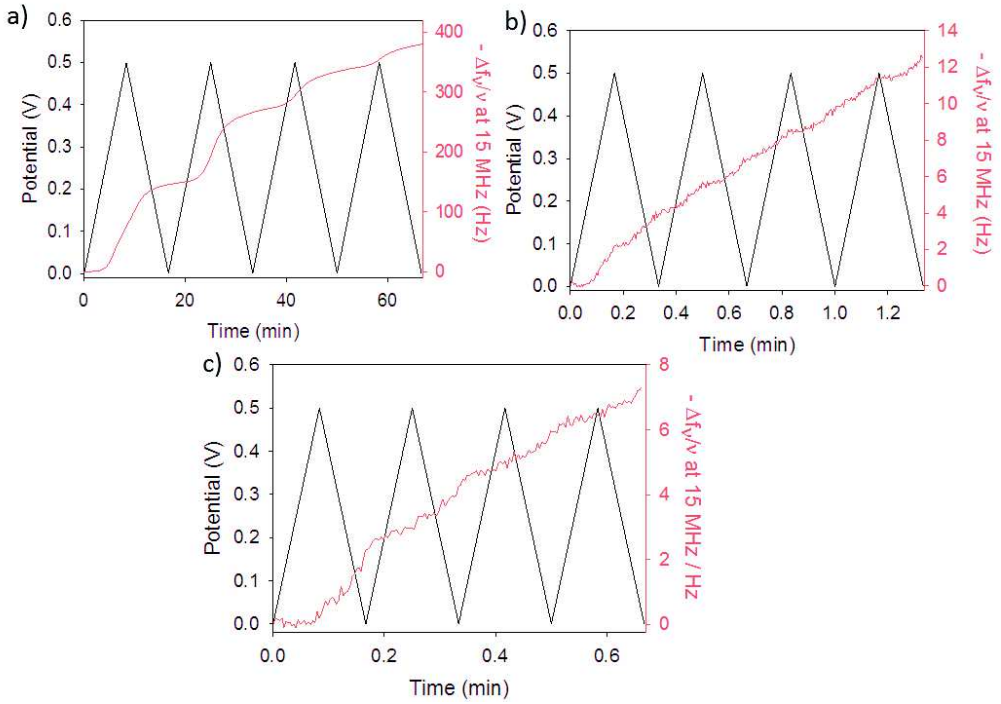

Figure 3.14: *Evolution of (black line) the potential applied and (red line) the normalized frequency shift of a PAH/bis-catechol mixture (at 0.23 in catechol/amine ratio) during the CV application between 0 and +500 mV (vs Ag/AgCl) at a) 1 mV/s in scan rate, b) 50 mV/s in scan rate and c) 100 mV/s in scan rate.*

By decreasing the scan rate from 50 mV/s to 1 mV/s, the mass deposited decreases. Likewise, when the scan rate increases to 200 mV/s the mass deposited decreases. An optimum of the buildup is obtained for a scan rate of 50 mV/s. The existence of an optimum scan rate in the film buildup reflects the fact that the buildup process must be governed by at least two antagonistic effects. During a CV cycle, catechol molecules near the electrode are oxidized into quinones during the period of the cycle corresponding to oxidation conditions. These quinones can be reduced back into catechols during the time of the cycle which corresponds to reduction conditions. At a slow scan rate, during one cycle both the oxidation and reductions periods are long. Large amount of oxidized molecules are formed before reduction of these molecules takes place. Therefore it can be assumed that at slow scan rates one forms dense films near the electrode. Because they are dense, the films rapidly reduce the diffusion of further bis-catechol molecules through. On the other hand, at very high scan rates, the each oxidation period is rapidly followed by a reduction period. The oxidized quinone molecules are then rapidly reduced back into their catechol "non-active" form. Thus the flux of quinone molecules diffusing towards the solution, responsible for the interaction with PAH and for the formation of the film, would become small. In the limit of a very small flux, no film would form. Indeed, the rare catechol molecules that would diffuse into the solution would react with PAH chains

without being able to form a network. There must thus exist an intermediate scan rate where the flux of quinones is sufficient to form efficiently a network with the PAH chains, forming a film that is not very dense at the beginning and thus allowing diffusion of catechol molecules through. Such a film will thus reach a thickness that is larger than at very low scan rates and of course larger than what is expected at very high scan rates. Yet as the buildup process goes on, the catechol molecules continue also to interact with the PAH chains near the electrode. This film becomes thus also denser with time and correlatively the diffusion of catechol molecules through is reduced. After a while this diffusion is hindered and the film buildup stops.

Finally, the effect of the molecular weight of PAH and of bis-catechol molecule on the self-construction was studied. All the previous results were obtained with PAH with a molecular weight of 58 000 g/mol. Figure 3.15 shows the normalized frequency shift obtained during the self-construction of PAH/bis-catechol mixture for two different PAH molecular weights (Mw = 58 000 and 15 000 g/mol) at the same catechol/amine ratio of 0.38.

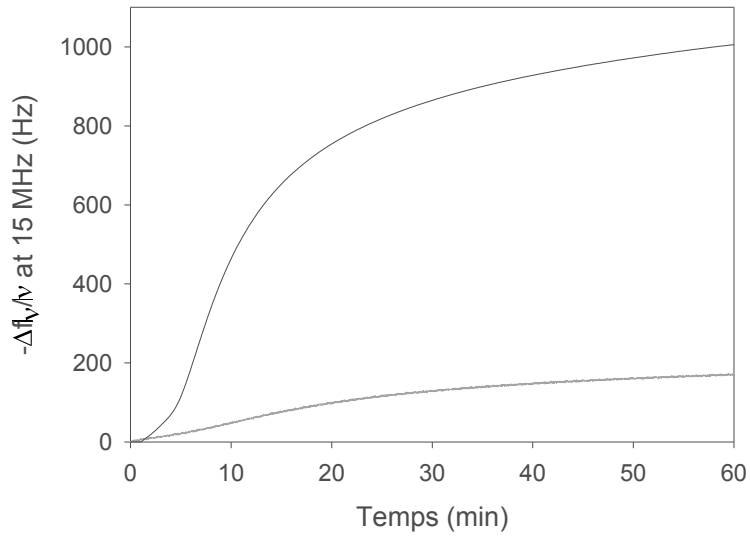

Figure 3.15: *Evolution of the normalized frequency shift of a PAH/bis-catechol mixture (at 0.38 in catechol/amine ratio) with a PAH of 15000 g/mol (grey line) and 58000 g/mol (black line), during a CV application between 0 and +500 mV (vs Ag/AgCl, scan rate 50 mV/s).*

By using a PAH with a smaller molecular weight, the self-construction still takes place but the kinetic of buildup is smaller. Indeed after 60 min of self-construction, a frequency shift of 200 Hz with PAH (Mw = 15 000 g/mol) is measured in comparison to 1000 Hz in the case of a PAH (Mw = 58 000 g/mol). This can be explained by the fact that PAH is the main building block of the assembly (in term of mass adsorbed). Then for the same kinetic of reaction between bis-

catechol and PAH, a smaller mass is adsorbed in the case of small PAH chains (Mw = 15 000 g/mol) than in the case of long PAH chains (Mw = 58 000 g/mol).

3.8 Conclusions

We designed a catechol based electrochemically triggered construction of films based on an organic morphogen, bis-catechol. By CV application, the oxidized bis-catechol spacers react with PAH forming a polymeric film that self-constructed exclusively on the surface of the electrode. A fast buildup is obtained that reaches a plateau after 20 min. These films present a spiky structure. This is attributed to the use of bifunctional molecules as film constituent. We show that the amine/catechol ratio is an important parameter which governs the film buildup. For a given amine/catechol ratio there exists an optimum CV scan rate leading to a maximum of the film thickness as a function of the scan rate. Smaller molecular mass of PAH leads to slower kinetic of buildup and a longer bis-catechol prevents the self-construction.

References

1. Waite, J. H.; Tanzer, M. L. Polyphenolic Substance of Mytilus-Edulis - Novel Adhesive Containing L-Dopa and Hydroxyproline. *Science* **1981,** *212*, 1038.

2. Waite, J. H. Nature's Underwater Adhesive Specialist. *Int. J. Adhesion and Adhesives* **1987,** *7*.

3. Lee, H.; Dellatore, S. M.; Miller, W. M.; Messersmith, P. B. Mussel-Inspired Surface Chemistry for Multifunctional Coatings. *Science* **2007,** *318*, 426.

4. Lee, B. P.; Messersmith, P. B.; Israelachvili, J. N.; Waite, J. H. Mussel-Inspired Adhesives and Coatings. In *Annual Review of Materials Research, Vol 41*, Clarke, D. R.; Fratzl, P., Eds., 2011; Vol. 41, pp 99.

5. Sedo, J.; Saiz-Poseu, J.; Busque, F.; Ruiz-Molina, D. Catechol-Based Biomimetic Functional Materials. *Advanced Materials* **2013,** *25*, 653.

6. Faure, E.; Falentin-Daudre, C.; Jerome, C.; Lyskawa, J.; Fournier, D.; Woisel, P.; Detrembleur, C. Catechols as Versatile Platforms in Polymer Chemistry. *Progress in Polymer Science* **2013,** *38*, 236.

7. Krylova, I. Painting by Electrodeposition on the Eve of the 21st Century. *Progress in Organic Coatings* **2001,** *42*, 119.

8. Wu, L. Q.; Gadre, A. P.; Yi, H. M.; Kastantin, M. J.; Rubloff, G. W.; Bentley, W. E.; Payne, G. F.; Ghodssi, R. Voltage-Dependent Assembly of the Polysaccharide Chitosan onto an Electrode Surface. *Langmuir* **2002,** *18*, 8620.

9. Boccaccini, A. R.; Keim, S.; Ma, R.; Li, Y.; Zhitomirsky, I. Electrophoretic Deposition of Biomaterials. *Journal of the Royal Society Interface* **2010,** *7*, S581.

10. Ngankam, A. P.; Van Tassel, P. R. Continuous Polyelectrolyte Adsorption under an Applied Electric Potential. *Proceedings of the National Academy of Sciences of the United States of America* **2007,** *104*, 1140.

11. Olsen, C.; Van Tassel, P. R. Polyelectrolyte Adsorption Kinetics under an Applied Electric Potential: Strongly Versus Weakly Charged Polymers. *Journal of Colloid and Interface Science* **2009,** *329*, 222.

12. Shi, X. W.; Tsao, C. Y.; Yang, X. H.; Liu, Y.; Dykstra, P.; Rubloff, G. W.; Ghodssi, R.; Bentley, W. E.; Payne, G. F. Electroaddressing of Cell Populations by Co-Deposition with Calcium Alginate Hydrogels. *Advanced Functional Materials* **2009,** *19*, 2074.

13. Cheng, Y.; Tsao, C. Y.; Wu, H. C.; Luo, X. L.; Terrell, J. L.; Betz, J.; Payne, G. F.; Bentley, W. E.; Rubloff, G. W. Electroaddressing Functionalized Polysaccharides as Model Biofilms for Interrogating Cell Signaling. *Advanced Functional Materials* **2012,** *22*, 519.

14. Johnson, E. K.; Adams, D. J.; Cameron, P. J. Directed Self-Assembly of Dipeptides to Form Ultrathin Hydrogel Membranes. *Journal of the American Chemical Society* **2010,** *132*, 5130.

15. Liu, Y.; Cheng, Y.; Wu, H. C.; Kim, E.; Ulijn, R. V.; Rubloff, G. W.; Bentley, W. E.; Payne, G. F. Electroaddressing Agarose Using Fmoc-Phenylalanine as a Temporary Scaffold. *Langmuir* **2011,** *27*, 7380.

16. Leisk, G. G.; Lo, T. J.; Yucel, T.; Lu, Q.; Kaplan, D. L. Electrogelation for Protein Adhesives. *Advanced Materials* **2010,** *22*, 711.

17. Wong, I. Y.; Footer, M. J.; Melosh, N. A. Electronically Activated Actin Protein Polymerization and Alignment. *Journal of the American Chemical Society* **2008,** *130*, 7908.

18. Waltman, R. J.; Bargon, J. Electrically Conducting Polymers - a Review of the Electropolymerization Reaction, of the Effects of Chemical-Structure on Polymer Film Properties, and of Applications Towards Technology. *Canadian Journal of Chemistry-Revue Canadienne De Chimie* **1986,** *64*, 76.

19. Rydzek, G.; Jierry, L.; Parat, A.; Thomann, J. S.; Voegel, J. C.; Senger, B.; Hemmerle, J.; Ponche, A.; Frisch, B.; Schaaf, P.; Boulmedais, F. Electrochemically Triggered Assembly of

Films: A One-Pot Morphogen-Driven Buildup. *Angewandte Chemie-International Edition* **2011,** *50*, 4374.

20. Rydzek, G.; Garnier, T.; Schaaf, P.; Voegel, J. C.; Senger, B.; Frisch, B.; Haikel, Y.; Petit, C.; Schlatter, G.; Jierry, L.; Boulmedais, F. Self-Construction of Supramolecular Polyrotaxane Films by an Electrotriggered Morphogen-Driven Process. *Langmuir* **2013,** *29*, 10776.

21. Rydzek, G.; Parat, A.; Polavarapu, P.; Baehr, C.; Voegel, J. C.; Hemmerle, J.; Senger, B.; Frisch, B.; Schaaf, P.; Jierry, L.; Boulmedais, F. One-Pot Morphogen Driven Self-Constructing Films Based on Non-Covalent Host-Guest Interactions. *Soft Matter* **2012,** *8*, 446.

22. Rydzek, G.; Polavarapu, P.; Rios, C.; Tisserant, J. N.; Voegel, J. C.; Senger, B.; Lavalle, P.; Frisch, B.; Schaaf, P.; Boulmedais, F.; Jierry, L. Morphogen-Driven Self-Construction of Covalent Films Built from Polyelectrolytes and Homobifunctional Spacers: Buildup and Ph Response. *Soft Matter* **2012,** *8*, 10336.

23. Rydzek, G.; Terentyeva, T. G.; Pakdel, A.; Golberg, D.; Hill, J. P.; Ariga, K. Simultaneous Electropolymerization and Electro-Click Functionalization for Highly Versatile Surface Platforms. *Acs Nano* **2014,** *8*, 5240.

24. Turing, A. M. The Chemical Basis of Morphogenesis. *Philos. Trans. R. Soc. Lond.* **1952,** *237*, 37.

25. Potter, J. D. Morphogens, Morphostats, Microarchitecture and Malignancy. *Nature Reviews Cancer* **2007,** *7*, 464.

26. Gray, K. M.; Liba, B. D.; Wang, Y. F.; Cheng, Y.; Rubloff, G. W.; Bentley, W. E.; Montembault, A.; Royaud, I.; David, L.; Payne, G. F. Electrodeposition of a Biopolymeric Hydrogel: Potential for One-Step Protein Electroaddressing. *Biomacromolecules* **2012,** *13*, 1181.

27. Cai, W. B.; Kwok, S. W.; Taulane, J. P.; Goodman, M. Metal-Assisted Assembly and Stabilization of Collagen-Like Triple Helices. *Journal of the American Chemical Society* **2004,** *126*, 15030.

28. Tian, Y. A.; Ye, S. Q.; Ran, Q.; Xian, Y. Z.; Xu, J. J.; Peng, R.; Jin, L. T. Generation of Surface-Confined Catechol Terminated Sams Via Electrochemically Triggered Michael Addition: Characterization, Electrochemistry and Complex with Ni(Ii) and Cu(Ii) Cations. *Physical Chemistry Chemical Physics* **2010,** *12*, 13287.

29. Apetrei, C.; de Saja, J. A.; Zurro, J.; Rodriguez-Mendez, M. L. Advantages of the Biomimetic Nanostructured Films as an Immobilization Method Vs. The Carbon Paste Classical Method. *Catalysts* **2012,** *2*, 517.

30. Lakshmi, D.; Bossi, A.; Whitcombe, M. J.; Chianella, I.; Fowler, S. A.; Subrahmanyam, S.; Piletska, E. V.; Piletsky, S. A. Electrochemical Sensor for Catechol and Dopamine Based on a Catalytic Molecularly Imprinted Polymer-Conducting Polymer Hybrid Recognition Element. *Analytical Chemistry* **2009,** *81*, 3576.

31. El Haitami, A. E.; Martel, D.; Ball, V.; Nguyen, H. C.; Gonthier, E.; Labbe, P.; Voegel, J.-C.; Schaaf, P.; Senger, B.; Boulmedais, F. Effect of the Supporting Electrolyte Anion on the Thickness of Pss/Pah Multilayer Films and on Their Permeability to an Electroactive Probe. *Langmuir* **2009,** *25*, 2282.

32. Kong, Y.; Mu, S. L. Investigation on the Electrochemical Polymerization of Catechol by Means of Rotating Ring-Disk Electrode. *Chinese Journal of Chemistry* **2003,** *21*, 630.

33. Marczewska, B.; Przegalinski, M. Poly(Catechol) Electroactive Film and Its Electrochemical Properties. *Synthetic Metals* **2013,** *182*, 33.

34. El Haitami, A. E.; Thomann, J. S.; Jierry, L.; Parat, A.; Voegel, J. C.; Schaaf, P.; Senger, B.; Boulmedais, F.; Frisch, B. Covalent Layer-by-Layer Assemblies of Polyelectrolytes and Homobifunctional Spacers. *Langmuir* **2010,** *26*, 12351.

35. Zangmeister, R. A.; Morris, T. A.; Tarlov, M. J. Characterization of Polydopamine Thin Films Deposited at Short Times by Autoxidation of Dopamine. *Langmuir* **2013,** *29*, 8619.

36. Bernsmann, F.; Ponche, A.; Ringwald, C.; Hemmerle, J.; Raya, J.; Bechinger, B.; Voegel, J. C.; Schaaf, P.; Ball, V. Characterization of Dopamine-Melanin Growth on Silicon Oxide. *Journal of Physical Chemistry. C* **2009,** *113*, 8234.

37. Wang, Z.; Sun, C. Y.; Vegesna, G.; Liu, H. Y.; Liu, Y.; Li, J. H.; Zeng, X. Q. Glycosylated Aniline Polymer Sensor: Amine to Imine Conversion on Protein-Carbohydrate Binding. *Biosensors and Bioelectronics* **2013,** *46*, 183.

38. Amaral, I. F.; Granja, P. L.; Barbosa, M. A. Chemical Modification of Chitosan by Phosphorylation: An Xps, Ft-Ir and Sem Study. *Journal of Biomaterials Science, Polymer Edition* **2005,** *16*, 1575.

39. Rosenthal, D.; Ruta, M.; Schlogl, R.; Kiwi-Minsker, L. Combined Xps and Tpd Study of Oxygen-Functionalized Carbon Nanofibers Grown on Sintered Metal Fibers. *Carbon* **2010,** *48*, 1835.

40. Figueiredo, J. L.; Pereira, M. F. R.; Freitas, M. M. A.; Orfao, J. J. M. Modification of the Surface Chemistry of Activated Carbons. *Carbon* **1999,** *37*, 1379.

41. Ando, R. A.; do Nascimento, G. M.; Landers, R.; Santos, P. S. Spectroscopic Investigation of Conjugated Polymers Derived from Nitroanilines. *Spectrochim. Acta. Part A* **2008,** *69*, 319.

42. Truica-Marasescu, F.; Wertheimer, M. R. Nitrogen-Rich Plasma-Polymer Films for Biomedical Applications. *Plasma Process. Polym.* **2008,** *5*, 44.

43. Compton, O. C.; Dikin, D. A.; Putz, K. W.; Brinson, L. C.; Nguyen, S. T. Electrically Conductive "Alkylated" Graphene Paper Via Chemical Reduction of Amine-Functionalized Graphene Oxide Paper. *Advanced Materials* **2010,** *22*, 892.

44. Huang, Y. L.; Tien, H. W.; Ma, C. C. M.; Yang, S. Y.; Wu, S. Y.; Liu, H. Y.; Mai, Y. W. Effect of Extended Polymer Chains on Properties of Transparent Graphene Nanosheets Conductive Film. *Journal of Materials Chemistry* **2011,** *21*, 18236.

45. Cheng, Y.; Gray, K. M.; David, L.; Royaud, I.; Payne, G. F.; Rubloff, G. W. Characterization of the Cathodic Electrodeposition of Semicrystalline Chitosan Hydrogel. *Materials Letters* **2012,** *87*, 97.

46. Shard, A. G.; Whittle, J. D.; Beck, A. J.; Brookes, P. N.; Bullett, N. A.; Talib, R. A.; Mistry, A.; Barton, D.; McArthur, S. L. A Nexafs Examination of Unsaturation in Plasma Polymers of Allylamine and Propylamine. *Journal of Physical Chemistry B* **2004,** *108*, 12472.

47. Briggs, D.; Brewis, D. M.; Dahm, R. H.; Fletcher, I. W. Analysis of the Surface Chemistry of Oxidized Polyethylene: Comparison of Xps and Tof-Sims. *Surface and Interface Analysis* **2003,** *35*, 156.

CHAPTER 4 : ELECTROTRIGGERED SELF-ASSEMBLY OF METAL-POLYPHENOL NANOCOATINGS USING A MORPHOGENIC APPROACH

CHAPTER 4 : ELECTROTRIGGERED SELF-ASSEMBLY OF METAL-POLYPHENOL NANOCOATINGS USING A MORPHOGENIC APPROACH

Summary

4.1 Abstract

In summary, a new electrotriggered self-assembly of metal-polyphenol nanocoatings was developed using a morphogenic approach. Tannic acid (TA)/Fe(III) nanofilms were self-assembled using a mixture of Fe(II) and TA on which an anodic current was applied leading to the oxidation of Fe(II) into Fe(III) at the surface of an electrode. The confined electro-generated gradient of Fe(III) allowed to control the buildup of TA/Fe(III) film based on di-coordinated complexes independent of the pH and Fe(II)/TA molar ratio of the building solution. The film thickness and the self-assembly kinetic could be tuned by the application time in current, the value of the current and Fe(II)/TA molar ratio of the building solution. We showed that this strategy should be applicable to a wide range of polyphenols.

4.2 Introduction

Supramolecular and molecular nanostructures attract increasing interest since they allow the design of new types of self-assembling materials with widespread applications ranging from tunable electronics, up to biomaterials.[1] A large variety of supramolecular interactions, including hydrogen bonding, hydrophobic interactions,[2] π-π stacking,[3] electrostatic interactions,[4] and metal-ligand coordination[5] were used to self-assemble molecular architectures on surface. Individual metal-ligand coordination sites can provide stable, yet reversible, crosslinking points between polymers to achieve the self-assembly. Incorporating metal-ions into a supramolecular architecture gives also access to their rich properties with potential applications for magnetic, electric and optical devices.[6] Most often the reported supramolecular self-assembly processes take place in the bulk whereas in Nature such processes are often generated locally. One prominent example in Nature is the formation actin fibers induced by focal adhesions during cell adhesion.[7] Localized self-assembly of compounds all present in solution represents a real challenge since the compounds present in solution are prone to interacting. Localized self-assembly thus requires the presence of a local stimuli to initiate the self-assembly process. Electrotriggered reactions constitute one way to address this challenge. Electrotriggered formation of films can be divided into three categories: (i) precipitation of polyelectrolytes,[8-10] (ii) self-assemblies of polyelectrolytes,[11-12] physical gel[13-14] or proteins[15-18] and (iii) formation of covalent bonds between monomers (electropolymerization).[19] In 2011, we introduced the morphogenic self-construction of films based on electrogenerated ions that induce the buildup of a film: a new concept in the field of electrodeposition of polymers. In order to induce the cross-linking between two polymers

chains, we first used the Cu^{I}-catalyzed click reaction between azide and alkyne.[20] More recently, we described the electrotriggered assembly of polyelectrolytes by using charge shifting polymers allowing for the localized deposition of active enzymes.[21]

Inspired by the exceptional ability of mussels to adhere on almost any type of surfaces and by the catechol based biochemistry behind this adhesion, a huge community of researchers designed different functional materials. Catecholic ligands with Fe(III) is one particular metal–ligand interaction widely observed in Nature. For instance, the stability constant of ferric ion complexes with enterobactin (tripodal tris-catecholate siderophore from E. coli) is equal to 10^{52}. This corresponds to a free energy 2 orders of magnitude higher than that of a single hydrogen bond, 3 times as high than that of the the biotin/avidin noncovalent interaction, and comparable to a covalent bond. The cuticle of the mussel byssal thread employs dopamine residues to establish catechol-based Fe(III) crosslinks. In addition to its strength and dynamic nature, catechol–Fe(III) complexation is highly pH-dependent. Binding stoichiometry changes from a 1:1 catechol:Fe(III) mono-complex at low pH to a highly stable 3:1 tris-complex at increased pH. Tannic acid (TA) is a polyphenol, composed of galloyl and catechol moieties present in abundance in nature and easily accessible. As catechol moieties, galloyl coordinates metals such as Fe(III) in a pH dependent manner. At high pH values (above its pKa 8.5), TA behaves as a rigid polyanion and can also form polyelectrolytes complexes with polycations like quaternized poly(4-vinylpyridine).[22] Using metal-polyphenol coordination, TA/Fe(III) multilayer films were designed having an enormous potential for biomedical applications.[23-25] In 2013, Caruso and coworkers introduced a new concept: the one-pot assembly of TA/Fe(III) films and capsules.[5] By mixing Fe(III) and TA in solution at basic pH, TA/Fe(III) coating was self-assembled by a simple dipping of the material (planar surfaces or microparticles). The concept was extended to others metallic ions such as aluminium, vanadium, chromium, cobalt[26] and to small phenolic molecules, such as gallic acid, pyrogallol and pyrocatechol.[27]

Using mussel-inspired chemistry, we showed in the previous chapter the electro-cross-linking deposition of polymers based on the confined oxidation of bis-catechol homobifunctional molecules.[28] Here, we go one step further in this field and introduce a new electrotriggered morphogenic self-assembly based on polyphenol – metal ion interactions, using a polyphenol (TA) and its ability of coordinating Fe(III) ions. A mixture solution of TA and Fe(II), forming a water-soluble ferrous complex,[29] was used as building solution in contact with a working electrode. The application of an anodic current allows to oxidize Fe(II) into Fe(III) in a confined

gradient in the vicinity of the electrode inducing the localized self-assembly of a TA/Fe(III) film (Figure 4.1).

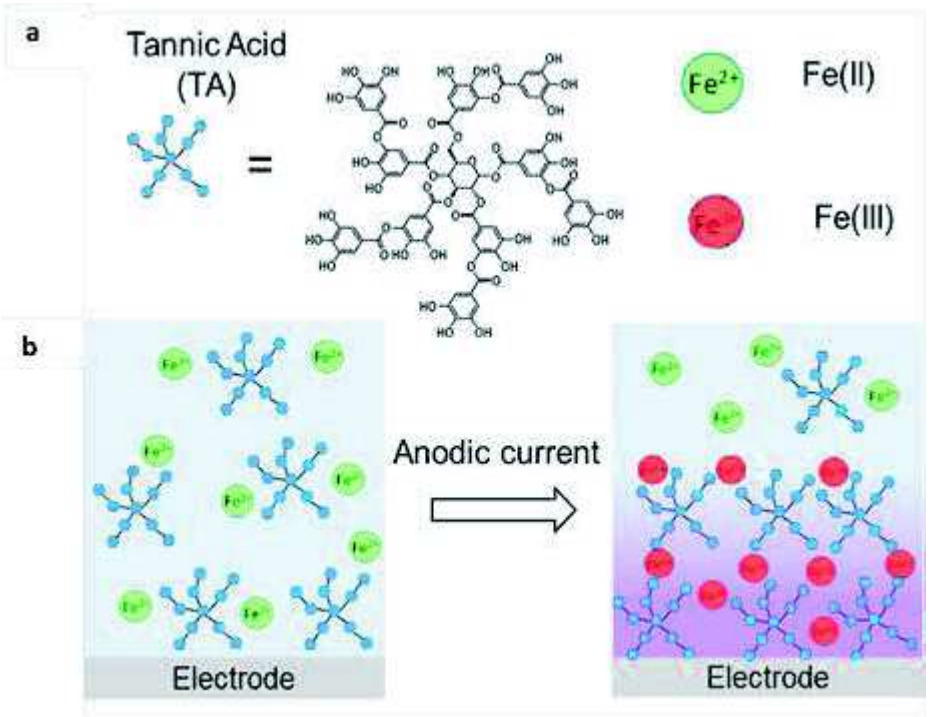

Figure 4.1: *(a) Chemical structure of tannic acid (TA) (b) Schematic representation of the one pot self-assembly of metal-polyphenol film based on the electro-oxidation of Fe(II) in Fe(III).*

4.3 Fe(II) and TA electrochemical characterization

We first investigated the electrochemical response of Fe(II), Tannic Acid (TA) and Fe(II)/TA mixture by cyclic voltammetry on an ITO coated QCM acting as the working electrode (Figure 4.2). The voltammogram of iron ions exhibits a couple of redox peaks which corresponds to the redox transitions Fe(II)/Fe(III). Oxidation and reduction peaks are centered at 1.2 V and -0.05 V (at 50 mV/s), respectively (Figure 4.2a). These values are quite different compared to the literature which are measured on a bare gold electrode (0.70 V and 0.29 V, respectively).[30] The wider separation of redox peaks is probably related to slower kinetics of Fe(II)/Fe(III) transition on ITO comparing to gold.[31] The oxidation of Fe(II) is already observed for potentials above 0.2 V. The voltammogram of TA exhibits an irreversible oxidation at 0.93 V (Figure 4.2b). The reduction peak is lacking, meaning that the electrochemical reaction is irreversible as described in the literature.[32] Electrochemical-quartz crystal microbalance with dissipation (QCM) was used to monitor *in situ* the evolution of frequency shift related to the deposition of mass on the ITO-crystal (Figure 4.2c). An increase of the frequency shift is observed during the application of the cyclic voltammetry (5 cycles at 50 mV/s). The irreversibility of the electrochemical signal

coupled with the increase of the mass might be due to chemical reactions between TA molecules, probably through aryloxy radical formation,[33] leading to an electro-cross-linking of TA (Figure 4.2c). Similarly to the CV signal of Fe(II), the oxidation peak of TA on ITO is shifted compared to values reported in literature (0.44 V). Fe(II)/TA mixture shows a first peak of oxidation at 0.25 V, attributed to Fe(II) oxidation, followed by a second larger peak at 0.80 V, corresponding to galloyl oxidation (Figure 4.2d). A small reduction peaks is visible at 0.12 V, which can be assigned to Fe(III) reduction. According to the cyclic voltammograms, it can be anticipated that by working at potentials between 0.1 and 0.5 V, the oxidation of Fe(II) to Fe(III) occurs while the oxidation of TA can be limited.

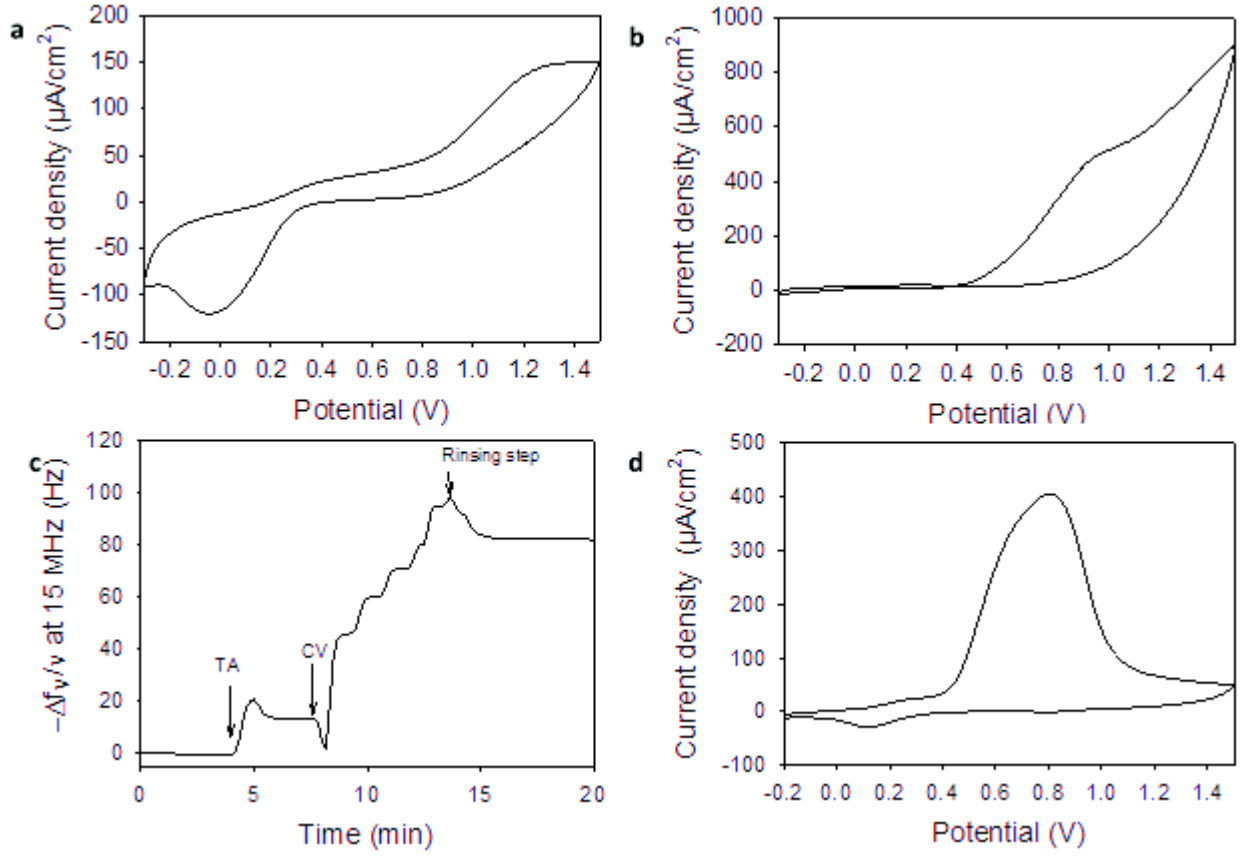

Figure 4.2: *Cyclic voltammograms, obtained on ITO-QCM crystal, of (a) Fe(II) solution ($FeSO_4$, 1 mg/mL) solution, (b) TA (10 mg/mL) over the potential range of -0.3 V to 1.5 V (scan rate 50 mV/s). (c) In-situ evolution of the normalized frequency shift, measured by QCM, as a function of time during the application of cyclic voltammetry on TA solution in contact with ITO-QCM crystal (-0.3 V to 1.5 V, scan rate 50 mV/s) (d) Cyclic voltammogram of Fe(II)/TA mixture at 2.5 in molar ratio over the potential range of -0.3 V to 1.5 V (scan rate 50 mV/s). The supporting electrolyte was 150 mM KPF_6 buffer solution at pH 3.*

4.4 Electro-triggered self-assembly of TA/Fe(III) films

In order to induce and control the self-assembly, the gradient of morphogens, Fe(III), was generated at the electrode surface by electrochemical oxidation of Fe(II) obtained galvanostatically. This method allows controlling the amount of exchanged charges and thus the quantity of morphogen generated at the working electrode. The application of a current allows to control the quantity of morphogens generated. Argon was flushed in all Fe(II) based solutions to prevent any oxidation in solution due to dissolved oxygen. The supporting electrolyte was a 150 mM KPF_6 buffer solution at pH 3 (unless otherwise stated). QCM was used to monitor *in situ* the self-assembly of TA/Fe(III) film during the application of an anodic current (galvanostatic conditions) with the ITO-QCM crystal acting as working electrode. When a TA/Fe(II) solution (2.5 in Fe(II)/TA ratio at pH 3) was brought in contact with the ITO-QCM crystal, a small frequency shift (20 Hz) was observed corresponding to TA adsorption (Figure 4.3a).

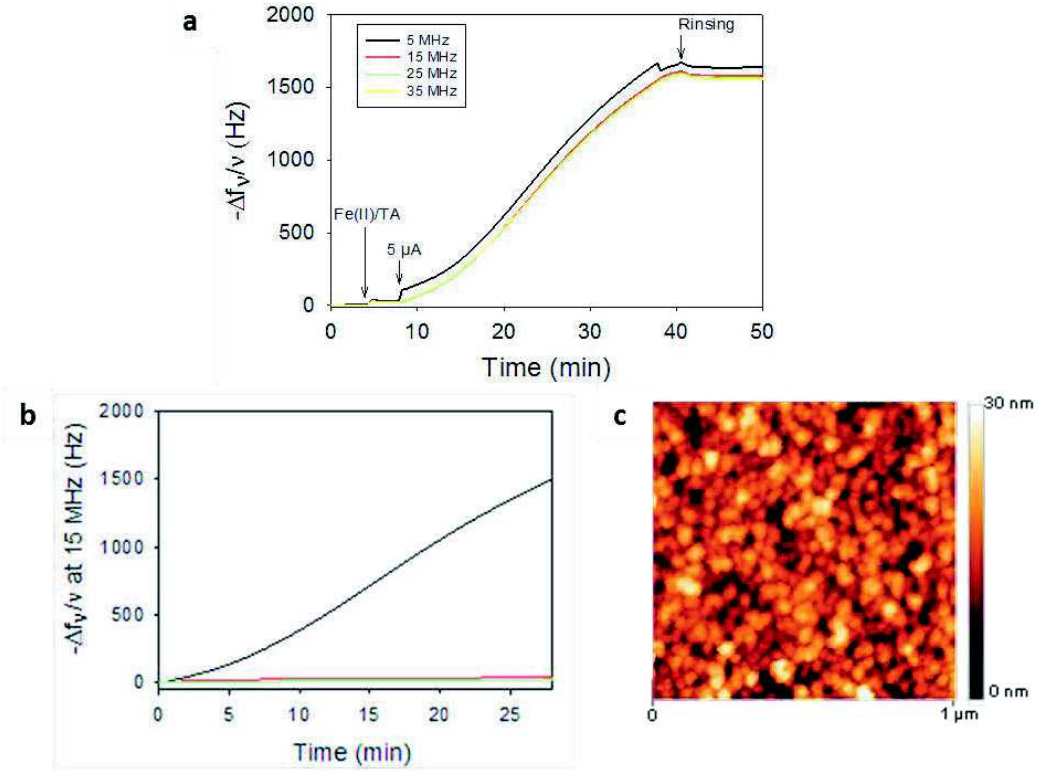

Figure 4.3: *(a) Evolution of the normalized frequency shift, measured by QCM at different frequencies, as a function of time of Fe(II)/TA mixture (2.5 in Fe(II)/TA ratio at pH 3) during the application of 6.25 µA/cm^2. (b) Evolution of the normalized frequency shift, measured by QCM-D, as a function of time of (black line) Fe(II)/TA mixture (2.5 in Fe(II)/TA ratio at pH 3), (red line) Fe(II) and (green line) TA solutions during the application of 6.25 µA/cm^2. (c) AFM image, obtained in contact mode and liquid state, of self-assembled TA/Fe(III) film obtained after 30 min.*

As soon as a current of 6.25 µA/cm^2 (corresponding to an applied current of 5 µA) was applied, the opposite of the normalized frequency shift increased, in first approximation, linearly with time showing the self-assembly of a TA/Fe(III) film (Figure 4.3b). When the application of the current is interrupted followed by a rinsing step, the evolution of the resonance frequency was stopped (Figure 4.3a). In the sole presence of TA or Fe(II), smaller frequency shifts (less than 30 Hz) were observed (Figure 4.3b). The presence of both partners is thus required which strongly indicates the self-assembly of a TA/Fe(III) film. The morphology of the deposited film was characterized by Atomic Force Microscopy (AFM) in contact mode and liquid state (Figure 4.3c).

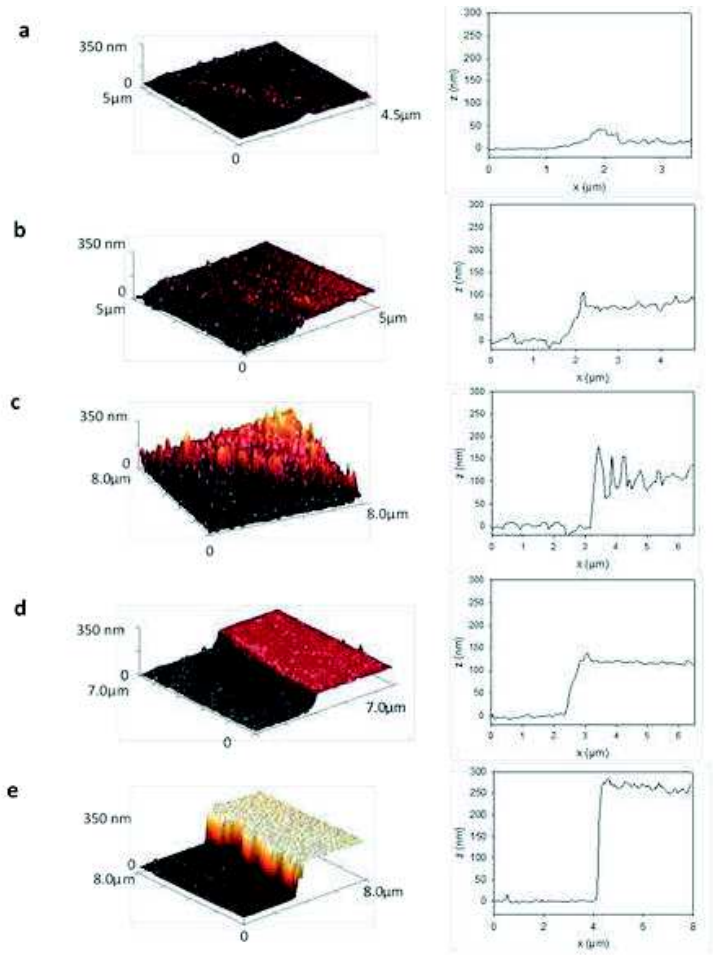

Figure 4.4: *Typical AFM 3D images, obtained in contact mode and liquid state, and respective cross-section profiles of a scratched TA/Fe(III) film, obtained after (a) 5 min, (b) 10 min, (c) 20 min and (d) 70 min of self-assembly. The film buildup was performed with a TA/Fe(II) solution at (2.5 in Fe(II)/TA ratio at pH 3) by applying a current value of 6.25 µA/cm^2.*

Figure 4.3b shows a typical topography corresponding to a TA/Fe(III) film self-assembled for 30 min with an applied current of 6.25 µA/cm^2. The film appears grainy with a roughness (root mean square roughness calculated on 10 × 10 µm^2 AFM images) of about 5.2 ± 1 nm. After

scratching, the thickness of the film could be determined (Figure 4.4). After 5 min of self-assembly, the film covers uniformly the whole substrate with a thickness of 16 ± 1 nm (determined from three measurements of the *z* section) and a roughness of 6.3 ± 0.1 nm. The film thickness increases as a function of the application time of the current until 263 ± 3 nm reached at 70 min. It can be noticed that the film roughness remains almost constant reaching 6.8 ± 0.1 nm (Figure 4.5).

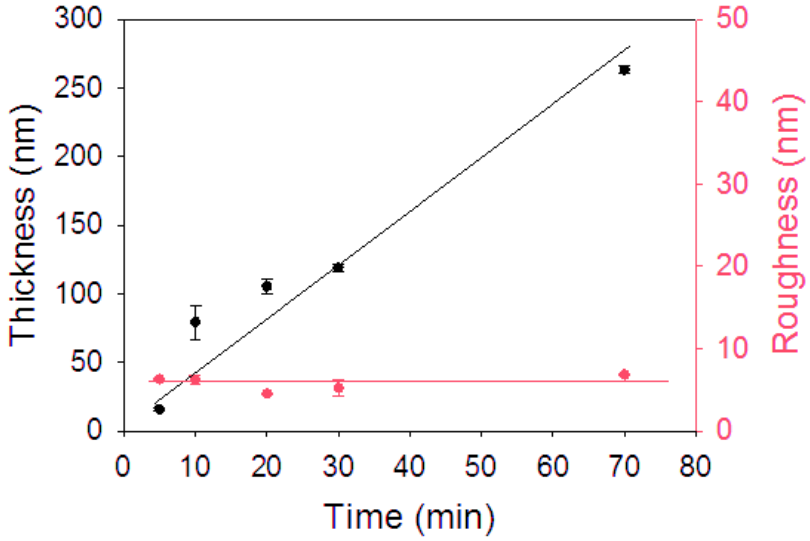

Figure 4.5: *Evolution of the thickness and the roughness, measured by AFM in contact mode in liquid state, of the self-assembled TA/Fe(III) film, after scratching, as a function of time. TA/Fe(II) mixture solution (2.5 in Fe(II)/TA ratio at pH 3) was putted in contact with the electrode with an applied current of 6.25 µA/cm^2. The film roughness was calculated on a 10 × 10 µm^2 AFM images. The data represents the mean and the standard deviation of three measurements. Lines are used to guide the eye.*

The constant roughness is due to the self-assembly of TA/Fe(III) complexes in the solution in the vicinity of the electrode which adsorb on the surface along the process. This is in accordance with AFM image where the film seems to be a homogeneous assembly consisting in 30 nm-diameter nanoparticles (Figure 4.3b). The electro-controlled generation of morphogenic Fe(III) from the electrode allows to control the self-assembly of TA/Fe(III) on its surface simply by adjusting the time over which the potential is applied. It is interesting to compare these electrogenerated TA/Fe(III) self-assembled films to the films obtained by Ejima *et al.* in one pot process by using pH changes of TA/Fe(III) solution. At similar iron ions/TA molar ratios, the roughness of both films are in the same range.[5]

4.5 Chemical analysis of the self-assembled TA/Fe(III) film

XPS investigation of self-assembled films allowed to determine both the atomic and chemical functions composition. A typical analysis of a TA/Fe(III) self-assembled film is given through

a buildup obtained from a TA/Fe(II) solution (2.5 in Fe(II)/TA ratio at pH 3) in contact with an ITO-QCM electrode with an applied current of 6.25 µA/cm^2 for 30 min. Following atoms were detected in the XPS spectrum: carbon (C), oxygen (O) and iron (Fe) (Figure 4.6a-b). The C 1s peak at 285 eV (used as an internal calibration peak) represents 70% of the elemental composition of the self-assembled film and confirms the presence of TA in the resulting film because it is the only one carbon-containing compound in the starting TA/Fe(II) solution. The position of Fe $2p_{1/2}$ and Fe $2p_{3/2}$ peaks, centered at 725.5 eV and 711.9 eV respectively, indicated the presence of Fe(III) species in the self-assembled film (Figure 4.6c).[34] By deconvolution of both peaks, the relative proportion of Fe(III) and Fe(II) were evaluated at 80-85% and 20-15%, respectively. These values of Fe(III)/Fe(II) ratio are in agreement with deconvoluated peaks of Fe 3p observed at 56.8 eV (Figure 4.7a). The presence of Fe(III) in major proportion validates our proposed model of film buildup based on the gradient of Fe(III) generated *in situ* from the electrode surface. In addition, by deconvolution of O 1s signal, two peaks centered at 533.5 eV and 531.8 eV can be attributed to H-O-Fe and O-Fe species, respectively (Figure 4.7b). Entities O-Fe provide the evidence that Fe(III) and TA are coordinated through phenol groups from gallic acid units as previously reported in the literature.[23, 35] The presence of Fe-O-H can be explained by the coordination of water molecules with Fe(III). This means that the six coordination sites of some Fe(III) atoms involved into the self-assembled architecture of the film are not all occupied by phenol groups from TA. This is in agreement with the atomic Fe/TA ratio calculated using $C_{76}H_{52}O_{46}$ as chemical formula of TA: by integration of the elemental peaks of Fe and C (with respect to their individual sensitivity factors) the Fe/TA ratio is about 1:2 which correspond to bis-coordinated complexes (1 Fe complexed by 2 TA).

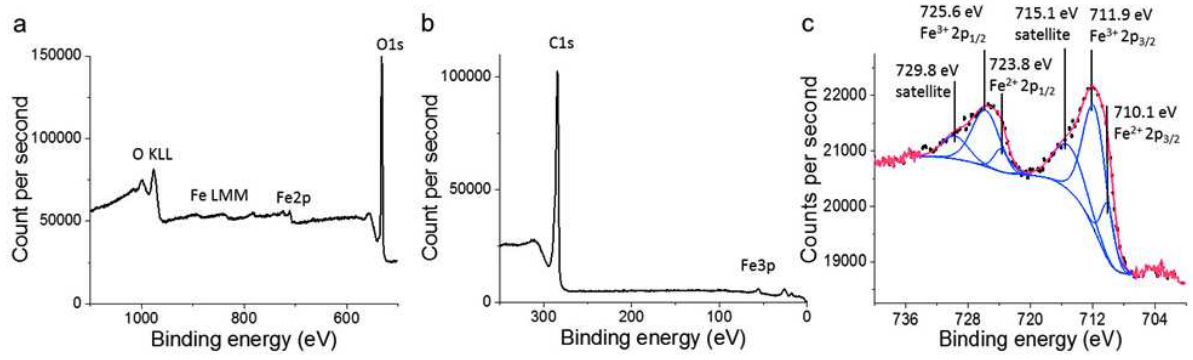

***Figure 4.6**: XPS spectra of TA/Fe(III) self-assembled film (a, b) survey spectrum and (c) Fe 2p core-level spectrum. Experimental data are drawn in dotted black line. TA/Fe(III) self-assembled film was obtained with TA/Fe(II) mixture solution (2.5 in Fe(II)/TA ratio at pH 3) in contact with an ITO-QCM electrode with an applied current of 6.25 µA/cm^2 for 30 min.*

Deconvolution of the C 1s peak located in the area going from 283 eV to 294 eV (Figure 4.8) gives access to the relative proportion of carbons involved in both C-OH and C=O groups. The carbon atom involved in the C-OH group is assigned to both phenol groups and all six carbons constituting the glucose central ring of TA. The other C=O carbon included the carbonyl moiety coming from ester groups bonding all gallic acid units all together to form TA.

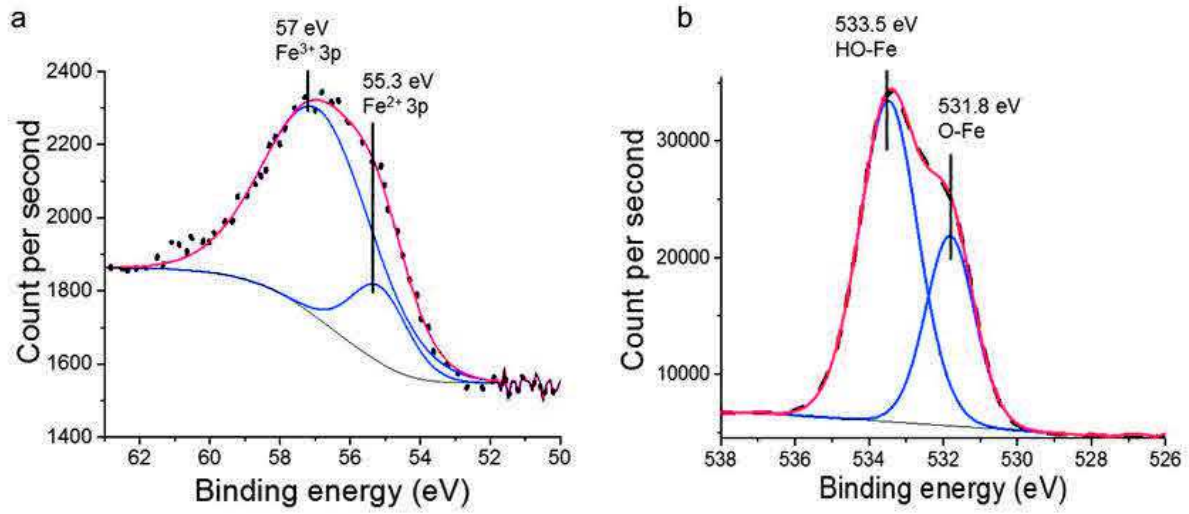

***Figure 4.7**: XPS analysis of (a) the Fe 2p and (b) O 1s core-level spectrum of TA/Fe(III) self-assembled film. Experimental data are drawn in dotted black line. TA/Fe(III) self-assembled film was obtained with TA/Fe(II) mixture solution (2.5 in Fe(II)/TA ratio at pH 3) in contact with an ITO-QCM electrode with an applied current of 6.25 µA/cm^2 for 30 min.*

According to the chemical structure of TA displayed in Figure 4.1a, the theoretical atomic ratio C-O/C=O is 3.60, a value close to the experimental ratio of 3.55 that we measured by XPS on pure TA powder (Figure 4.8). Surprisingly, XPS analysis of the TA/Fe(III) self-assembled film lead to an atomic ratio C-O/C=O of 2.80, a value indicating a higher proportion of C=O compared to C-O. This value is independent of the Fe(II)/TA molar ratio of the building solution used to self-assemble the film. The presence of more C=O groups than expected can be explained by the oxidation of some phenol groups into quinones either due to the current applied to self-assemble the film, to dissolved oxygen or to iron ions acting as catalysts.[36] It is interesting to note that polyphenol-based coatings such as polydopamine films always contain a small proportion (20-30%) of stable quinone groups into their architecture coming from the oxidation of phenol.[37]

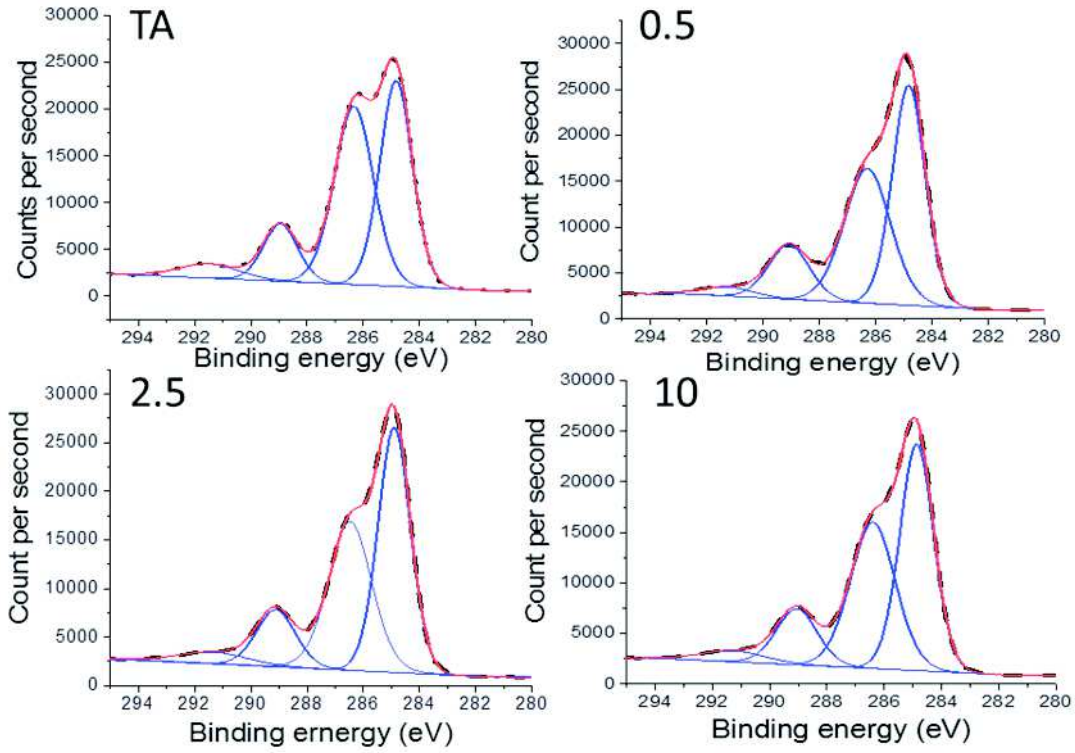

Fe(II)/TA molar ratio of the building solution	0	0.5	2.5	10
O-C/O=C peak area ratio	3.55	2.85	2.8	2.86

Figure 4.8: *High resolution spectra of C1s peaks measured by XPS analysis of TA/Fe(III) self-assembled films obtained from building solutions with Fe(II)/TA molar ratio of 0 (pure TA), 0.5, 2.5 and 10 (black dotted line). Peaks obtained after decomposition are drawn in blue and their sum in red. In all spectra, four components localized respectively at 291 eV, 288.9 eV, 286.3 eV and 284.8 eV were found. They are respectively attributed to π-π* satellite, O=C-O, O-C and C-C bonds. Corresponding peak ratios between O=C and O-C are presented in the table.*

4.6 Influence of the physico-chemical conditions on the self-assembly

To gain more mechanistic insight into the self-assembly process, several parameters that might influence the buildup process were varied. The current intensity was varied from 1.25 to 31.25 $\mu A/cm^2$ while keeping the pH of the mixture solution at 3. It comes out that the TA/Fe(III) film self-assembly kinetic strongly depend on the applied current: higher current intensities lead to a faster buildup kinetic (Figure 4.9a). Higher current intensity leads to higher quantity of electrogenerated Fe(III) ions, the morphogen, in the vicinity of the working electrode leading to the assembly of more TA molecules on the surface and thus making the film thicker. A level

off of TA/Fe(III) self-assembly occurs after reaching a characteristic value in frequency shift and in time. Both values depend on the applied current and the measured potential (Figure 4.9b).

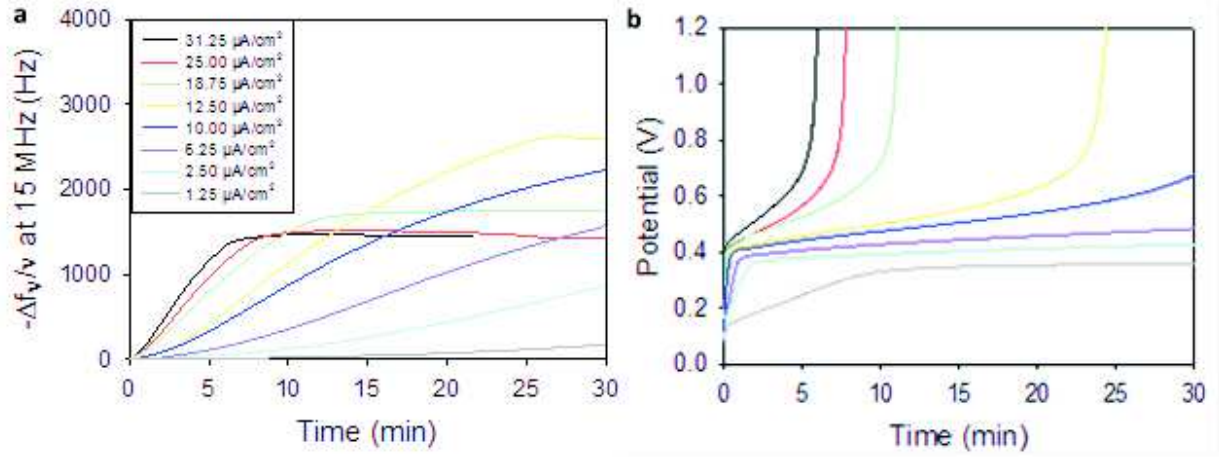

Figure 4.9: *(a) Evolution of the normalized frequency shift, measured by EC-QCM, and (b) of the potential during the self-assembly of TA/Fe(III) film as a function of time performed at different current intensities. TA/Fe(II) mixtures were prepared with 2.5 in Fe(II)/TA ratio at pH 3.*

During the effective self-assembly of TA/Fe(III), the potential required to maintain the current constant in the electrochemical cell increases until a threshold value that is below 0.6 V (Figure 4.9b). Above this value, the buildup of TA/Fe(III) film slows down until a plateau is reached. Before the frequency shift plateau is reached, most of the current corresponds to Fe(II) oxidation into Fe(III). The increase in potential above 0.6 V is related to the oxidation of TA molecules, present in the self-assembled film, that probably cross-link on the surface of the electrode (Figure 4.2b-c).[38-39] Interestingly, a thicker film is formed, before reaching the blocking plateau, with a slower self-assembly kinetic, *i.e.* with lower current intensities. During the buildup, a shift of the applied potential toward more oxidative conditions occurs, so that the current in the system remains constant. This result suggests that the electronic transfer becomes less favorable while the film growth because the diffusion of Fe(II) to the electrode is too slow. For systems reaching 0.6 V or above, the measured frequency shift levels off, indicating the end of the film growth (Figure 4.9b). At this potential, the oxidation current is predominantly due to the oxidation and cross-linking of TA present in the self-assembled film, leading to lower quantity of electrogenerated Fe(III) and thus leading to a slower buildup until no more buildup, when the film becomes impermeable to Fe ions.

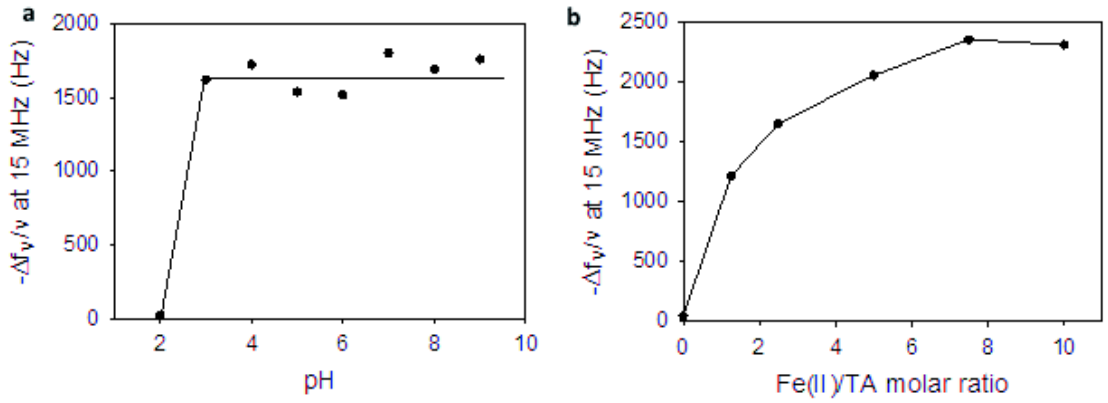

Figure 4.10: *Evolution of the normalized frequency shift during TA/Fe(III) self-assembly as a function (a) of the buildup pH with 2.5 in Fe(II)/TA molar ratio and (b) of Fe(II)/TA molar ratio with a buildup pH of 3. The applied current intensity was fixed at 6.25 µA/cm² for 30 min.*

The influence of the pH and the Fe(II)/TA molar ratio of the building solution were also investigated for an applied current of 6.25 µA/cm² (Figure 4.10). Below pH 3 with a Fe(II)/TA molar ratio of 2.5, a small buildup is obtained (about 25 Hz). Above pH 3 until pH 9, there is no influence of the pH and the frequency shift observed is around 1600 Hz after 30 min of self-assembly (Figure 4.10a). The coordination between TA and Fe(III) is pH-dependent leading to mono-complex at pH < 2, di-complex at 3 < pH < 6 and tris-complex at pH > 7.[5] For a pH buildup below 3, the electrogeneration of Fe(III) does not lead to film self-assembly due to the formation of mono-complex mainly. Above this pH value, the pH has thus almost no influence on the self-assembly of TA and Fe(III). Next, keeping the applied current intensity fixed (6.25 µA/cm²), the Fe(II)/TA molar ratio of the buildup mixture was varied from 0 to 10 with TA concentration fixed at 10 mg/mL. Thicker TA/Fe(III) films are obtained with higher Fe(II)/TA molar ratio reaching a plateau for a Fe(II)/TA molar ratio of 8 (Figure 4.10b). We performed XPS measurements on three different self-assembled films obtained with Fe(II)/TA molar ratios of 0.5, 2.5 and 10 in the buildup mixture (Figure 4.8). The Fe/TA molar ratio of the self-assembled film is about 1:2 independently of the Fe(II)/TA molar ratio of the buildup mixture. The relative percentages of Fe(III) and Fe(II) are also similar for the three tested films. By keeping the applied current intensity fixed, the same quantity of Fe(III) is electrogenerated in the solution. However, the kinetic of the self-assembly increases by increasing Fe(II)/TA ratio (Figure 4.11). In the building solution, monomeric Fe(II)/TA soluble complexes are formed. Taking into account the molecular formulae of TA, 10 moieties (5 pyrogallol and 5 catechoyl moities) per TA molecule can be complexed with Fe(II). By increasing the Fe(II)/TA molar ratio in the building solution, each molecule of TA will be complexed with an increasing

number of Fe(II) ions until saturation (Fe(II)/TA = 10). A the saturation, all TA molecules present in the bulk and in contact with the electrode are surrounded by Fe(II) ions which increases the probability of the electro-generated Fe(III), from Fe(II), to interact with TA. These experiments highlight the crucial role of the Fe(II)/TA molar ratio on the self-assembly of the film.

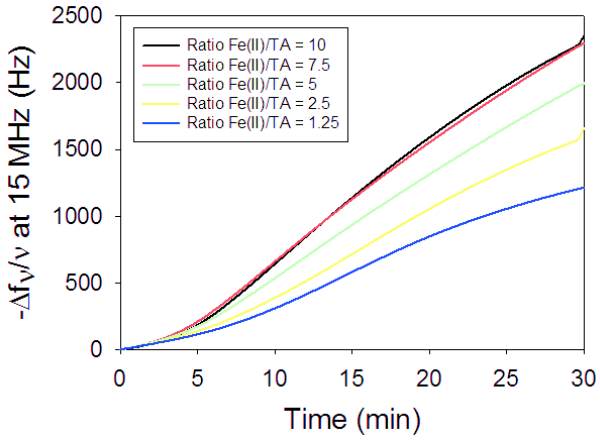

***Figure 4.11**: Evolution of the normalized frequency shift, measured by QCM, as a function of time of TA/Fe(II) mixtures at pH 3 at different Fe(II)/TA ratio during the application of 6.25 µA/cm².*

4.7 Stability of the coating

To test the stability of TA/Fe(III) self-assembled films, EDTA solutions, known to chelate metal cations, were put in contact with films obtained at two different pHs: pH 3 and pH 7.4. The pH of the EDTA solution was similar to that of the film buildup solution. We found previously that the same mass is deposited on the electrode at these two pHs.

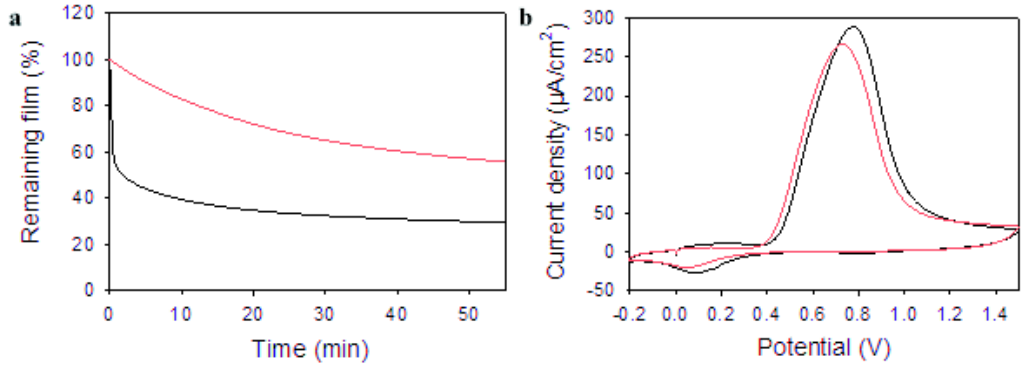

***Figure 4.12:** (a) Percentage of remaining TA/Fe(III) films, self-assembled at (black curve) pH 3 and (red curve) pH 7.4, as a function of time when putted in contact with 100 mM EDTA at the buildup pH. The percentage is calculated from the frequency shift obtained by QCM signal at the injection of the EDTA solution. (b) First cycle of the cyclic voltamogramm of TA/Fe(III) films after self-assembly (black curve) at pH 3 and (red curve) at pH 7.4. The cyclic voltammetry was performed in contact with 150 mM KPF_6 solution between -0.2 V and 1.5 V at 50 mV/s. The self-assembled films were obtained using an applied current of 6.25 µA/cm² for 30 min with 2.5 Fe(II)/TA ratio mixture solution.*

After 55 min of contact with EDTA, the percentage of the remaining film was about 56% at pH 7.4 and 30% at pH 3 (Figure 4.12a). The film seems thus to be more stable when self-assembled at pH 7.4 than at pH 3. This is consistent with the fact that the number of coordination bonds increases with the pH leading to more stable TA/Fe(III) complexes.[5] When a cyclic voltammetry was performed on TA/Fe(III) self-assembled films at pH 3 and pH 7.4, we observed a similar irreversible oxidation peak of TA (between 0.7 and 0.8 V) and the peak of oxido/reduction of iron (at 0.2 V and 0.1 V) (Figure 4.12b). However, the Fe(III)/Fe(II) oxido-reduction peaks are more visible at pH 3 than at pH 7.4 in the potential range of 0 V and 0.3 V. This result is in accordance with the fact that di-coordinated complexes are mainly formed at pH 7.4. Self-assembly of TA/Fe(III) at pH 7.4 leads to more coordinated and thus less sensitive Fe(III) ions than at pH 3. Indeed, mono-coordinated complexes of catechol, similar to galloyl moieties, can be involved in electron transfer reactions in contrast to di- or tris-coordinated complexes that prevent redox reactions.[40] The stability of TA/Fe(III) coating was also tested by the application of reductive potentials to induce the reduction of Fe(III) into Fe(II) (Figure 4.13).

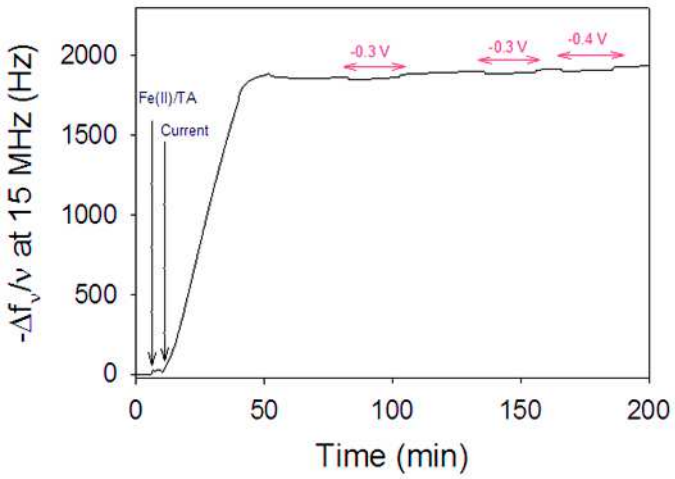

***Figure 4.13**: Evolution of the normalized frequency shift, measured by QCM, as a function of time of TA/Fe(II) mixture (2.5 in Fe(II)/TA ratio at pH 3) during the application of 6.25 µA/cm^2 followed by the application of three reductive potentials.*

No visible dissolution of the film was observed at -0.4 V indicating the stability of TA/Fe(III) complexes. To go further, several cycles of cyclic voltammetry have been applied on both self-assembled films (Figure 4.14).

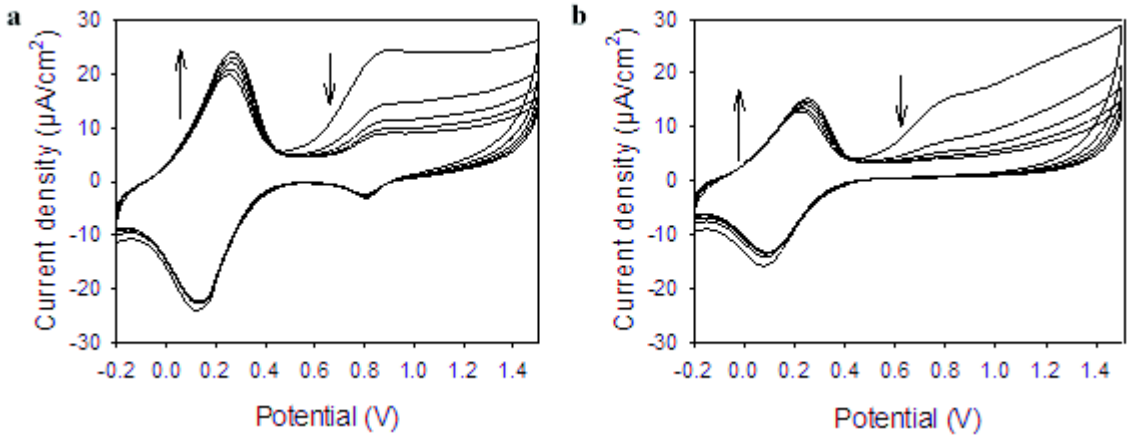

***Figure 4.14**: Cyclic voltamogramms of TA/Fe(III) films after self-assembly at (a) pH 3 and (b) pH 7.4. The cyclic voltammetry was performed in contact with 150 mM KPF_6 solution between -0.2 V and 1.5 V at 50 mV/s (5 cycles). The first cycle is represented in Figure 4.12b. The black arrows indicate the evolution of the signal during the cyclic voltammetry. The self-assembled films were obtained by using an applied current of 6.25 µA/cm² for 30 min with 2.5 Fe(II)/TA ratio mixture solution.*

After the first cycle (Figure 4.12b), the oxidation peak of TA decreases about 10 fold followed by a slower continuous decrease during the following cycles. This indicates an irreversible TA oxidation, probably at the vicinity of the electrode. At the same time, the oxido-reduction signal of Fe(II)/Fe(III) increases. This could be explained by the release of Fe(III) from di-coordinated complexes simultaneously with the irreversible oxidation of galloyl moieties of TA. The oxidation of TA seems to be partially reversible at pH 3 (presence of a reduction peak of TA at 0.8 V) in comparison to pH 7.4. This may be tentatively explained by the better oxidation of pyrogallol at higher pH.[41]

4.8 Generalization of the concept and Conclusion

To generalize the concept, two other polyphenols, gallic acid and rosmarinic acid (Figure 4.15a-b), were used in mixtures with Fe(II) to self-assemble a film. Figure 4.15c-d demonstrates that the concept of electrochemically induced self-assembly of TA can be generalized to other polyphenols.

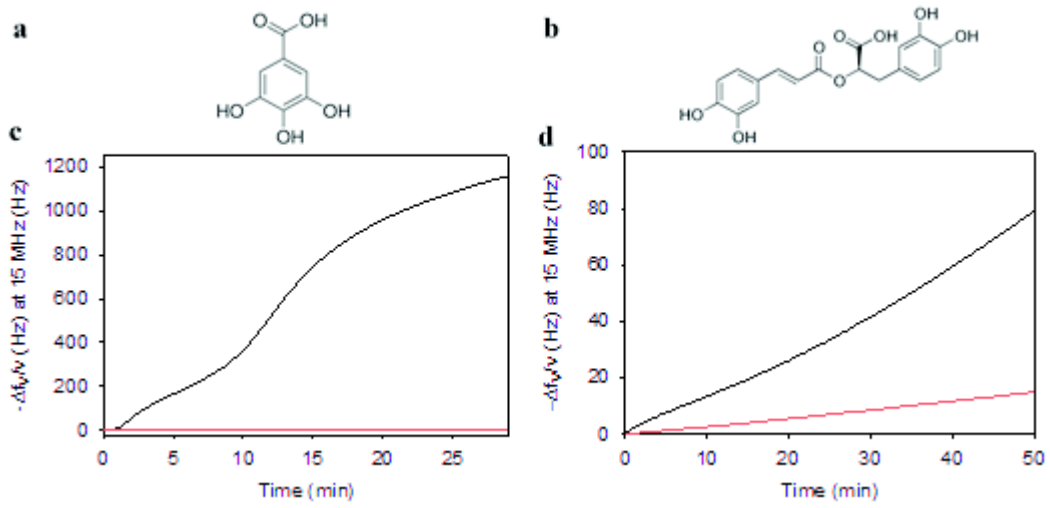

Figure 4.15: *Chemical formulae of (a) gallic acid and (b) rosmarinic acid. Evolution of the normalized frequency shift as a function of time of (c) gallic acid/Fe(II) mixture, 1:2 Fe(II)/gallic acid molar ratio at pH 3 (black curve) and gallic acid (red curve), at an applied current of 62.5 µA/cm^2 (d) rosmarinic acid/Fe(II) mixture, 1:1 Fe(II)/rosmarinic acid molar ratio at pH 3, (black curve) and rosmarinic acid (red curve) at an applied current of 6.25 µA/cm^2.*

In summary, a new electrotriggered self-assembly of metal-polyphenol nanocoatings was developed using a morphogenic approach. TA/Fe(III) nanofilms were self-assembled using a mixture of Fe(II) and TA on which an anodic current was applied leading to the oxidation of Fe(II) into Fe(III) at the surface of an electrode. The confined electro-generated gradient of Fe(III) allowed to control the buildup of TA/Fe(III) film based on di-coordinated complexes independent of the pH and Fe(II)/TA molar ratio of the building solution. The film thickness and the self-assembly kinetic could be tuned by the application time, the value of the current and Fe(II)/TA molar ratio of the building solution. We showed that this strategy should be applicable to a wide range of polyphenols.

References

1. Webber, M. J.; Appel, E. A.; Meijer, E. W.; Langer, R. Supramolecular Biomaterials. *Nature Materials* **2016,** *15*, 13.

2. Whitesides, G. M.; Boncheva, M. Beyond Molecules: Self-Assembly of Mesoscopic and Macroscopic Components. *Proceedings of the National Academy of Sciences of the United States of America* **2002,** *99*, 4769.

3. Vigier-Carriere, C.; Garnier, T.; Wagner, D.; Lavalle, P.; Rabineau, M.; Hemmerle, J.; Senger, B.; Schaaf, P.; Boulmedais, F.; Jierry, L. Bioactive Seed Layer for Surface-Confined Self-Assembly of Peptides. *Angewandte Chemie-International Edition* **2015,** *54*, 10198.

4. Decher, G. Fuzzy Nanoassemblies: Toward Layered Polymeric Multicomposites. *Science* **1997,** *277*, 1232.

5. Ejima, H.; Richardson, J. J.; Liang, K.; Best, J. P.; van Koeverden, M. P.; Such, G. K.; Cui, J.; Caruso, F. One-Step Assembly of Coordination Complexes for Versatile Film and Particle Engineering. *Science* **2013,** *341*, 154.

6. Friese, V. A.; Kurth, D. G. From Coordination Complexes to Coordination Polymers through Self-Assembly. *Current Opinion in Colloid & Interface Science* **2009,** *14*, 81.

7. Case, L. B.; Waterman, C. M. Integration of Actin Dynamics and Cell Adhesion by a Three-Dimensional, Mechanosensitive Molecular Clutch. *Nature Cell Biology* **2015,** *17*, 955.

8. Krylova, I. Painting by Electrodeposition on the Eve of the 21st Century. *Progress in Organic Coatings* **2001,** *42*, 119.

9. Wu, L. Q.; Gadre, A. P.; Yi, H. M.; Kastantin, M. J.; Rubloff, G. W.; Bentley, W. E.; Payne, G. F.; Ghodssi, R. Voltage-Dependent Assembly of the Polysaccharide Chitosan onto an Electrode Surface. *Langmuir* **2002,** *18*, 8620.

10. Boccaccini, A. R.; Keim, S.; Ma, R.; Li, Y.; Zhitomirsky, I. Electrophoretic Deposition of Biomaterials. *J. R. Soc. Interface* **2010,** *7*, S581.

11. Ngankam, A. P.; Van Tassel, P. R. Continuous Polyelectrolyte Adsorption under an Applied Electric Potential. *Proceedings of the National Academy of Sciences of the United States of America* **2007,** *104*, 1140.

12. Olsen, C.; Van Tassel, P. R. Polyelectrolyte Adsorption Kinetics under an Applied Electric Potential: Strongly Versus Weakly Charged Polymers. *Journal of Colloid and Interface Science* **2009,** *329*, 222.

13. Shi, X. W.; Tsao, C. Y.; Yang, X. H.; Liu, Y.; Dykstra, P.; Rubloff, G. W.; Ghodssi, R.; Bentley, W. E.; Payne, G. F. Electroaddressing of Cell Populations by Co-Deposition with Calcium Alginate Hydrogels. *Advanced Functional Materials* **2009,** *19*, 2074.

14. Cheng, Y.; Tsao, C. Y.; Wu, H. C.; Luo, X. L.; Terrell, J. L.; Betz, J.; Payne, G. F.; Bentley, W. E.; Rubloff, G. W. Electroaddressing Functionalized Polysaccharides as Model Biofilms for Interrogating Cell Signaling. *Advanced Functional Materials* **2012,** *22*, 519.

15. Johnson, E. K.; Adams, D. J.; Cameron, P. J. Directed Self-Assembly of Dipeptides to Form Ultrathin Hydrogel Membranes. *Journal of the American Chemical Society* **2010,** *132*, 5130.

16. Liu, Y.; Cheng, Y.; Wu, H. C.; Kim, E.; Ulijn, R. V.; Rubloff, G. W.; Bentley, W. E.; Payne, G. F. Electroaddressing Agarose Using Fmoc-Phenylalanine as a Temporary Scaffold. *Langmuir* **2011,** *27*, 7380.

17. Leisk, G. G.; Lo, T. J.; Yucel, T.; Lu, Q.; Kaplan, D. L. Electrogelation for Protein Adhesives. *Advanced Materials* **2010,** *22*, 711.

18. Wong, I. Y.; Footer, M. J.; Melosh, N. A. Electronically Activated Actin Protein Polymerization and Alignment. *Journal of the American Chemical Society* **2008,** *130*, 7908.

19. Waltman, R. J.; Bargon, J. Electrically Conducting Polymers - a Review of the Electropolymerization Reaction, of the Effects of Chemical-Structure on Polymer Film Properties, and of Applications Towards Technology. *Can. J. Chem.* **1986,** *64*, 76.

20. Kolb, H. C.; Finn, M. G.; Sharpless, K. B. Click Chemistry: Diverse Chemical Function from a Few Good Reactions. *Angewandte Chemie-International Edition* **2001,** *40*, 2004.

21. Dochter, A.; Garnier, T.; Pardieu, E.; Chau, N. T. T.; Maerten, C.; Senger, B.; Schaaf, P.; Jierry, L.; Boulmedais, F. Film Self-Assembly of Oppositely Charged Macromolecules Triggered by Electrochemistry through a Morphogenic Approach. *Langmuir* **2015,** *31*, 10208.

22. Erel-Unal, I.; Sukhishvili, S. A. Hydrogen-Bonded Multilayers of a Neutral Polymer and a Polyphenol. *Macromolecules* **2008,** *41*, 3962.

23. Rahim, M. A.; Ejima, H.; Cho, K. L.; Kempe, K.; Mullner, M.; Best, J. P.; Caruso, F. Coordination-Driven Multistep Assembly of Metal-Polyphenol Films and Capsules. *Chemistry of Materials* **2014,** *26*, 1645.

24. Ringwald, C.; Ball, V. Layer-by-Layer Deposition of Tannic Acid and Fe 3+ Cations Is of Electrostatic Nature but Almost Ionic Strength Independent at Ph 5. *Journal of Colloid and Interface Science* **2015,** *450* 119.

25. Yang, L.; Han, L.; Ren, J.; Wei, H.; Jia, L. Coating Process and Stability of Metal-Polyphenol Film. *Colloids and Surfaces A: Physicochem. Eng. Aspects* **2015,** *484*, 197.

26. Guo, J. L.; Ping, Y.; Ejima, H.; Alt, K.; Meissner, M.; Richardson, J. J.; Yan, Y.; Peter, K.; von Elverfeldt, D.; Hagemeyer, C. E.; Caruso, F. Engineering Multifunctional Capsules through the Assembly of Metal-Phenolic Networks. *Angewandte Chemie-International Edition* **2014,** *53*, 5546.

27. Rahim, M. A.; Kempe, K.; Mullner, M.; Ejima, H.; Ju, Y.; van Koeverden, M. P.; Suma, T.; Braunger, J. A.; Leeming, M. G.; Abrahams, B. F.; Caruso, F. Surface-Confined Amorphous Films from Metal-Coordinated Simple Phenolic Ligands. *Chemistry of Materials* **2015,** *27*, 5825.

28. Maerten, C.; Garnier, T.; Lupattelli, P.; Chau, N. T. T.; Schaaf, P.; Jierry, L.; Boulmedais, F. Morphogen Electrochemically Triggered Self-Construction of Polymeric Films Based on Mussel-Inspired Chemistry. *Langmuir* **2015,** *31*, 13385.

29. Hingston, F. J. Activity of Polyphenolic Constituents of Leaves of Eucalyptus and Other Species in Complexing and Dissolving Iron Oxide. *Australian Journal of Soil Research* **1963,** *1*, 63.

30. Nagasaka, M.; Yuzawa, H.; Horigome, T.; Hitchcock, A. P.; Kosugi, N. Electrochemical Reaction of Aqueous Iron Sulfate Solutions Studied by Fe L-Edge Soft X-Ray Absorption Spectroscopy. *Journal of Physical Chemistry C* **2013,** *117*, 16343.

31. Kisler, K.; Kim, B. N.; Liu, X.; Berberian, K.; Fang, Q.; Mathai, C. J.; Gangopadhyay, S.; Gillis, K. D.; Lindau, M. Transparent Electrode Materials for Simultaneous Amperometric Detection of Exocytosis and Fluorescence Microscopy. *J Biomater Nanobiotechnol* **2012,** *3*, 243.

32. Wan, H. J.; Zou, Q. L.; Yan, R.; Zhao, F. Q.; Zeng, B. Z. Electrochemistry and Voltammetric Determination of Tannic Acid on a Single-Wall Carbon Nanotube-Coated Glassy Carbon Electrode. *Microchimica Acta* **2007,** *159*, 109.

33. Burzio, L. A.; Waite, J. H. Cross-Linking in Adhesive Quinoproteins: Studies with Model Decapeptides. *Biochemistry* **2000,** *39*, 11147.

34. Moulder, J. F.; Stickle, W. F.; Sobol, P. E.; Bomben, K. D. *Handbook of X-Ray Photoelectron Spectroscopy*; Physical Electronics: Chanhassen, MN, 1995.

35. Gust, J.; Suwalski, J. Use of Mossbauer-Spectroscopy to Study Reaction-Products of Polyphenols and Iron Compounds. *Corrosion* **1994,** *50*, 355.

36. Mander, L.; Liu, H. W. *Comprehensive Natural Products Ii: Chemistry and Biology*; Elsevier: Kildington, U. K., 2010; Vol. 1.

37. d'Ischia, M.; Napolitano, A.; Ball, V.; Chen, C. T.; Buehler, M. J. Polydopamine and Eumelanin: From Structure-Property Relationships to a Unified Tailoring Strategy. *Acc. Chem. Res.* **2014,** *47*, 3541.

38. Mu, S. L.; Chen, C. Electrochemical Oxidation of Pyrogallol: Formation and Characterization of Long-Lived Oxygen Radicals and Application to Assess the Radical Scavenging Abilities of Antioxidants. *Journal of Physical Chemistry B* **2012,** *116*, 12567.

39. Mochizuki, M.; Yamazaki, S.; Kano, K.; Ikeda, T. Kinetic Analysis and Mechanistic Aspects of Autoxidation of Catechins. *Biochimica Et Biophysica Acta-General Subjects* **2002,** *1569*, 35.

40. Avdeef, A.; Sofen, S. R.; Bregante, T. L.; Raymond, K. N. Coordination Chemistry of Microbial Iron Transport Compounds .9. Stability-Constants for Catechol Models of Enterobactin. *Journal of the American Chemical Society* **1978,** *100*, 5362.

41. Deming, T. J. Mussel Byssus and Biomolecular Materials. *Current Opinion in Chemical Biology* **1999,** *3*, 100.

CHAPTER 5: ELECTROTRIGGERED SELF-CONSTRUCTION OF ENZYMATIC FILMS FOR BIOSENSING APPLICATION

CHAPTER 5: ELECTROTRIGGERED SELF-CONSTRUCTION OF ENZYMATIC FILMS FOR BIOSENSING APPLICATION

Summary

5.1 Abstract

During my PhD, we focused on the design of an enzyme-based electrode using electrotriggered film self-construction based on the two strategies developed so far. The idea was to immobilize an enzyme on the electrode using the cross-linking strategy based on the self-construction by catechol/gallol oxidation and the physical entrapment strategy based on the self-assembly of TA/Fe(III) by coordination bonds. In the first case, bis-catechol was used has an electro-activated crosslinker of enzymes through chemical reaction between quinone of the oxidized bis-catechol and amine functions of the enzyme. In the second case, we attempt to physically entrap enzymes in TA/Fe(III) self-assembled films by co-deposition.

5.2 Introduction

Environmental monitoring, food industry or clinical analyses require the development of selective tools for biomolecule detection. Biosensors can be regarded as complementary tools to classical analytical methods (e.g. high performance liquid chromatography) due to their unique feature, their inherent simplicity, relative low cost, rapid response and miniaturization, thereby allowing continuous monitoring. A biosensor is a device composed of two intimately associated elements: (i) a bioreceptor, that is an immobilized sensitive biological element (e.g. enzyme) recognizing the analyte (e.g. enzyme substrate). (ii) a transducer, that is used to convert the (bio)chemical signal resulting from the interaction of the analyte with the bioreceptor into an electronic one. The intensity of the generated signal is directly or inversely proportional to the analyte concentration. Transduction of the biological activity of the functional surface into a quantifiable electric signal can be performed by different ways, depending on the chemical or physical interaction substrate/receptor (Figure 5.1). Enzyme-based electrodes represent an important class of biosensors where byproducts of enzymatic breakdown of an analyte are detected electrochemically.[1-2]

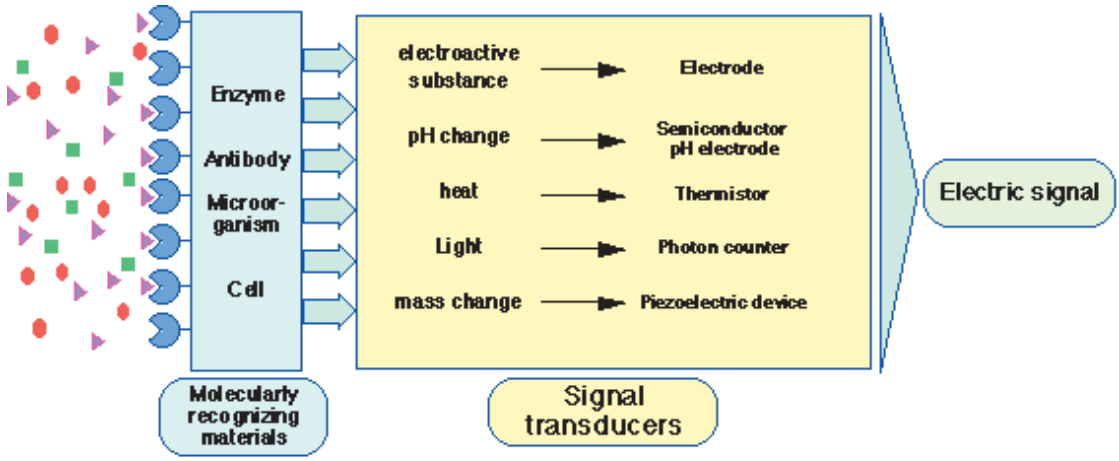

Figure 5.1: *Schematic representation of the general working of biosensors. (www.jaist.ac.jp)*

Electrodeposition of polymers, widely used for biosensing applications, is a simple and attractive approach for the controlled immobilization of enzymes on electrode surfaces.[3-5] It presents many advantages such as localized and fast deposition, working in soft conditions and offers the possibility of co-deposition with others components such as enzymes or nanomaterials. Enzymes are mainly physically entrapped in an electrodeposited film.[6-7] Only few examples of one-pot covalent cross-linking of enzymes exist.[8]

5.3 Electrocrosslinking of enzyme through catechol/gallol oxidation

5.3.1 Introduction and concept

As it was shown in the third chapter, bis-catechol designed in our group can be used for the electro-crosslinking of a polyamine. The principle of this process is based on the reaction of oxidized bis-catechol (bis-quinone) molecules with amine functions of the polymer. We can imagine to use this process to electro-crosslink other compounds bearing amine moieties, such as enzymes. We used alkaline phosphatase (AP) as an enzyme with the same experimental conditions as in chapter 3 (Figure 5.2).

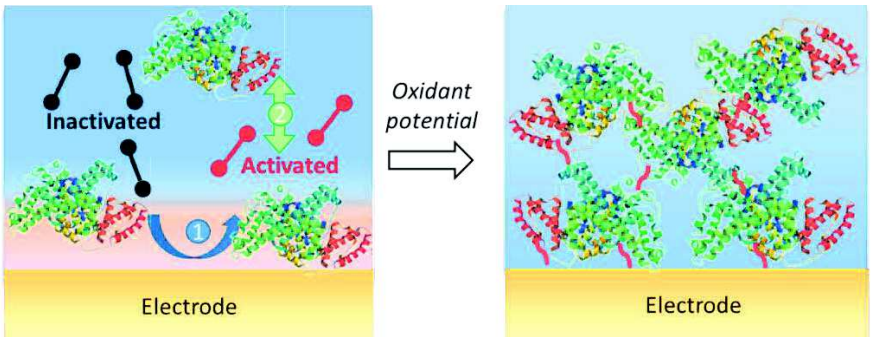

Figure 5.2: *Principle of the one pot self-construction of AP film based on the oxidation of bis-catechol molecules.*

Bis-catechol and AP are unable to crosslink together mixed in an aqueous solution. In contact with an electrode where a defined electrochemical signal is applied, bis-catechol molecules are oxidized into bis-quinones which further react with the amino groups of AP through Michael addition and Schiff's base condensation.

5.3.2 Electrocrosslinking using bis-catechol

First, we tried to electrocrosslink AP using the same optimal conditions, determined for the PAH/bis-catechol system (see Chapter 3). AP (1 mg/mL) and bis-catechol (1 mg/mL) mixtures were prepared in 10 mM HEPES - 150 mM $NaNO_3$ aqueous buffer at pH 7.4. Figure 5.3a shows a typical QCM signal relative to the obtained buildup. After the injection of AP/bis-catechol mixture or bis-catechol alone, a small increase of the normalized frequency is observed due to coordination bonding between catechol and gold QCM crystal. The application of a cyclic voltammetry (CV) (0 - 500 mV, *vs* Ag/AgCl, scan rate of 50 mV/s) results in a very slow increase of the normalized frequency shift in both cases. After 60 min and a rinsing step, the frequency shift reached 40 Hz for AP/bis-catechol mixture and bis-catechol alone in solution.

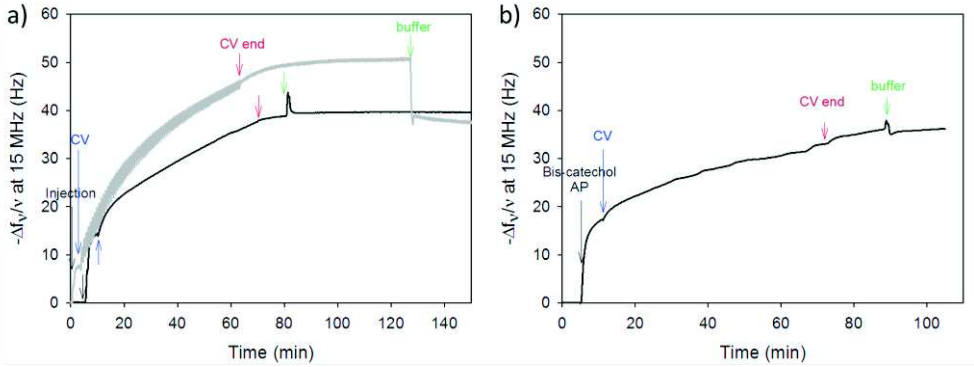

Figure 5.3: *Evolution of the normalized frequency shift, measured by EC-QCM, as a function of time of (a) AP/bis-catechol mixture with bis-catechol (1 mg/mL) and AP (1 mg/mL) (black curve) and bis-catechol (1 mg/mL) solution (grey line) and (b) AP/bis-catechol mixture with bis-catechol (1 mg/mL) and AP (6 mg/mL) during the application of CV between 0 and +500 mV (vs Ag/AgCl, scan rate 50 mV/s).*

In comparison when a PAH/bis-catechol mixture is used in the same conditions, a frequency shift of almost 800 Hz was obtained (Chapter 3, Figure 3.5). The mass deposited with bis-catechol solution can be explained by the electroreticulation of the molecule.[9-10] Indeed, bis-quinone can react with bis-catechol leading to the formation of a free radical that can further react with bis-catechol molecules.[11] As a similar buildup is obtained with and without the enzyme, AP is probably entrapped in the cross-linked bis-catechol matrix. Electrocrosslinking of AP is not possible in this condition. In comparison with PAH, AP, and more generally enzymes, have much lower amine functions density involved in their conformational structure which limits their accessibility for chemical reactions with bis-quinone.[12-13] This could explained the lower adsorbed mass of AP/bis-catechol mixture during the electrodeposition. To increase the probability of cross-linking between bis-catechol and AP, we first increase the concentration of AP and the pH of the solution. The oxidation of catechol is improved at high pH values and amine moieties of AP are deprotonated favoring the reaction with quinone.[14] Figure 5.3b shows the QCM signals obtained during the application of CV (0 - 500 mV, vs Ag/AgCl, 50 mV/s) in the presence of AP (6 mg/mL) and bis-catechol (1 mg/mL) mixture, prepared in the same buffer at pH 8. A similar buildup is obtained in the previous conditions. Thus, increasing AP concentration and the pH does not favor the buildup.

In order to increase the probability of reaction between bis-quinone and amine functions of AP, the concentration of bis-catechol was increased until its limit of solubility maintaining the pH of the solution at 8. When AP (1 mg/mL) and bis-catechol (3 mg/mL) mixture prepared at pH 8 is used and the CV applied for 60 min, the normalized frequency increases until a value of 650 Hz before the rinsing step (Figure 5.4). However, the rinsing step induced a decrease of the frequency shift of almost 350 Hz. The final frequency shift reaches 250 Hz after the rinsing step when using bis-catechol solution.

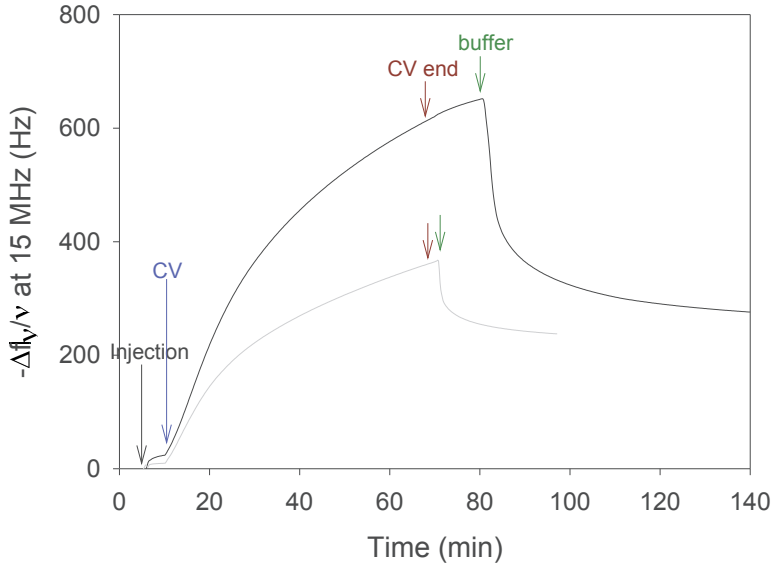

Figure 5.4: *Evolution of the normalized frequency shift, measured by EC-QCM, as a function of time of AP/bis-catechol mixture (black line) and bis-catechol (grey line) with AP at 1 mg/mL and bis-catechol at 3 mg/mL during the application of CV between 0 and +500 mV (vs Ag/AgCl, scan rate 50 mV/s).*

Even if the deposition of AP/bis-catechol mixture is twice faster than the deposition of bis-catechol, a similar mass is deposited with and without the presence of the enzyme. Increasing the concentration in bis-catechol allows to deposit more material on the surface due to its polymerization.[9-10] The decrease in mass at the rinsing step, observed for both buildups, is probably due to loosely adsorbed polymerized bis-catechol on the surface of QCM crystal. Using bis-catechol at higher concentration favors its polymerization. AP is probably physically entrapped in the bis-catechol matrix instead of cross-linked.

5.3.3 Electrocrosslinking using others phenol molecules

Using the same strategy, we used polyphenol molecules having more phenolic moieties (gallol) and a better solubility to improve the electrotriggered crosslinking of AP. Tannic acid (TA) and a dendrimer bearing gallol moieties synthesized in our laboratory were used with AP.

TA is a polyphenol bearing 5 gallol moieties which is soluble at high concentration (2850g/L). As catechol, gallol can be electrochemically oxidized to react covalently with nucleophilic functions such as amine.[15] We first tried to electrodeposit PAH as a proof of concept. TA was mixed at different concentrations with PAH (1 mg/mL) in $NaNO_3$ 150 mM HEPES 10 mM at pH = 7.4. The mixture of TA/PAH were always turbid due to strong electrostatic interactions[16] and were thus filtrated with 0.20 µm filters. CV were applied between 200 and 700 mV because TA is oxidized at a higher potential compared to bis-catechol (see Chapter 3, Figure 3.4a and Chapter 4, Figure 4.2b). Figure 5.6a shows QCM signals measured during the application of

CV (200 - 700 mV, vs Ag/AgCl, 50 mV/s) for TA/PAH mixture and TA solution both with TA at 3 mg/mL. As soon as the CV is applied, the normalized frequency shift starts to increase in both cases. After one hour of CV, the frequency shift reached 120 Hz for the TA/PAH mixture and 70 Hz for TA alone. As catechol, oxidized gallol moieties of TA can react between each other leading to a deposition of mass.[17] Yet, a better mass deposition is obtained in the presence of PAH. Both compounds are needed to measure a significant mass deposition on the crystal. In order to improve the mass deposition, the concentration of TA was increased at 10 mg/mL and we used a fixed potential of 1.0 V (vs Ag/AgCl) to induce the buildup (Figure 5.6b). ITO coated QCM crystals were used to be able to work at this potential. The normalized frequency shift reached 350 Hz for the TA/AP mixture and 100 Hz for TA alone in solution. Working at higher concentrations and at a constant potential of 1.0 V allows to deposit thicker films. These results show that TA can be used as an electro-activated crosslinker of polyamine.

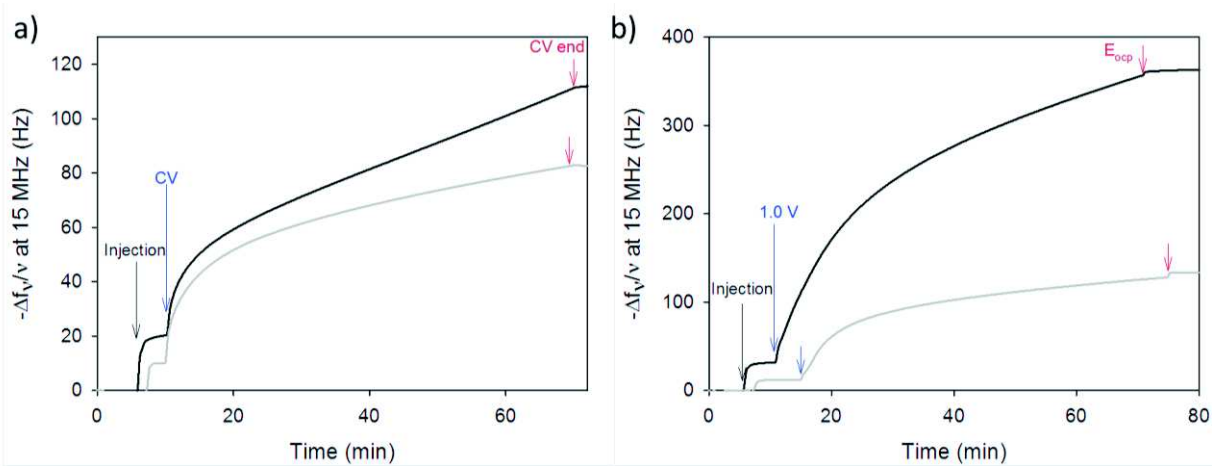

Figure 5.6: *Evolution of the normalized frequency shift, measured by EC-QCM, as a function of time of (a) TA/PAH (black line) and TA (grey line) mixture during the application of CV between +200 and +700 mV (vs Ag/AgCl, scan rate 50 mV/s).(b) TA/PAH (black line) and TA (grey line) during the application of +1.0 V (vs Ag/AgCl) for 1h alternated with OCP.*

After the validation of the process with PAH/TA mixture, AP/TA mixture were prepared with AP at 1 mg/mL and TA at 10 mg/mL, in $NaNO_3$ 150 mM HEPES 10 mM at pH = 7.4. As soon as both compounds are mixed, the solution becomes turbid. This is due to the complexation between the enzyme and TA.[18-20] A filtrated solution was used for the following experiments. After 1 h of potential application (1.0 V) followed by a rinsing step, the measured frequency shifts are of 40 Hz for AP/TA mixture and 60 Hz for TA in solution (Figure 5.7). As with bis-catechol, AP does not contribute to the film buildup in these conditions. Moreover, a similar decrease of QCM signal at the rinsing step is observed for both TA/AP and TA solutions, probably related to loosely adsorbed material.

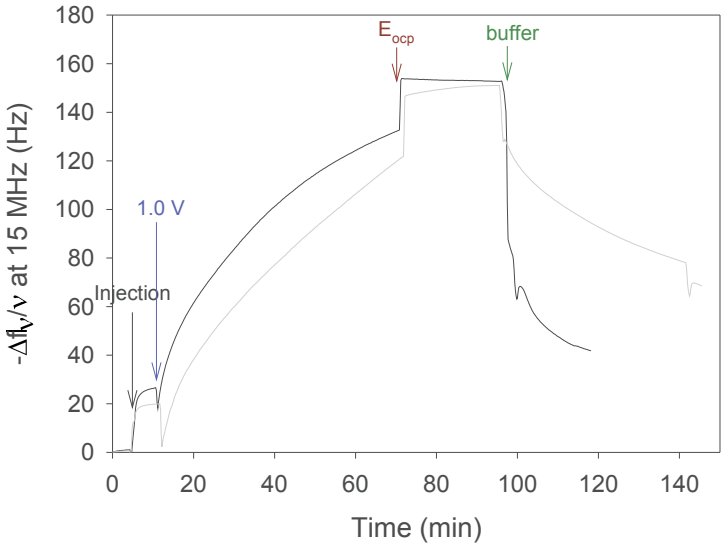

Figure 5.7: *Evolution of the normalized frequency shift, measured by EC-QCM, as a function of time of TA/AP (black line) and TA (grey line) from a filtrated mixture during the application of a constant potential of +1.0 V (vs Ag/AgCl, 1h).*

In order to avoid the complexation of AP by TA due to its numerous gallol moieties and the other phenolic functions in its structure, a gallol-dendrimer was synthesized by Dr. Paolo Luppatelli, post doctorant in the team (Figure 5.8). Presenting three gallol moieties, gallol-dendrimer does not form aggregates with AP in solution.

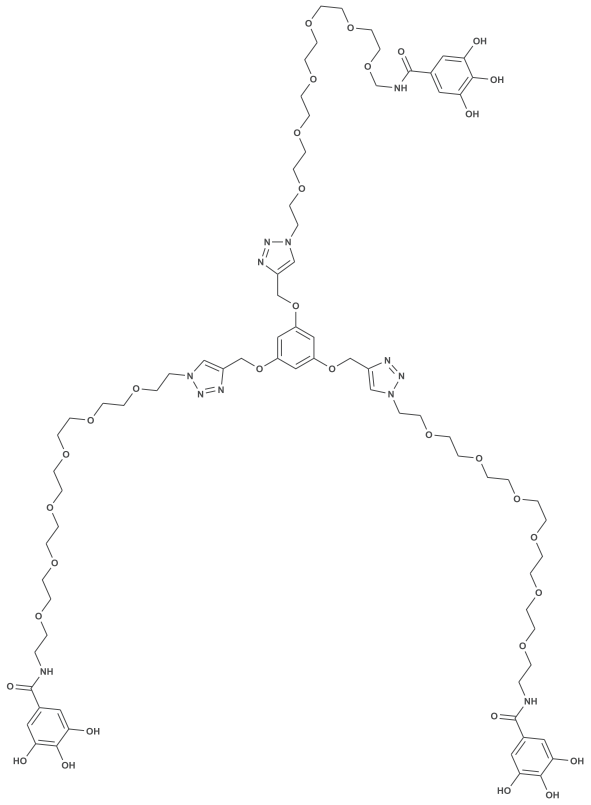

Figure 5.8: *Molecular representation of the gallol-dendrimer.*

AP/Gallol-dendrimer mixtures were prepared by mixing the gallol-dendrimer at 1 mg/mL and AP at 1 mg/mL in $NaNO_3$ 150 mM HEPES 10 mM at pH = 7.4. Figure 5.9 shows the QCM signals measured during the application of CV between -500 mV and 700 mV (vs Ag/AgCl, 50 mV/s) for a mixture of AP/gallol-dendrimer and gallol-dendrimer alone in solution. The evolution of the frequency shifts are very similar for the mixture and the control. Most of the buildup occurs during the first 10 min leading to 450 Hz in frequency shift followed by a plateau, probably due to the limited diffusion of gallol-dendrimer.

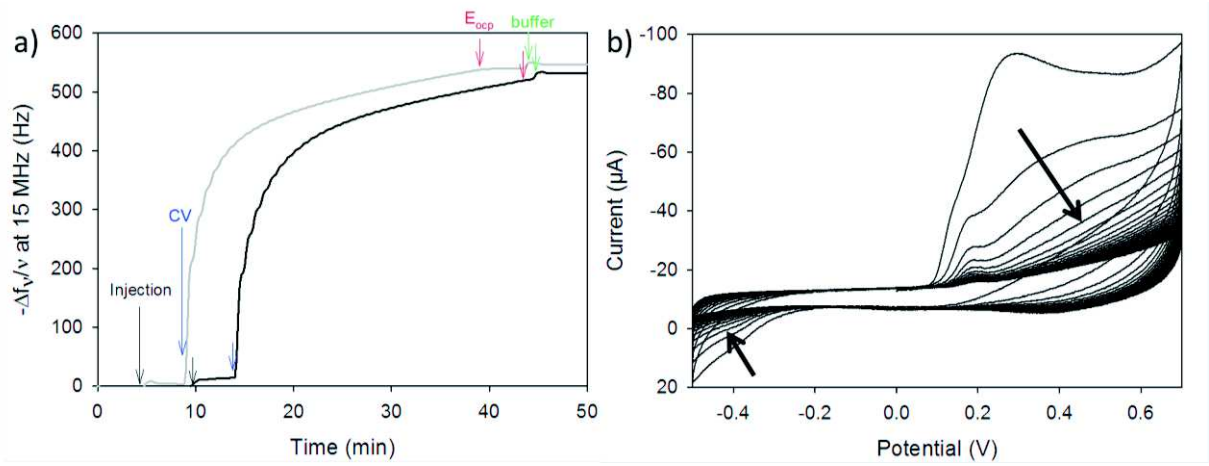

Figure 5.9: *(a) Evolution of the normalized frequency shift, measured by EC-QCM, as a function of time of a gallol-dendrimer/AP (black line) and gallol-dendrimer (grey line) mixture during the application of CV between -500 mV and +700 mV (vs Ag/AgCl, scan rate 50 mV/s). (b) Cyclic voltammogram with 90 cycles (30 min, 20s between each cycle) of gallol-dendrimer (1 mg/mL) solution over the potential range of -0.5 to 0.7 V (vs Ag/AgCl, scan rate 50 mV/s).*

To check the incorporation of AP, we tested the activity of the coating. To do so, a multidetector spectroscope UV (Xenius XC, SAFAS, Monaco) equipped with a microplate reader was used to monitor the catalytic activity of AP within the film. Paranitrophenyl phosphate (PNPP) solution substrate of AP was prepared at 10% w/w with $NaNO_3$ 150mM - 10 mM HEPES buffer at pH 7.4. The enzymatic reaction yields para-nitrophenol, a yellow soluble product monitored at the wavelength of 405 nm (Figure 5.11). The coating appears to be active (data not shown), meaning that AP might be physically entrapped in the film.

5.4 Entrapment of enzymes in electrodeposited TA/Fe(III) films

5.4.1 Introduction concept

As a second approach, we tried to physically entrap enzymes in the self-assembled TA/Fe(III) films. More precisely, enzymes were mixed with TA and Fe(II) in solution and were putted in

contact with an electrode. By applying an oxidant potential, the self-assembly of TA and Fe(III) films is triggered in the presence of the enzyme (Figure 5.10). AP was used. It should be remembered that TA interact with enzymes, thus AP/TA/Fe(II) mixtures were turbid. In contrast to previous experiments, the solutions were not filtrated.

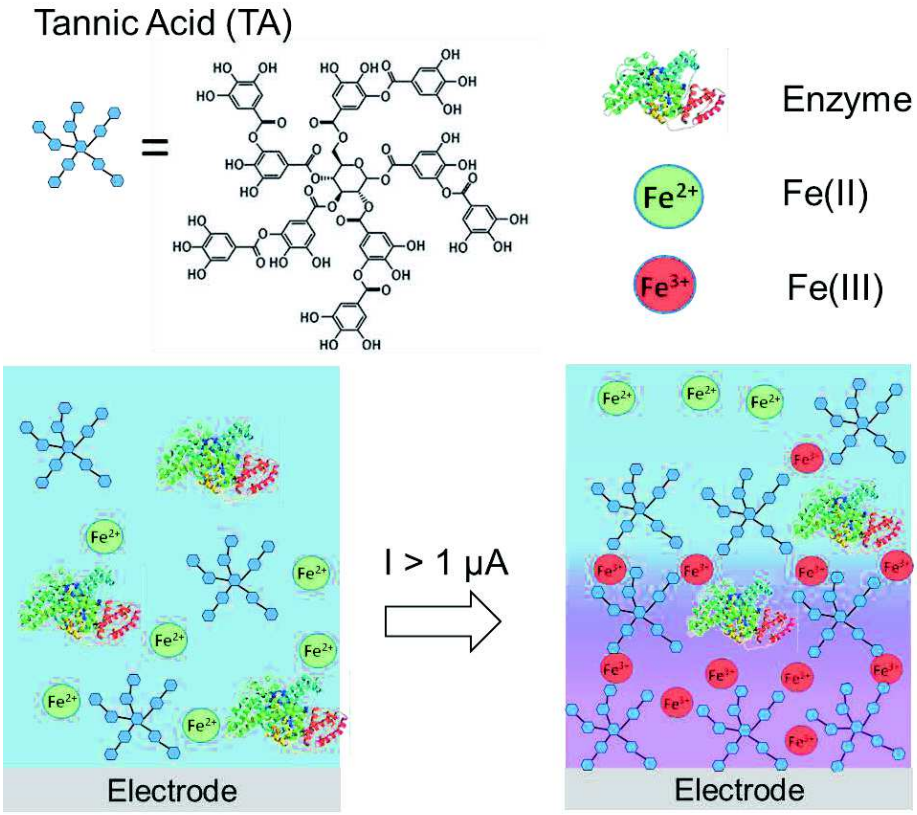

Figure 5.10: *Principle of the physical entrapment of enzymes in one pot self-assembled Fe/TA films.*

5.4.2 Entrapment of alkaline phosphatase into TA/Fe(III) films

AP was mixed at 1 mg/mL with TA (10 mg/mL) and Fe (II) (4 mg/mL) in KPF_6 150 mM at pH = 3 and pH = 7.4. Figure 5.11 shows the evolution of the QCM signals measured during the application of a constant current of 5 µA for mixtures of AP/TA/Fe(II) at pH = 3 (Figure 5.11a) and at pH = 7.4 (Figure 5.11b). In both case after one hour, a normalized frequency shift of approximatively 1000 Hz is reached. This is consistent with the fact that TA/Fe(II) buildup is pH independent (see Chapter 4).

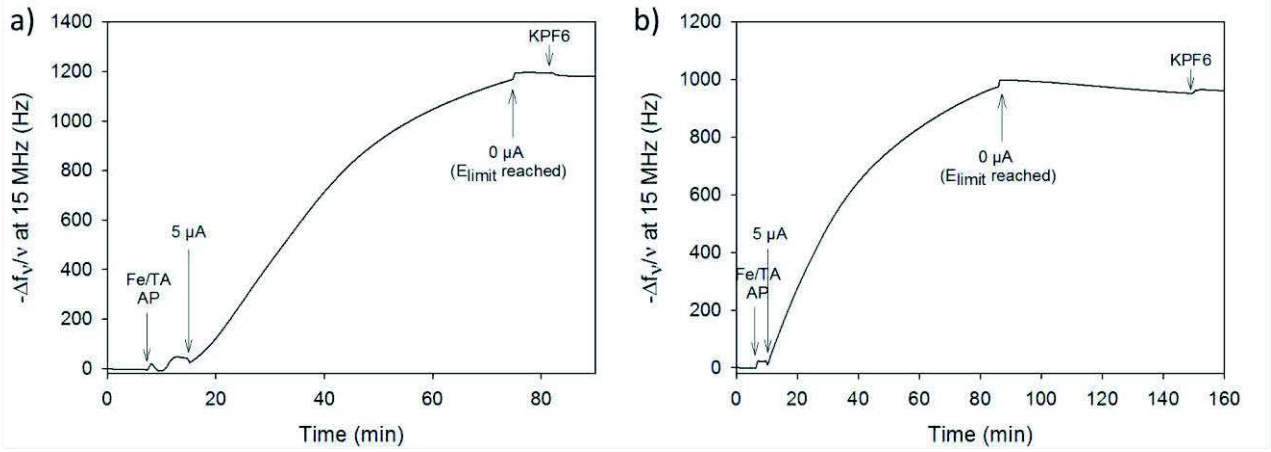

Figure 5.11: *Evolution of the normalized frequency shift, measured by EC-QCM, as a function of time during the application of a constant current of 5µA for TA/FeII/GO mixture a) at pH = 3. b) at pH = 7.4.*

In the presence of AP, TA/Fe(III) self-assembly is slowed down. In comparison, the normalized frequency shift measured is of 2500 Hz for TA/Fe(III) solution for the same duration (1h). Moreover during the current application, a potential of 1.2 V (the limit of potential at which the potentiostat stops) is reached at the normalized frequency shift of 1000 Hz, leading to the current stop. The increase in potential leads to the oxidation of gallol moities of TA, inducing TA self-polymerization. Due to the non-desired precipitation of AP substrate (PNPP), we were not able to test the enzymatic activity of the film.

5.5 Outlook

As it was mentioned in the first part of this chapter, electro-crosslinking of AP by phenolic crosslinkers was not possible because of the low density of amine functions of AP and because of self-polymerization of phenolic crosslinker (which occurs through radical formation). It is known in literature that hydroquinone prevents radical species formation.[21] Electro-crosslinking of AP through catechol/gallol oxidation could be performed in the presence of hydroquinone in order to limit the self-polymerization of phenolic crosslinker and promote the crosslinking of the enzyme.

References

1. Thevenot, D. R.; Toth, K.; Durst, R. A.; Wilson, G. S. Electrochemical Biosensors: Recommended Definitions and Classification - (Technical Report). *Pure and Applied Chemistry* **1999,** *71*, 2333.

2. Sarma, A. K.; Vatsyayan, P.; Goswami, P.; Minteer, S. D. Recent Advances in Material Science for Developing Enzyme Electrodes. *Biosensors and Bioelectronics* **2009,** *24*, 2313.

3. Kurzawa, C.; Hengstenberg, A.; Schuhmann, W. Immobilization Method for the Preparation of Biosensors Based on Ph Shift-Induced Deposition of Biomolecule-Containing Polymer Films. *Analytical Chemistry* **2002,** *74*, 355.

4. Luo, X. L.; Xu, J. J.; Du, Y.; Chen, H. Y. A Glucose Biosensor Based on Chitosan-Glucose Oxidase-Gold Nanoparticles Biocomposite Formed by One-Step Electrodeposition. *Analytical Biochemistry* **2004,** *334*, 284.

5. Suginta, W.; Khunkaewla, P.; Schulte, A. Electrochemical Biosensor Applications of Polysaccharides Chitin and Chitosan. *Chemical Reviews* **2013,** *113*, 5458.

6. Ahuja, T.; Mir, I. A.; Kumar, D.; Rajesh. Biomolecular Immobilization on Conducting Polymers for Biosensing Applications. *Biomaterials* **2007,** *28*, 791.

7. Miao, Y. Q.; Chen, J. R.; Wu, X. H. Using Electropolymerized Non-Conducting Polymers to Develop Enzyme Amperometric Biosensors. *Trends in Biotechnology* **2004,** *22*, 227.

8. Poller, S.; Koster, D.; Schuhmann, W. Stabilizing Redox Polymer Films by Electrochemically Induced Crosslinking. *Electrochemistry Communications* **2013,** *34*, 327.

9. Kong, Y.; Mu, S. L. Investigation on the Electrochemical Polymerization of Catechol by Means of Rotating Ring-Disk Electrode. *Chinese Journal of Chemistry* **2003,** *21*, 630.

10. Marczewska, B.; Przegalinski, M. Poly(Catechol) Electroactive Film and Its Electrochemical Properties. *Synthetic Metals* **2013,** *182*, 33.

11. Burzio, L. A.; Waite, J. H. Cross-Linking in Adhesive Quinoproteins: Studies with Model Decapeptides. *Biochemistry* **2000,** *39*, 11147.

12. Bradshaw, R. A.; Cancedda, F.; Ericsson, L. H.; Neumann, P. A.; Piccoli, S. P.; Schlesinger, M. J.; Shriefer, K.; Walsh, K. A. Amino-Acid-Sequence of Escherichia-Coli Alkaline-Phosphatase. *Proceedings of the National Academy of Sciences of the United States of America-Biological Sciences* **1981,** *78*, 3473.

13. Inouye, H.; Barnes, W.; Beckwith, J. Signal Sequence of Alkaline-Phosphatase of Escherichia-Coli. *Journal of Bacteriology* **1982,** *149*, 434.

14. Deming, T. J. Mussel Byssus and Biomolecular Materials. *Current Opinion in Chemical Biology* **1999,** *3*, 100.

15. Krogsgaard, M.; Andersen, A.; Birkedal, H. Gels and Threads: Mussel-Inspired One-Pot Route to Advanced Responsive Materials. *Chemical Communications* **2014,** *50*, 13278.

16. Shutava, T.; Prouty, M.; Kommireddy, D.; Lvov, Y. Ph Responsive Decomposable Layer-by-Layer Nanofilms and Capsules on the Basis of Tannic Acid. *Macromolecules* **2005,** *38*, 2850.

17. Sileika, T. S.; Barrett, D. G.; Zhang, R.; Lau, K. H. A.; Messersmith, P. B. Colorless Multifunctional Coatings Inspired by Polyphenols Found in Tea, Chocolate, and Wine. *Angewandte Chemie-International Edition* **2013,** *52*, 10766.

18. Spencer, C. M.; Cai, Y.; Martin, R.; Gaffney, S. H.; Goulding, P. N.; Magnolato, D.; Lilley, T. H.; Haslam, E. Polyphenol Complexation - Some Thoughts and Observations. *Phytochemistry* **1988,** *27*, 2397.

19. Goldstein, L. J. S., T. The Inhibition of Enzymes by Tannins. *Phytochemistry* **1965,** *4*, 185.

20. Martin, M. M.; Rockholm, D. C.; Martin, J. S. Effects of Surfactants, Ph, and Certain Cations on Precipitation of Proteins by Tannins. *Journal of Chemical Ecology* **1985,** *11*, 485.

21. Palumbo, A.; Dischia, M.; Misuraca, G.; Prota, G. Mechanism of Inhibition of Melanogenesis by Hydroquinone. *Biochimica et Biophysica Acta* **1991,** *1073*, 85.

Conclusions and outlooks

Electrotriggered one-pot self-assembly through morphogenic approach has proven to be a very efficient way of surface functionalization. Here, we generalized the pioneering work made in our team in this field to new systems showing the versatility of this process. To do so, we looked at natural phenomena proving once again that nature, far from being obsolete, grants us ideas towards new technological advances. The mussel adhesion phenomenon and the role of polyphenols in nature are both based on the chemical properties of catechol and gallol moieties. Two systems based on this biochemistry were successfully designed by a morphogenic approach during my PhD. The first one relies on the redox properties of catechol moieties. We developed a system based on the electrotriggered covalent self-construction of a polyamine: PAH by a bis-catechol spacer (the morphogen). Oxidation of both catechol moieties into quinones leads to a gradient of activated bis-quinone molecules from the electrode. Bis-quinone reacts on both sides on amine functions of PAH leading to self-construction of a film on the surface. In the second system, the ability of gallol moieties of TA to coordinate Fe(III) was exploited. By applying an oxidant potential in the presence of a TA/Fe(II) mixture, Fe(II) ions were oxidized into Fe(III) ions, the morphogens here, from the surface of the electrode leading to the self-assembly of TA on the surface through coordination bonding with Fe(III). In the last part, we tried to use both systems to immobilize enzymes for biosensing applications.

In the first part of this work, the electrotriggered self-construction of polymer films by catechol oxidation was studied. We showed that bis-catechol molecules, when electrochemically activated by oxidation of catechol into quinone, are able to covalently react on amine functions of PAH leading to the buildup of a film. In this case, cyclic voltammetry was performed to trigger the self-construction. However, the buildup of these films is limited at some point due to the limited diffusion of bis-catechol molecules to the electrode all along the film buildup. Indeed, compared to other morphogens (ions) used in the previous works, bis-catechol is much bigger and its diffusion into the film is prevented. XPS analysis confirmed both presence of bis-catechol and PAH covalently linked through Michael addition and imine formation. Films imaged by AFM appeared to be extremely rough, due to the use of homobifunctional catechol molecule. A study of the effect of the concentration in morphogen (bis-catechol) and of the scan rate of the CV showed optimal buildup conditions at a catechol/amine ratio of 0.3 and at a scan rate of 50 mV/s.

In the second part of my Ph.D, we demonstrated the electro-self-assembly of TA through coordination bonding with ions. In this part, morphogens, Fe(III) ions generated by oxidation of Fe(II), induce an assembly of a TA/Fe(III) network on the surface of the electrode through coordination bonding between gallol moieties of TA and Fe(III). A anodic current was applied in this case. Compared to the previous developed system, AFM study showed that thicker and smoother films are built, probably due to the small size of TA/Fe(III) complexes that assembled on the surface. The chemical composition of the self-assembled film, studied by XPS, proved the presence of both TA and iron, mainly Fe(III) ions and a small amount of Fe(II) ions, confirming our concept. The film buildup kinetic, and so the thickness, can be tuned by controlling the current applied and TA/Fe(II) molar ratio of the buildup solution. The buildup turns out to be pH independent. Finally, the stability of the films was tested by contact with EDTA or application of a reductive potential. The contact with an EDTA solution partially dissolves the self-assembled TA/Fe(III) film. In contrast, the film is stable under reductive potential.

In the last chapter, we tried to use both systems developed for biosensing applications. The idea was to immobilize an enzyme on the electrode using the cross-linking strategy using the self-construction by phenol oxidation and the physical entrapment strategy using the self-assembly by coordination bonds. Firstly, different phenolic cross-linkers (bis-catechol, TA and a dendrimer gallol) were used to electro-crosslink alkaline phosphatase (AP) by reaction of oxidized catechol or gallol moieties with amine functions of AP. Yet, no significant buildup with the enzyme/phenolic crosslinker solution was observed. This could be due the low density and accessibility of amine functions on AP. By increasing the concentration of catechol/gallol based molecules, a competitive self-polymerization was observed preventing the crosslinking of AP. Secondly, we tried to entrap AP in the electrodeposited TA/Fe(III) network by co-deposition. In the presence of the enzyme, the buildup kinetics is slower compared to TA/Fe(III) film and the morphogen diffusion limit is reached probably due to crosslinking between TA and the enzyme. Yet, because of experimental issues, no activity of the enzyme was measured.

The first outlook of this work would be to dig further in the immobilization of an enzyme by a morphogenic approach notably by using hydroquinone to limit the self-polymerization of phenolic cross-linker while increasing the concentration of the late one. Indeed, preliminary results showed that hydroquinone can suppress self-polymerization of bis-catechol during the application of a CV. Other strategies could be implemented to override the low amine density

of the enzyme: electrocrosslink of PAH/enzyme complexes, chemical modification of enzyme to increase its amine functions density, using cluster of enzymes...

Moreover, other applications could be considered. Indeed, XPS measurement showed that the electrodeposited films present free catechol (first system) or free gallol (second system) moieties. As it is described in Chapter 1, these functions can promote further immobilization of biomolecules, or nanoparticles. Thus, the developed films could be used as immobilization platforms of antimicrobial peptides or silver nanoparticles for the design of antimicrobial surfaces. Moreover, these films might have relevant anticorrosion properties.

Finally, the last but not the least outlooks would be to move towards more complex electrotriggered morphogenic systems. In Turing's model, formation of patterned assemblies from unpatterned ones is always induced by at least two morphogens whereas in our case one morphogen is used. Designing systems based on two morphogens would allow to create complex structures with peculiar properties.

UNIVERSITÉ DE STRASBOURG

Résumé de Thèse

présentée par

Clément MAERTEN

Auto-construction et auto-assemblage bio-inspirés de films organiques par électrochimie

Directrice de thèse : Dr. Fouzia Boulmedais

Institut Charles Sadron, CNRS

Les revêtements de surfaces sont étudiés depuis le début du XXème siècle et sont présents en abondances dans notre vie quotidienne. Ils nous permettent de conférer aux matériaux de nouvelles fonctionnalités, par exemple des propriétés magnétiques, électriques, optiques, de biocompatibilité, etc. Un grand nombre de procédés ont été développés pendant ces dernières années pour modifier la surface de tout type de matériaux en fonction de la propriété voulue (métaux, céramiques, polymères).

L'électrodéposition de matière molle est un procédé se basant sur l'utilisation d'un signal électrique pour déclencher et contrôler l'assemblage de films minces qui offre de nombreuses opportunités pour diverses applications et attire de plus en plus l'attention du monde scientifique. En effet, ce procédé a l'avantage d'être rapide et facile à mettre en place sur des matériaux conducteurs présentant des géométries complexes. De plus, le signal électrique pouvant être appliqué avec une sélectivité spatiotemporelle parfaite, il permet l'assemblage séquentiel de différents composants sur des électrodes micro ou nano-structurées.

Il y a cinq ans, notre équipe a introduit l'autoconstruction morphogénique de films : un nouveau concept basé sur la génération électrochimique d'un gradient de catalyseur déclenchant l'assemblage covalent de films polymériques. En biologie, la morphogénèse englobe les théories décrivant le développement de la forme et de la structure d'un organisme biologique. En 1952, le mathématicien Alan Turing a publié un article fondateur appelé « The Chemical Basis of Morphogenesis » *(Philosophical Transactions of the Royal Society, Vol 237, 1953)* où il a introduit un modèle expliquant la formation de motifs pendant la création d'organismes vivants. D'après ce modèle, la conjonction de réactions chimiques et de la diffusion moléculaire d'espèces réactives appelées morphogènes mènent spontanément à des variations spatiales de concentration de ces espèces induisant la formation de motifs en raies ou en taches. Pour illustrer ce modèle, Turing utilise l'exemple des taches de la fourrure du guépard, la position des tentacules de l'hydre ainsi que la phase du développement embryonnaire appelé gastrulation.

En chimie, un morphogène peut être défini comme une molécule ou un ion généré à une interface qui diffuse en solution produisant la formation d'un gradient, ce gradient induisant un processus chimique localisé. Ce concept a été appliqué pour construire des films composés de deux polymères interagissant par création de liaisons covalentes par chimie click. Le Cu (I), le morphogène, est produit par électrochimie, *i.e* par réduction du Cu (II) à une électrode, et catalyse la réaction click entre les fonctions alcynes et azotures des deux polymères créant un

assemblage localisé à la surface de l'électrode *(Angewandte Chemie International Edition, Vol 123, 2011)*.

Le but de ma thèse était d'étendre cette stratégie à d'autres systèmes en utilisant une approche bio-inspirée. Le concept du morphogène a été appliqué à l'autoconstruction de films de polymères et d'acide tannique en se basant sur une biochimie inspirée des moules et des polyphénols.

1) Introduction Bibliographique

1.1) La Nature : notre inspiration

Le biomimétisme a pour but de comprendre des phénomènes naturels afin non seulement d'élargir notre connaissance de la Nature, mais également de trouver des idées afin de créer de nouveaux concepts, particulièrement en science des matériaux. Bien que l'humanité ait réalisé d'énormes progrès pendant les derniers siècles, la nature possède encore une avance considérable. Cela fait déjà plusieurs siècles que l'homme essaye d'imiter la nature : Leonard de Vinci par exemple, qui essaya de créer une machine volante imitant les oiseaux. Depuis de Vinci, de nombreux exemples de concepts biomimétiques ont été créées. La soie d'araignée présente des propriétés mécaniques exceptionnelles et pourrait remplacer le Kevlar. La microstructure des feuilles de Lotus a inspiré la création de surfaces super hydrophobes. Les geckos sont capables de marcher sur n'importe quelle surface sans tomber, encourageant la création de nouveaux adhésifs.

Pour ce travail, notre inspiration provient de deux observations : la capacité unique des moules à adhérer à tout type de surface dans l'eau et dans des conditions extrêmes, ainsi que la capacité des polyphénols a coordiner les métaux contribuant à la coloration des plantes. Ces deux phénomènes sont basés sur la chimie diversifiée des groupements catéchols et gallols (Figure 1). Les catéchols sont des dérivés du benzène présentant deux groupes hydroxyles en ortho. Ils sont répandus dans le monde animal et végétal, par exemple la dopamine est un neurotransmetteur bien connu, et le L-Dopa est l'acide aminé responsable des fortes propriétés d'adhésion de protéines sécrétée par moule. Les gallols ont une structure chimique très proche des catéchols, avec trois groupes hydroxyles au lieu de deux. Avec les catéchols, ils sont présents dans les polyphénols des plantes.

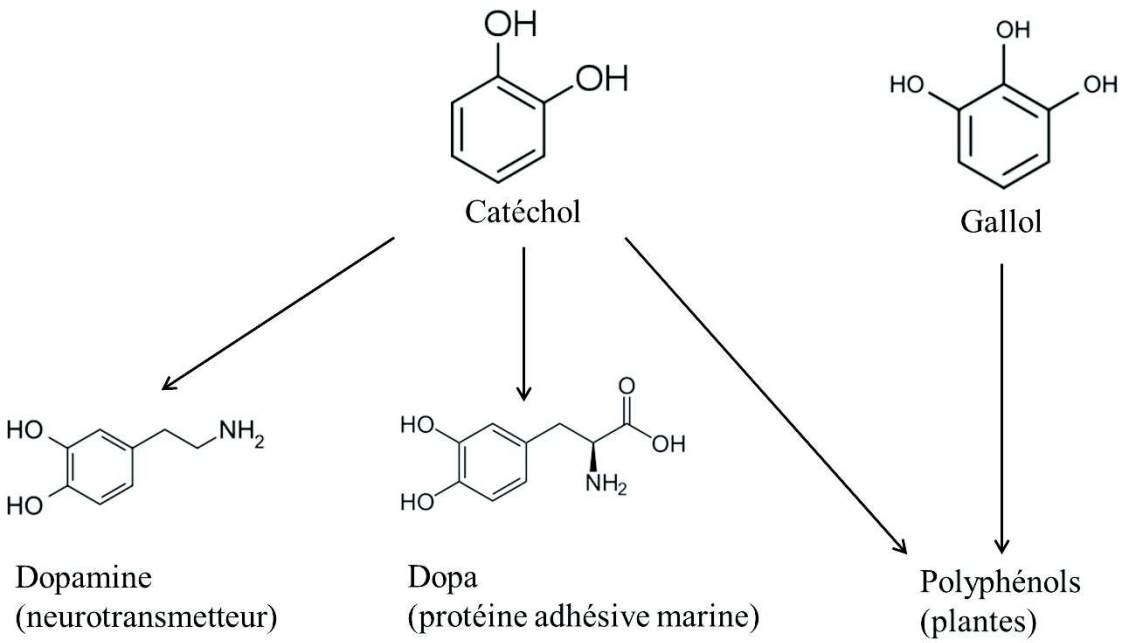

Figure 1 *: Structure chimique des groupements catéchols et gallols.*

Les catéchols et par extension les gallols peuvent interagir avec des atomes ou des fonctions chimiques de différentes manières (Figure 2) : ils peuvent former des liaisons hydrogènes, des complexes de coordinations avec les métaux notamment les ions Fe(III),[1] des complexes de transfert de charges et oxydés en quinones, réagir de façon covalente avec des groupements nucléophiles comme les amines ou les thiols.[2]

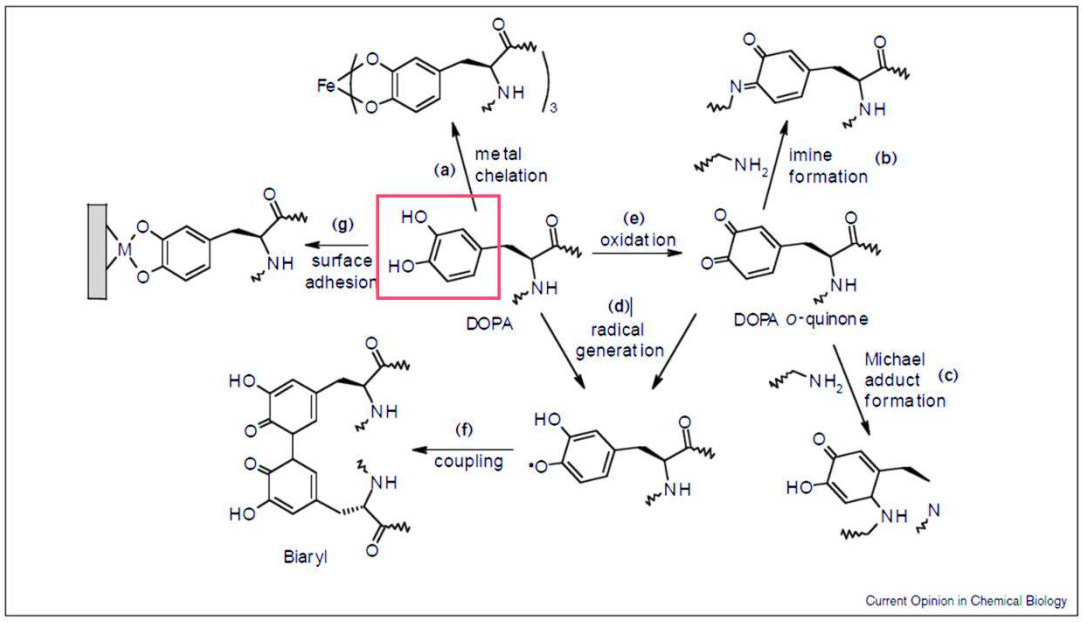

Figure 2 *: Les différentes interactions possibles que les catéchols (encadré rouge) peuvent former.*[2]

C'est cette biochimie qui nous a inspiré pour créer de nouveaux systèmes pour l'électrodéposition de films organiques.

1.2) L'électrodéposition morphogénique de macromolécules

Depuis 40 ans, de nombreuses structures complexes et organisées ont été réalisées par mélange de molécules en solution. Cependant, les architectures moléculaires qui se forment exclusivement au voisinage d'une interface restent rares. En effet, les molécules composant la structure interagissent en général immédiatement ou très rapidement en solution, empêchant un assemblage restreint à la surface. Utiliser un stimulus localisé apparaît comme le meilleur moyen pour induire la formation d'un assemblage ou d'un film. L'électrodéposition est un procédé ou des signaux « électriques » sont imposés pour déclencher et contrôler la construction de films minces. Ces procédés peuvent être séparés en trois catégories :

L'électrodéposition par précipitation de macromolécules

Découverte au début du XXème siècle puis appliquée aux peintures dans l'industrie automobile notamment,[3] l'électrodéposition par précipitation de macromolécules a été récemment revalorisé par l'usage d'un polysaccharide naturel : le chitosan.[4] Le chitosan possède la propriété d'être soluble dans l'eau à un pH < pKa (autour de 6,3) à cause de la protonation de ses groupements amines et insoluble à un pH > pKa. La Figure 3 montre le mécanisme d'électrodéposition du chitosan.

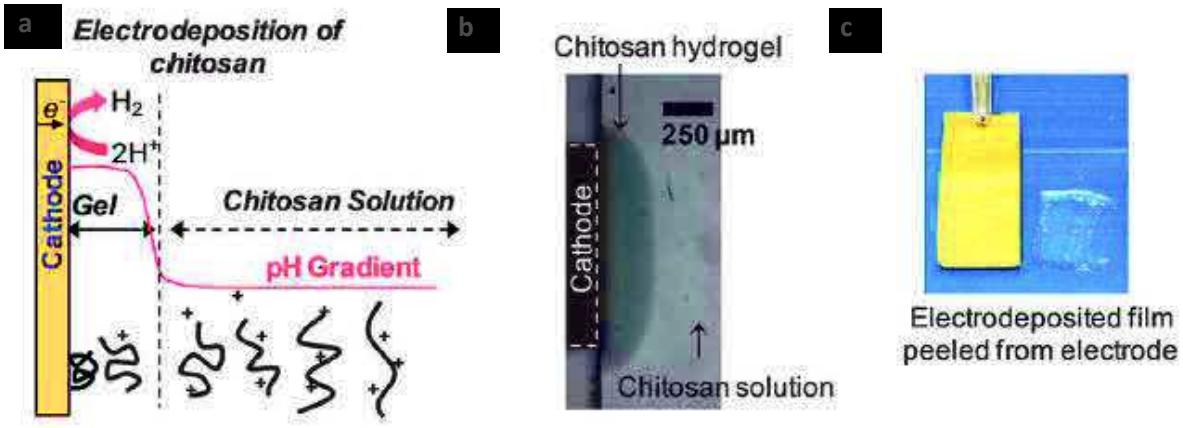

***Figure 3** : (a) Mécanisme d'électrodéposition du chitosan avec photos (b) du chitosan déposé d'un système micro-fluidique et (c) d'un hydrogel de chitosan décollé d'une électrode.*[5]

Plus précisément, un gradient de protons, de pH, est généré depuis l'électrode par électrolyse de l'eau (-2 V). Ceci va mener à la déprotonation des groupements amines du chitosan dans le voisinage de l'électrode et donc à une précipitation du polymère sur la surface.

Il est à noter que ce procédé a également été appliqué aux enzymes.[6] Deux procédés sont décrits dans la littérature : la déposition électrochimique et la déposition électrophorétique des enzymes. Ils sont tous deux basés sur la génération d'un gradient de proton par électrolyse de l'eau dans une solution enzymatique ce qui déclenche l'agrégation et la précipitation des enzymes quand le pH atteint le point isoélectrique de l'enzyme au voisinage de l'électrode.

L'auto-assemblage de polyélectrolytes par électrochimie

L'auto-assemblage de polyélectrolytes regroupe plusieurs procédés :

- La méthode assistée de multicouches par champ électrique qui consiste à améliorer les interactions électrostatiques entre des polyélectrolytes et une surface en appliquant un potentiel électrique.[7]
- L'électro-auto-assemblage de polyélectrolytes, mis en évidence par Van Tassel.[8]
- L'électro-auto-assemblage par activation ionique développé par Payne pour les gels d'alginate/calcium (II).[9]

L'électrodéposition de polymères par formation de liaisons covalentes

Ces procédés regroupent : l'électropolymérisation qui se base sur l'utilisation d'un potentiel électrochimique pour oxyder des monomères, les transformant en espèce radicalaire réactive qui polymérise pour former un film,[10] les multicouches couplées par électrochimie introduite par notre équipe en 2010[11] et enfin l'électro-réticulation de polymères. Comme mentionné précédemment, cette dernière a été introduite dans notre en groupe en 2011.[12]

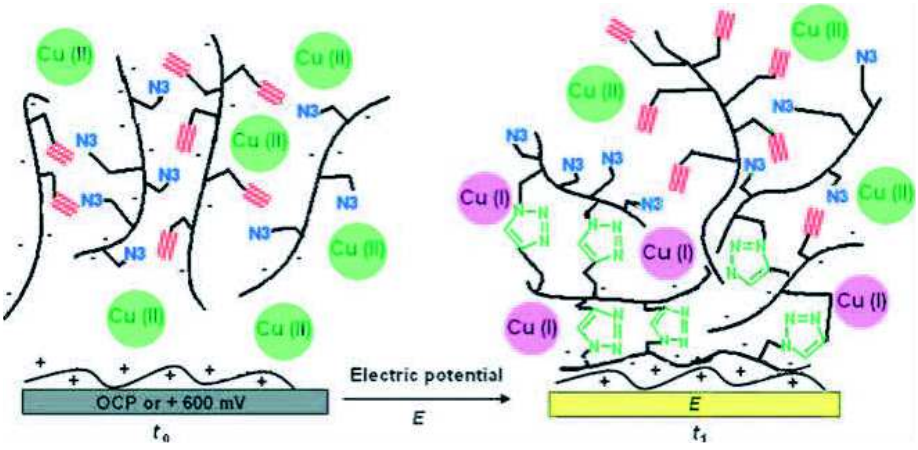

Figure 4 *: Formation « une-étape » de films par chimie click contrôlée électrochimiquement.*[12]

Dans ce cas, la réaction click entre les fonctions azotures et les alcynes de polymères fonctionnalisés a été exploitée. La Figure 4 illustre le concept d'électroréticulation basé sur

deux polymères modifiés chimiquement, l'un présentant des fonctions azotures et l'autre des fonctions alcynes. Les deux polymères sont mélangés en solution en présence de Cu (II) et sont incapables d'interagir entre eux. Quand un potentiel électrique réducteur est appliqué, le Cu (II) est réduit en Cu (I) qui catalyse la réaction entre les fonctions azotures et alcynes et donc l'assemblage d'un film de polymères réticulés sur la surface de l'électrode.

2) Autoconstruction morphogénique de film polymériques par électrochimie

Inspirés par la versatilité chimique des groupements catéchols pour réagir de façon covalente avec d'autres groupes fonctionnels, nous avons introduit un nouvel exemple de construction morphogénique basée sur l'utilisation de chaîne courtes d'éthylène glycol portant des groupements catéchols de chaque côté. Ces espaceurs homobifonctionnels seront appelés par la suite « bis-catechol » (Figure 5a). Un polymère commercial : le poly(allylamine hydrochlorure) (PAH) et ces molécules de bis-catéchol sont mélangés dans une solution aqueuse et ne peuvent réagir ensemble. Par mise en contact avec une électrode et application d'un potentiel électrochimique défini, les molécules de bis-catéchols sont oxydées à l'électrode, ce qui les « active » en bis-quinone (Figure 5b). Dans cet état activé, les molécules de bis-quinone peuvent réagir avec les fonctions amines du PAH par addition de Michael ou condensation de base de Schiff.

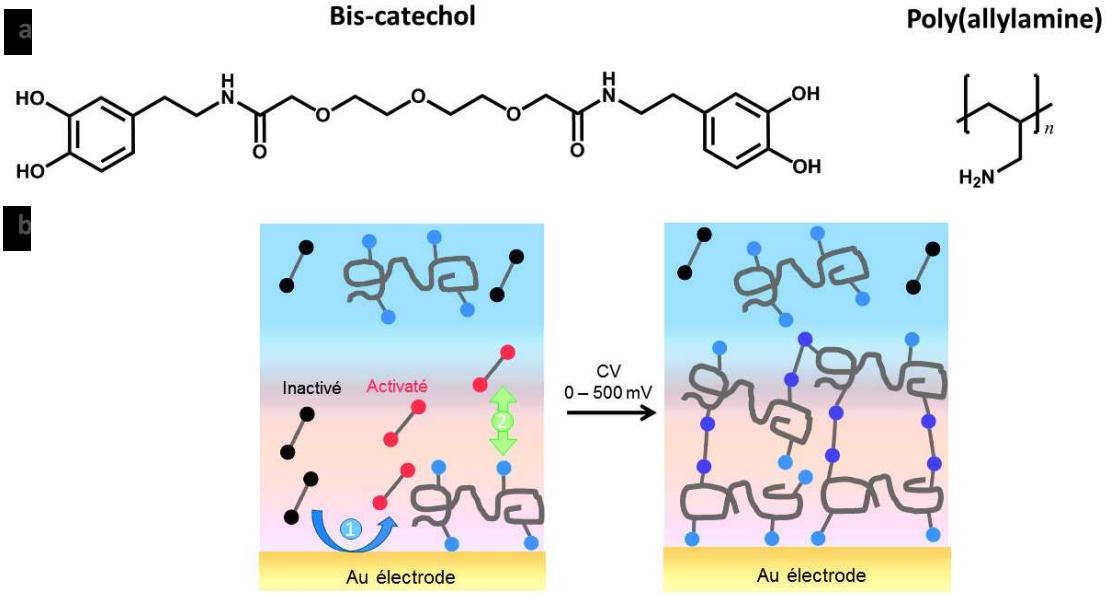

***Figure 5** : (a) Structure chimique du bis-catéchol et du poly(allylamine hydrochlorure) (PAH). (b) Principe de l'autoconstruction en « une étape » d'un film de polymères basée sur l'oxydation d'un morphogène (biscatéchol).*

L'assemblage du film, qui intervient de façon localisée au niveau de l'électrode, est loin d'être évidente à cause (i) de la diffusion des molécules de bis-catéchols jusqu'à l'électrode qui doit être assurée tout au long du processus de construction et ce, même après le début de la formation du film, et (ii) de la possibilité de réaction des deux extrémités des espaceurs sur une même chaine de polymère devenant inaccessible pour continuer le processus d'autoconstruction. Contrairement aux autres systèmes morphogéniques présentés par notre équipe jusqu'ici, il s'agit du premier exemple de construction où le morphogène fait partie intégrante du film.

Les constructions ont été réalisées à l'aide d'un potentiostat (Chi 660, CH Instrument) et ont été suivies *in-situ* par microbalance à cristal de quartz avec mesure de la dissipation couplé à l'électrochimie (EC-QCM, Q sense). Plus précisément, le suivi des différentes harmoniques de la fréquence de résonance d'un cristal de quartz permet de suivre le dépôt de masse sur le cristal. Seule la fréquence normalisée, mesurée à 15 MHz, sera représentée. La topographie et l'épaisseur des films obtenus ont été déterminées par microscopie à force atomique (AFM) en mode contact et en liquide.

Afin de déclencher la construction, notre idée a été de travailler en voltammétrie cyclique (CV). Cette technique permet d'appliquer une différence de potentiel définie et de mesurer simultanément le courant électrique. Les bornes de potentiel choisies sont de 0 à 500 mV (vs Ag/AgCl). Nous avons tout d'abord étudié le comportement électrochimique des molécules de bis-catéchols en voltammétrie cyclique (Figure 6).

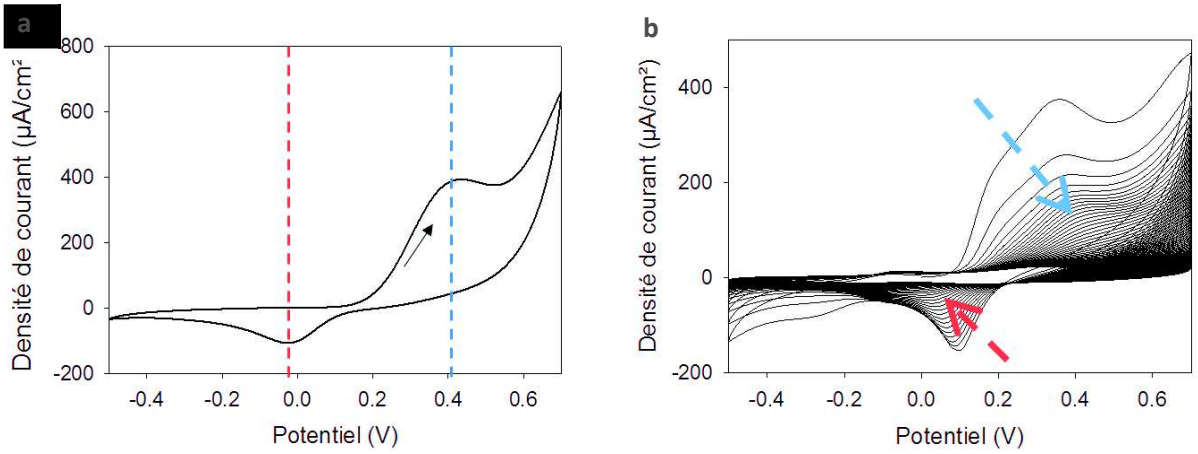

Figure 6 *: CV de -0,5 à 0,7V (vs Ag/AgCl, vitesse de scan 50 mV/s) avec (a) un cycle de solution de biscatéchol (1 mg/mL) et (b) 180 cycles (1h, 20s par cycles) d'un mélange de biscatéchol (1 mg/mL) et PAH (1 mg/mL). Réalisé dans un tampon 10 mM Hepes-150 mM $NaNO_3$ à pH = 7,4.*

Les pics d'oxydations (tirets bleus) et de réduction (tirets rouges) sont mesurés respectivement à 0,4V et -0,03V (vs Ag/AgCl). Ces valeurs sont en accord avec celles dans la littérature.[13]

L'autoconstruction d'un film de PAH (Mw = 58000 g/mol) et de bis-catéchol a été étudié par EC-QCM qui permet de suivre la construction *in-situ* des films pendant l'application d'un stimulus électrique. Les mélanges de PAH et de biscatéchol ont été préparés dans un tampon aqueux 10 mM HEPES – 150 mM $NaNO_3$ à pH = 7,4. Le tampon HEPES compense la production de proton provenant de l'oxydation des catéchols en quinones. Toutes les solutions ont été dégazées avec de l'argon pour éviter l'oxydation des catéchols par l'oxygène dissous en solution. La Figure 7 montre le suivi d'une construction pour une CV appliquée pendant une heure avec une vitesse de balayage de 50 mV/s.

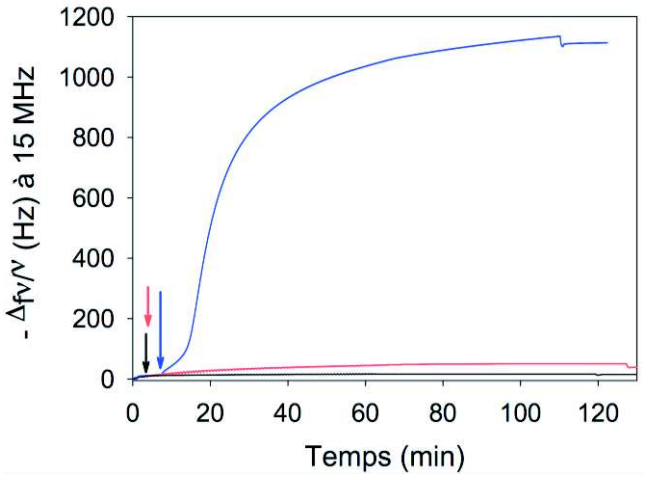

***Figure 7** : Evolution de la fréquence normalisée, mesurée par EC-QCM, en fonction du temps (ligne bleue) d'un mélange PAH/biscatéchol (catéchol/amine ratio de molaire 0,38), (ligne rouge) d'une solution de biscatéchol et (ligne noire) d'une solution de PAH pendant l'application d'une CV entre 0 et +500 mV (vs Ag/AgCl, vitesse de balayage 50 mV/s). Après injections des solutions, une CV a été appliquée aux temps marqués par des flèches de couleurs respectives.*

Avant d'appliquer la CV, une solution contenant un mélange de PAH et de bis-catéchol à pH = 7,4 est injectée, une légère augmentation de la fréquence est observée (Figure 7) due à l'adsorption électrostatique du PAH sur le cristal d'or. Lors de l'application de la CV, la fréquence normalisée augmente due au dépôt de film. La construction ralentit avant la fin de la durée de la CV. Cet effet est dû à la formation d'un film isolant sur le substrat qui limite la diffusion du bis-catéchol. La Figure 7 montre également les expériences de contrôle réalisées avec le PAH seul et le bis-catéchol seul en solution. Aucune construction n'est obtenue. Un mélange de PAH et bis-catéchol est donc nécessaire pour observer une autoconstruction.

Des mesures AFM ont été réalisées afin de caractériser la topographie des films auto-construits et de déterminer leur épaisseur après rayure. La Figure 8a montre l'évolution de l'épaisseur mesurée (distance minimum z entre le substrat nu est la hauteur du film où celui-ci recouvre tout le substrat) mesurée par AFM à différents temps de constructions.

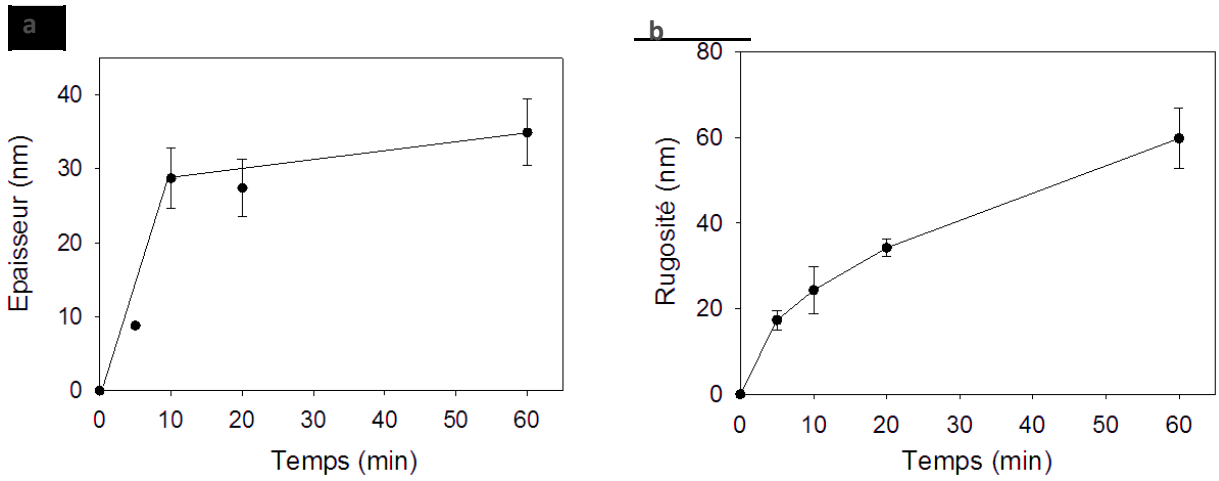

Figure 8 *: Evolution de l'épaisseur et de la rugosité, mesurées par AFM en mode contact et à l'état liquide, en fonction du temps d'autoconstruction d'un film obtenu à partir d'un mélange PAH/biscatéchol avec un ratio catéchol/amine de 0,38 en appliquant une CV entre 0 et + 500 mV (vs Ag/AgCl, vitesse de scan 50 mV/s). La rugosité a été calculée à partir d'images AFM de dimension 10 µm × 10 µm.*

Après 5 min d'application de la CV, le film PAH/bis-catéchol couvre entièrement et uniformément le substrat avec une épaisseur de 9 nm. L'épaisseur du film augmente avec la durée d'application de la CV, atteignant 35 nm après 60 min d'autoconstruction. On peut remarquer que l'épaisseur du film évolue de la même façon que la variation de fréquence mesurée en QCM, *i.e* une augmentation rapide pendant les 15 premières minutes de la construction suivie d'un pseudo plateau. On peut également remarquer que les films sont très rugueux et que la rugosité augmente tout au long du processus (Figure 8b). Des films rugueux similaires, caractérisés par la présence de nombreux pics, ont été obtenus dans d'autres exemples de constructions morphogéniques par électrochimie impliquant une petit molécule bi-fonctionnel.[14] Il semble donc logique de corréler cette structure en pic avec l'usage d'espaceurs éthylène glycol bi-fonctionnels. L'influence de deux paramètres a été étudié : le ratio catéchol/amine et la vitesse de balayage de la CV. Après 60 minutes de construction, la variation de fréquence mesurée en QCM augmente avec le ratio catéchol/amine jusqu'à atteindre un palier pour un ratio de 0,25 (Figure 9a). Cet effet peut être expliqué par une gêne stérique qui empêche tous les groupements amines d'être réticulés par les catéchols oxydés. La Figure 9b montre l'influence de la vitesse de balayage sur la construction. Un optimum est observé pour une vitesse de 50 mV/s. A vitesse de balayage supérieur, moins de temps est laissé au bis-catéchol pour qu'il soit oxydé et qu'il diffuse depuis l'électrode pour réticuler les chaînes de PAH. Dans ce cas c'est la diffusion du bis-catéchol qui est limitante. A faible vitesse de balayage c'est l'effet inverse qui se produit, le bis-catéchol a beaucoup de temps pour être oxydé

et diffuser depuis la surface et dans ce cas c'est la diffusion du PAH depuis la solution vers la surface qui limite la construction.

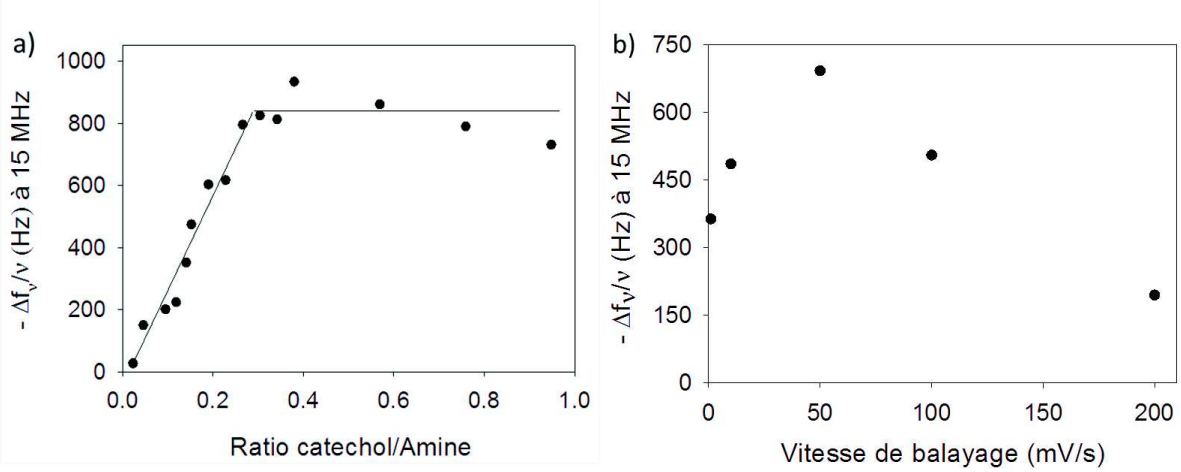

***Figure 9** : (a) Evolution de la fréquence normalisée mesurée en EC-QCM d'une solution de PAH/biscatéchol obtenue après 60 min d'application d'une CV entre 0 et +500 mV (vs Ag/AgCl, vitesse de balayage 50 mV/s) en fonction du ratio molaire catéchol/amine. (b) Evolution de la fréquence normalisée mesurée en EC-QCM d'une solution de PAH/biscatéchol avec un ratio catéchol/amine de 0,23, obtenue après 60 min d'application d'une CV entre 0 et +500 mV (vs Ag/AgCl) en fonction de la vitesse de balayage.*

3) Autoconstruction par électrochimie de films d'acide tannique basée sur des liaisons covalentes fer(III)/pyrogallol

La Figure 10 schématise le principe du second système basé sur la formation de liaisons de coordination. Dans ce cas, le morphogène est l'ion Fer (III). En effet l'ion Fer (III) peut être complexé par un, deux ou trois groupements pyrogallol selon le pH. Nous avons utilisé un mélange d'acide tannique (TA) qui est une molécule présentant cinq groupements pyrogallols et d'ions Fer (II) à pH = 3, qui a été mis en contact avec l'électrode. L'application du potentiel électrique conduisant à l'oxydation de l'ion Fer (II) en ion Fer (III) permet l'assemblage d'acide tannique à partir de la surface de l'électrode.

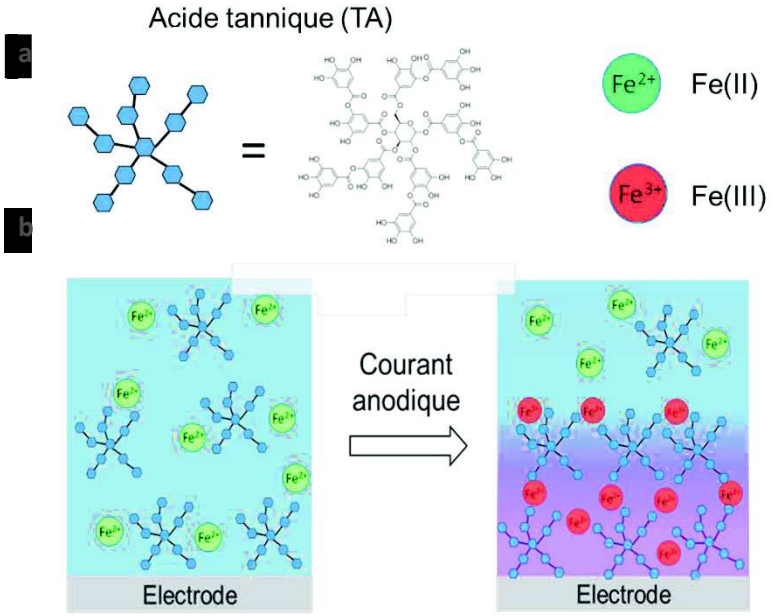

Figure 10 *: (a) Structures chimique de l'acide tannique. (b) Principe de l'autoconstruction en « une étape » d'un film d'acide tannique basé sur l'oxydation d'un morphogène (ion Fer (III)).*

Nous avons tout d'abord étudié la réponse électrochimique du Fe(II), de l'acide tannique et du mélange des deux composés par CV sur un cristal de QCM recouvert d'ITO et agissant comme électrode de travail (Figure 11). Le voltamogramme des ions ferriques présente un couple de pics redox correspondant aux transitions redox Fe(II)/Fe(III). Les pics d'oxydation et de réduction sont situés à 1,2 V et -0,05 V (à 50 mV/s) respectivement (Figure 11a). Ces valeurs sont très différentes de celles retrouvées dans la littérature sur des électrodes d'or (0,70 V et 0,29 V respectivement) probablement à cause d'une plus faible conductivité de l'ITO par rapport à l'or.[15] On observe une augmentation du courant mesurée et donc un début d'oxydation du Fe(II) pour les potentiels supérieurs à 0,2 V. Le voltamogramme du TA montre une oxydation irréversible oxydation à 0,93 V (Figure 11b). Aucun pic de réduction n'est observé ce qui signifie que la réaction électrochimique est irréversible comme décrit dans la littérature.[16] Tout comme pour le Fe(II), le pic d'oxydation du TA en CV sur l'ITO est décalé par rapport aux valeurs données dans la littérature (0,44 V). Le mélange Fe(II)/TA montre un premier pic d'oxydation à 0,25 V, attribué à l'oxydation du Fe(II), suivi d'un pic plus large à 0,80 V correspondant à l'oxydation des gallols (Figure 11c). Un pic de réduction de faible intensité est visible à 0,12 V qui peut être attribué à la réduction du Fe(III). D'après ces voltamogrammes on peut anticiper que travailler à des potentiels entre 0,1 et 0,5 V permet d'oxyder le Fe (II) en Fe (III) tout en limitant l'oxydation des gallols du TA.

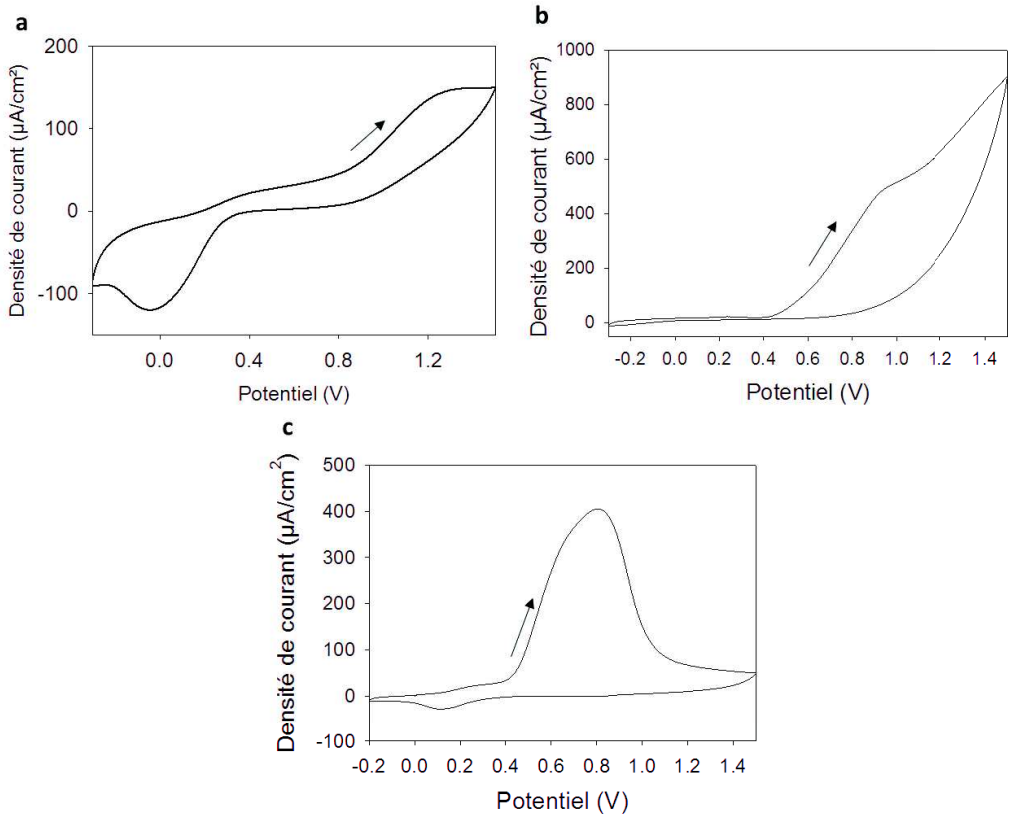

Figure 11 *: CV sur cristaux d'ITO de -0,3 à 1,5V (vs Ag/AgCl, vitesse de scan 50 mV/s) (a) d'une solution de Fe(II) ($FeSO_4$, 1 mg/mL), (b) d'une solution de TA (10 mg/mL) et (c) d'un mélange Fe(II)/TA (ratio molaire de 2,5). Réalisé dans un électrolyte 150 mM KPF_6 à pH = 3.*

Afin d'induire et de contrôler l'auto-assemblage, un gradient de Fe (III) a été généré à l'électrode par oxydation électrochimique du Fe (II) en mode galvanostat, c'est à dire une densité de courant appliquée constante. Cette méthode permet de contrôler le nombre de charges échangées et donc la quantité de morphogène généré. Nous avons utilisé ici un électrolyte 150 mM KPF_6 à pH = 3. Les expériences ont été réalisées sous Argon afin de prévenir une oxydation de TA en solution due à l'oxygène dissous. La Figure 12a montre le suivi d'une construction en EC-QCM pour un courant appliqué de 6,25 µA/cm² pendant 30 minutes. Avant d'appliquer le potentiel, une solution contenant un mélange de TA et d'ions Fe (II) à pH = 3 est injectée. Lors de l'application du potentiel, la fréquence normalisée augmente due au dépôt de film. La Figure 12a montre également les expériences de contrôles réalisées avec le TA et le Fe (II) seuls en solution. Aucune construction n'est obtenue. Un mélange des deux est donc nécessaire pour observer une auto-assemblage.

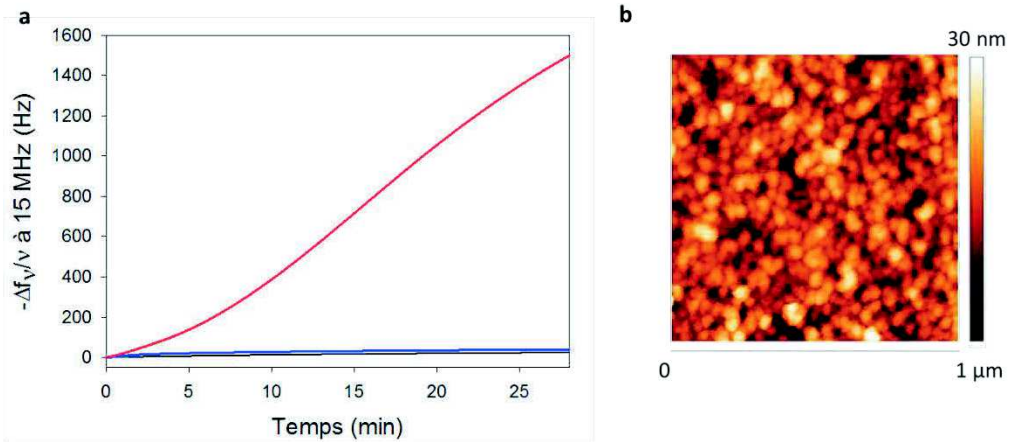

Figure 12 *: a) Evolution de la fréquence normalisée, mesurée par EC-QCM, en fonction du temps (ligne rouge) d'un mélange fer (II)/TA (ratio fer/TA de 2.5), (ligne noire) d'une solution de TA, (ligne bleue) d'une solution de fer (II) pendant l'application d'une densité de courant de 6.25 µA/cm². b) Image AFM obtenue en milieu liquide et en mode contact d'un film TA/Fer(III) autoconstruit pendant 30 minutes.*

La morphologie des films déposés a été caractérisée par AFM en mode contact à l'état liquide. La Figure 12b montre une topographie caractéristique d'un film TA/Fe(III) auto-assemblé pendant 30 minutes avec une densité de courant appliquée de 6,25 µA/cm². Le film présente des grains avec une rugosité aux environs de 5 nm. Une fois le film rayé, son épaisseur a pu être déterminée et ce, à différents temps de construction (Figure 13). Après 5 min d'auto assemblage, le film couvre uniformément tout le substrat avec une épaisseur de 16 nm et une rugosité de 6,3 nm. L'épaisseur du film augmente avec le temps d'application du courant jusqu'à atteindre 263 nm à 70 min. On peut remarquer que la rugosité du film reste presque constante atteignant 6,8 nm après 70 min.

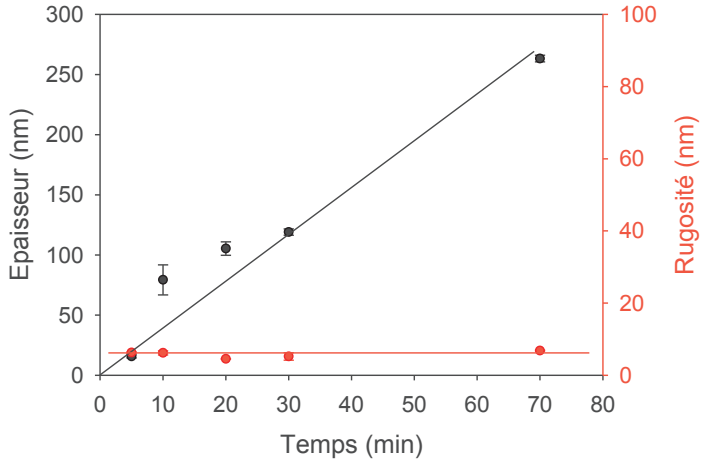

Figure 13 *: Evolution de l'épaisseur et de la rugosité d'un film auto-assemblé de TA et de Fe(III) mesurée par AFM après rayure en mode contact et en milieu liquide, en fonction du temps. Un mélange TA/Fe (II) (ratio Fe(II)/TA de 2,5 pH =3) a été mis en contact avec l'électrode et une densité de courant de 6,25 µA/cm² a été appliquée. La rugosité du film a été calculée à partir d'images AFM de dimensions10 µm × 10 µm.*

Cette rugosité constante est due à l'auto-assemblage de complexes TA/Fe(III) en solution dans le voisinage de l'électrode qui s'adsorbent sur la surface tout au long du processus. Ceci est en accord l'image topographique AFM représentant le film comme un assemblage homogène constitué de nanoparticules de 30 nm de diamètre (Figure 12b). Nous montrons ici que la génération de Fe (III), électrocontrôlée depuis l'électrode, permet le contrôle de l'auto-assemblage de TA/Fe (III) sur la surface simplement en ajustant le temps pendant lequel le courant est appliqué. Il est intéressant de comparer ces films de TA/Fe (III) électro-générés à ceux obtenus par changement de pH en solution par Ejima et al. A des ratios molaires Fe/TA similaires les rugosités des deux films sont dans le même ordre de grandeur.[17]

Les films construits sont stables même si un potentiel réducteur (-0,4V) est appliqué. Une étude par XPS a mis en évidence la présence de l'acide tannique et du fer (III) dans le film. L'influence de certains paramètres de construction a également été étudiée. La densité de courant appliquée a été variée de 1,25 à 31,25 µA/cm² et l'épaisseur du film augmente avec celui-ci. Le ratio Fe(II)/TA a également un impact sur la construction, l'épaisseur des films augmente avec celui-ci jusqu'à atteindre un plateau pour des ratios supérieurs à 8. Le type de complexe formé étant dépendant du pH de la solution, l'effet de ce dernier a aussi été examiné. Il a été montré que le pH n'a pas de répercussions sur la construction pour des pH supérieurs à 2. A pH=2 et en dessous, aucune construction n'est observée ce qui est attribué à la formation de mono-complexes de Fe (III)/TA et donc l'absence d'assemblage sur la surface.

4) Application des nouveaux procédés d'électrodéposition aux biocapteurs

Un des objectifs majeurs de ce travail était la création d'une électrode fonctionnalisée avec une enzyme en utilisant les deux stratégies d'autoconstruction de films induit par électrochimie présentées précédemment. L'idée était d'immobiliser une enzyme sur l'électrode soit par réticulation *via* l'oxydation de catéchols/gallols, soit en piégeant l'enzyme dans un auto-assemblage de TA et de Fe (III). Dans le premier cas, le biscatéchol, une fois activé par l'application d'un potentiel, a été utilisé pour réticuler enzymes réaction chimique entre les quinones du biscatéchol oxydé et les fonctions amines de l'enzyme. Dans le deuxième cas, nous avons essayé de piéger physiquement l'enzyme par co-déposition avec un film TA/Fe(III) auto-assemblé. Comme il est montré dans la deuxième partie de ce résumé, le biscatéchol créé dans notre équipe peut être utilisé pour électroréticulé un polyamine. Nous pouvons donc imaginer utiliser ce procédé pour électroréticuler d'autres composés présentant des fonctions amines, ce

qui est le cas pour les enzymes. Nous avons utilisé la phosphatase alcaline (AP) comme enzyme dans les mêmes conditions optimales déterminées pour le système PAH/bis-catéchol (voir partie 2). La Figure 14a montre un signal typique de construction obtenue en EC-QCM. Après l'injection du mélange AP/biscatéchol ou du biscatéchol seul, une légère augmentation de la fréquence normalisée est observée due à la coordination de l'or du crystal de QCM par les catéchols. L'application d'une CV (0-500 mV, vs Ag/AgCl, vitesse de scan 50 mV/s) induit une très lente augmentation de la fréquence normalisée dans les deux cas. Après 60 minutes et une étape de rinçage, la variation de fréquence a atteint 40 Hz pour le mélange AP/biscatéchol et le biscatéchol seul en solution.

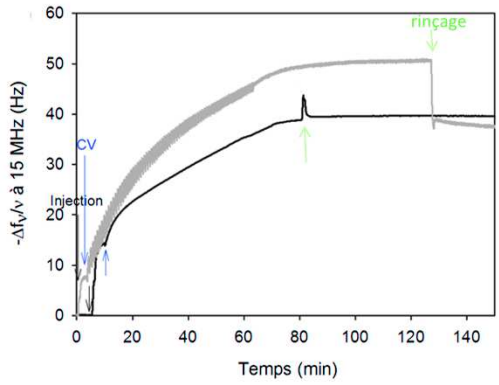

Figure 14 *: Evolution de la variation de fréquence normalisée mesurée par EC-QCM en fonction du temps pendant l'application d'une CV entre 0 et +500 mV (vs Ag/AgCl, vitesse de scan 50 mV/s) pour un mélange AP/biscatéchol à 1 mg/mL en biscatéchol et 1 mg/mL en AP.*

En comparaison, quand un mélange PAH/bis-catéchol est utilisé dans les même conditions, une variation de fréquence de 800 Hz est mesurée (Figure 7). La masse déposée avec la solution de bis-catéchol peut être expliqué par l'électroréticulation de la molécule.[18] Une construction similaire étant obtenue avec ou sans enzyme, celle-ci n'est probablement pas piégée dans le matrice de bis-catechol réticulé. Il est donc impossible d'immobiliser l'enzyme dans ces conditions. L'AP et les enzymes en général possède une densité d'amine assez faible (en comparaison avec le PAH) avec une accessibilité limitée par leur conformation ce qui défavorise la réaction avec les fonctions quinones du bis-catechol.[19]

Notre deuxième approche a été d'essayer de piéger physiquement l'enzyme dans le film auto-assemblé TA/Fe(II). Plus précisément, l'AP a été mélangée avec le TA et le Fe (II) en solution et le mélange a été mis en contact avec une électrode. En appliquant un potentiel oxydant, l'auto-assemblage de films TA et de Fe (III) des films est induit en présence de l'enzyme.

La Figure 15 montre l'évolution d'un signal de QCM mesuré pendant l'application d'un courant constant de 5 µA (densité de courant 6,25 µA/cm²) pour des mélanges AP/TA/Fe(II) à pH = 3 et à pH = 7,4. Dans les deux cas après une heure, une variation de fréquence normalisée d'approximativement 1000 Hz est atteinte.

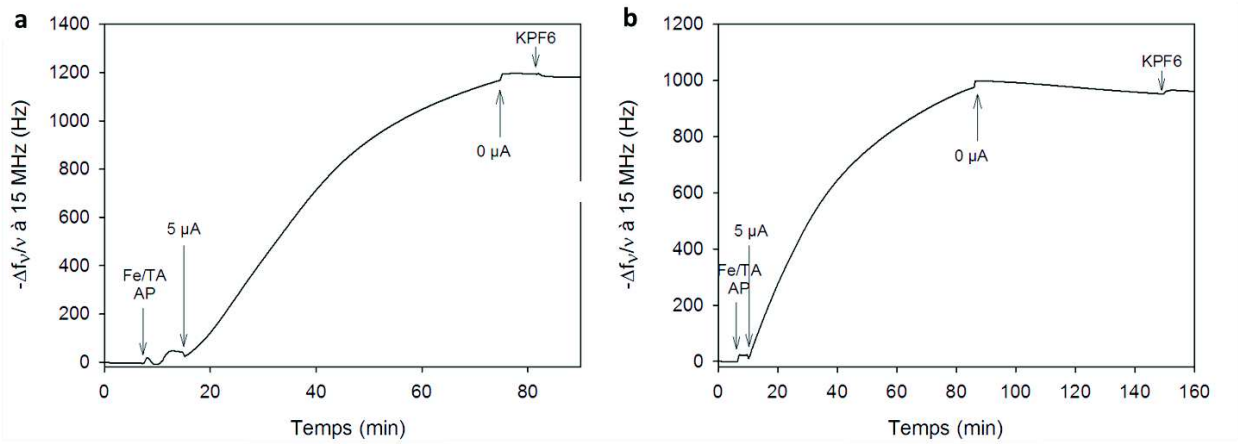

Figure 15 *: Evolution de la variation de fréquence normalisée mesuré en EC-QCM en fonction du temps pendant l'application d'un courant de 5µA (densité de courant 6.25 µA/cm²) pour un mélange TA/Fe(II)/AP à a) pH = 3 et b) pH = 7,4.*

En présence d'AP, l'auto-assemblage de TA/Fe(III) est ralenti. En comparaison, la variation de fréquence normalisée est de 2500 Hz pour une solution de TA/Fe (III) pendant la même durée (1h). A cause de la précipitation du substrat test de l'AP (PNPP), nous n'avons pas été capables de tester l'activité enzymatique du film et de vérifier la présence de l'AP dans le film.

Conclusion

Nous prouvons avec ce travail que l'auto-assemblage « une-étape » par l'approche morphogénique est un procédé de fonctionnalisation très efficace. Ici, nous généralisons le travail précurseur réalisé par notre équipe dans ce domaine à de nouveaux systèmes, montrant ainsi la versatilité du procédé. C'est dans ce but que nous nous sommes inspirés de phénomènes naturels prouvant encore une fois que la nature, loin d'être obsolète, peut nous fournir des idées innovantes et générer des nouvelles avancées technologiques. Le phénomène d'adhésion des moules et le rôle des polyphénols dans la nature sont tous deux basés sur les propriétés chimiques des groupements catéchols et gallols. Deux systèmes basés sur cette biochimie ont été créés par une approche morphogénique. Le premier repose sur les propriétés redox des catéchols. Plus précisément, il est basé sur l'autoconstruction covalente d'une polyamine : le PAH, par un espaceurs biscatéchol (le morphogène) activé par électrochimie. L'oxydation des deux groupements catéchols en quinones mène à la formation d'un gradient de molécules bis-

quinones activées depuis l'électrode. Les bis-quinones réagissent des deux cotés sur les fonctions amines du PAH menant à l'autoconstruction d'un film sur la surface. Le second système repose sur la capacité des groupements gallols de l'acide tannique à complexer le Fe (III). En appliquant un potentiel d'oxydation en présence d'un mélange TA/Fe (II), les ions Fe (II) sont oxydés en ions Fe (III), le morphogène ici, à la surface de l'électrode déclenchant l'auto-assemblage de TA sur la surface par liaisons de coordinations avec le Fe (III). Enfin nous avons essayé d'appliquer ces deux systèmes à l'immobilisation d'enzymes pour des applications de biocapteurs.

La première ouverture de ce travail serait de persévérer dans le développement d'une approche morphogénique pour immobiliser une enzyme, notamment en utilisant l'hydroquinone pour limiter l'auto-polymérisation du biscatéchol et donc pouvoir augmenter sa concentration. Une autre stratégie pourrait être d'utiliser des complexes PAH/enzymes, de modifier chimiquement une enzyme pour augmenter sa densité d'amines ou encore d'utiliser des clusters d'enzymes. Une seconde ouverture serait d'exploiter les fonctions catéchols ou gallols libres restantes dans les deux systèmes afin de développer des plates-formes d'immobilisation pour des macromolécules ou des nanoparticules.

Références

[1] Monahan, J.; Wilker, J. J. Specificity of Metal Ion Cross-Linking in Marine Mussel Adhesives. *Chemical Communications* **2003**, 1672.

[2] Deming, T. J. Mussel Byssus and Biomolecular Materials. *Current Opinion in Chemical Biology* **1999,** *3*, 100.

[3] Krylova, I. Painting by Electrodeposition on the Eve of the 21st Century. *Progress in Organic Coatings* **2001,** *42*, 119.

[4] Wu, L. Q.; Gadre, A. P.; Yi, H. M.; Kastantin, M. J.; Rubloff, G. W.; Bentley, W. E.; Payne, G. F.; Ghodssi, R. Voltage-Dependent Assembly of the Polysaccharide Chitosan onto an Electrode Surface. *Langmuir* **2002,** *18*, 8620.

[5] Payne, G. F.; Kim, E.; Cheng, Y.; Wu, H. C.; Ghodssi, R.; Rubloff, G. W.; Raghavan, S. R.; Culver, J. N.; Bentley, W. E. Accessing Biology's Toolbox for the Mesoscale Biofabrication of Soft Matter. *Soft Matter* **2013,** *9*, 6019.

[6] Ammam, M. Electrochemical and Electrophoretic Deposition of Enzymes: Principles, Differences and Application in Miniaturized Biosensor and Biofuel Cell Electrodes. *Biosensors and Bioelectronics* **2014,** *58*, 121.

[7] Sun, J. Q.; Gao, M. Y.; Zhu, M.; Feldmann, J.; Mohwald, H. Layer-by-Layer Depositions of Polyelectrolyte/Cdte Nanocrystal Films Controlled by Electric Fields. *Journal of Materials Chemistry* **2002,** *12*, 1775.

[8] Ngankam, A. P.; Van Tassel, P. R. Continuous Polyelectrolyte Adsorption under an Applied Electric Potential. *Proceedings of the National Academy of Sciences of the United States of America* **2007,** *104*, 1140.
[9] Shi, X. W.; Tsao, C. Y.; Yang, X. H.; Liu, Y.; Dykstra, P.; Rubloff, G. W.; Ghodssi, R.; Bentley, W. E.; Payne, G. F. Electroaddressing of Cell Populations by Co-Deposition with Calcium Alginate Hydrogels. *Advanced Functional Materials* **2009,** *19*, 2074.
[10] Waltman, R. J.; Bargon, J. Electrically Conducting Polymers - a Review of the Electropolymerization Reaction, of the Effects of Chemical-Structure on Polymer Film Properties, and of Applications Towards Technology. *Canadian Journal of Chemistry-Revue Canadienne De Chimie* **1986,** *64*, 76.
[11] Rydzek, G.; Thomann, J. S.; Ben Ameur, N.; Jierry, L.; Mesini, P.; Ponche, A.; Contal, C.; El Haitami, A. E.; Voegel, J. C.; Senger, B.; Schaaf, P.; Frisch, B.; Boulmedais, F. Polymer Multilayer Films Obtained by Electrochemically Catalyzed Click Chemistry. *Langmuir* **2010,** *26*, 2816.
[12] Rydzek, G.; Jierry, L.; Parat, A.; Thomann, J. S.; Voegel, J. C.; Senger, B.; Hemmerle, J.; Ponche, A.; Frisch, B.; Schaaf, P.; Boulmedais, F. Electrochemically Triggered Assembly of Films: A One-Pot Morphogen-Driven Buildup. *Angewandte Chemie-International Edition* **2011,** *50*, 4374.
[13] Tian, Y. A.; Ye, S. Q.; Ran, Q.; Xian, Y. Z.; Xu, J. J.; Peng, R.; Jin, L. T. Generation of Surface-Confined Catechol Terminated Sams Via Electrochemically Triggered Michael Addition: Characterization, Electrochemistry and Complex with Ni(Ii) and Cu(Ii) Cations. *Physical Chemistry Chemical Physics* **2010,** *12*, 13287.
[14] Rydzek, G.; Terentyeva, T. G.; Pakdel, A.; Golberg, D.; Hill, J. P.; Ariga, K. Simultaneous Electropolymerization and Electro-Click Functionalization for Highly Versatile Surface Platforms. *Acs Nano* **2014,** *8*, 5240.
[15] Nagasaka, M.; Yuzawa, H.; Horigome, T.; Hitchcock, A. P.; Kosugi, N. Electrochemical Reaction of Aqueous Iron Sulfate Solutions Studied by Fe L-Edge Soft X-Ray Absorption Spectroscopy. *Journal of Physical Chemistry C* **2013,** *117*, 16343.
[16] Wan, H. J.; Zou, Q. L.; Yan, R.; Zhao, F. Q.; Zeng, B. Z. Electrochemistry and Voltammetric Determination of Tannic Acid on a Single-Wall Carbon Nanotube-Coated Glassy Carbon Electrode. *Microchimica Acta* **2007,** *159*, 109.
[17] Ejima, H.; Richardson, J. J.; Liang, K.; Best, J. P.; van Koeverden, M. P.; Such, G. K.; Cui, J.; Caruso, F. One-Step Assembly of Coordination Complexes for Versatile Film and Particle Engineering. *Science* **2013,** *341*, 154.
[18] Burzio, L. A.; Waite, J. H. Cross-Linking in Adhesive Quinoproteins: Studies with Model Decapeptides. *Biochemistry* **2000,** *39*, 11147.
[19] Bradshaw, R. A.; Cancedda, F.; Ericsson, L. H.; Neumann, P. A.; Piccoli, S. P.; Schlesinger, M. J.; Shriefer, K.; Walsh, K. A. Amino-Acid-Sequence of Escherichia-Coli Alkaline-Phosphatase. *Proceedings of the National Academy of Sciences of the United States of America-Biological Sciences* **1981,** *78*, 3473.

Résumé en français suivi des mots-clés en français

Les architectures moléculaires qui se forment exclusivement sur une surface sont encore rares. L'électrodéposition est un procédé exploitant des « signaux » électriques afin de déclencher et contrôler l'assemblage de films. Récemment, une nouvelle méthode : l'autoconstruction de films en « une étape » par l'utilisation d'un morphogène (un gradient de catalyseur généré depuis une électrode), a attiré l'attention de la communauté scientifique. En effet, elle permet l'auto-assemblage rapide de films polymériques robustes. Cependant, cette technique était limitée à des systèmes basés sur la chimie click du Cu (I).

Le but de ce travail était d'étendre cette stratégie à d'autres systèmes en utilisant une approche bio-inspirée. Le concept du morphogène a été appliqué pour développer deux nouveaux systèmes d'autoconstruction déclenchées par électrochimie. Le premier système est basé sur l'autoconstruction covalente de films polymériques induite par l'oxydation d'une molécule organique, inspirée de la moule. Le deuxième est basé sur l'auto-assemblage de films de polyphénols par électro-assemblage par liaisons de coordinations. Enfin, nous avons appliqué ces deux concepts pour immobiliser électrochimiquement une enzyme sur une électrode afin de créer un biosenseur.

Mots clés : polymère, électrodéposition, enzyme, catéchol, polyphénol, chimie de surface, fonctionnalisation

Résumé en anglais suivi des mots-clés en anglais

Molecular architectures that spontaneously grow exclusively near a surface are rare. Electrodeposition is a process in which imposed electrical « signals » are employed to direct the assembly of thin films. Recently, a new method based on the one-pot self-construction of films by means of a morphogen (a catalyst gradient generated from a surface) has attracted attention since it allows the quick self-assembly of robust films. Nevertheless, this technique was quite limited to systems based on click chemistry.

The purpose of this work was to extend this strategy to other systems using a bio-inspired approach. The one-pot morphogen concept was applied to design two new electro-triggered self-construction concepts. The first one is based on the self-construction of covalent polymer films triggered by mussel-inspired molecule oxidation. The second one is based on the electro-self-assembly of polyphenols films based on ionic bonds coordination. Finally, we tried to apply these concepts in order to electrochemically immobilize an enzyme on an electrode to create a biosensor.

Keywords : polymer, electrodeposition, enzyme, catechol, polyphenol, surface-chemistry, functionalization